National Aeronautics and
Space Administration

George C. Marshall Space Flight Center
Marshall Space Flight Center, Alabama 35812

PROCEEDINGS OF THE SHUTTLE-BASED COMETARY SCIENCE WORKSHOP

A Forum for the Presentation and Discussion of
Possible Shuttle-Based Experiments and
Observations of Comets and
Cometary-Like Materials

Sponsored by

The University of Alabama in Huntsville
and
The George C. Marshall Space Flight Center

Huntsville, Alabama

November 4-5, 1976

FOREWORD

The Proceedings of the Shuttle-Based Cometary Science Workshop is the initial result of a forum for the presentation of possible Shuttle-based experiments and observations of comets and cometary-like materials. The two-day workshop on the various possibilities of this new orbiting laboratory was held in November 1976. The workshop was sponsored by the George C. Marshall Space Flight Center and presented by the University of Alabama in Huntsville. The encouragement of Bertram Donn of NASA Headquarters, the support of Charles Lundquist of the Marshall Space Flight Center and Ernst Stuhlinger of the University of Alabama in Huntsville, and the enthusiastic participation of the attendees made the workshop a success, as the proceedings reflect. It is hoped that the final results of the workshop will be cometary science experiments and observations from the Space Shuttle. The data obtained from this research will increase greatly our knowledge of comets.

The session chairmen for the workshop were C. Lundquist, B. Donn, M. Dubin, and C. R. O'Dell. The material from the last session (IV) of the workshop has been incorporated in the proceedings into the other sessions.

G. Allen Gary and K. Stuart Clifton
Editors
Space Sciences Laboratory
Marshall Space Flight Center

PREFACE

The motivation of this meeting was to examine the prospects of cometary research from the Space Shuttle. Clearly, the Shuttle provides a potentially valuable set of capabilities for such research. Many advantages appear quite obvious. However, as one looks into them more closely a variety of problems and difficulties begin to appear. In some cases the value of Shuttle research compared to ground-based experiments or observations appears less favorable.

Dr. Lundquist suggested that a conference or workshop with a small set of active cometary scientists could be very useful. Such an effort, in which a number of individual points of view and scientific disciplines would simultaneously consider this question, seemed very worthwhile. This would be true not only for the participants, but for all potential investigators of comets by circulating the workshop proceedings. As a result of a group discussion, not only could the more obvious prospects and problems be explored, but new ideas could develop and otherwise unforeseen difficulties become apparent. One objective was to delineate opportunities for research unique to the Shuttle.

The workshop was divided into four sessions with a chairman who had experience in the area covered by that session. The papers were intended to introduce the subject and provide background material and stimulation for the discussion by all the participants. The first session dealt with the Shuttle as research environment. The second was concerned with on-board experiments at zero-gravity and release of gas and dust to simulate cometary phenomena. Cometary observations from space were treated in the third session. The final session discussed objectives and results of the workshop and additional information on Shuttle opportunities.

The participants felt the meeting indeed was worthwhile and that they would remain an informal working group for cometary science from the Shuttle. We hope that these proceedings will be useful and stimulating to others in planning Shuttle-based cometary research. That was the initial and primary goal of the Shuttle-Based Cometary Science Workshop.

Bertram Donn
National Aeronautics and Space Administration

TABLE OF CONTENTS

TABLE OF CONTENTS (Concluded)

omit 70
P.5

INTRODUCTORY COMMENTS

Ernst Stuhlinger
Organizing Chairman
University of Alabama in Huntsville

Professor Fred Whipple, discussing comets at a meeting of astronomers several years ago, mentioned almost casually that a "dirty snowball", resembling at least qualitatively his model of a comet nucleus, could be built on earth and transported into a low earth orbit onboard a spacecraft. The snowball would then be expelled from the spacecraft and observed with instruments while it orbited the earth in close proximity to the orbiting spacecraft.

At the time of that remark, a project of this kind seemed to be far in the future. Today, only five years separate us from the operational Shuttle, and a "snowball" project would appear feasible. In fact, the Shuttle with its capability for large payloads, instrumentation, and even scientists onboard would be quite applicable to a snowball project, provided that such a project should appear meaningful and desirable after careful scientific scrutiny.

Dr. Bertram Donn, Office of Space Sciences at NASA Headquarters, asked the G. C. Marshall Space Flight Center to organize and convene a meeting of cometary sciences specialists with the objective of discussing feasibility and desirability of a snowball project, and of other comet-related projects in space. Dr. Charles Lundquist was assigned responsibility for this meeting, and he in turn selected the University of Alabama in Huntsville to be the host of the conference. The UAH is very happy to welcome the participants today. We hope that the meeting

will be enjoyable and successful for all of you.

The organizing committee included Kenneth S. Clifton and Allen G. Gary from the G. C. Marshall Space Flight Center, and Carl Cramer from the University of Alabama in Huntsville.

The National Aeronautics and Space Administration is very intent on making the capabilities of space projects available to science; however, NASA desires to obtain from members of the scientific community a clear indication of the usefulness and desirability of a specific science project before work on the project is started.

It is hoped that this working group meeting on Shuttle-based cometary science will bring out those objectives in comet research which can and should be pursued by Shuttle-related projects.

SESSION I
SHUTTLE SPACECRAFT

SPACE SHUTTLE OPPORTUNITIES FOR COMETARY RESEARCH

Charles A. Lundquist
Space Sciences Laboratory
NASA, Marshall Space Flight Center, Alabama

The Marshall Center is pleased to welcome this Workshop to Huntsville, Alabama. The Space Shuttle's impact on future modes of scientific investigation is particularly evident here. Early in the Shuttle planning cycle, this Center had the privilege to aid NASA Headquarters by modeling sequences of typical Shuttle missions. These mission models helped identify places where improvements could be made to better accommodate experiments on the Shuttle. The Marshall Center is also the principal United States interface with the Spacelab Program of the European Space Agency. Spacelab will, of course, provide resource support for much of the specialized equipment prepared for space investigations. Also, Marshall has been given management responsibility for the first three Spacelab missions and for the science payload to be flown on the sixth of the Orbital Test Flights of Shuttle preceding the Spacelab missions.

From the vantage point that these responsibilities provide, we are keenly aware that the Shuttle era is approaching very rapidly. This is a realization that I want specifically to convey and emphasize today. A few weeks ago, on September 17, the first Space Shuttle was rolled out in a ceremony in Palmdale, California. Proposals for experiments on the first Spacelab mission in 1980 have been received and are being evaluated. The selection of experiments to be carried will be announced in the next 2 or 3 months. Proposals for experiments on Orbital Test Flights (OFT-2 through OFT-6) and for the second Spacelab mission are due on December 3, 1976 — approximately 1 month from today. Their evaluation will begin immediately thereafter. Further opportunities to propose experiments for subsequent flights will be forthcoming soon.

To establish appropriate insight and common foundations for participation in the Shuttle missions, various scientific disciplines have held meetings analogous to this Workshop. Indeed, several major disciplines have been quite busy seeking to understand how to optimize the use of the Shuttle for their fields of interest. Truthfully, there would have been advantages in a somewhat earlier date for this Workshop. Nevertheless, some time remains for the consequences of the Workshop to be registered in proposals for specific cometary experiments, even for the OFT and second Spacelab missions. Certainly, we must fully appreciate a real sense of urgency in recognition of the pace at which the Shuttle era is approaching.

Several distinct modes of cometary investigation are offered by the Shuttle. First, there is a mode in which instrumentation for observations of a natural comet is carried to orbit on Spacelab. This is the mode used successfully for Comet Kohoutek during the Skylab mission of 1973-1974. Second is a mode in which gaseous or solid material is released from Shuttle to simulate some aspect of cometary physics. Such an artificial comet option was discussed in some of the mission model studies. Another mode uses the near weightlessness within Spacelab to allow laboratory experiments with materials as they may exist on the surface of a comet nucleus. Surely, the sponsors of this Workshop hope that all of these opportunities to use Shuttle will be examined in the course of the Workshop.

Ultimately, a Shuttle may be used to stage a mission to or near a comet. This eventual mission should be kept in mind as the other opportunities for cometary research are considered. Early investigations from Earth orbit, if thoughtfully designed, can significantly enhance the value of a later comet visit.

The first session on the Workshop agenda provides a synopsis of the Shuttle characteristics that influence possible cometary research. The organizers of the Workshop trust that this will supply the desired background for our subsequent discussions.

SHUTTLE/SPACELAB DESIGN, PERFORMANCE, ACCOMMODATIONS AND CONSTRAINTS

The purpose of this paper is to describe the main characteristics of the Shuttle/Spacelab system in order to provide an introduction for individual experimenters who may propose cometary science experiments. The information contained herein was derived from the "Spacelab Payload Accommodations Handbook PDR-B 1976". Specific information is subject to change; however, the salient design, performance, accommodations, and constraints for the experimenter are expected to remain as presented. Major Spacelab/experiments interfaces, Spacelab payload support systems, and requirements with which experiments must comply are described in the referenced document.

General Spacelab System

Spacelab, as a shuttle payload, is carried to and from orbit by the Space Shuttle (Figure 1). It remains attached to the Orbiter (within the payload bay) of the Space Shuttle throughout the flight.

Spacelab consists of two basic elements in the orbiter bay - a pressurized module and an unpressurized pallet which can be used separately or in combination. The modular design of the module and the pallet allows a variety of flight configurations which can be grouped into three basic configuration types - module only, module plys pallet, and pallet only.

The module provides a controlled pressurized environment for the users and their equipment. It supplies basic services such as power,

heat rejection, and data management, together with certain basic support equipment such as standard racks, airlock, etc. which may be used as required. In general, the module consists of either a single cylindrical segment (core segment) or two segments (core plus experiment segment). The pallet is an unpressurized platform to which instruments, which require direct exposure to space, such as telescopes and antennas may be mounted. The pallet provides basic services, such as power distribution, heat rejection, and data acquisition and commands.

The pallet only configuration may contain up to 15 m mounting length. Up to three pallet segments can be combined with a short module (core segment only) and up to two pallet segments can be combined with a long module (core and experiment). The module diameter is slightly over 4 meters and each cylindrical segment is approximately 2.7 meters long. The pallet segments are approximately 3 meters long and 4 meters wide. Major external design features of Spacelab in a typical module plus pallet configuration are shown in Figure 2. The presented configuration consists of a two-segment module and one pallet segment.

The module itself is formed of a cylindrical pressure shell and cone-shaped end closures (end cones) and is covered with high-performance insulation. The module is structurally attached to the Orbiter by attach fittings located on the main ring frames of the module cylindrical segments. The forward-located module segment (core segment) contains subsystem equipment and crew work space, but also leaves about 60 percent of the rack volume for experiment installation. The experiment segment is dedicated entirely to experiment installation and operations.

The center of gravity of the Orbiter with the integrated Spacelab must lie within certain limits which result from aerodynamic constraints during re-entry and landing. For this reason the Spacelab module cannot be located at the very forward end of the Orbiter cargo bay. A tunnel is therefore provided for crew and equipment transfer between the Orbiter and the Spacelab module. In addition, a tunnel adapter/EVA airlock combination is attached to the Orbiter forward bulkhead. Extra-vehicular activity (EVA) can be performed through the EVA airlock on the top of the tunnel adapter. The design of this unit is such that access to Spacelab from the Orbiter is not interrupted during EVA.

The top of the core segment contains provisions for mounting a high quality window/viewport assembly and the top of the experiment segment contains provision for mounting either a high quality window/ viewport assembly or an airlock. If neither airlock nor window/viewport are flown, the top openings are closed by coverplates. A second viewport is located in the aft end cone to give an unobstructed view of the pallet. The forward and aft end cones also provide for feedthrough panels for utility routing. Figure 3 shows the major Spacelab flight elements.

The U-shaped pallet segments, also seen in Figure 3, are covered with aluminum honeycomb panels. They are integral parts of the pallet structure, but can also be used for mounting of light weight payload equipment. A series of hardpoints attached to the main structure of the pallet segment is provided for mounting of heavy payload equipment. The pallet segments are mounted to the Orbiter with a set of attach fittings. Up to three pallet segments may be structurally linked together to form a pallet train and attached to the Orbiter by a single set of

attach fittings. Up to five pallet segments may be flown on a single mission.

The interior design of the module is modular and provides flexibility to the user. Racks are arranged in single and double rack assemblies for mounting of equipment. The floor is segmented. The most forward floor in the core segment provides support for the subsystem double rack assembly on each side. A second floor segment provides for support of rack assemblies for experiments.

The core segment can accommodate one single and one double rack assembly for experiments, while the experiment segment can accommodate one single and two double rack assemblies for experiments, on each side. The sequence of single and double racks must be as indicated in Figure 3. The racks are independently attached to the floor and overhead structure so that as many racks as necessary may be installed for a given mission. If some racks are not required, other special experiment equipment may be attached in their place.

The subsystem racks are also detachable but will normally remain installed in the core segment between flights. In operational use, the equipment racks and floors will normally be pre-integrated and checked out as a complete assembly. This assembly will then be rolled into the module shell. The necessary interface connections will then be made with the primary structure and the subsystems in the core segment.

In the module only and module plus pallet configurations, Spacelab subsystems are mounted in the subsystem racks and on the subfloor as shown in Figure 3. In these configurations the module can accommodate crew members for operation of subsystems and experiments. Signal, power and other utility lines to and from the Orbiter are routed from the forward end cone. In module plus pallet configuration lines between module and pallet are routed via a utility support structure. For pallet configurations an "Igloo", a pressurized cylinder attached to a pallet, is provided for installation of certain subsystem hardware which is needed for pallet-only configurations. In pallet-only configurations, operations of subsystems and experiments will be performed from the Orbiter's aft flight deck (AFD) or from the ground. Signal and other utility lines to and from the Orbiter are routed through the igloo. Spaced pallet segments are connected via a utility support structure.

The Spacelab equipment in the aft flight deck (AFD) of the Orbiter permits the control of Spacelab subsystems and experiments, and permits the display of data. This aft flight deck equipment is independent of the Spacelab configuration flown. In the aft flight deck there are also limited space and resources available for payload use.

A prime consideration in designing Spacelab was the provision of as many services as possible for the users within the given con-

straints. This has led to a modular design of subsystems. A certain part of the subsystem equipment may be selected by the users in order to satisfy the specific need for a flight in an optimal manner. This subsystem equipment, which can be removed without affecting the basic operation of the Spacelab system is defined as "mission dependent" equipment.

The Spacelab flight hardware is divided into the following subsystems: Structure, environmental control, electrical power and distribution, command and data management, and common payload support equipment. The environment control subsystem (ECS) comprises elements for environmental control, life support, and passive and active thermal control. Oxygen/nitrogen atmosphere at sea level pressure is provided in the module by this subsystem. Crew habitability support such as food, drink, sleep, hygiene, and waste management facilities is provided by the Orbiter. The ECS includes a valve in the forward bulkhead by which experiment chambers etc. inside the module can be connected with the outside vacuum. This facility is referred to as the small experiment vent assembly.

The electrical power and distribution subsystem (EPDS) conditions the basic electric power derived from the Orbiter's fuel cells and distributes it to Spacelab subsystems and Spacelab payloads.

The command and data management subsystem (CDMS) provides support functions, such as data acquisition, command, formatting, display and

recording. The CDMS includes three identical computers: one dedicated to Spacelab payloads, one dedicated to subsystems and one back-up computer for either of the two dedicated computers. The CDMS subsystem is largely independent from the Orbiter. Communication with ground facilities, either directly to a Spaceflight Tracking and Data Network (STDN) Station or via the Tracking and Data Relay Satellite System (TDRSS), is provided through the Orbiter's communication system. System activation and monitering (SAM) of Spacelab is performed through dedicated hardware and CDMS.

Common payload support equipment (CPSE) consists of an airlock, a top cover plate, a top cover plate with a high quality window and viewport and film storage provisions.

The Spacelab program also provides software for operation of Spacelab on orbit and check-out of Spacelab on the ground. Furthermore, the program includes mechanical and electrical ground support equipment for integration and checkout of Spacelab.

Coarse pointing of Spacelab payloads is provided by the Orbiter. A Spacelab-supplied instrument pointing subsystem (IPS) permits high precision pointing of Spacelab payloads.

The typical operation cycles of Spacelab are: Pre-integrated equipment of the user(s) is integrated into Spacelab which is subsequently installed in the Orbiter. In the launch configuration the Space Shuttle consists of the Orbiter, a large External Tank which provides propellant to the Orbiter during launch and two Solid Rocket Boosters.

The Solid Rocket Boosters are jettisoned after burn-out and retrieved. The External Tank is jettisoned in the final ascent phase. The nominal flight duration of the Orbiter is seven days. However, the Orbiter/Spacelab is being designed so as not to preclude extended missions of up to thirty days duration. After launch the doors of the Orbiter cargo bay will be opened in order to expose Spacelab to space. Subsequent to completion of check-out operations Spacelab will be activated and operated. Before re-entry and landing the Spacelab systems will be de-activated and the doors of the Orbiter cargo bay will be closed. After landing, Spacelab and the Orbiter will be refurbished as required and prepared for the next flight in separate ground operation cycles.

Physical Constraints:

Figure 4 illustrates the physical envelope for Spacelab and its payload in the Orbiter cargo bay and the location of this envelope within the Orbiter. The dynamic envelope is that envelope which must not be exceeded by any Spacelab or payload hardware in launch or landing configuration (except for interface connections) under the maximum predicted dynamic environment, excluding Orbiter crash landing loads.

The dynamic envelope is of cylindrical shape with a diameter of 4.572 m (15 feet) around a center-line parallel to the Orbiter Xo-axis at Orbiter stations Yo = 0 and Zo = 400 inches (10.16 m). The length of the dynamic envelope is 18.288 m (60 feet), extending from Orbiter station Xo ==582 inches (14.783 m) to Orbiter station Xo = 1302 inches (33.071 m).

Technical drawings of the dynamic envelopes in the Orbiter cargo bay are given in Figure 5.

Particular attention of the users is drawn to the fact that transportation envelopes for various ground transportation modes may impose more severe constraints than the dynamic envelope of the Orbiter cargo bay.

Field of View Constraints of the Orbiter Cargo Bay:

The Orbiter has the capability of exposing the entire length and width of the Orbiter cargo bay to space environment. With the Orbiter cargo bay doors and radiators open, the Orbiter provides an unobstructed 180-degree lateral field of view (except for localized interference due to the manipulator supports and the door hinges) for any point along the line $Y_o = 0$, $Z_o = 427$ (10,845.8 mm) between $X_o = 582$ (14,782.8 mm) and $X_o = 1302$ (33,070.8 mm). The manipulator supports are not removed from the Orbiter, even if the remote manipulator is not flown. From the midpoint of the dynamic envelope $X_o = 942$ (23,926 mm) $Y_o = 0$, $Z_o = 400$ (10,160 mm), the following clearance angles, measured from the Z axis toward the X axis are maintained:

To the forward Orbiter bulkhead	75^o (1.309 radians)
To the aft Orbiter bulkhead	75^o (1.309 radians)
To the vertical stabilizer	57^o (0.99408 radians)

These clearance angles are shown in Figure 6.

Center of Gravity Constraint:

The center of gravity of the assembly Orbiter and Spacelab with its payload must be located within very close tolerances because of aerodynamic effects during re-entry and landing. Therefore, the location of the center of gravity of Spacelab with its payload with respect to the center of gravity of the empty Orbiter has specific constraints.

Orbits and Orbital Maneuvering Constraints:

The Space Shuttle provides for transportation of Spacelab to and from earth orbits and utilizes two launch sites. The Eastern Test Range (ETR) located at the Kennedy Space Center (KSC) is used for launches into low inclination orbits and the Wester Test Range (WTR) located at the Vandenberg Air Force Base (VAFB) is used for launches into high inclination orbits.

The thrust required to accelerate the Orbiter to suborbital velocity is supplied by two Solid Rocket Boosters and the main engines of the Orbiter which are supplied with propellant from an External Tank. The Solid Rocket Boosters and the External Tank are jettisoned during the launch phase. An Orbital Maneuvering Subsystem (OMS) is used to acquire orbital velocity and to place the Orbiter into the desired orbit (Figure 7). Furthermore, the OMS provides the propulsive thrust to perform orbit corrections, orbit transfer, rendez-vous and de-orbit maneuvers. The thrust required for Orbiter separation and translational braking is provided by the Reaction Control Subsystem (RCS) which is operated in a special mode for this purpose, although the prime function of this subsystem is attitude control.

The integral OMS tanks of the Orbiter are sized to provide a usable capacity of 11294 kg (24900 lb). The velocity increment which can be imparted to the Orbiter by this amount of propellant is 304.8 m/sec (1000 ft/sec) for a 29484 kg (65000 lb) and about 366 m/sec (1200 ft/sec) for a 14515 kg (32000 lb) cargo weight respectively. Up to three extra propellant tanks, referred to as OMS kits can be installed in the Orbiter cargo bay for increased operational flexibility. These extra

OMS kits are installed at the aft end of the Orbiter cargo bay.

The dry- and wet weight, as well as the velocity increment which can be imparted to the Orbiter with various cargo weights are summarized in Table 1.

The dry- and wet weight of the OMS-kits will be charged to the landing and launch weight of the Spacelab payload, respectively. These weight have to be duly accounted for in mission planning and in the assessment of the center of gravity. The velocity increments outlined in Table 1 indicate that the OMS-kits are not intended to perform significant inclination changes e.g. from 28.5 to 0 degree inclination, but to perform orbit corrections or transfer maneuvers in the orbital plane. The maximum achievable inclination change per OMS-kit is about 2 degrees. The achievable inclination decrease below 28.5 degree is about 1 degree per OMS kit only because the inclination has to be restored to 28.5 degree prior to descent. The use of OMS-kits to obtain orbits with high altitude is shown in Figure 8.

Achievable Orbits:

In Figure 8 typical ranges of circular orbits attainable for Spacelab missions are presented. This figure is based on a total Spacelab weight, including Spacelab payload, of 14515 kg (32000 lb). It is assumed that launch takes place from KSC for inclinations between 28.5^{o} and 57^{o} and from VAFB for inclinations between 56^{o} and 104^{o}.

Figure 8 represents the capabilities of the Space Shuttle for typical sets of operational requirements. In this figure, a RCS propellant consumption of 1408 kg (3100 lb) is assumed. It should be noted

that the suborbital disposal of the External Tank presents limitations on some discrete inclinations between 56 and 70 degrees for launches from VAFB. Missions in this inclination region will have to be individually planned, because the performance shown in the maximum expected and trajectory changes to accommodate safe External Tank disposal will degrade performance.

Figure 8 is derived from performance curves of the Space Shuttle for launches from KSC and VAFB (Figures 9 and 10). The curves present the cargo weight to be placed into circular orbits as a function or orbital altitude, for various inclinations and number of OMS-kits. The weight of the OMS propellant in the integral OMS-tankage and OMS-kits necessary to obtain the indicated orbits has already been taken into account in establishing the performance curves of Figures 9 and 10 and, therefore, need not be subtracted from the cargo weight given in these figures.

The Space Shuttle also has the capability to place Spacelab into elliptical orbits. This capability depends significantly on the de-orbit mode. Orbits with maximum eccentricity can be obtained in a direct de-orbit mode, i.e. a procedure where the de-orbit maneuver is initiated at apogee. An alternative de-orbit mode (indirect de-orbit mode) is to return to a low altitude orbit prior to re-entry. The maximum achievable heights of apogee are shown in Table 2 for various inclinations and the two described de-orbit modes. This table is based on a height of perigee of 185 km (100 nautical miles) and a Spacelab weight, including payload, of 14515 kg (32000 lb). For the direct de-orbit maneuver there exist operational limitations such as the relationship of the landing site to the location of the de-orbit maneuver or constraints due to thermal

protection system capabilities. In Table 2 an ideal relationship between the landing site and the location of the de-orbit maneuver and no constraint due to the Orbiter thermal protection system are assumed. The data concerning the indirect de-orbit mode are based on an 185 km (100 nautical miles) circular orbit prior to re-entry. The indirect de-orbit mode can always be flown. The exact capability of the Space Shuttle to obtain elliptical orbits will have to be assessed on an individual basis and will, in general, be between the figures for the two de-orbit modes, quoted in Table 2.

The Shuttle System has the capability to place the Orbiter into sun synchronous orbits which have nodal precession rates exactly matching the earth's angular motion around the sun.

It has already been pointed out that the data for the direct de-orbit modes given in Table 2 are based on an ideal location of the perigee with respect to the landing site. Other locations of the perigee and control of the location of perigee are possible, but these cases will have to be calculated on an individual basis.

In principle the Shuttle System is capable of covering the whole range of possible angles of right ascension of ascending nodes. Mission requiring specific angles of right ascension of ascending node have to be evaluated on an individual basis.

Attitude Control:

Orbiter pointing and attitude control are performed by the Reaction Subsystem (RCS) using either primary or vernier thrusters. Basic RCS data and the arrangement of thrusters and tanks are given in Figure 11.

The Orbiter contains a structural reference, referred to as Navigation Base. For Orbiter pointing, this Navigation Base is related to an inertial reference which is derived in the Inertial Measurement Unit (IMU). The IMU contains gyros whose accuracy can be up-dated by star trackers. The Navigation Base and the IMU with its star trackers are located in the forward end of the Orbiter. The Orbiter Guidance, Navigation and Control System has the capability of pointing any vector defined in the Orbiter Navigation Base Axis System at any desired inertial, earth fixed or orbiting target or in the direction of the local vertical. In order to describe the pointing performance the terms "accuracy" and "stability" are used. These terms are defined in Figure 12. Pointing accuracy for inertial or earth referenced directions is within a $\pm$ 0.5 degree (3-sigma) half cone angle. The pointing error for continuous pointing will increase with time due to drift of the IMU. Also, the duration of continuous pointing is limited by the thermal constraints. The pointing accuracy specified above when utilizing the Orbiter IMU for Spacelab payload pointing does not include orientation alignment uncertainty between the Orbiter Navigation Base and, for example, a Spacelab payload. This alignment uncertainty can be greater than 2 degrees. In order to minimize the effect of this uncertainty the Orbiter Guidance, Navigation and Control System is capable of accepting compatible attitude information from a Spacelab payload supplied and Spacelab mounted sensor of comparable accuracy to the Orbiter IMU. The Orbiter Guidance, Navigation and Control computer will receive and process the attitude error signals from such a sensor. In order to meet the pointing accuracy this sensor information must be updated to the Orbiter Guidance, Navigation and Control computer at rates compatible with sample rates of the general

purpose computer and consistent with the chosen method for determining angular rates and accelerations during payload pointing. The combined effect of quantization and noise on sensor readout must be no greater than 30 arc seconds (1 sigma) per axis. Details of the interfaces between the Spacelab payload supplied sensor and the Orbiter are TBD. Utilizing this information, the Orbiter Guidance, Navigation and Control System is capable of pointing a vector defined in the sensor-fixed reference axis system at any direction defined above to within the same pointing accuracy. The rate of change of this pointing accuracy will now also depend upon the drift characteristics of the Spacelab payload sensor.

The Orbiter Guidance, Navigation and Control computer will be able to provide the following initialization or ephermeris data, also to Spacelab and its payload:

a) position and velocity of Orbiter

b) attitude orientation angles and attitude rate

c) time

The specific frame, data format etc. is TBD.

Pointing Stability:

For Spacelab payload pointing utilizing the Vernier Thruster, the Orbiter Flight Control System provides a stability of $\pm$ 0.1 deg/axis. This figure is in essence identical to the dead band of the Flight Control System. The maximum stability rate is $\pm$ 0.01 deg/sec/axis for the limit cycle of the control system when no Vernier Thrusters have failed. When using the primary thrusters, the Orbiter Flight Control System is capable of providing a stability of $\pm$ 0.1 deg/axis and a stability rate

of ± 0.1 deg/sec/axis. For pointing and/or stability requirements beyond the capability of the Orbiter, the Orbiter is capable of accepting compatible commands from a Spacelab payload supplied and Spacelab mounted stabilization and control system.

Pointing Accuracy:

The Orbiter capability to point a vector defined in the navigation base axes utilizing the Orbiter IMU for attitude information is summarized in Table 3 and described below:

IMU Inertial Attitude Hold: The error in pointing the Orbiter into an inertial direction utilizing the Orbiter IMU includes

- errors due to the deadband (± 0.1 deg/axis) of the Flight Control System
- errors due to the IMU alignment uncertainty of ± 0.133 deg/axis (3 sigma)
- read-out errors of the IMU (± 0.073 deg/axis, 3 sigma)
- drift rate of IMU (± 0.105 deg/hour/axis, 3 sigma)

Based upon these values, a vector defined in the Orbiter navigation base axes may be maintained to an inertial pointing accuracy of ± 0.5 deg for durations up to 1.0 hour, subsequent to which IMU realignment is required. Active IMU realignment can require interruption of attitude hold for durations up to 15 minutes and the Orbiter may require maneuvering to acquire the necessary stars. It is possible to realign the IMU during the sunlit part of the orbit, but this is a function of the stars available to the Orbiter star tracker(s) to acquire. Pointing duration can be extended beyond one hour by IMU inflight calibration

(i.e. IMU realignment without interruption of attitude hold provided the necessary stars are within the field of view of the Orbiter star trackers).

For the second case shown in Table 3 (augmented inertial) the Orbiter star trackers are continuously tracking a suitable star pair which permits frequent updates of the IMU reference. For this case the attitude error due to drift is essentially eliminated; thus, the vector defined in the navigation base axes may be maintained to within $\pm$ 0.44° of the desired direction for an indefinitely long period of time (determined by other factors such as propellant consumption, thermal conditioning and heat rejection requirements, etc.).

Passive Attitude Control:

The Orbiter can also operate in either a free drift or (possibly, depending upon the magnitude and direction of disturbances resulting from crew motion and venting) a passive gravity gradient stabilized mode to satsify acceleration levels below 10^{-4} g. A passively stable gravity gradient drift mode ($\pm$Xo-axis along local vertical) would only experience thermal constraints on attitude hold duration for angles between orbital plane and Earth-Sunline equal to or greater than 60 degrees. Star trackers of the Orbiter can passively keep the IMU platform aligned to within 1 degree as long as the field of view of the star trackers is kept on or above the local horizontal and suitable star pairs are available. A gravity gradient attitude of a Xo-upward along the local vertical and $\pm$ Zo perpendicular to the orbital plane would, therefore, have either no or occasional thermal constraints, and be compatible with the star tracker field of view constraint for passive

platform alignment.

Translational accelerations due to the atmospheric drag acting on the Orbiter while in a free drift mode are given in Figure 13. Drift mode translational acceleration level time histories could, however, also be expected to be affected by other mission dependent variables which include venting forces, disturbances from crew movement, orbit altitude, Orbiter orientation, and attitude control changes due to communication requirements. Experiment timeline and crew timeline constraints also need to be known before total meaningful attitude hold duration capabilities and requirements can be specified.

During normal Orbiter attitude-control activities, thrusting of the Orbiter RCS will cause slight acceleration to be exerted on Spacelab equipment depending on its location with respect to the center of rotation. Values are given in Table 4 for the RCS thrusters. The values shown are based on an Orbiter prior to the deorbit burn with a 14515 kg (32 K lb) cargo.

All three angular accelerations may occur simultaneously and the linear acceleration at any point of Spacelab may be calculated based on the distance from the Orbiter's center of gravity. This location will vary to some extent with the particular payload weight distribution.

Crew Tasks and Crew Size:

The Orbiter crew consists of the commander and pilot who are always required to operate and manage the Orbiter. Additional crewmen who may be required to conduct Orbiter/Spacelab payload operations are a mission specialist and one or more payload specialists.

The crew size will be a function of the mission complexity and duration, but the maximum crew is seven persons: commander, pilot, mission specialist and 4 payload specialists.

For Spacelab flights for a continuous 24 hour operation a total crew of 4 is required: commander and pilot to monitor and control Orbiter and Spacelab subsystems in alternating shifts, mission specialist and a payload specialist to serve as Spacelab crew for experiment operation in alternating shifts.

It is foreseen that for each crew-member a sleep cycle of 8 hours is followed by an awake cycle of 16 hours. 8½ to 10½ hours of productive work can be expected within 16 hours awake time. Crew cycles may be arranged such that an overlap for all crew-menbers of approximately 8 hours will be achieved. This will give convenient time each day for the total crew for briefings, flight plan updates, checklist reviews etc.

Crew Compartment and Accommodation:

The Orbiter crew compartment is a two-level cabin consisting of the flight deck and the mid-deck as shown in Figure 14.

The forward area of the flight deck is dedicated primarily to Orbiter operations during ascent and descent. It is equipped with displays, controls and two seats for the commander and pilot. These seats are not removable.

The aft area of the flight deck (aft flight deck) contains two seats for a mission specialist and a payload specialist during ascent and re-entry. These seats are removed for on-orbit operations. Controls and displays for orbiter systems operations, Spacelab subsystem oper-

ation are located on the aft flight deck.

The layout of the aft flight deck is shown in Figure 15: Three work stations, namely the "mission station", the "on-orbit station" and the "payload station" can be distinguished. Furthermore, attention is drawn to the panel R7 which is the only panel which can be accessed by the mission specialist during ascent and descent. Figure 15 indicates the panels which are available for Spacelab and payload. The physical accommodation for Spacelab and its payload is summarized in Table 5. The entire R11 and L10 panels and the Spacelab dedicated parts of the panels A6 and A7, together with volumes associated with all these panel areas are allocated to Spacelab payloads. However, if the instrument pointing system (IPS) is flown, a small IPS panel will be located either in the A6 or A7 panel.

As indicated in Figure 15 the consoles in the mission and payload station are removable from the Orbiter in order to permit equipment integration off-line from the turn-around cycle of the Orbiter. It is envisaged that the Spacelab subsystem hardware in the aft flight deck is independent of the Spacelab configuration to be flown.

In the present operational concept for Spacelab it is foreseen that the Spacelab subsystems can be operated from the mission station

using the Orbiter display and keyboard located in the panel R11 and from the Spacelab integrated control panels located in panel R7. This panel contains also provisions for switches and indicators for payload safing function required during ascent and descent. The payload station and part of the on-orbit station are dedicated to experiment operation.

The power for Spacelab and its payload at the aft flight deck is 350 W continuous and 420 W peak during ascent/descent and 750 W continuous and 1000 W peak for on-orbit operation. The available heat rejection is compatible with the quoted power figure.

The Orbiter provides, at no weight penalty to the Spacelab payload, 28 mandays of expendables for normal operations plus 16 mandays of expendables for rescue operations for four men and for a duration of 4 days. In addition, volume can be provided for expendables for up to 42 mandays whose weight and volume above the outlined provisions will be charged to the Spacelab payload. (Figure 18 gives a survey of the items and services charged to the Spacelab payload.)

The crew compartment is connected with the Spacelab module through a tunnel. For this purpose a tunnel adapter must be attached to the rear end of the mid-deck. A hatch separates the crew compartment from the tunnel adapter, tunnel and module. On top of the tunnel adapter the "EVA airlock" is attached permitting to perform Extra Vehicular Activities (EVA) without interrupting the connection between the crew compartment and the module. For pallet-only missions the tunnel and tunnel adapter are not required. For these missions the EVA airlock can be attached to the opening at the rear end of the mid-deck at

Xo = 576" (14.630 m) and be placed either inside or outside of the mid-deck.

Electrical Power and Energy:

Hydrogen/oxygen fuel cells provide the DC electrical energy for the Orbiter and Spacelab. The required fuel is stored in tank sets, referred to as energy kits, each energy kit providing approximately 840 kWh in the Orbiter baseline configuration. The Orbiter baseline provides only 50 kWh of electrical energy for Spacelab use; the weight of one additional energy kit is included in the Spacelab weight so that 890 kWh are available to Spacelab and its payload. Volume for three additional energy kits will be provided outside the dynamic envelope of the Orbiter cargo bay. Further energy kits may be added, but they must be located within the dynamic envelope and, therefore, result also in a volume penalty for the Spacelab payload. The dry and wet weight of additional energy kits will be charged to the landing and launch weight of the Spacelab payload, respectively. The weight of the fuel and the energy kits has to be accounted for in mission planning and in the assessment of the center of gravity.

Although additional energy kits may be used to increase the electrical energy available to the Spacelab payload, it is pointed out that the use of electrical power must be consistent with the available head rejection capability.

Active Thermal Control Subsystem (ATCS):

The heat generated by Spacelab and its payload is dissipated in Spacelab supplied coolant loops, transferred to the coolant loops of ATCS via a heat exchanger and finally transferred to space via radiators

on the doors of the Orbiter cargo bay. The heat rejection can be supplemented by the operation of a flash evaporator when the Orbiter attitude is thermally unfavorable. Vaporized water produced by the hydrogen/oxygen fuel cell is expelled overboard through the flash evaporator. Heat generated in the Orbiter is rejected by this process. The ATCS will provide a nominal on-orbit heat rejection of 8.5 kW for Spacelab and its payload with the doors of the Orbiter cargo bay open. This level of heat rejection capability is the maximum the Orbiter can supply. It is achieved by supplementing the basic Orbiter ATCS (6.3 kW capability) with a heat rejection kit which is included in the basic Spacelab weight, i.e. the increased heat rejection capability is not weight chargeable to the Spacelab payload.

EVA And Rescue Accommodation:

The Orbiter provides the capability for Extra-Vehicular Activity (EVA) and rescue. The equipment and expendables required to support three, two-man EVA operations is supplied by the Orbiter. Two of these three operations may be utilized by Spacelab or payloads for either planned or unscheduled EVA operations, the third operation is for rescue. There is no weight credit to Spacelab or payloads if no EVA is planned for a flight. Additional EVA operations in support of Spacelab and/or its payload may be provided with the expendables being provided as items which will be charged to the weight of the Spacelab payload.

EVA operations will utilize a self-contained life support system capable of supporting a six-hour EVA. At lease three (3) hours of oxygen prebreathing is required; post EVA operations take approximately 1.5 hours. Mose of the first two hours of the three-hour prebreathing

scheduled to begin 3.5 hours before the start of an EVA, can be used to accomplish useful, non-EVA related, activities by the EVA crewmen. The remaining 1.5 hours are used for EVA preparation.

Avionics:

The Orbiter avionics provides for:

a) Receiving, transmission and distribution of voice

b) Transmission of operational telemetry

c) Receiving and transmission of Spacelab data (including payload data)

d) Transmission of commands from the ground or Orbiter to Spacelab CDMS subsystem

e) Furnishing Guidance, Navigation and Control data to Spacelab or its payload

f) Transmission and distribution of television signals

g) Tracking of active and passive targets

h) Transmission and reception of EVA data and voice

i) Recording (MSS-PCM recorder)

The Orbiter avionics also provide the interface between the Oribiter and:

a) Tracking and Data Relay Satellite (TDRS) operating in KU-band and S-band

b) Space Tracking and Data Network (STDN) during ascent and descent.

c) Spacelab

d) EVA crewmen

e) Other space vehicles

f) Landing site facilities of the Orbiter

Remote Manipulator System:

The Remote Manipulator System and its installations in the Orbiter are shown in Figures 16 and 17. The Orbiter provides one manipulator 50 ft (15.240 m) in length on the left side of the Orbiter. In orbit the manipulator is capable of removing and installing a 15 ft (4.572 m) diameter, 60 ft (18.288 m) long, 65.000 lb (29.510 kg) pbject. The Remote Manipulator System in its stored position does not infringe on the dynamic envelope to Spacelab and its payload.

The manipulator provides a light for illumination and a TV camera for remote viewing.

If not required for a particular mission the Remote Manipulator System may be removed to provide additional payload weight capability, provided compensations are made for the effect on the Orbiter center of gravity.

A second manipulator arm can be installed if required.

The capability is provided to operate two Remote Manipulator Systems in a series, not simultaneously. However, it is possible to hold or lock one manipulator arm while operating the other one.

SPACELAB SYSTEM CAPABILITIES:

The Spacelab system provides versatile services to payloads as depicted in Figure 18. The overall system capabilities and resources will be described below. A description of the design aspects of the various subsystems of interest to the user is also provided.

Flight Configurations:

The modular elements of Spacelab introduced earlier can be arranged in various flight configurations to suit the needs of specific mission/payload requirements and to meet Orbiter constraints.

Eight basic flight configurations are presented in detail with respect to their physical accommodation capabilities. While other configurations are basically possible, only these eight configurations are under configuration control with respect to the mechanical interfaces to the Orbiter. In addition, of these eight basic configurations, four are formal baseline design configurations and as such are under formal configuration control within the Spacelab project. The formal baseline design configurations are

- o Short module/9 m pallet (3 pallet segments)
- o Long Module
- o 15 m pallet (5 pallet segments)
- o 9 m pallet (3 independently suspended pallet segments)

The hardware of the Spacelab project, however, allows all eight basic and other possible flight configurations to be implemented by combination/deletion/addition of appropriate hardware elements.

Long Module Configuration (Baseline Design Configuration):

The long module configuration is shown in Figure 19. It consists of the core and experiment segment and provides the largest pressurized volume for Spacelab payloads. It is accessible from the Orbiter cabin through the transfer tunnel. Utility services are routed from the Orbiter to the forward end cone feedthrough provisions and from there into the module interior. Basic Spacelab dimensions are shown (in mm),

as well as the Orbiter stations of the module attach fittings. Orbiter stations Xo 660" have to be kept clear of Spacelab and Spacelab payload equipment, since this volume is reserved for the EVA airlock and tunnel adapter.

Long Module plus 3 m Pallet Configuration:

Figure 20 depicts the long module/3 m pallet configuration. This configuration provides both pressurized volume for payloads and pallet mounting area for experiments requiring exposure to space environment. Utility services to the pallet are routed from module aft end cone feed-through plates to the pallet.

Long Module plus 6 m Pallet Configuration:

This configuration (Figure 21) increases the pallet mounting area by connecting two pallet segments to form a pallet train. Utility routing is the same as for the long module plus 3 m-pallet-configuration.

Short Module plus 6 m Pallet Configuration:

A short module may be used in place of the long module to provide the configuration shown in Figure 22 .

Short Module plus 9 m Pallet Configuration (Baseline Design Configuration):

This configuration offers the largest area which may be used in a module/pallet configuration, as shown in Figure 23. The three pallet segments are rigidly attached to form a single pallet train.

9-Meter-Pallet-Configuration (Baseline Design Configuration):

As shown in Figure 24, this configuration consists of three independently suspended pallet segments. The pallet segments are placed

along the length of the cargo bay. Utility routing between pallet segments is not described in this paper. The "Igloo" at the forward pallet provides a controlled pressurized environment for a set of Spacelab subsystem equipment similar to that located in the core segment of the module. Utility services are routed directly from the Orbiter to the Igloo/first pallet segment.

For the accommodation of experiment structures, it must be ensured that such structures do not act as a rigid connection between the pallet segments.

12-Meter-Pallet-Configuration:

A potentially well suited configuration for a number of astronomy missions is depicted in Figure 25, consisting of two independently suspended pallet trains composed of two pallet segments each. For the accommodation of payload structures, it must be ensured that such structures do not act as a rigid connection between the two pallet trains.

15-Meter-Pallet-Configuration (Baseline Design Configuration):

This configuration provides the longest possible experiment platform for Spacelab payloads requiring exposure to the space environment. The configuration shown in figure 26 consists of two independently suspended pallet trains separated by a dynamic clearance gap. One pallet train consists of three and the other consists of two structurally connected pallet segments.

For the accommodation of payload structures, it must be ensured that such structures do not act as a rigid connection between the two pallet trains.

MODUIAR ELEMENTS OF SPACEIAB - OVERALL CONFIGURATION:

The pressurized module consists of a combination of either one or two 4-m-diameter cylindrical segments of 2.7 m length. The module end closures are conical sections of equal angle. The forward end cone is truncated at the diameter required to interface with the crew transfer tunnel which connects to the Orbiter. The aft end cone is truncated to provide an opening closed by a cover plate.

One segment, the Core Segment, and the forward and aft end cones compose the Short Module. Two segments, Core Segment and Experiment Segment, together with the end cones compose the Long Module. The module exterior is covered with high-performance insulation. EVA mobility aids are also located at the exterior.

Each segment is equipped with a flange ring of 1.3 m internal diameter on the top to provide accommodation for the following Common Payload Support Equipment (CPSE):

- top airlock (experiment segment only)

or

- optical window/viewport assembly

When not used for any of the above items, the CPSE opening is closed with a coverplate.

Planned and/or contingency access constraints during ground operations (late access in vertical position) do not allow the use of the top airlock in the CPSE opening of the core segment.

Accommodation Capability:

All module flight configurations contain the same basic internal arrangement of subsystem equipment, the main difference being the volume available for experiment installation.

Subsystem equipment is primarily located forward in the core segment. It is installed in the first double rack on each side and on the subfloor extending the whole length of the core segment.

Experiment equipment can be accommodated in the remaining 60% of the core segment and in the experiment segment as shown in Figure 27.

The main floor is designed to carry the racks with their equipment and consists of segments. Racks and floor are interconnected at the integration site. The floor segments allow adaptability of the secondary structure to both module sizes. The main floor itself consists of a load-carrying beam structure and is covered by panels on the main walking surface providing also for noise attenuation from the subfloor area. The floor also contains openings equipped with debris traps to allow cabin air return flow. Except for the center floor panels, all panels are hinged to allow underfloor access in orbit and on the ground, as can be seen in Figure 29. Major features shown are the floor with the equipment rack assemblies pre-integrated. If experiment racks are replaced by stand-alone ezperiment equipment, the same attachment points as those for racks have to be used.

The racks are standard 19 inch racks to accommodate standard as well as non-standard laboratory equipment. The total number of experiment racks is two double and two single racks in the core segment and

four double and two single racks in the experiment segment.

Payload equipment (with or without racks) will normally be integrated with the main floor structure when this is removed from the module. The complete floor/payload assembly, the "experiment train", will then be integrated in the module.

There is only a single interface plane between the subsystem equipment remaining inside the module and the experiment train for electrical and avionics cooling loop connections after roll-in and before roll-out of the experiment train.

Figure 28 shows a frontal view of the module. The left and right hand sections through the module are shown in Figures 29 and 30, illustrating the subsystem arrangement, the airlock and the rack numbering scheme. The control center and the work bench rack contain subsystem equipment only. The experiment racks are shown with the location of the experiment power switching panels and intercom remote stations. Subsystem equipment in the underfloor space of the core segment is mounted on a 2.7 m subfloor attached to the primary module structure.

While an underfloor space for experiment is available in the experiment segment, only attachment points in the primary structure are provided but no subfloor.

Overhead stowage containers marked with asterisk might not be installed during launch/descent because of late access through the core segment CPSE opening (detailed late access provisions are currently under investigation).

Standard Experiment Racks:

The nominal envelope for experiment and the subsystem equipment mounted in the standard experiment racks is shown in Figure 31. Minor protrusions of experiment equipment beyond the nominal allowable depth may be possible, if compatible with the experiment rear cabling, the spacing of the cabling support struts, and the ECS ducts.

Experiments which require no standard ECS air cooling ducts, no standard ECS fire suppression system nor rear struts for cabling attachments, may utilize the entire internal depth allowed by the basic rack structure.

The height available for experiment (and Spacelab mission dependent) equipment is also shown.

Projections of experiments in front of the front panel mounting plane is normally limited to knobs, switches and similar small protrusions. Larger protrusions in front of the racks may be allowed, subject to case-to-case restrictions due to:

- possible interference and operational constraints with the MGSE rack-floor support braces kit.
- possible interference and operational constraints with the MGSE late access kit.
- possible interference with the floor hinged panels
- crew habitability considerations.
- excessive aisle obstruction due to similtaneous presence of center aisle equipment.

The following maximum equipment masses, including Spacelab mission

dependent equipment and experiment cabling, may be accommodated in the experiment racks:

- single rack 290 kg
- double rack (overall) 580 kg
- either side of a double rack (left or right) 290 kg
- double rack (center frame removed) 480 kg

Pallet Segment:

The pallet cross-section is U-shaped providing hard points for mounting heavy experiments and a large panel surface area to accommodate lighter payload elements. Pallet segments are of 3 m length and 4 m width and can be flown independently or interconnected. As many as three pallets can be interconnected to form one pallet train supported by one set of attach fittings; whereas pallet-configurations may consist of one to five pallet segments.

Figure 32 shows a basic pallet segment with hardpoints and typical sandwich skin panels with inserts (not shown here). Each segment consists of the basic structure and subsystem equipment which includes:
Mission Independent Equipment:

- subsystem and experiment electrical power busses
- subsystem and experiment data busses
- a subsystem equipment package consisting of:
  - 1 experiment power distribution box
  - 1 subsystem RAU (Remote Acquisition Units)
  - 1 subsystem interconnection station
  - 2 experiment interconnection station

Mission Dependent Equipment:

- up to 4 experiment RAU's
- cold plates and thermal capacitors
- plumbing
- thermal insulation blankets

It is currently foreseen to mount the mission independent subsystem equipment package on experiment cold plates located on each pallet segment. It has to be pointed out, however, that it might not be required to always fly a complete basic subsystem package on each pallet segment, depending on specific experiment requirements.

Igloo/Pallet Front Frame:

In pallet-only configurations, subsystem equipment necessary for the operation of Spacelab is located in the "Igloo" which is mounted to the front frame of the first pallet segment. The Igloo, as shown in Figure 33 is a pressurized cylinder equipped with a removable bulkhead providing full access to the interior. The weight of an equipped Igloo is about 640 kg, the usable volume is 2.2 m^3. Thermal control of subsystem equipment is achieved by cold plates which are connected to the pallet freon cooling loop.

A set of Spacelab subsystem equipment, similar to a set which in module only and module/pallet configuration is integrated within the module, is installed within the Igloo in the pallet-only mode. Operator interface equipment, such as CRT's, keyboards, TV monitor and Spacelab control panels are located in the Orbiter aft flight deck.

The following is the list of the equipment (basic and mission dependent) which is located in the Igloo:

- 3 computers (subsystem, experiment and back-up computer)
- 2 I/O units (subsystem and experiment I/O)
- 1 mass memory
- 2 subsystem RAU's
- 1 subsystem interconnecting station
- 1 emergency box
- 1 power control box
- 1 subsystem power distribution box
- 1 remote amplifier and advisory box (RAAB)
- 1 high rate multiplexer (HRM)

In addition to the Igloo the following major subsystem equipment is also mounted to the front frame of the first pallet segment.

- 1 subsystem 400 Hz inverter (only in pallet-only configurations)
- 1 experiment 400 Hz inverter (only in pallet-only configurations)
- freon cooling loop components

Thermal control of the 400 Hz inverters is also achieved by cold plates connected to the pallet freon cooling loop.

Transfer Tunnel:

The transfer tunnel (NASA furnished) will enable crew and equipment transfer between the Spacelab module and the Orbiter in a shirtsleeve environment. It is capable of functioning under orbital as well as ground operation conditions. It will have a minimum of about 1 m clear diameter, sufficient for handling a box of 0.56 x 0.56 x 1.27 m size

and moving of a 1.95 m tall crew member with a maximum elbow width of 0.75 m. The same internal atmosphere as in the Spacelab module is provided. Lighting is installed in the tunnel, as well as mobility aids for internal movements.

Figure 34 shows in a simplified form the mode of interfaces with the Orbiter and the Spacelab module. The tunnel adapter/airlock combination is provided by the Orbiter.

The tunnel consists of a S-shaped tunnel segment, a number of cylinder segments to accommodate different flight configuration locations and flexible elements for dynamic decoupling and tolerance compensation.

The baseline tunnel hardware will allow to assemble the five basic module-only/module-pallet configurations.

COMMAND AND DATA MANAGEMENT SUBSYSTEM:

The Command and Data Management Subsystem (CDMS) provides a variety of services to Spacelab experiments and subsystems.

These services include:

- data acquisition
- data processing
- data formatting
- data transmission
- recording
- large volume bulk-storage
- monitoring
- display

- command and control capability for experiments
- command and control capability for subsystems
- audio intercommunication
- caution and warning
- provisions for closed circuit television

The equipment provided by the CDMS to Spacelab experiments is listed in Table 6.

Figure 35 presents a functional block diagram of the CDMS.

Experiment outputs delivering housekeeping and low speed scientific data that need further on-board processing, are sampled by Remote Acquisition Units (RAU's) and transferred to the experiment computer via interconnecting Stations (IS), the experiment data bus, and the Input/Output (I/O) unit.

On the same path, serial PCM and On/Off commands are transferred from the experiment computer, via the RAU's to the experiments.

The RAU User Time Clock delivers precision reference timing information.

Typical functions for on-board processing of scientific data by the experiment computer are quick look analysis, data compression, etc. Programs for control and processing of experiments and subsystems exceeding the capability of subsystem and/or experiment computer can be loaded at execution time from the Mass Memory Unit (MMU).

A backup computer, which is primarily intended as backup for the subsystem computer, is also available to experiments in case of experi-

ment computer failure. The backup computer is normally filled with subsystem programs. Before operating as experiment computer the core memory has to be loaded with the appropriate experiment software from the MMU.

The subsystem and experiment branches of the CDMS are identical and are composed of the same components, (computer, I/O unit, data bus, and RAU modules) except the user time clock capability which is unique for experiments. However, it should be noted that there is no direct link between the subsystem and experiment branch.

Experiment and subsystem monitoring and control is in principle automatically performed by CDMS equipment. These functions are initiated automatically through pre-programmed computer sequences stored in the MMU, or semi-automatically by inter-action of the keyboard/DDU with the computer, or by telecommands through the Orbiter uplink (2kb/s).

Data, processed by the experiment or subsystem computer can be displayed on Data Display Units (DDU's) having vactor display capability.

Low bit rate scientific and housekeeping data processed by the experiment computer can be transmitted by the Orbiter downlink via the Tracking and Data Relay Satellite System (TDRSS).

Medium and high rate scientific data are acquired by the High Rate Data Acquisition part of the CDMS. This part consists of the High Rate Multiplexer (HRM), the High Rate Digital Recorder (HRDR), the Orbiter Payload Recorder and the Voice Digitizer. This system is able to multiplex up to 16 experiment input channels for direct downlink via the Tracking and Data Relay Satellite System or for recording during non-transmission times of the Orbiter KU-Band System (HRDR or the Orbiter

Payload Recorder). The recorded data may be interleaved with real time experiment data for transmission to ground.

The Voice Digitizer will convert analog Spacelab audio signals into a HRM compatible digital form to allow voice tagging of data multiplexed by the HRM.

Spacelab provides the necessary electrical interfaces for experiment provided CCTV equipment to form an extension of the Orbiter CCTV. There is space for a TV monitor in the control center rack and an electrical interface for a video camera with EIA standard signal output characteristics (Monitor and camera have to be experiment provided).

The spacelab provides a 4.2 MHz analog channel for use by the experiment, e.g. to accommodate non-EIA-standard TV signals.

CCT and analog signals are transmitted to the ground through the same analog channel of the KU-Band down link, TDRSS non-coverage times are not bridged by an analog recorder.

Duplex voice links for onboard or Orbiter ground communication are provided by the Intercom System.

Emergency, warning and caution conditions are detected and displayed by the Caution and Warning System (C & W).

Low Rate Data Acquisition and Control:

Low rate data acquisition from experiments and experiment control is performed by the experiment computer through the experiment I/O unit, the experiment data bus and the experiment RAU's. Although the experiments interface only with the RAU's, the following paragraphs describe

the complete data and command transfer in more detail. The purpose of the detailed description is to provide visibility into a system that has to be shared with many users constraining each other.

The low rate data link is designed to achieve a word error rate (WER) $\leq 1.7 \times 10^{-7}$ for the data flow between any RAU digital input and the Orbiter PCM Master Unit.

Remote Acquisition Unit:

The RAU's are the principal interfaces for the bidirectional link between experiments and the CDMS for acquisition of low bit rate digital data, analog data and commands. The data exchange between RAU's and the I/O unit is performed via a simplex serial bus with a 1 Mb/s clock rate. The data are encoded in a self-clocking bi-phase code (Manchester II).

Each experiment RAU incorporates the following user interfaces:

Inputs: 128 flexible differential inputs for analog or discrete signals
4 serial PCM data channels with associated clocks, code NRZ-L

Output: 64 ON/OFF command channels
4 serial PCM command channels with associated clocks, code NRZ-L
1 User Time Clock 1024 kHz
1 User Time Clock Update, 4 pulse cycles/s pseudo-synchronized with on-board GMT

A block diagram of the RAU is given in Figure 36.

The RAU data acquisition is based on a software controlled concept. The software for subsystem data acquisition and control is provided by Spacelab. The software for experiment data acquisition and control has to be provided by the experimenter in accordance with his requirements. Applicable portions of the Spacelab software can be used by the experimenter.

The RAU's will be scanned periodically with periods of 10 ms, 100 ms, or 1 s. Each scan cycle will be initiated and controlled by the General Measurement Loop which is part of the Spacelab computer software. The experimenters may design their own software to generate additional measurement cycles using the operating system task scheduler. This scheduler will accept priority levels and queue to experiment software requests for data and command transmission.

Experiment RAU's can be connected to the experiment data bus at a number of interconnecting stations (IS) in the module and on each pallet. There are 2 interconnecting stations in the core segment, 3 in the experiment segment, and 2 on each pallet segment.

Each station accommodates two RAU's. The Spacelab baseline contains 8 experiment RAU's. The electrical characteristics of the experiment bus allow the accommodation of up to 22 RAU's although the computer allows the address of up to 32 RAU's.

In the Spacelab baseline standard locations for RAU's are provided in the lower part of the experiment rack. However, the concept allows the users to integrate RAU's together with his experiment equipment, if he uses his own racks and/or experiment equipment mounted directly to the center aisle or to the pallet.

In every case the user has to take care that

- the cabling between RAU and Interconnecting Station is below 5 m
- the environmental specifications of the RAU are met.

Computer:

The CDMS has three identical MITRA 125 S general purpose computers with characteristics as shown in Table 7.

These computers have the inherent potential of an interrupt capability. Eight hardware interrupts are wired from the computer to the I/O unit. Only four of these are presently required to support I/O unit activities. At the experiment computer experiments can access to the remaining four interrupts to enhance experiment use of the CDMS. The basic software of CDMS is non-synchronous and can be adapted to handle these interrupts.

The three computers are used as S/S Computer, Experiment Computer and Back-up Computer. S/S and Experiment Computers are connected to the dedicated CDMS equipment each via their own I/O unit, Data Bus and RAU's. There is no direct link between each computer.

The third computer is available as a back-up either for the S/S or the Experiment Computer and can be switched over manually.

Due to the concept of routing all S/S and experiment peripherals through dedicated I/O units, this switching connects the Back-up Computer to the appropriate I/O unit and all peripherals.

Normally the Back-up Computer is loaded with subsystem software (operating system and application software) since a S/S Computer failure

is more critical with respect to the overall performance of Spacelab. However, in case of Experiment Computer failure, the experiment software may be loaded from the Mass Memory Unit (MMU) by an operator command.

In the Module or Module/Pallet configuration, the computers are located in the Work Bench Rack. The location in the Pallet-Only configuration is the Igloo.

The computer facilities allow general purpose processing by user provided software written in HAL/S or another appropriate language for such purposes as:

- Checkout of Experiments
- Sequencing of Experiment Operations
- Monitoring and Control of Experiments
- Processing of DATA Acquired by Experiment RAU's

Examples of Data Processing are:

- Filtering
- Data Reduction
- Histograms
- Averaging
- Interpolation, etc.

The processed data may be delivered back to experiments, displayed on-board or transmitted to ground, depending on the mission requirements.

For experiment sequencing the user may provide several program packages for each experiment stored in the MMU. Depending on actual experiment results or data and information from ground via keyboard

entries or directly via uplink commands, a running sequence of operation steps may be stopped or changed or a new program may be initialized to be executed in the Experiment Computer.

INSTRUMENT POINTING SYSTEMS:

The Instrument Pointing Subsystem (IPS) will be delivered under the same general terms as the Spacelab and will be available for use on the second and subsequent flights.

IPS Description:

The Instrument Pointing Subsystem (IPS) provides precision pointing for payloads which require greater pointing accuracy and stability than is provided by the Orbiter. The IPS can accommodate a wide range of payload instruments of different sizes and weight.

The Gimbal System (shown in Figure 37) is attached to the payload when on-orbit, and performs the control maneuvers required by the observation program. During launch and landing the gimbal system and payloads are separated, whereas the payload is supported by the IPS Payload Clamp Assembly. The gimbal system comprises the following assemblies and subassemblies:

- 3 Bearing/drive units
- Payload/gimbal separation mechanism
- replaceable extension column
- soft mount with soft mount clamp
- emergency jettisoning device
- lower support structure
- thermal control system

The three identical drive units are arranged in such a way that their axes intersect at one point. Each drive assembly employs three wetlubricated ball bearings, two brushless DC-torquers, and two single speed/multi-speed resolvers. The design of the drive assembly includes a main shaft, and auxiliary shaft and a load by-pass mechanism which allows the loads occurring during the ascent and descent to be taken by the assembly housing without the need for additional clamping devices, while at the same time off-loading the ball bearings. All electrical services for IPS and payload functions are carried across each drive unit by a cable follower device consisting of two flexible flatband cable bundles wound in opposite directions.

The soft mount consists of a radially symmetrical arrangement of six spring/damper units which reduce the attitude disturbances caused by Orbiter thruster firings, crew motions, etc. Damping without static friction is achieved by employing two metal bellows, between which a liquid is pushed to and from through an orifice. During ascent and descent the soft mount is clamped, forming a rigid connection between gimbal structure and pallet. A replaceable extension column between the soft mount and the gimbal support structure, can be changed between missions to adjust the gimbal point of rotation for particular payload requirements.

Pointing and Stabilization:

The IPS optical sensor package includes the capability to have two roll sensors LOS at a skewed angle of either 45 degrees or 12 degrees with respect to the LOS of the centrally mounted optical sensor. The LOS's of all three optical sensors are arranged in one plane. Provision

is also made for the mounting of a light baffle system, designed for specific mission conditions, at the aperture of each optical sensor but structurally decoupled from the sensor.

The IPS provides 3-axis attitude control and stabilization for experiments. The characteristics of nominal 2000 kg and 200 kg payload are given in Table 8 and these are used as design reference payloads except when a requirement specifically states otherwise. Error requirements apply during solar and stellar fine pointing of the IPS, with the Orbiter in either an inertially stabilized mode or a free-drift mode with angular rates up to 10 deg/min with respect to inertial space. The values of pointing accuracy and quiescent stability error mean, in each case, that the probability of the error being less than the required values is 67% (see Figure 38). Bias error will include all sources of error with time constant equal to or greater than one orbital period. The pointing and stabilization characteristics are summarized in Table 9 and are presented in more detail in the following paragraphs.

Pointing Accuracy:

The pointing accuracy of the experiment LOS with respect to a reference star or an idealized solar disk is less than 2 arc-sec (design goal 0.8 arc-sec) in the two axes perpendicular to the experiment LOS and less than 40 arc-sec (design goal 15 arc-sec) in roll about the experiment LOS.

Quiescent Stability Error:

The quiescent stability error (achieved when there are no disturbances from the Orbiter) will be less than 1.0 arc-sec (design goal 1.6 arc-sec) in roll about the experiment LOS. These values apply for all angles

within the LOS range and for both the nominal 2000 kg and 200 kg payloads.

Disturbance Response Errors:

The disturbance errors discussed herein are defined as including the quiescent stability error and apply for the nominal 2000 kg payload with the IPS located at the forward end of a five pallet train and pointed to any attitude within the LOS range. Since the disturbance error for a given input disturbance varies significantly with IPS location and pointing direction, the disturbance response error values corresponds to worst case values.

For a nominal 200 kg payload the distrubrnce error is expected to be 2 or 3 times higher. Assuming similar shape and mass distribution, smaller payloads will, in general, experience larger errors than larger payloads. Although smaller payloads will have closer c.g. locations with respects to the gimbal axes, the lower moment of inertia being the dominating parameter, will result in a higher sensitivity to Orbiter disturbances.

Man Motion Disturbance

The disturbance error (peak value) due to a standardized man motion disturbance (corresponding to a typical wall push-off by the crew) is less than 3 arc-sec (design goal is 1 arc-sec) in the two axes perpendicular to the experiment LOS and less than 10 arc-sec (design goal is 4 arc-sec) about the roll axis.

Orbiter Limit Cycle Disturbance:

The limit cycle errors (peak value) arising in each axis due to Shuttle limit cycle motion of $\pm$ 0.1 degree and 30 m sec duration thruster firing are not greater than those caused by man-motion disturbance, for

the same payload and IPS configuration.

Stability Rate:

During fine pointing, peak stability rate is less than 2 arc-min/sec for a nominal 2000 kg payload. This is an instantaneous value occuring during the response of the IPS to a man-motion disturbance; a typical value during undisturbed quiescent pointing is TBD.

Pointing Range:

The IPS has a LOS pointing range of at least steradians without payload.

The range of roll angle about the experiment LOS is at least π radians at any position within the π steradians LOS pointing range. In order to prevent the payload from contacting any surrounding equipment due to error or failure, the IPS contains a redundant system for controlling angular range and rate. This must be adjusted for the configuration of surrounding equipment on each mission, and since a further angular range is required in order to account for dynamic effects, the achievable LOS range and allowable rate are restricted to less than the maximum as shown in Figure 39.

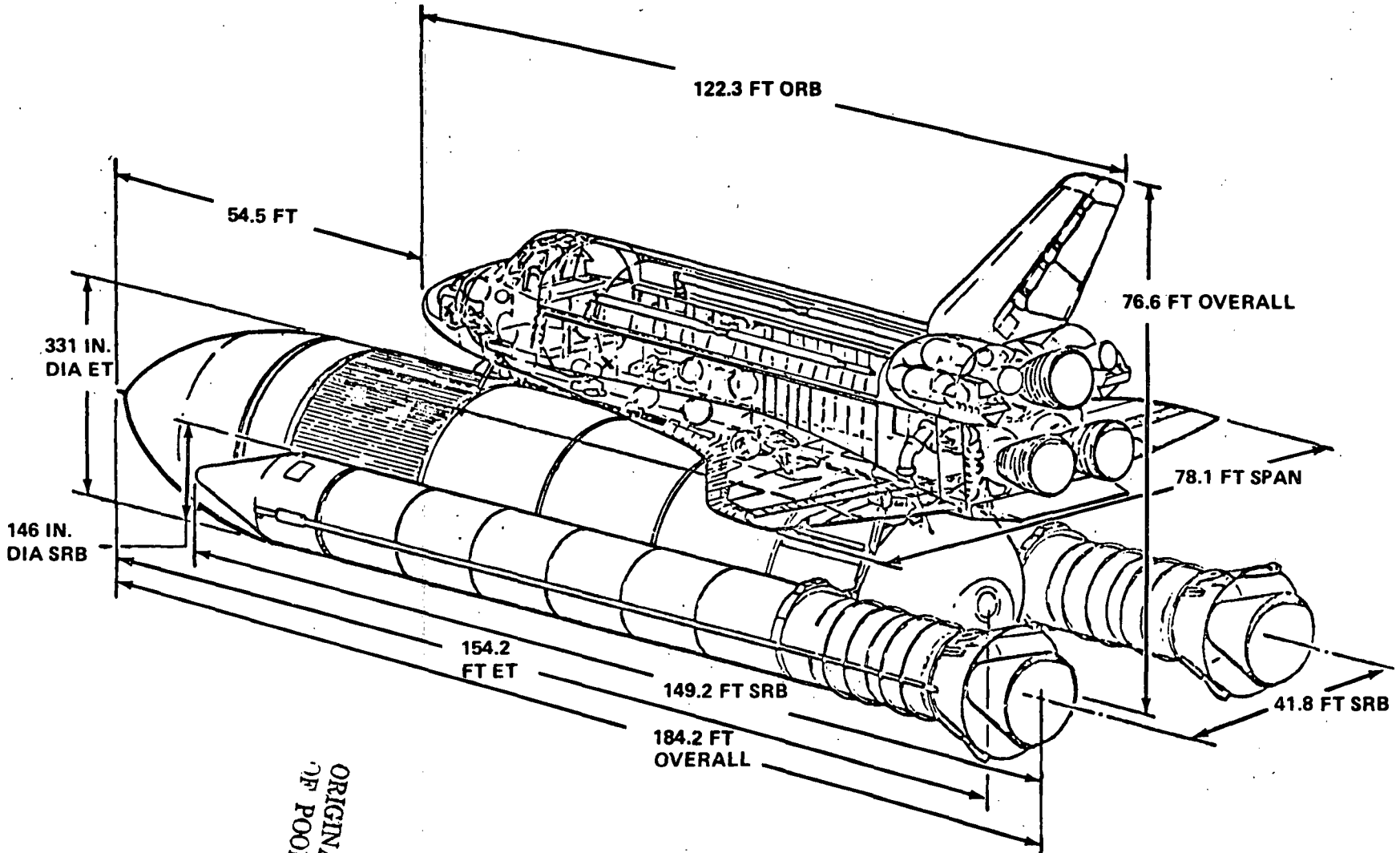

Figure 1. The Space Shuttle vehicle.

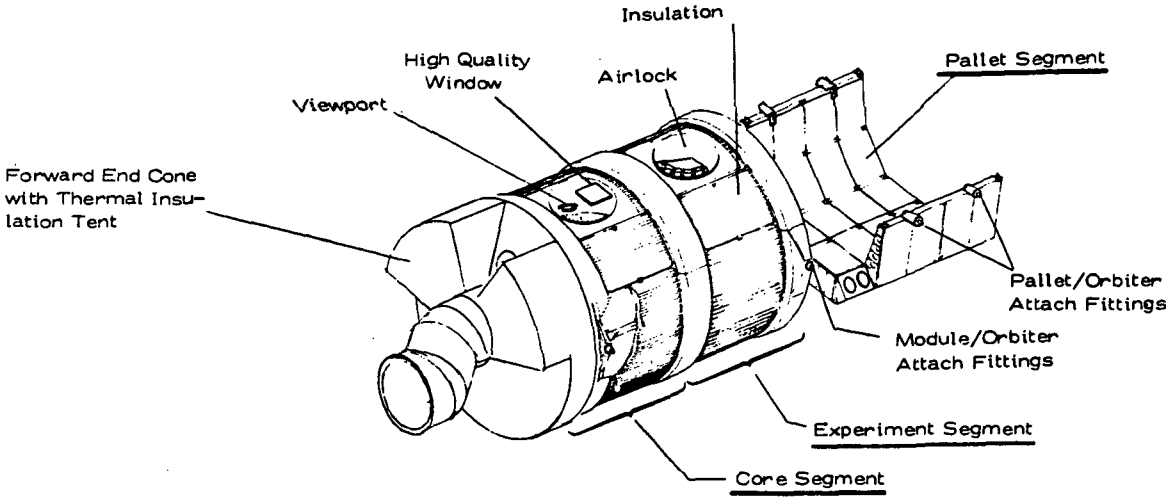

Figure 2. Spacelab external configuration within the Orbiter bay.

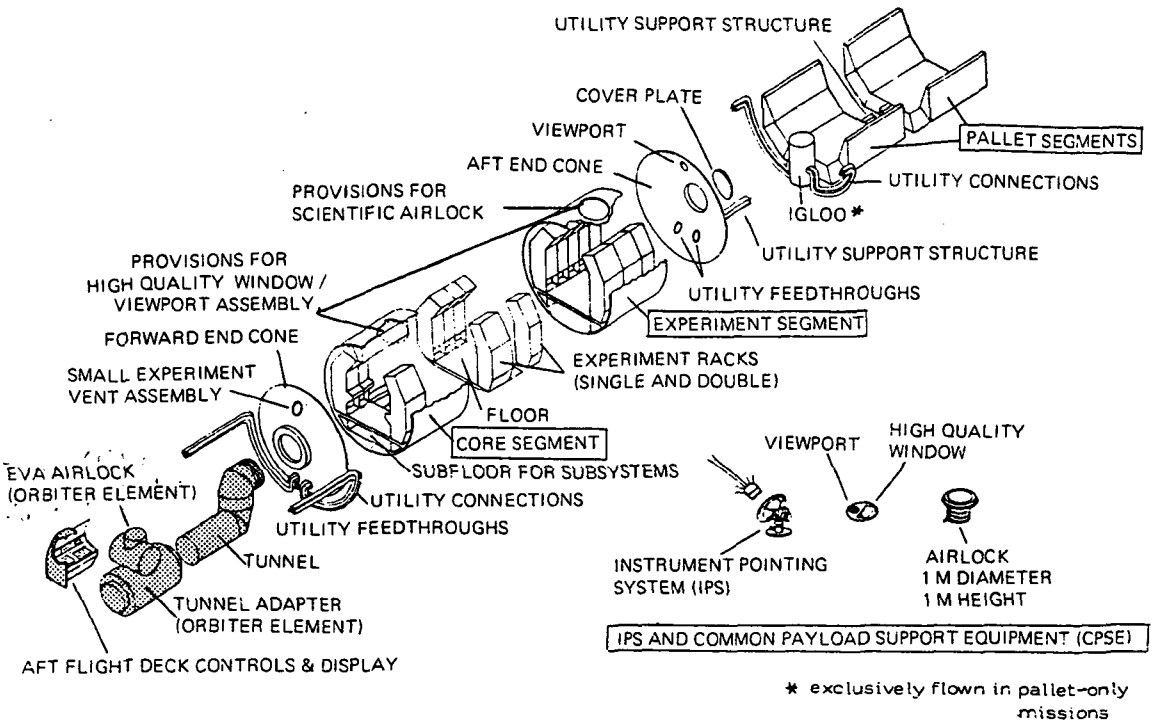

Figure 3. Major Spacelab flight elements.

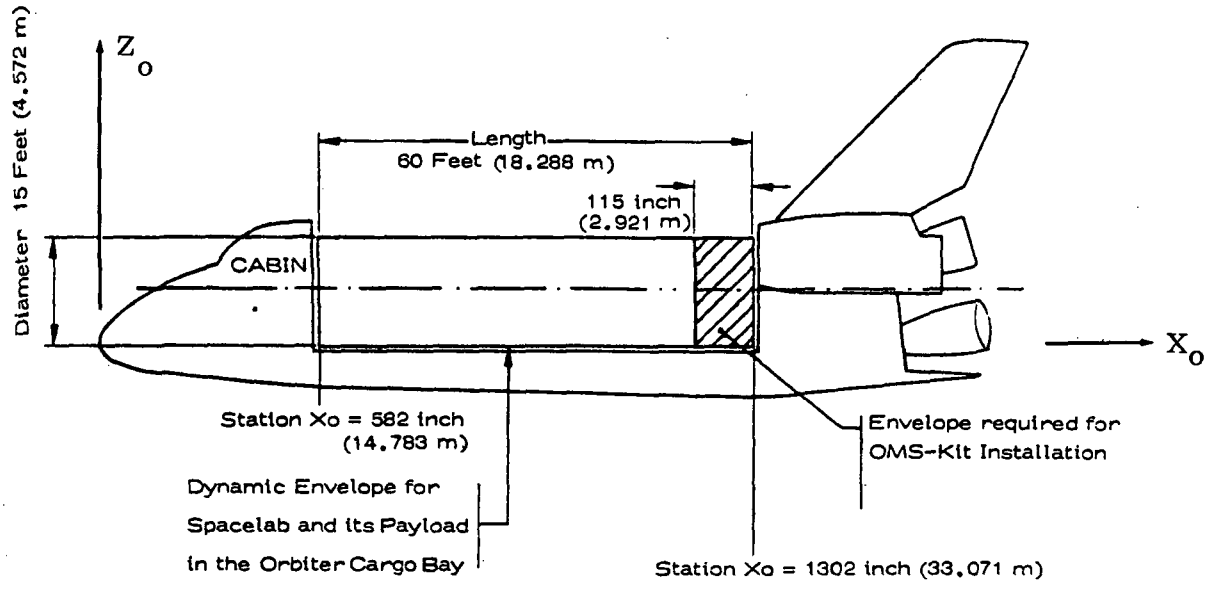

Figure 4. Dynamic envelope for Spacelab and its payload in the Orbiter cargo bay.

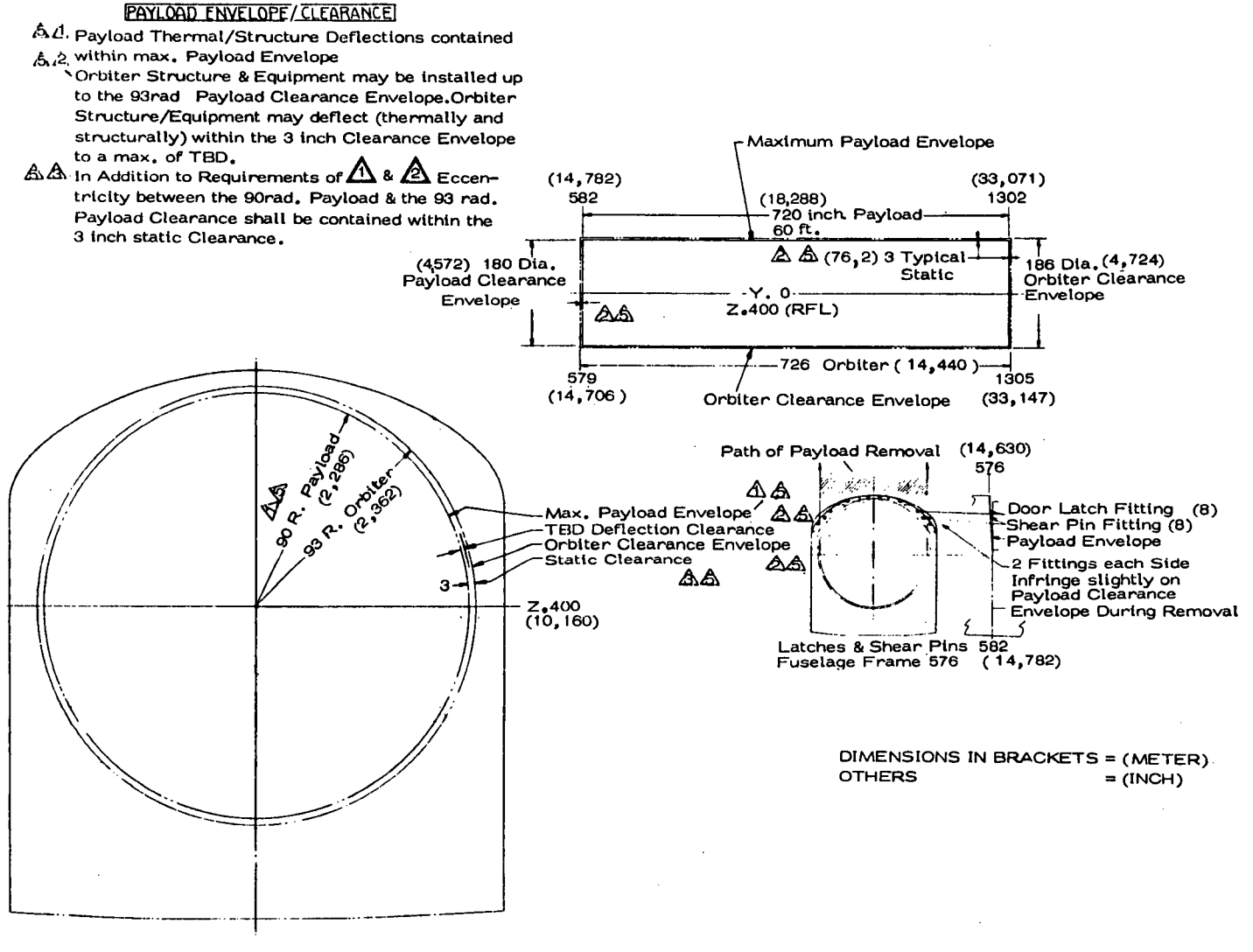

Figure 5. Technical drawings of the dynamic envelope in the Orbiter cargo bay. (Note: The term "payload" used on this page includes Spacelab.)

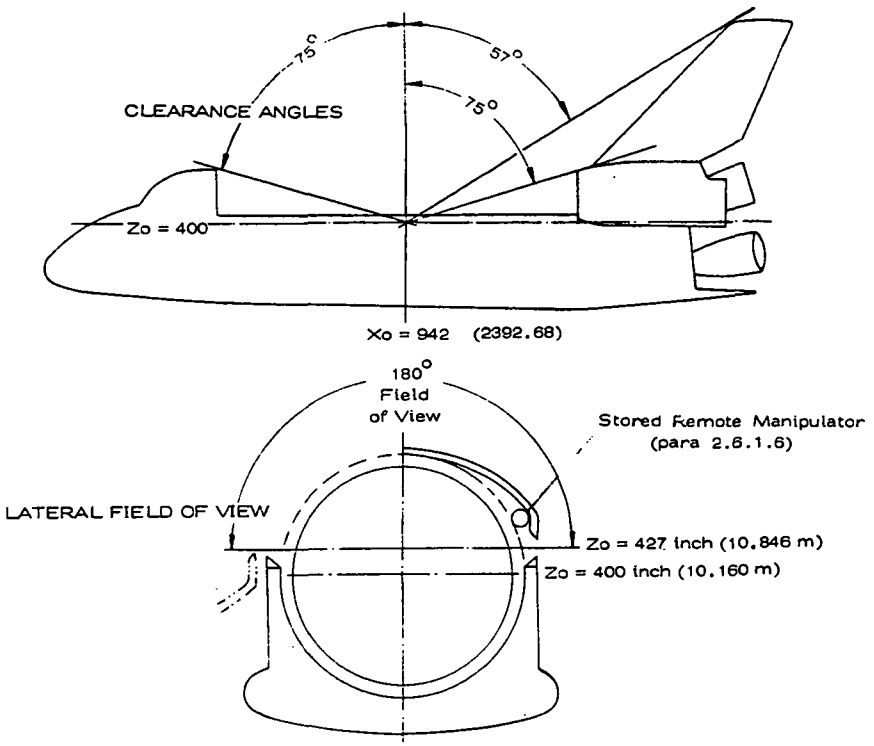

Figure 6. Field of view and clearance angles of Orbiter.

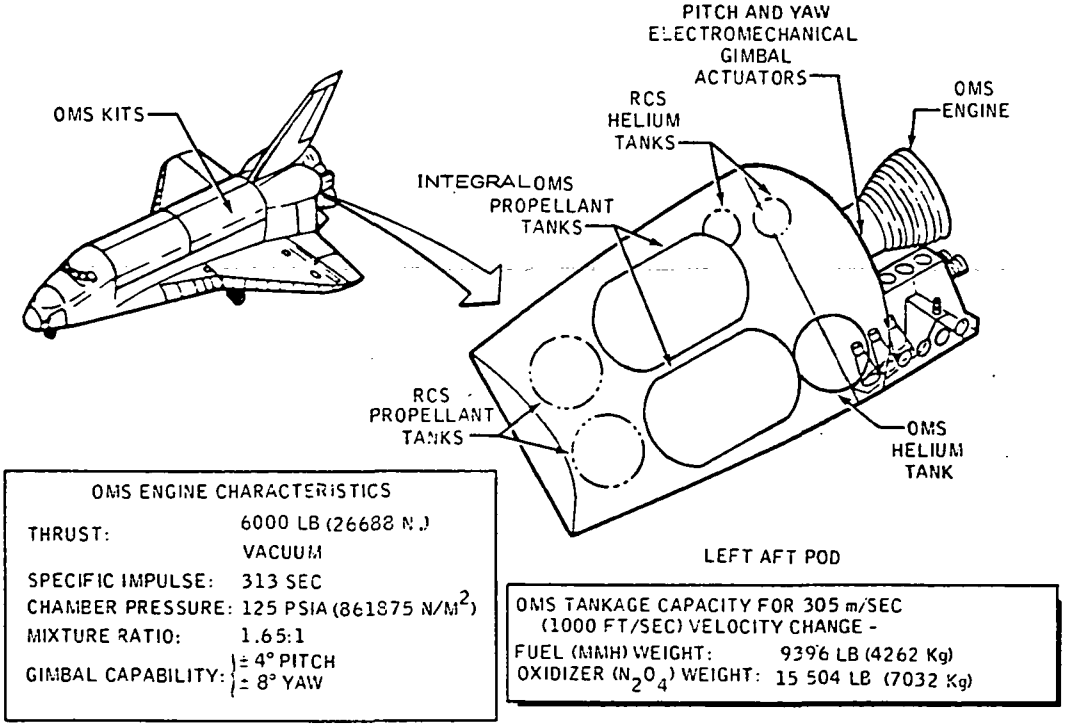

Figure 7. Orbital maneuvering subsystem (tank arrangement and engine characteristics).

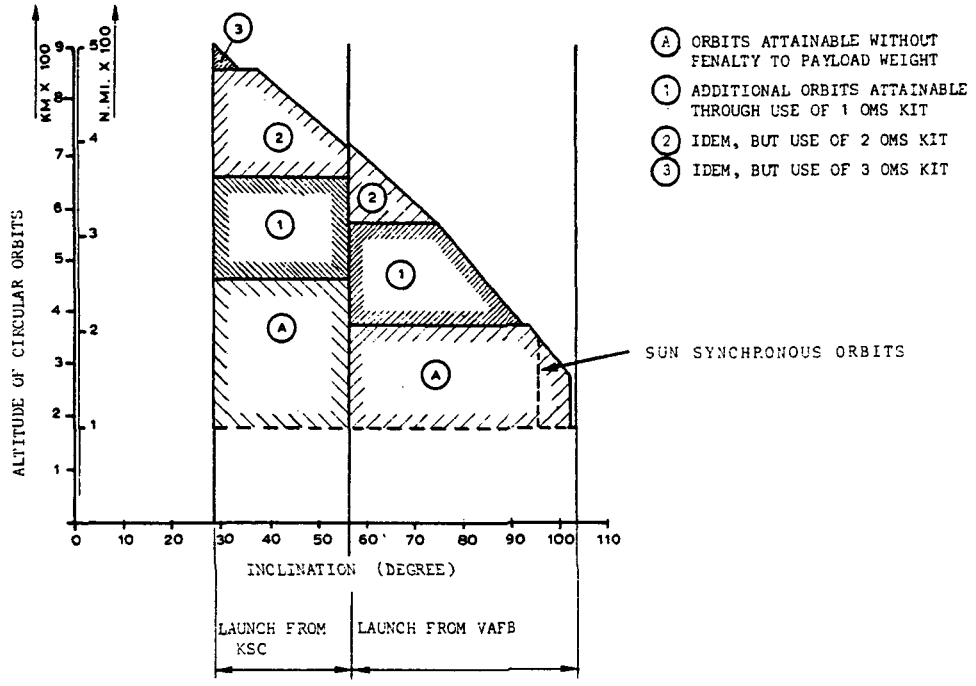

Figure 8. Typical ranges of circular orbits for Spacelab missions (14 515 kg, 32 000 lb).

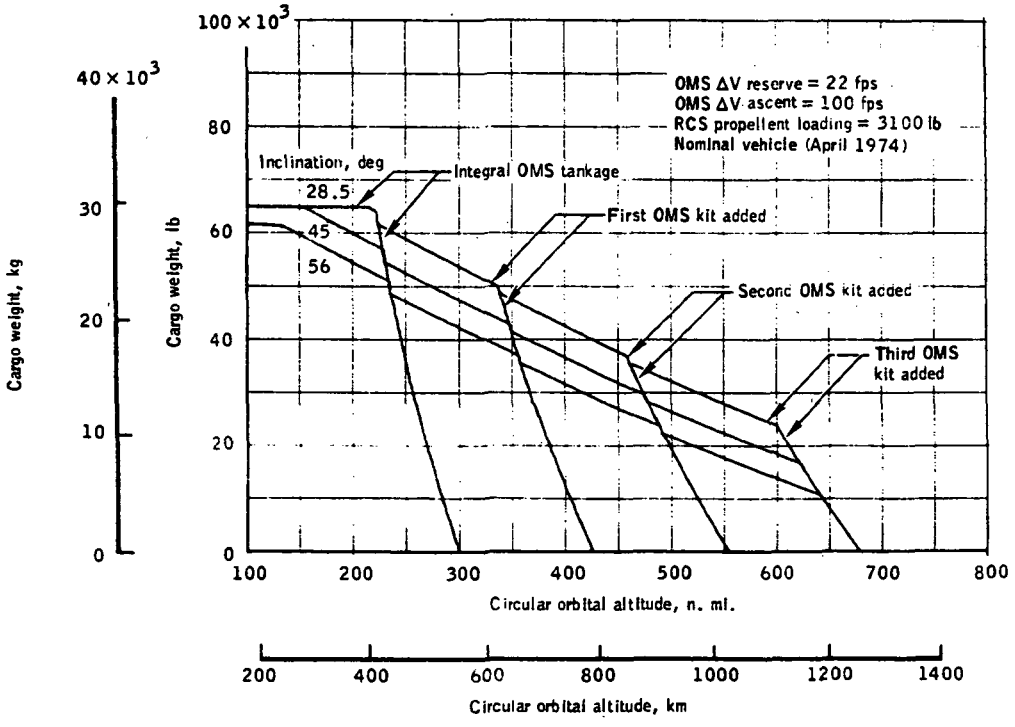

Figure 9. Cargo weight versus circular orbital altitude – KSC launch.

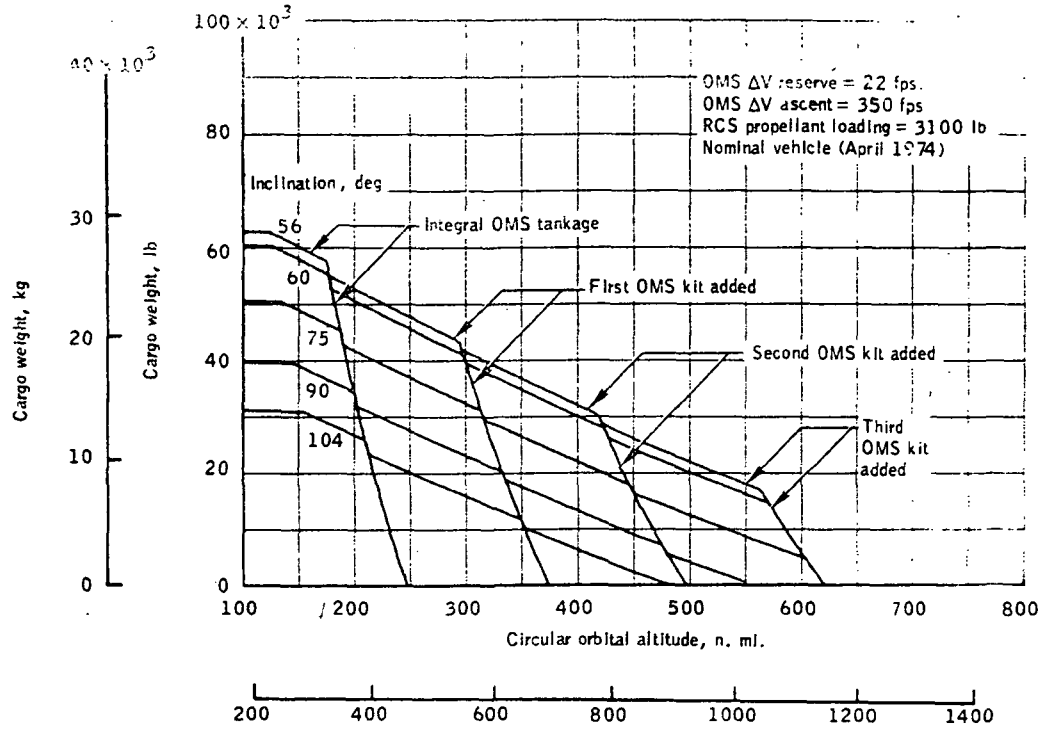

Figure 10. Cargo weight versus circular orbital altitude – VAFB launch.

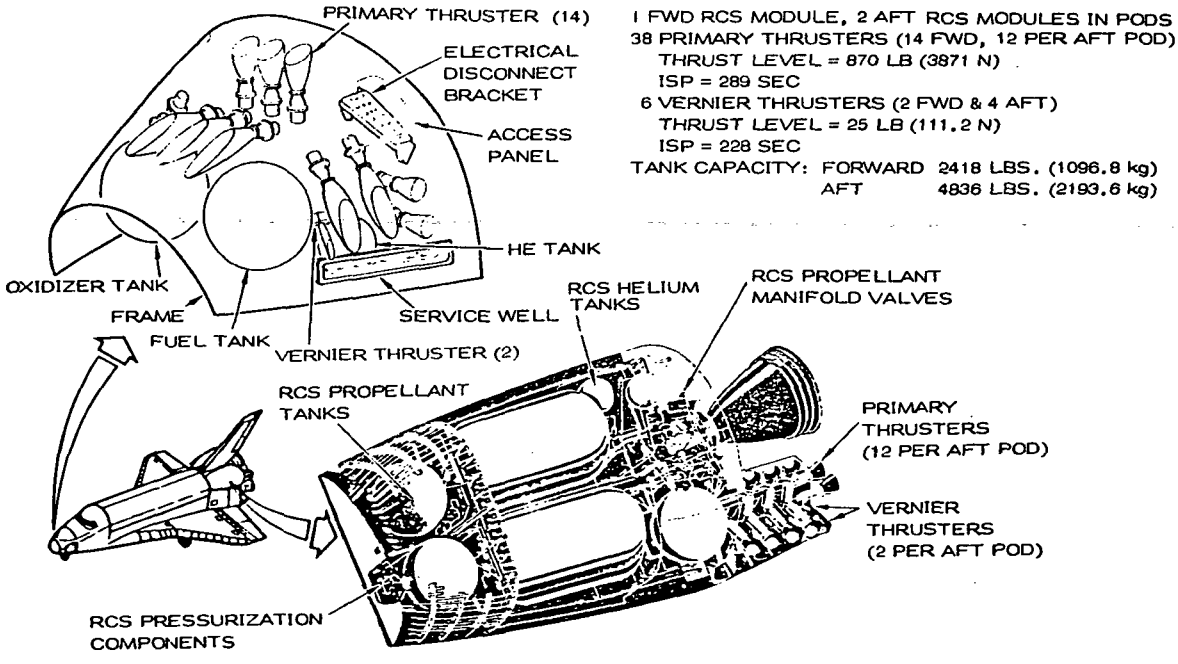

Figure 11. Orbiter reaction control subsystem (RCS) (tank and thruster arrangement).

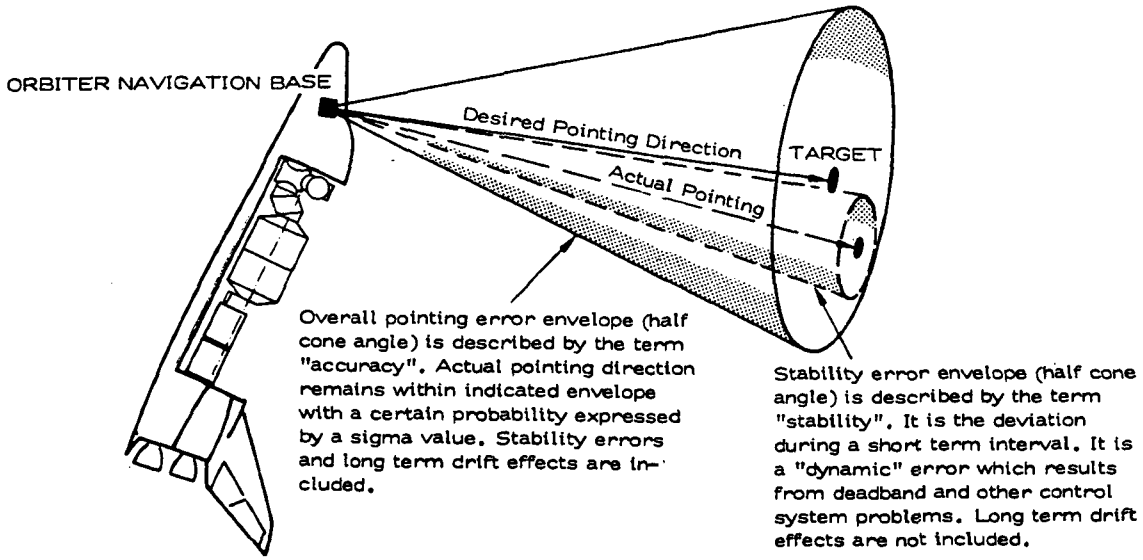

Figure 12. Definition of Orbiter pointing accuracy and stability.

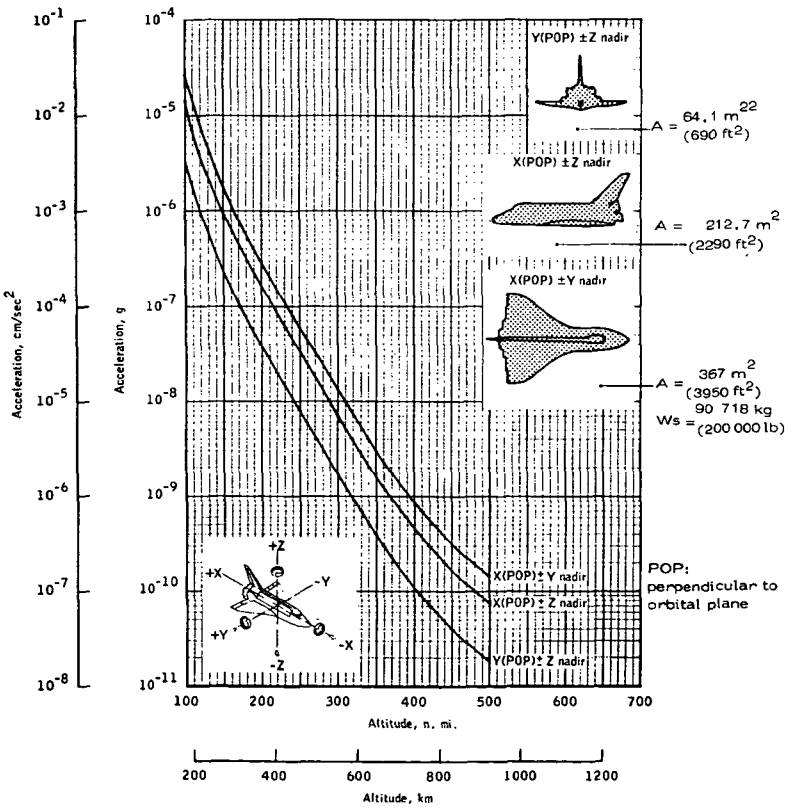

Figure 13. Effects of atmospheric drag on the Orbiter.

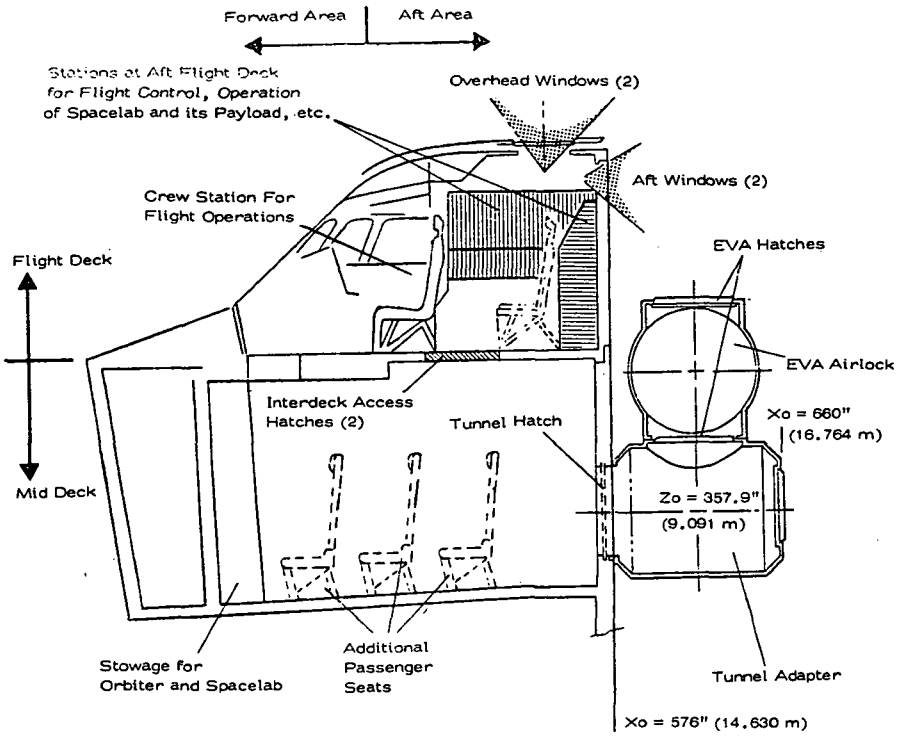

Figure 14. Crew compartment concept.

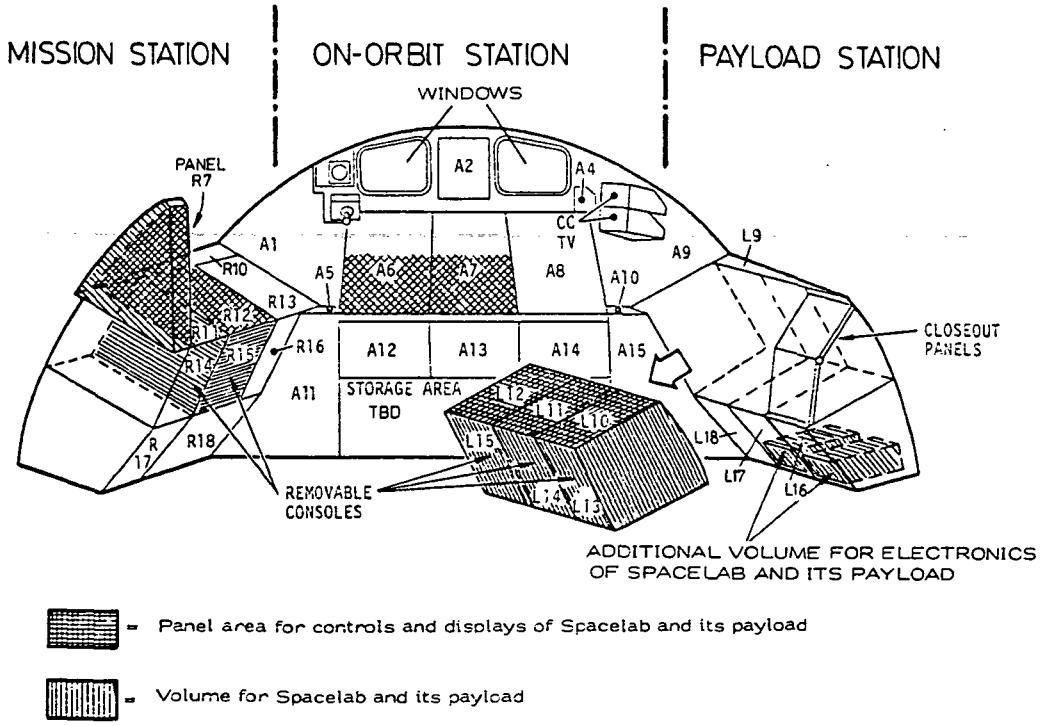

Figure 15. Layout of aft flight deck (view looking aft).

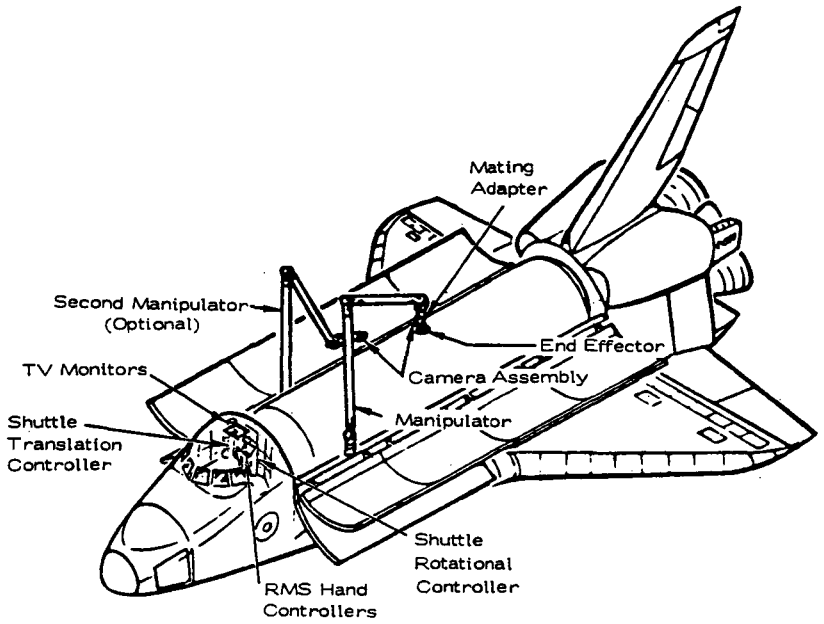

Figure 16. Orbiter remote manipulator system.

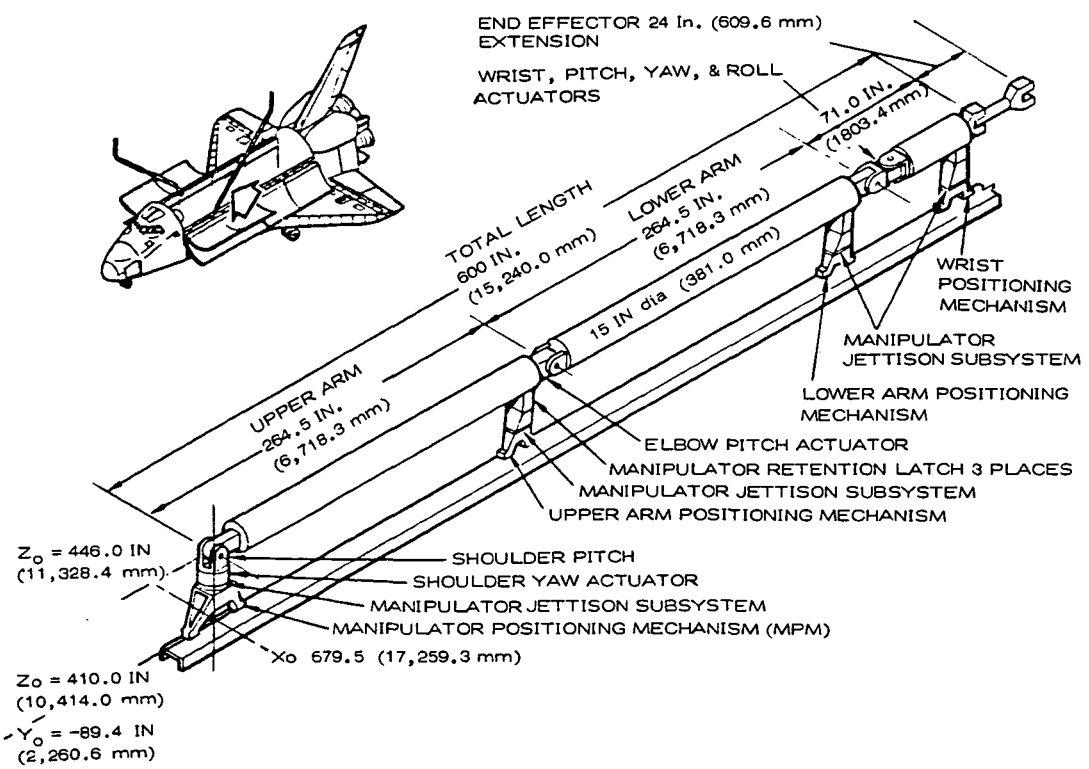

Figure 17. Manipulator arm of the remote manipulator system.

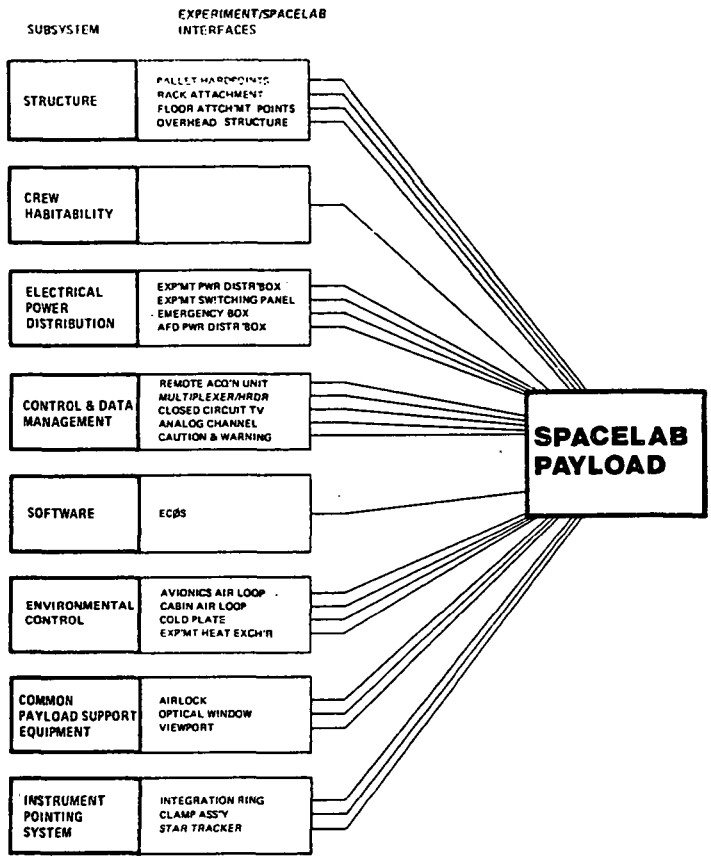

Figure 18. Spacelab services to payloads.

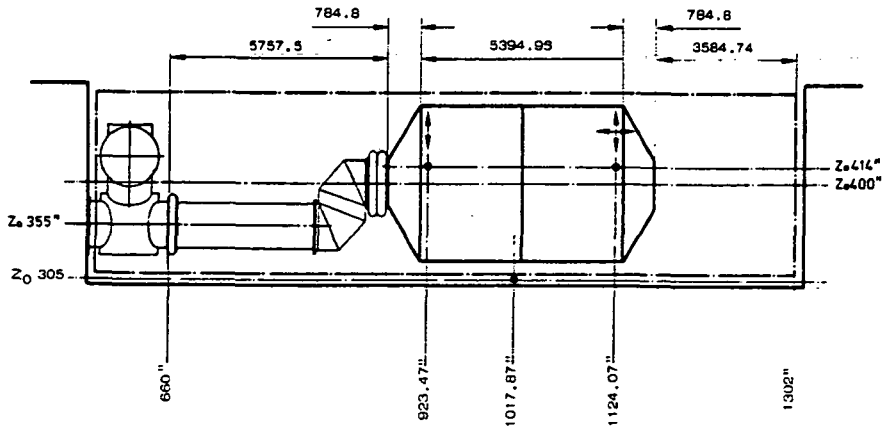

These signs indicate the load carrying direction of the attach fittings

Figure 19. Long module.

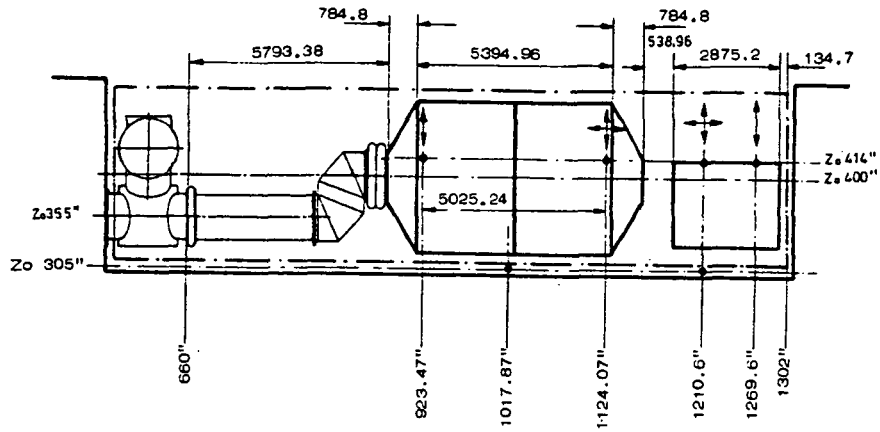

Figure 20. Long module plus 3 m pallet configuration.

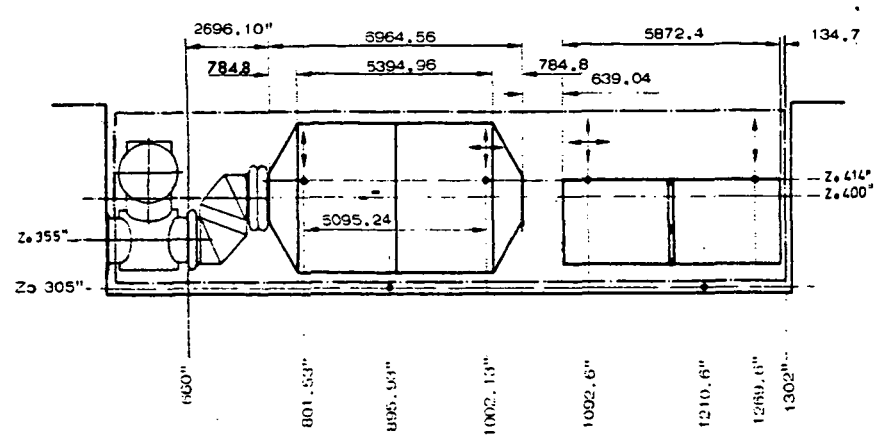

Figure 21. Long module plus 6 m pallet configuration.

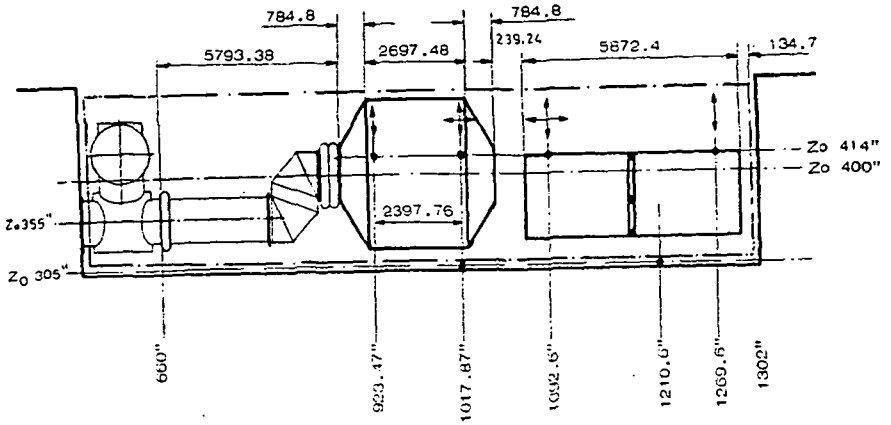

Figure 22. Short module plus 6 m pallet configuration.

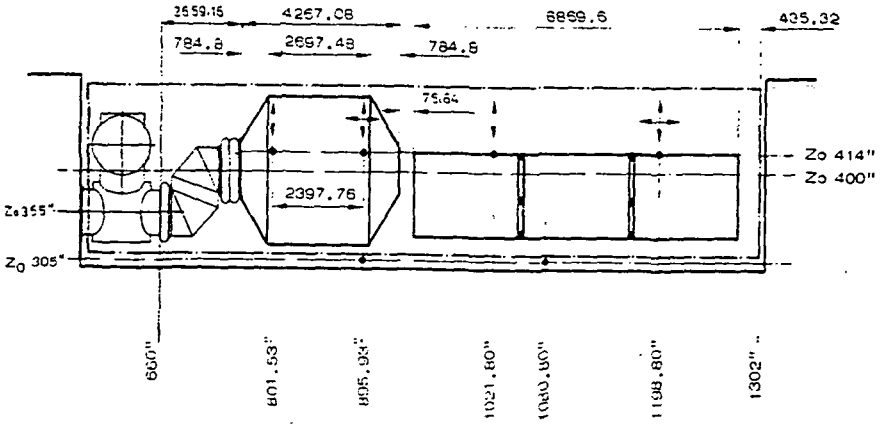

Figure 23. Short module plus 9 m pallet configuration.

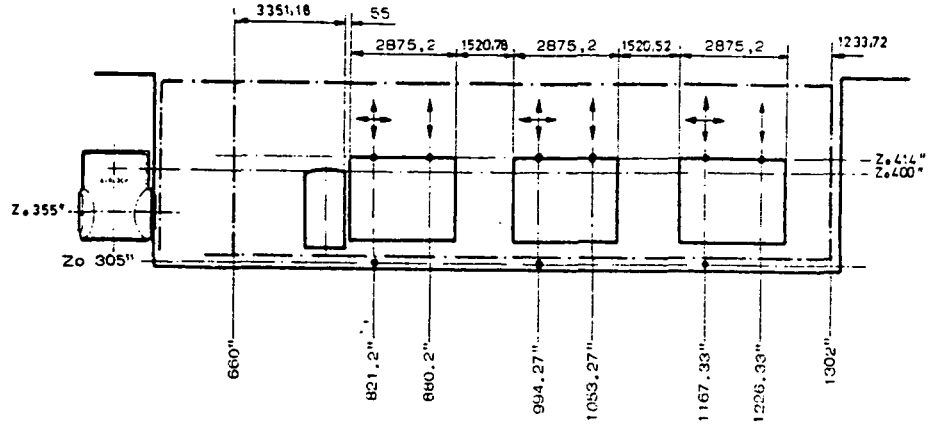

Figure 24. 9 m pallet configuration.

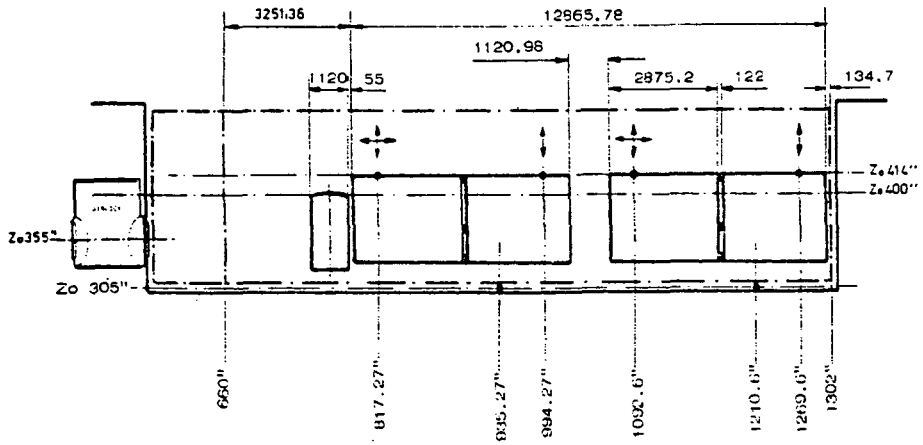

Figure 25. 12 m pallet configuration.

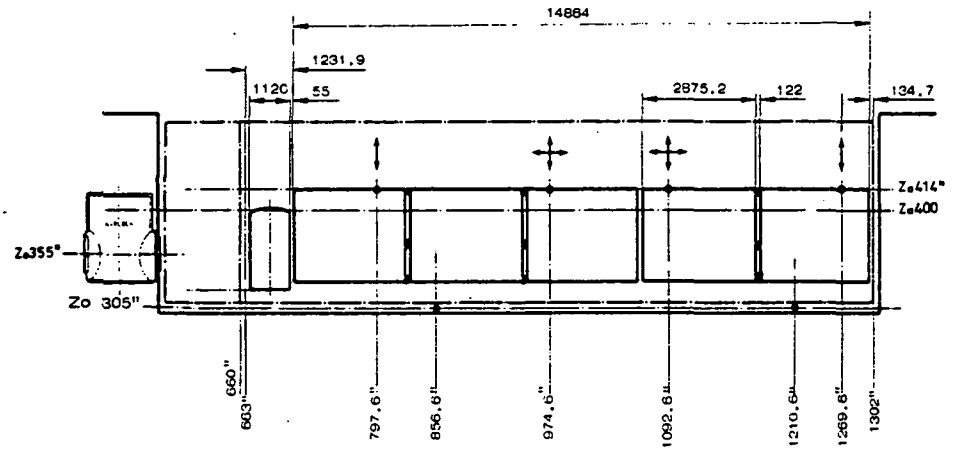

Figure 26. 15 m pallet configuration.

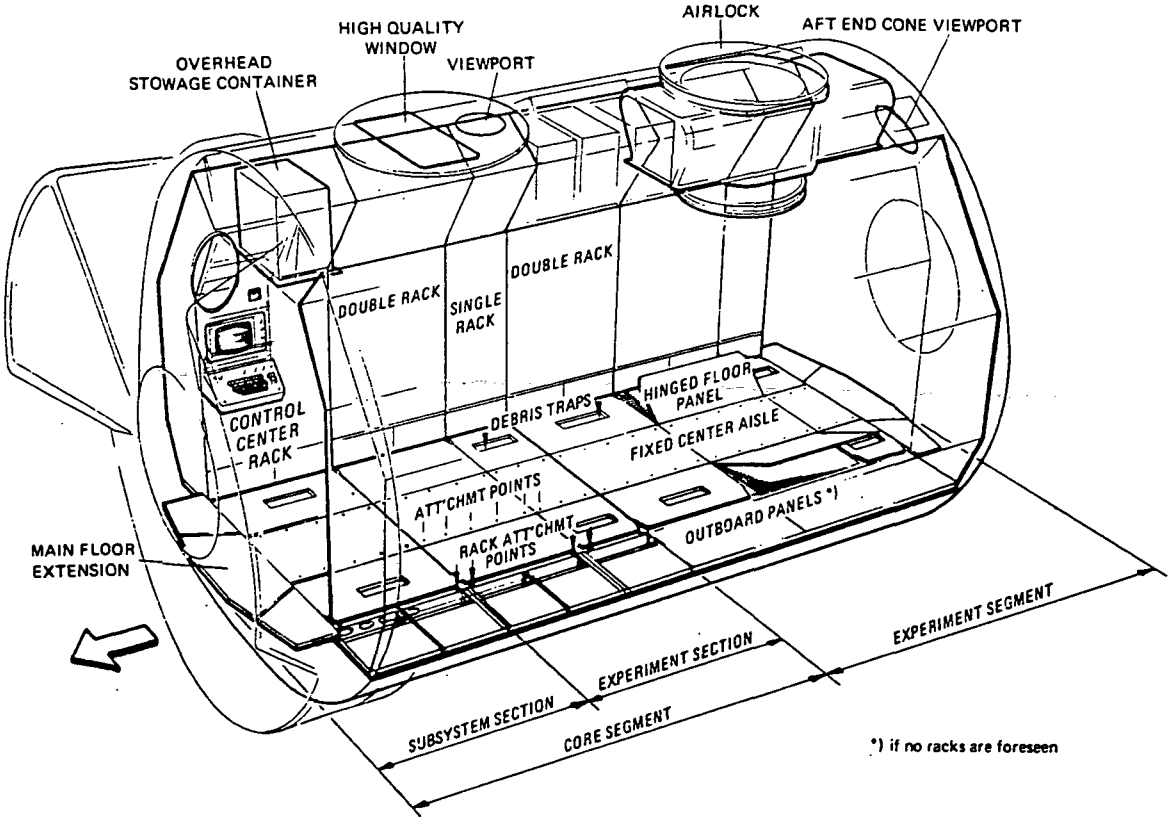

Figure 27. Internal accommodation layout.

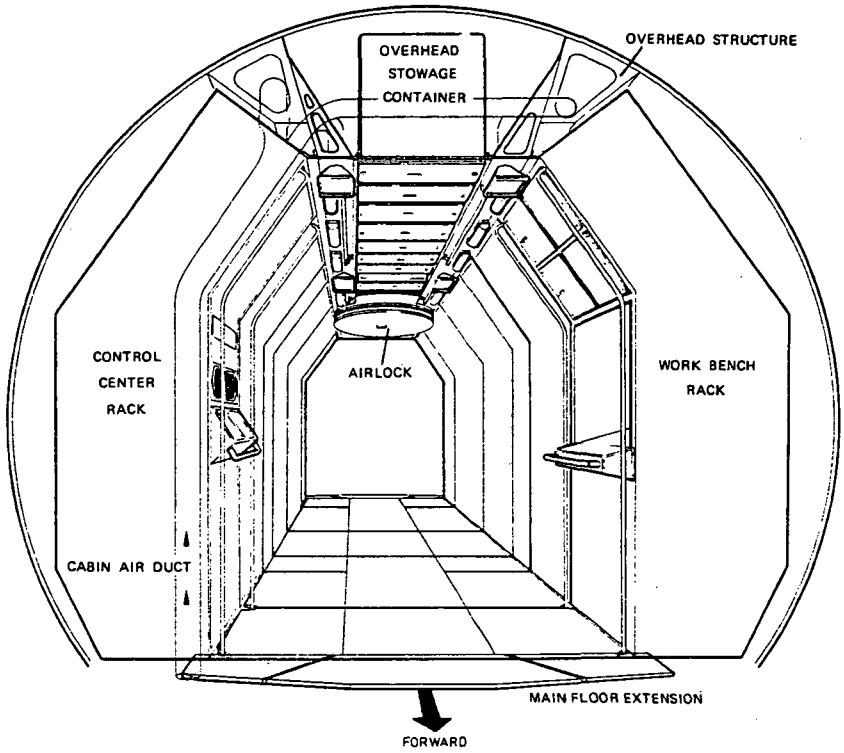

Figure 28. Module frontal view (end cone removed).

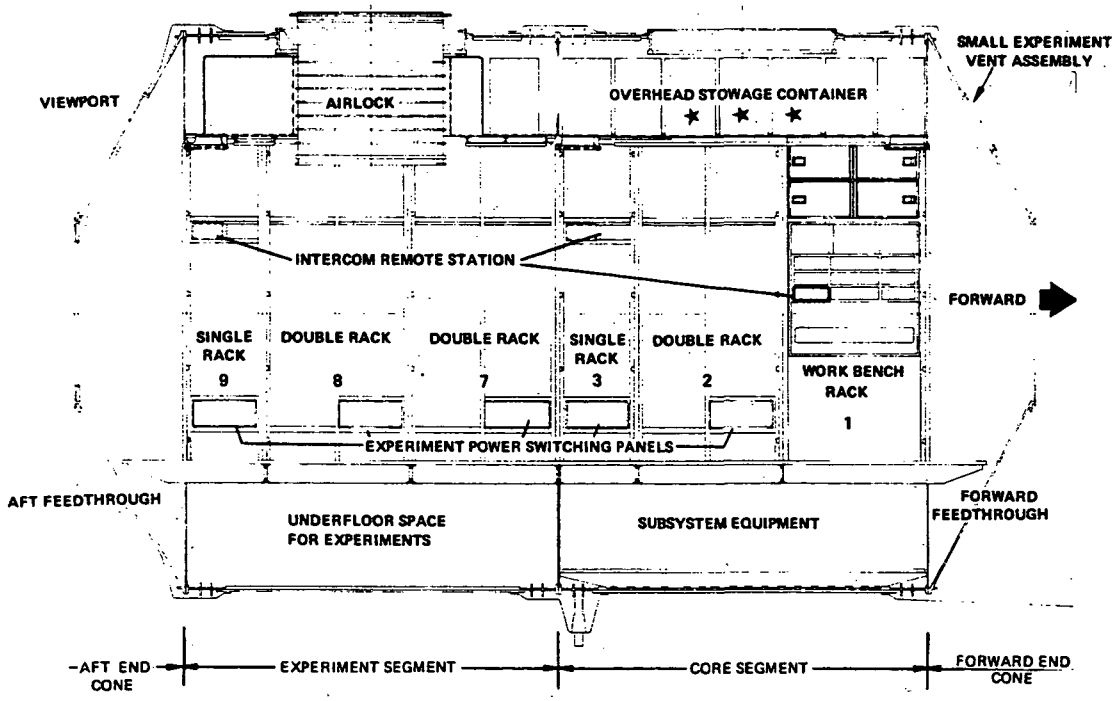

Figure 29. Sectional view port side.

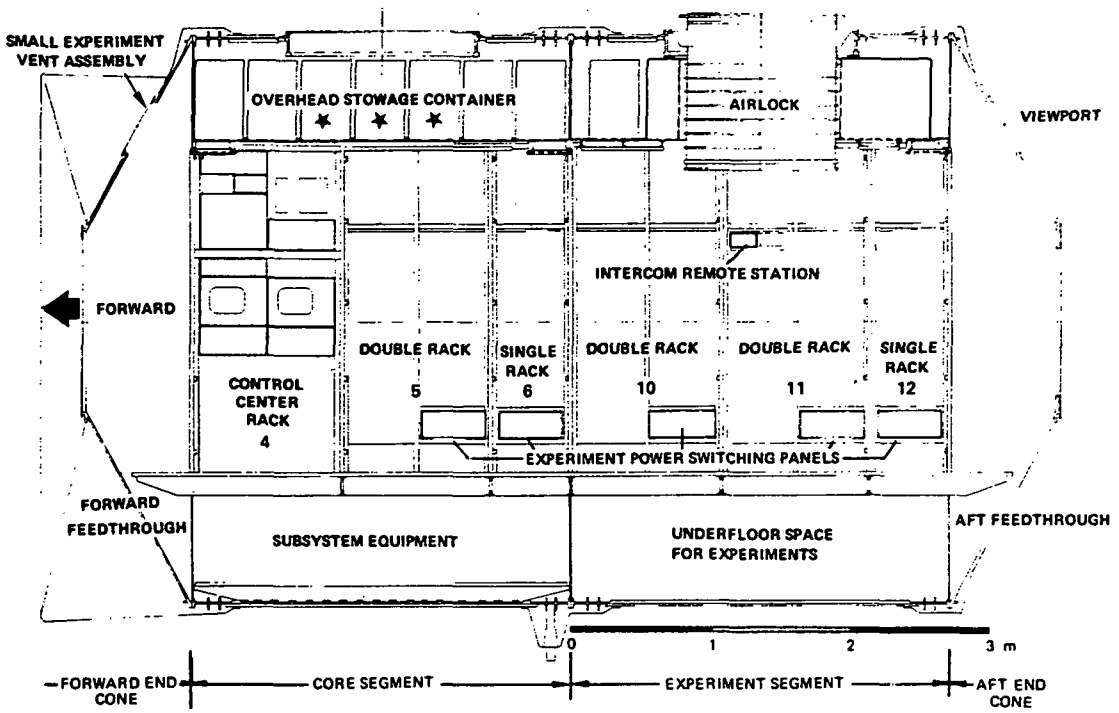

Figure 30. Sectional view starboard side.

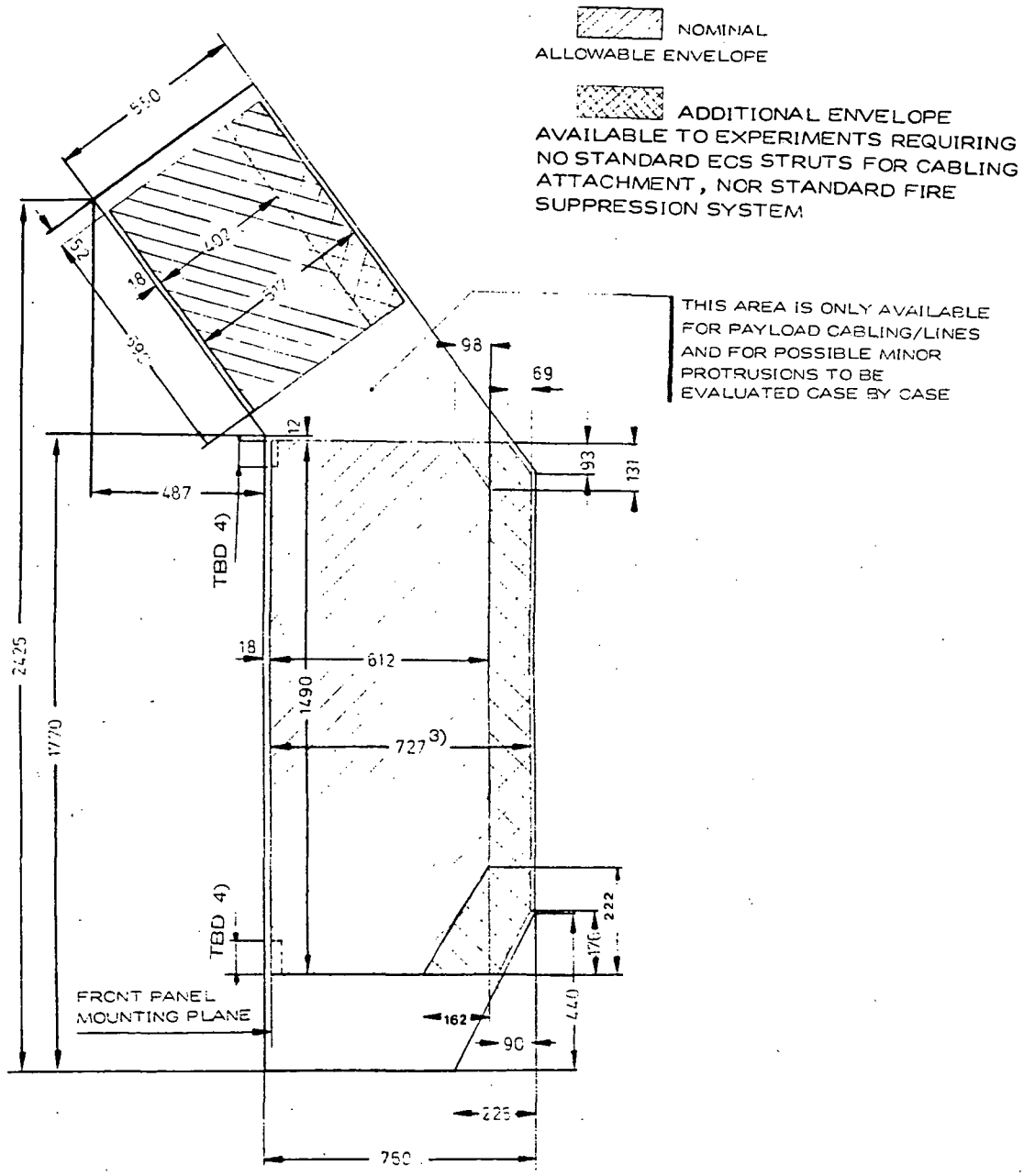

WITHOUT MIDDLE FRAME:

3) REDUCED UP TO 687

4) MINOR PROJECTION INTO EXPERIMENT ENVELOPE OF MIDDLE FRAME FITTING ACCORDING WITH FIG. 4.1-6

WIDTH OF PAYLOAD ENVELOPE:

1. STANDARD SINGLE RACK 451
2. STANDARD DOUBLE RACK: 2 x 451 (WITHOUT MIDDLE FRAME: 940

Figure 31. Nominal experiment allowable envelope inside the racks.

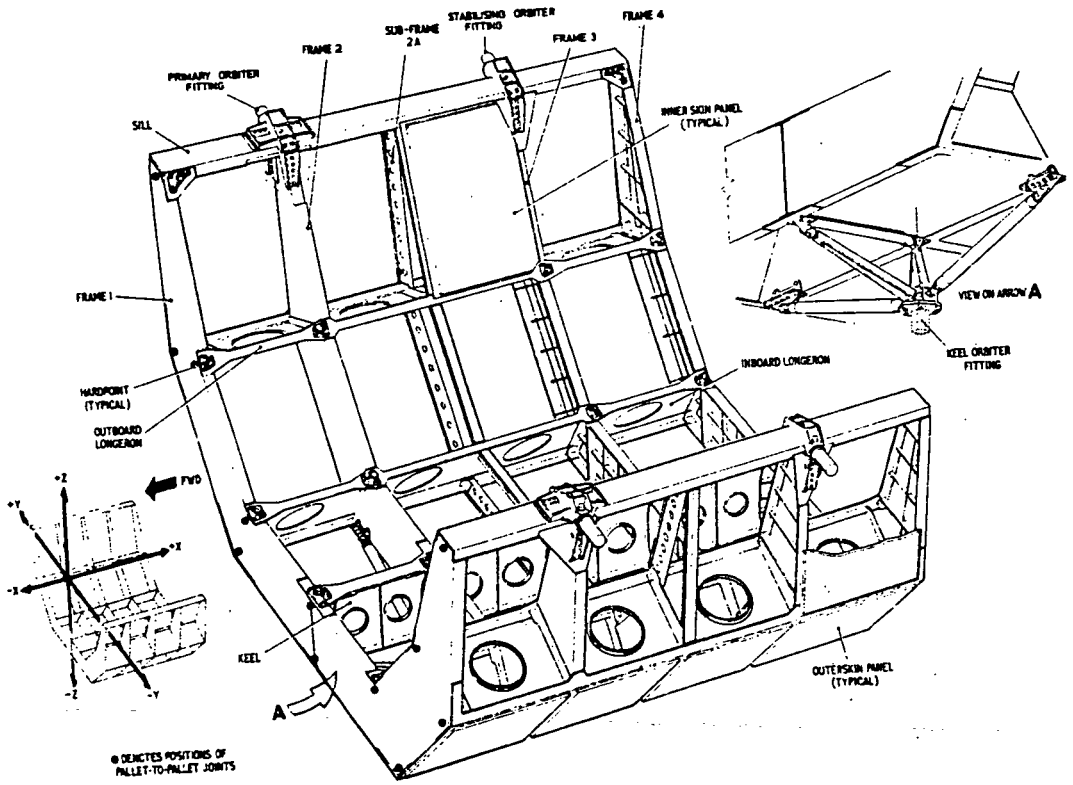

Figure 32. Pallet segment.

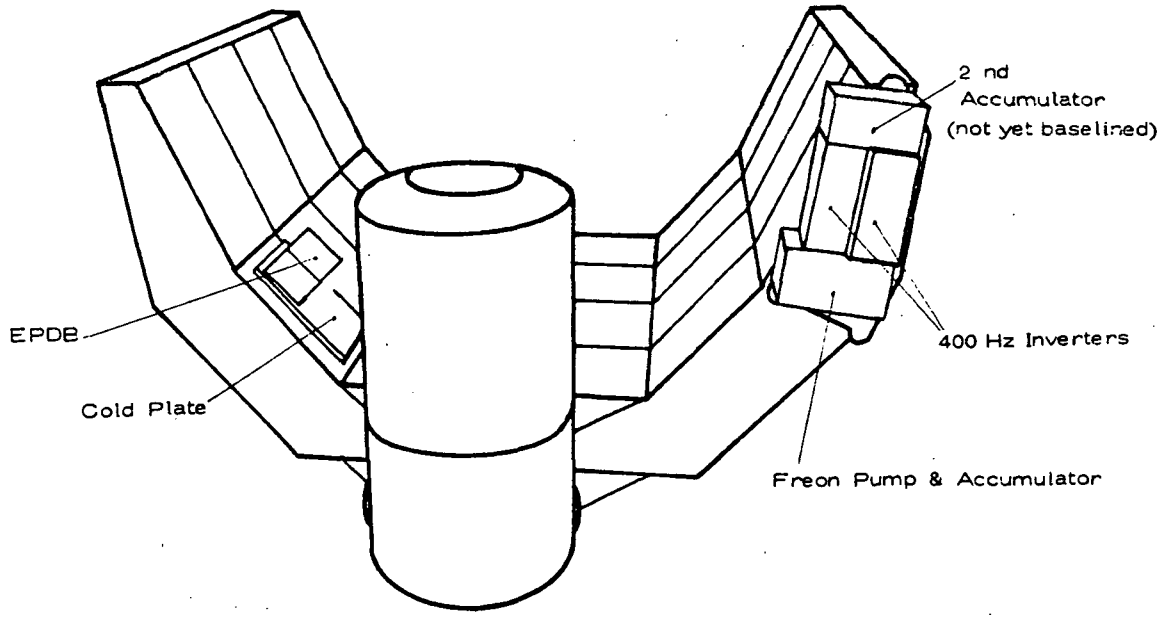

Figure 33. Igloo and front frame.

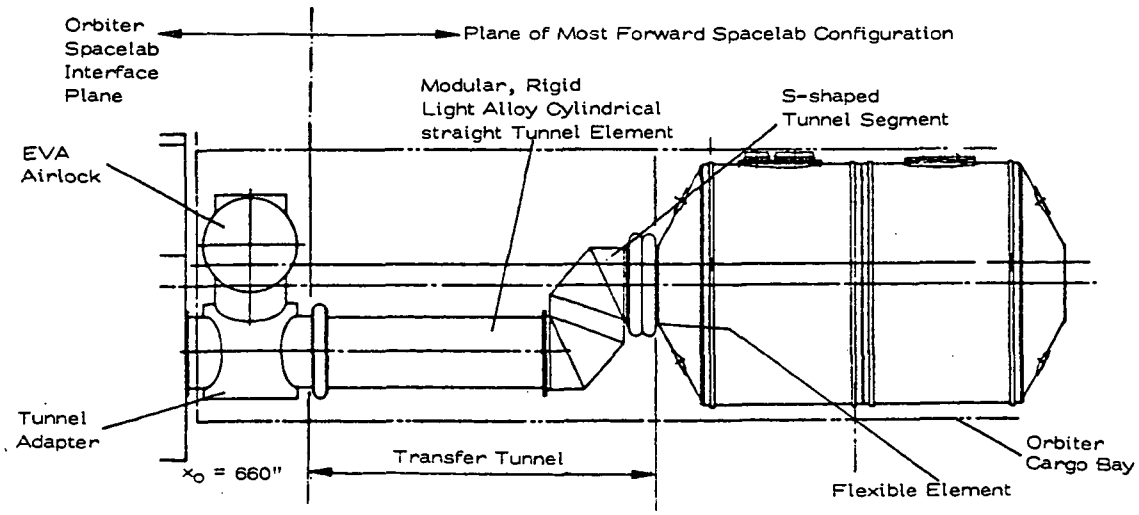

Figure 34. Transfer tunnel.

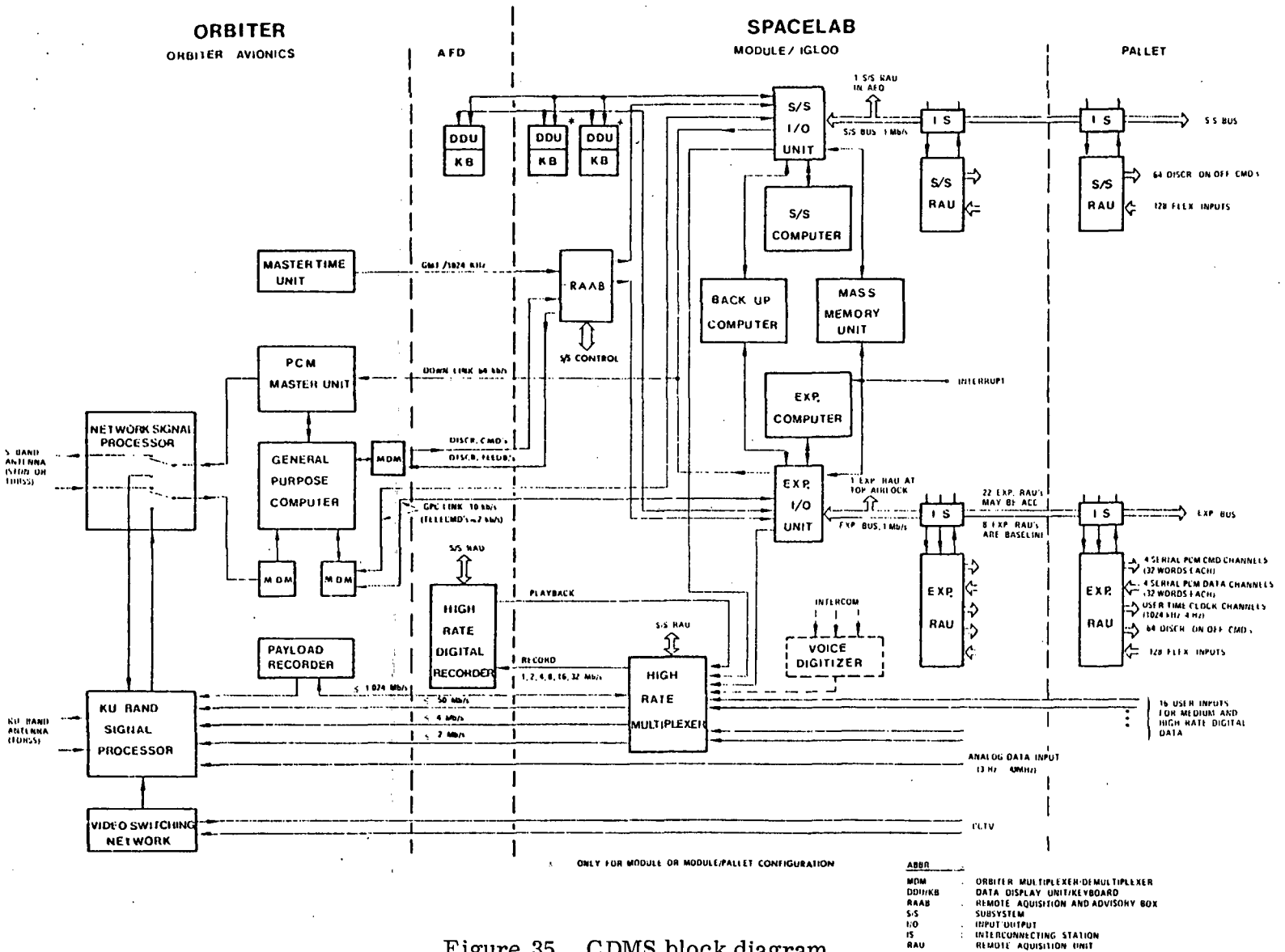

Figure 35. CDMS block diagram.

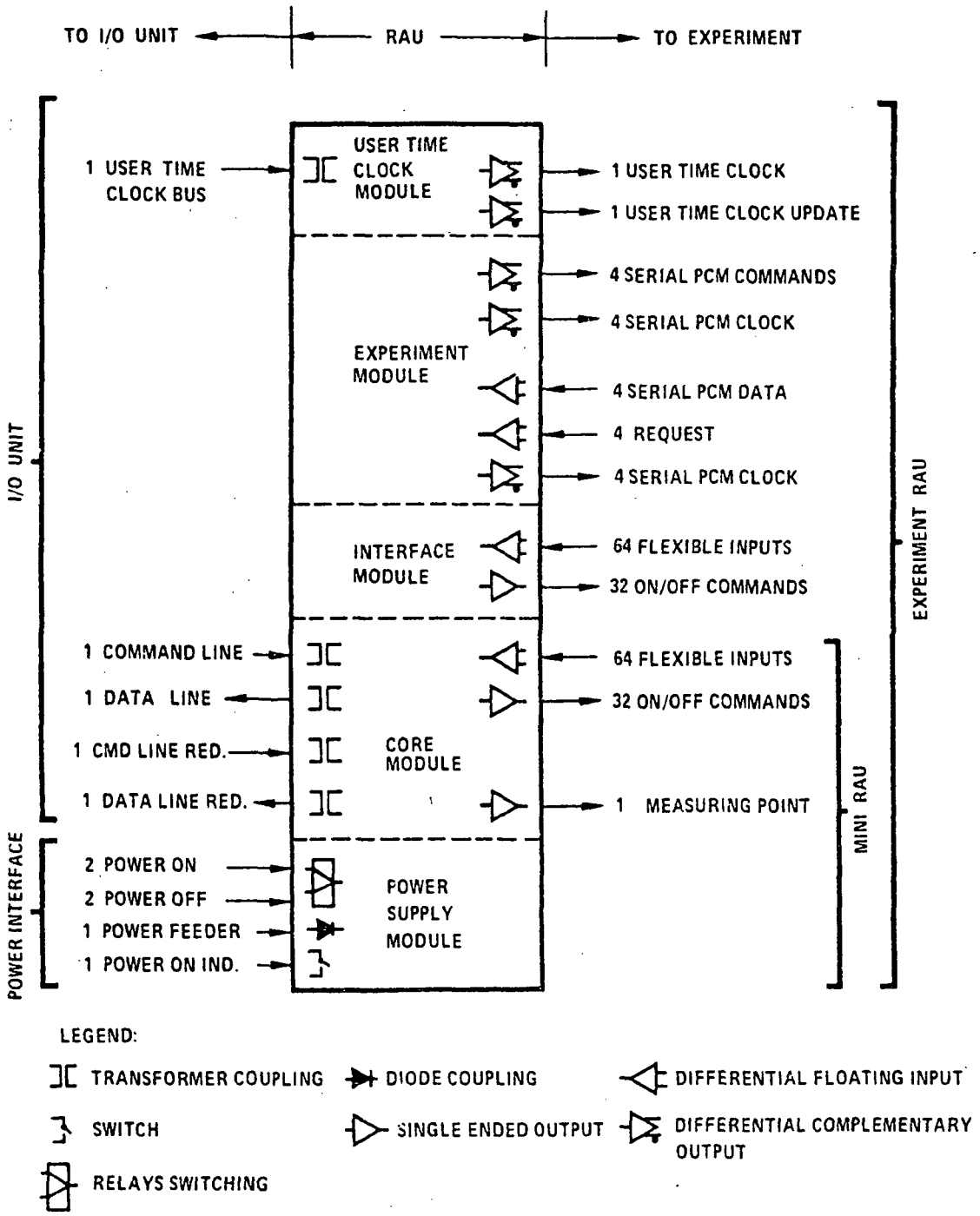

Figure 36. Remote acquisition unit block diagram.

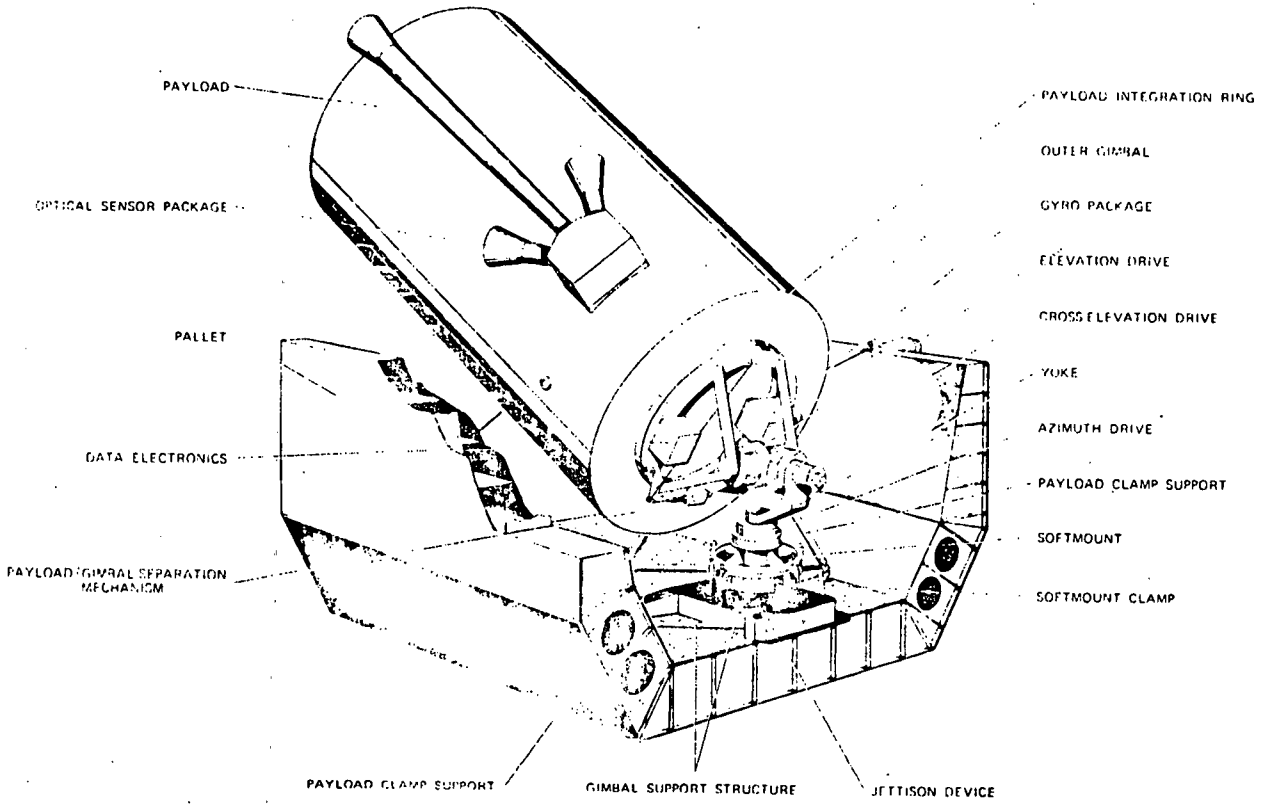

Figure 37. Instrument pointing subsystem.

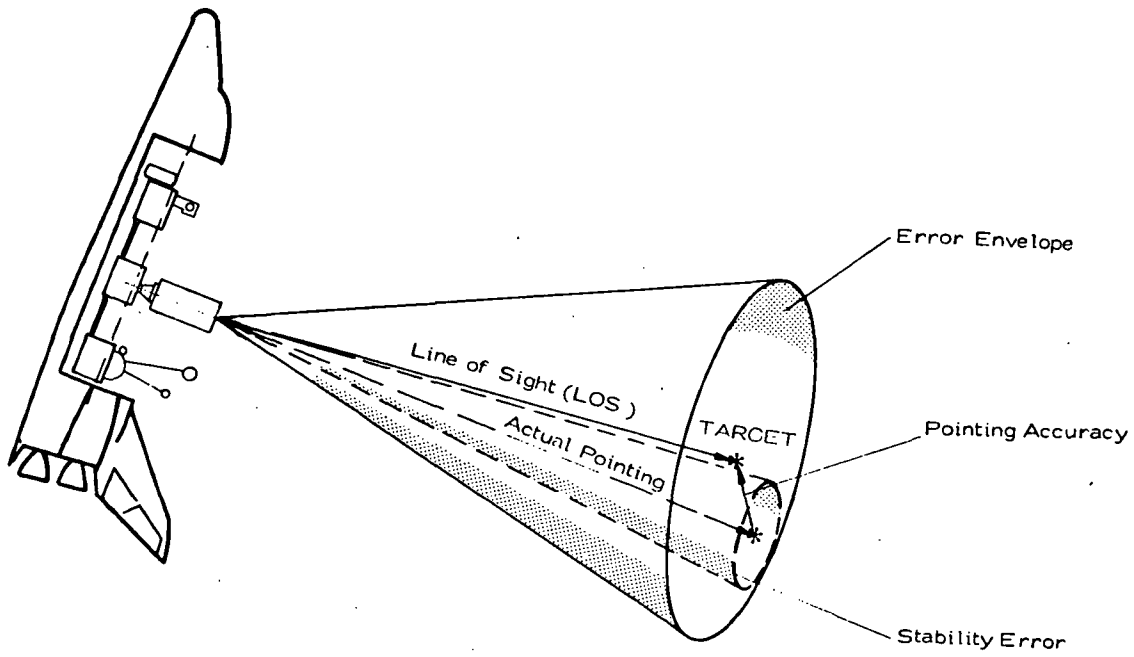

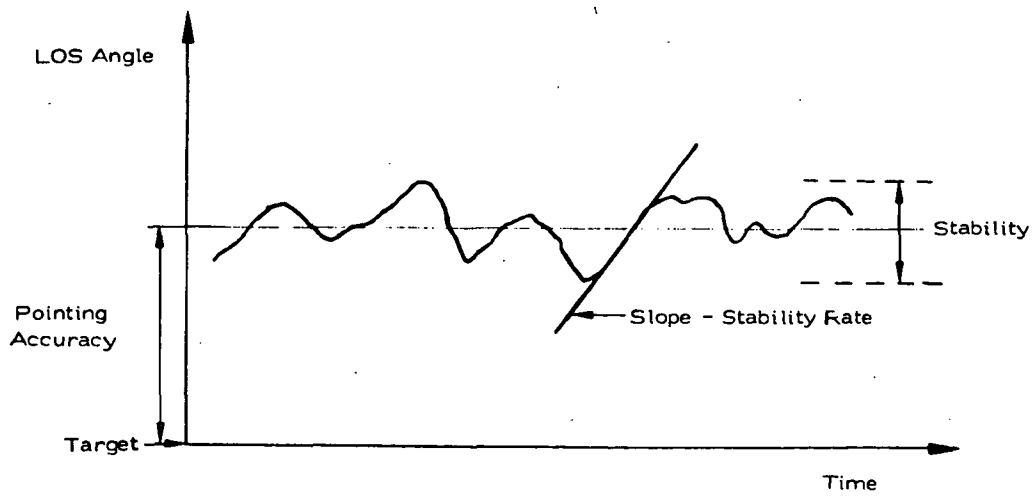

Figure 38. Error definitions.

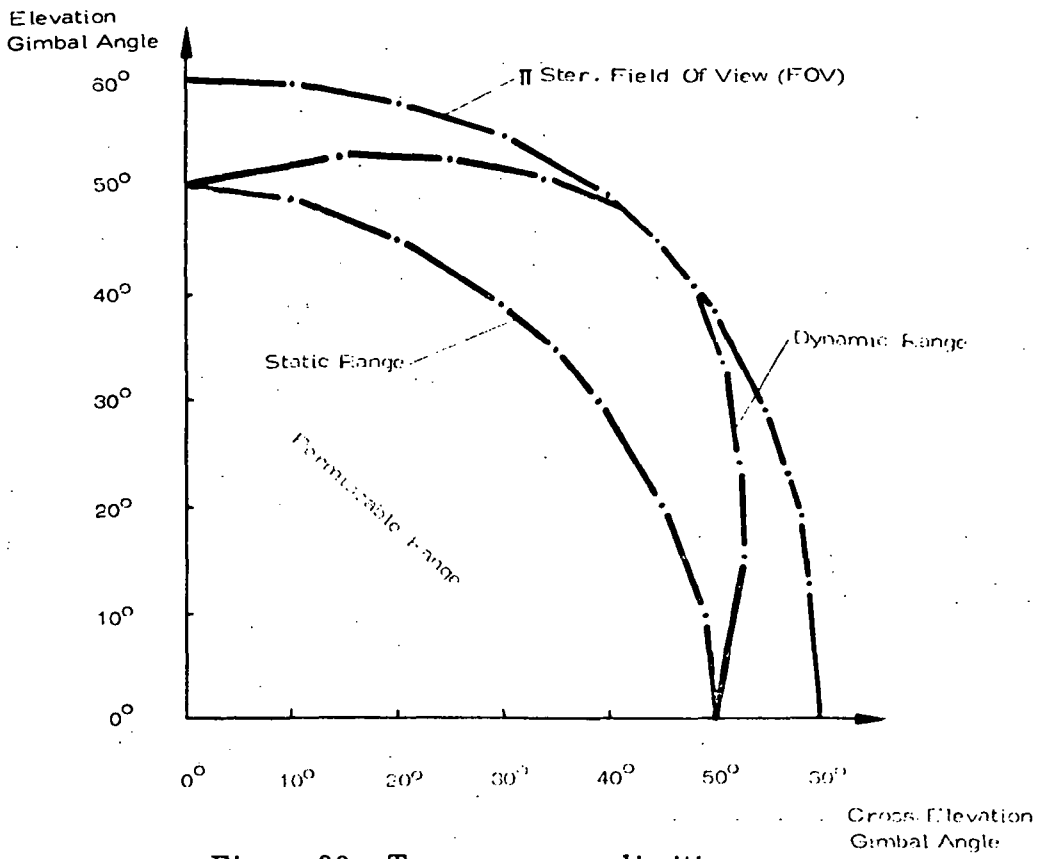

Figure 39. Two axes range limiting curve.

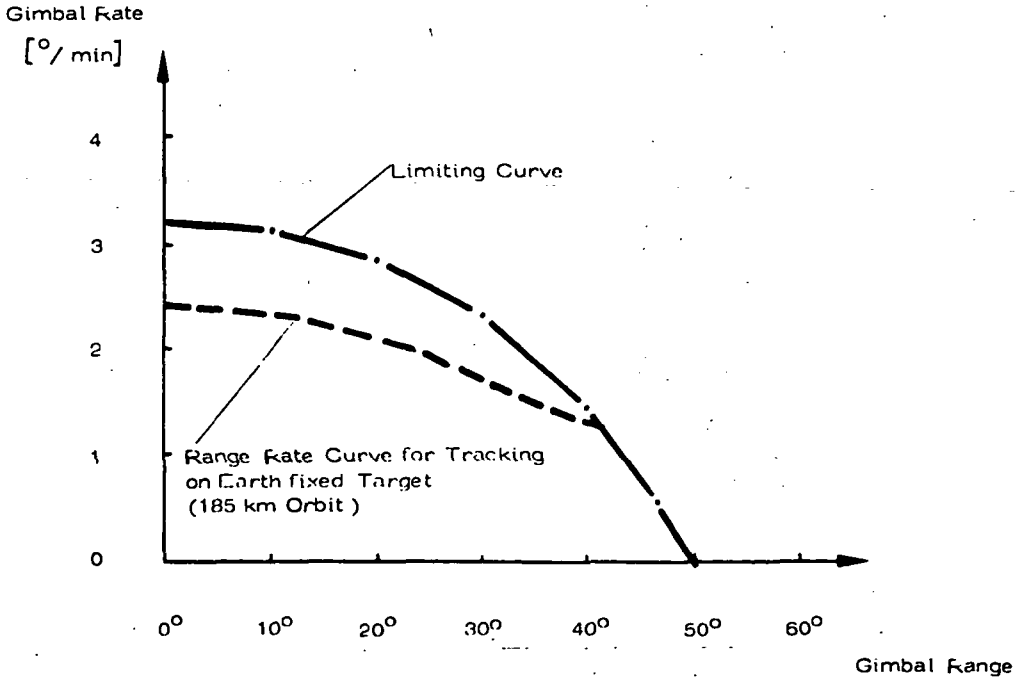

Figure 40. Range-rate limiting curve.

TABLE 1: WEIGHT AND VELOCITY INCREMENTS OF OMS-KIT

Number of OMS-kits	Dry Weight kg (lb)	Wet Weight kg (lb)	Velocity increments m/sec (ft/sec)	
			for 14 515 kg (32 000 lb) cargo weight	for 29 484 kg (65 000 lb) cargo weight
1	TBD	6466 (14255)	~ 183 (~ 600)	152.4 (500)
2	TBD	12533 (27631)	~ 366 (~1200)	304.8 (1000)
3	TBD	18601 (41009)	~ 549 (~ 1800)	457.2 (1500)

TABLE 2: ECCENTRIC ORBITS ACHIEVABLE

(Spacelab including its payload: 14 515 kg, 32 000 lb)

Inclination	direct de-orbit		indirect de-orbit	
	apogee in km (n.mi.)	number of OMS-kits	apogee in km (n.mi.)	number of OMS-kits
28.5°	2 500 (1 350)	3	1 150 (620)	3
55°	2 050 (1 100)	2	950 (510)	2
104°	280 (150)	0	550 (300)	0

Perigee 185 km (100 n.mi.)

TABLE 3: POINTING ACCURACY (HALF-CONE ANGLE) UTILIZING ORBITER IMU

Type of Pointing	Pointing Accuracy (3 Sigma) (Half-Cone Angle)	IMU-Drift Rate (3 Sigma)	Duration Between IMU Alignments
Inertial	± 0.5 deg	0.105 deg/hr/axis	1.0 hours
Augmented Inertial	± 0.44 deg	0	N/A
Earth-Surface-Fixed Target*	± 0.5 deg	0.105 deg/hr/axis	0.5 hours
Orbital Object	TBD	TBD	TBD
Local Vertical*	± 0.5 deg	0.105 deg/hr/axis	1 hour

*Tracking with TDRS, 100 n mi. (185 km) circular orbit.

TABLE 4: ORBITER RCS MAXIMUM ACCELERATION LEVELS

Direction	Translational, m/sec^2 (ft/sec^2)					Rotational, degrees/sec^2			
RCS System	$+x_b$	$-x_b$	$\pm y_b$	$+z_b$	$-z_b$	$\pm\ddot{\phi}$	$+\ddot{\theta}$	$-\ddot{\theta}$	$\pm\ddot{\psi}$
Primary Thruster	0.18 (0.6)	0.16 (0.5)	0.22 (0.7)	0.4 (1.3)	0.34 (1.1)	1.2	1.4	1.5	0.8
Vernier Thrusters	0	0	0.0021 (0.0070)	0	0.0024 (0.0080)	0.04	0.03	0.02	0.02

TABLE 5: PHYSICAL ACCOMMODATIONS ON THE AFT FLIGHT DECK FOR SPACELAB AND ITS PAYLOAD

Location at Aft Flight Deck	Panel Depth	Panel Width	Panel Area	Volume	Mass [1]
	inch (m)	inch (m)	ft^2 (m^2)	ft^3 (m^3)	lbs (kg)
• Panel R7	8 (0.203)	TBD	2.3 (0.21)	1.5 (0.042)	45 (20.4)
• Mission Station R12	20 (0.508)	19 (0.48) Size M	2.8 (0.26)	4.6 (0.130)	138 (62.6)
• On-orbit Station (Part of A6 & A7)	5-10 (0.127 - 0.254)	19 (0.48) Size G	3.7 (0.34)	2.4 (0.068)	72 (32.6)
• Payload Station (L10, L11, L12)	20 (0.508)	19 (0.48) Size M	8.3 (0.77)	13.8 (0.391)	414 (187.8)
• Additional Volume for electronics (L16, L17, L18)	-		-	1.3 (0.036)	39 (17.7)
Total	-		17.1 (1.59)	23.6 (0.668)	708 (321.1)

Note 1: Maximum loading based on 30 lbs/ft^3 (480 kg/m^3).

TABLE 6: CDMS EQUIPMENT FOR EXPERIMENTS

Basic Spacelab	Mission Dependent
1. Exp. Data Bus	1. Experiment Computer
2. Mass Memory	2. Experiment I/O Unit
3. Keyboard/Data Display Unit (2)	3. Experiment RAU's (6 total) (22 may be accommodated)
4. Intercom	4. Keyboard/Data Display Unit (1)
	5. High Rate Multiplexer
	6. Voice Digitizer
	7. High Rate Digital Recorder

TABLE 7: COMPUTER CHARACTERISTICS

Formats

Operands: 8, 16, 32 and 24 + 8 (floating points) bits

Instructions: 16 bits

Control Unit

Micro-programmed control unit

Cycle time 300 ns

Micro-interrupt capability

Micro-instructions 4 K words of 16 or 20 bits

Instruction Set

- Number of instructions 128
- Format 16 bits

  Immediate 8 bits
- Addressing capability

  Direct 256 Bytes

  Indirect memory double word

  Relative 512 bytes

  Based 256 bytes

  Indexed 64 K bytes
- Type

  Call and store

  Logic and comparison operations

  Shift operations

  Fixed-to-floating and floating-to-fixed conversions

  Conditional and unconditional jumps

Addressing Modes

Immediate, direct, indirect, relative to a base, indexed, relative to a program counter, half word, word, character, double word

- Addressing capability

  Byte, word, double word

Number of Adressable Registers

4 Specialized registers

62 Dedicated registers

7 Base registers

Computing Speed

Fixed Point :6 Bits

Add/Sub	Direct:	2	µs
	Indirect:	3	µs
Mul/Div	Direct	4	µs
	Indirect:	5	µs

Fixed Point: 32 Bits

Add/Sub	Direct:	5.5	µs
	Indirect:	6.5	µs
Mul/Div	Direct:	9.3	µs
	Indirect:	9.3	µs

Floating Point 32 Bits (24 + 8)

Add/Sub	Direct	5	µs
	Indirect	6	µs
Mul/Div	Direct	6	µs
	Indirect	7	µs

Gibson Mix $3.5 * 10^5$ Operations/Second

Input/Output

- Interrupts
  - Number of external: 8 Levels
  - Number of internal: 5 Levels
  - Number of software: Program dependent
  - Interrupt control: Microprogram + Software
  - Priority scheduler: Software
- Data transfer mode
  - Program controlled
    - data rate: 60 µs /word
    - no of addressable periferals: 65 k
  - Direct memory access
    - data rate: 400 to 800 K word/sec
    - control: direct
- Word length: 16 bits plus 1 parity + 1 protection
- Discretes: 8 inputs and 8 outputs
- Real time work: 1 µs to 2^{32} ms

Memory

- Type: :8 mil ferrits cores, 2 1/2 D configuration
- Capacity: 64 K 16-bit words (plus 1 parity bit and 1 protection bit)
- Modularity: 16 K words
- Cycle time: 920 ns
- Addressing, Quantum: Byte, word
- Access time: 420 ns
- Ports: 2

TABLE 8: CHARACTERISTICS OF NOMINAL 2000 kg AND 200 kg PAYLOADS

	LARGE PAYLOAD	SMALL PAYLOAD
Mass	2000 kg	200 kg
Dimensions	2 m Ø x 4 m	1 m Ø x 1.50 m
Moment of inertia about payload CG:		
about axis perp. to LOS	1200 kgm^2	20 kgm^2
about LOS axis	1000 kgm^2	25 kgm^2
CG offset from center of rotation of gimbal axes:		
along LOS	2.5 m	1.50 m
perp. to LOS	0.30 m	0.10 m
Structural characteristics frequency (TBD mode)	TBD Hz	TBD Hz

TABLE 9: POINTING AND STABILITY CHARACTERISTICS

	Requirements	Goals	
Bias Error			
LOS	2 arc sec	0.8 arc sec	1 sigma
ROLL	40 arc sec	15 arc sec	1 sigma
Quiescent Stab. Error			
LOS	1 arc sec	0.33 arc sec	1 sigma
ROLL	3 arc sec	1.6 arc sec	1 sigma
Man Motion Dist. Error			
LOS	3 arc sec	1 arc sec	peak
ROLL	10 arc sec	4 arc sec	peak
Stability Rate (max.)	2 arc min/sec	./.	
Pointing Range			
LOS	πSter.	N/A	
ROLL	πRad.		
Slewing Rate (max.)	2.5 deg/sec		

APPENDIX

SHUTTLE AND SPACELAB SCHEDULES

(As presented by Kenneth S. Clifton)

Flights of the Shuttle spacecraft will commence in 1979 with the first of six Orbital Flight Test (OFT) missions. A limited amount of experimentation will be accomplished on OFT flights 2 through 6, brief profiles of which are presented in Table A-1. An Announcement of Opportunity has already been released to the scientific community with a proposal due date of December 3, 1976. Likewise, the Announcements of Opportunity have been released for the First and Second Spacelab missions with proposal due dates of June and December 1976. Both of these Spacelab flights will occur in 1980. Spacelab 1 will place an experimental emphasis on the atmospheric sciences, while astrophysics will be emphasized on Spacelab 2. Spacelab 3, to be launched in 1981, is expected to emphasize space processing and life sciences. No Announcement of Opportunity has yet been released for this flight.

Table A-2 portrays a summary of typical missions to be flown in the years 1980-1982 in addition to those already specified. It should be emphasized, however, that the table represents only a typical mission plan for the early Shuttle flights in the years 1980-1982. The definitions of many of the payloads included in this payload model are limited at this time and subject to change. However, the missions shown are representative of the types, frequency, and cargo mixes during the period considered. More definitive data for each individual mission will be prepared as payload and mission planning evolves. At present it is envisioned that a general Announcement of Opportunity for the Spacelab missions will be issued on an annual basis. It might be noted that Spacelab payloads will be flown

at monthly intervals by 1982, with general Shuttle missions launched at the rate of two per month. Also, with the use of various upper stages, a variety of orbits may be achieved, including synchronous orbits and highly elliptical orbits, thus increasing the versatility for orbital experimentation.

TABLE A-1
OFT FLIGHT PROFILES

FLIGHT PARAMETERS						
Launch Date		July 79	Sept 79	Dec 79	Feb 80	March 80
Inclination (Deg.)		32-40	32-40	50-57	50-57	TBD
Payload Weight (lbs)	Up	10K	20K	22K	22K	22-55K
	Down	10K	10K	22K	22K	22K
Altitude (nm)		90-150	150	225	225	225
Duration (days)		Up to 5	Up to 7	Up to 7	7	7
Crew Size		2	2	2	3 or 4	4
Landing Site		EAFB**	EAFB	EAFB	KSC***	KSC

*Subject to change. Refer to "OFT Payload Requirements and Constraints."
**Edwards Air Force Base
***Kennedy Space Center

TABLE A-2. EARLY STS MISSIONS PLAN

FY-1980-1982
CARGO MANIFEST

Revised 6/21/76

YEAR	FLIGHT NO.	DATE	CONFIGURATION	PAYLOADS	ALTITUDE Km	INC. DEG.
1981	17	June	Spacelab - L+P	• Multi-User 81-3	450	55
	18	July	SSUS-A	• INTELSAT	Syn.	0
			SSUS-D	• WESTAR	Syn.	0
	19	Aug.	Spacelab - L+P	• ATL Emphasis	450	50
	20	Sept.	Shuttle	• LDEF - Deploy	500	28.8
				• BESS - Deploy	500	28.8
	21	Sept.	Spacelab	• Multi-User 81-2	325	57
	22	Oct.	IUS (2-Stage)	• Very Long Baseline Inter.	1 AU	--
			Shuttle	• Gravity Probe B - Deploy	460	33
				• SMM - Retrieval	460	33
	23	Oct.	Spacelab - L	• Life Science (Mod 1)	370	28.5
	24	Nov.	IUS	• DOD - 3	--	--
	25	Nov.	Spacelab - P	• Combined Astr.	--	--
	26	Dec.	IUS	• DOD - 4	--	--
	27	Dec.	Spacelab - L+P	• Multi-User 82-1	400	28.5
				• APPS**	400	28.5

**Altitude and Inclination Unconstrained

TABLE A-2 (Continued)

YEAR	FLIGHT NO.	DATE	CONFIGURATION	PAYLOADS	ALTITUDE Km	INC. DEG.
1980	7	May	IUS	• DOD-STP-1	--	--
			Shuttle	• LDEF Retrieval	250	32
	8	July	Spacelab - L+P	• First Spacelab	250	57*
	9	Sept.	SSUS-D	• Aerosat	Syn.	0
			SSUS-D	• Aerosat	Syn.	0
			SSUS-D	• GOES	Syn.	0
	10	Oct.	Spacelab - P	• Second Spacelab	450	35*
	11	Dec.	IUS	• DOD-2	--	--
1981	12	Jan.	Spacelab - L	• Multi-User 81-1	400	28.5
				• APPS**	400	28.5
	13	Feb.	IUS (2-Stage)	• STORMSAT	Syn.	0
			Shuttle	• Soft X-Ray - Deploy	400	28.5
	14	Mar.	Spacelab - L	• Life Science (Mod 1)	370	28.5
	15	Apr.	SSUS-A	• INTELSAT	Syn.	0
			SSUS-D	• WESTAR	Syn.	0
	16	May	SSUS-D	• Foreign Comm.	Syn.	0
			Shuttle	• APPS**	300	28.5
				• Vestibular Function - Deploy	300	28.5
			IUS (2-Stage)	• SPHINX B/C	36,000/1000	20

*Dependent on Experiments Selected from Announcement of Opportunity
**Altitude and Inclination Unconstrained

TABLE A-2 (Continued)

YEAR	FLIGHT NO.	DATE	CONFIGURATION	PAYLOADS	ALTITUDE Km	INC. DEG.
1982	28	Jan.	IUS (4-Stage)	• Out-of-Ecliptic Solar Observatory	Escape	--
	29	Jan.	IUS (4-Stage)	• Outer Planet Orbiter/Probe (Jup.)	Escape	--
	30	Feb.	Spacelab - L+P	• Multi-User 82-2	400	57
	31	Feb.	IUS	• DOD - 5	--	--
	32	Mar.	IUS	• DOD - 6	--	--
	33	Apr.	SSUS-D	• WESTAR	Syn.	0
			SSUS-D	• Foreign Comm.	Syn.	0
			Shuttle	• BESS - Retrieval	475	28.8
	34	Apr.	Spacelab - L	• Life Science (Mod II)	370	28.5
	35	May	IUS (2-Stage)	• Disaster Warning	Syn.	0
			Shuttle	• LDEF - Retrieval	470	28.8
				• APPS	470	28.8
	36	May	Spacelab - L+P	• AMPS	260x425	57
	37	May	IUS	• DOD - 7	--	--
	38	June	Spacelab - L+P	• Multi-User 82-4	250	55

TABLE A-2 (Concluded)

YEAR	FLIGHT NO.	DATE	CONFIGURATION	PAYLOADS	ALTITUDE Km	INC. DEG.
1982	39	July	IUS	• DOD - 8	--	--
	40	July	Spacelab - L+P	• ATL Emphasis	370	55
	41	Aug.	IUS (2-Stage)	• Very Long Baseline Inter.	5000	0
			Shuttle	• BESS - Deploy	500	28.8
				• APPS**	500	28.8
	42	Aug.	Spacelab - L+P	• EVAL		
	43	Sept.	IUS	• DOD - 9	--	--
	44	Sept.	Spacelab - L+P	• Multi-User 82-3	350	55
	45	Oct.	SSUS-A	• COMSTAR	Syn.	0
			SSUS-A	• COMSTAR	Syn.	0
	46	Oct.	Spacelab - L	• Life Science (Mod II)	370	28.5
	47	Nov.	IUS	• DOD -10	--	--
	48	Nov.	Spacelab - P	• Astr./High Energy	--	--
	49	Dec.	IUS (4-Stage)	• Sat. Uran. Titan Probe	Escape	--
	50	Dec.	Shuttle - WTR (OMS Kit)	• Earth Survey Sat.	907.7	99.1

**Altitude and Inclination Unconstrained

omit

SHUTTLE ENVIRONMENTAL PARAMETERS

R. Naumann
Space Sciences Laboratory
Marshall Space Flight Center

(No paper submitted for publication)

Reference can be made to the following documents:

Space Shuttle System Payload Accommodations, JSC 07700, Vols. 10 and 14, Lyndon B. Johnson Space Center, NASA, Houston, Texas, 1975.

C-2

N81-24131

D3

A LOW LIGHT LEVEL TELEVISION SYSTEM

B. J. Duncan
Marshall Space Flight Center

A proposal has been submitted in response to the announcement of opportunities for Skylab I involving low-light-level imaging techniques. While the observational objectives are not necessarily pertinent to cometary experimentation and observation, the instrumentation possibly would be, and is potentially available if the proposal is successful.

Dr. Steve Mende of LMSC is the principal investigator, with Dr. Bob Eather of Boston College, and the following MSFC personnel as co-investigators: Drs. Robert Naumann, Gary Swenson, and David Reasoner as well as Stuart Clifton and the author. The proposed observations are of natural and induced atmospheric glows and near vehicle aerosol distribution.

A dual detector system is proposed (see figures 1 & 2) mounted on a Z-axis gyrostabilized gymbal system which is under computer control for pointing and tracking. One channel is a low resolution array of 10 x 10 photodiodes on the rear of a microchannel plate (MCP) intensifier. The system field of view is 4 degrees with folded reflective optics having a 5-inch aperture. A pair of filter wheels allows a choice of interference and neutral density filters. Not shown in Figure 1 is the capability to insert a narrow-band tunable birefregent filter and another filter wheel for blocking filters.

The detector operates in a discrete pulse counting mode with each register position capable of storing up to 2^{16} counts. Sampling rates of up to 1000 per sec are possible. The data is stored on digital magnetic tape.

The other channel utilizes an intensified SEC video tube operating in an integration mode (i.e., integration on the SEC target). It has an identical 4 degree field of view optical system and, in addition, a 20 degree field of view refractive optical system is selectable via a flip mirror. Quartz optics allows ultraviolet observations down to 200 nm. Integrations of up to 1 second are possible on the SEC target. This single frame of inherently analog data is digitized (8 bits/pixel) and placed into a solid state memory from where it may be fed into the computer for arithmetic operations with subsequent frames. The data then can be placed on digital magnetic tape or fed back thru a D/A system for image reconstruction for on-board real-time display. This allows the payload specialist to interact for experiment operation and control via the CRT display.

Figure 2 is a conceptual depiction of the experiment instrumentation mounted on the gymbal system on a Spacelab pallet.

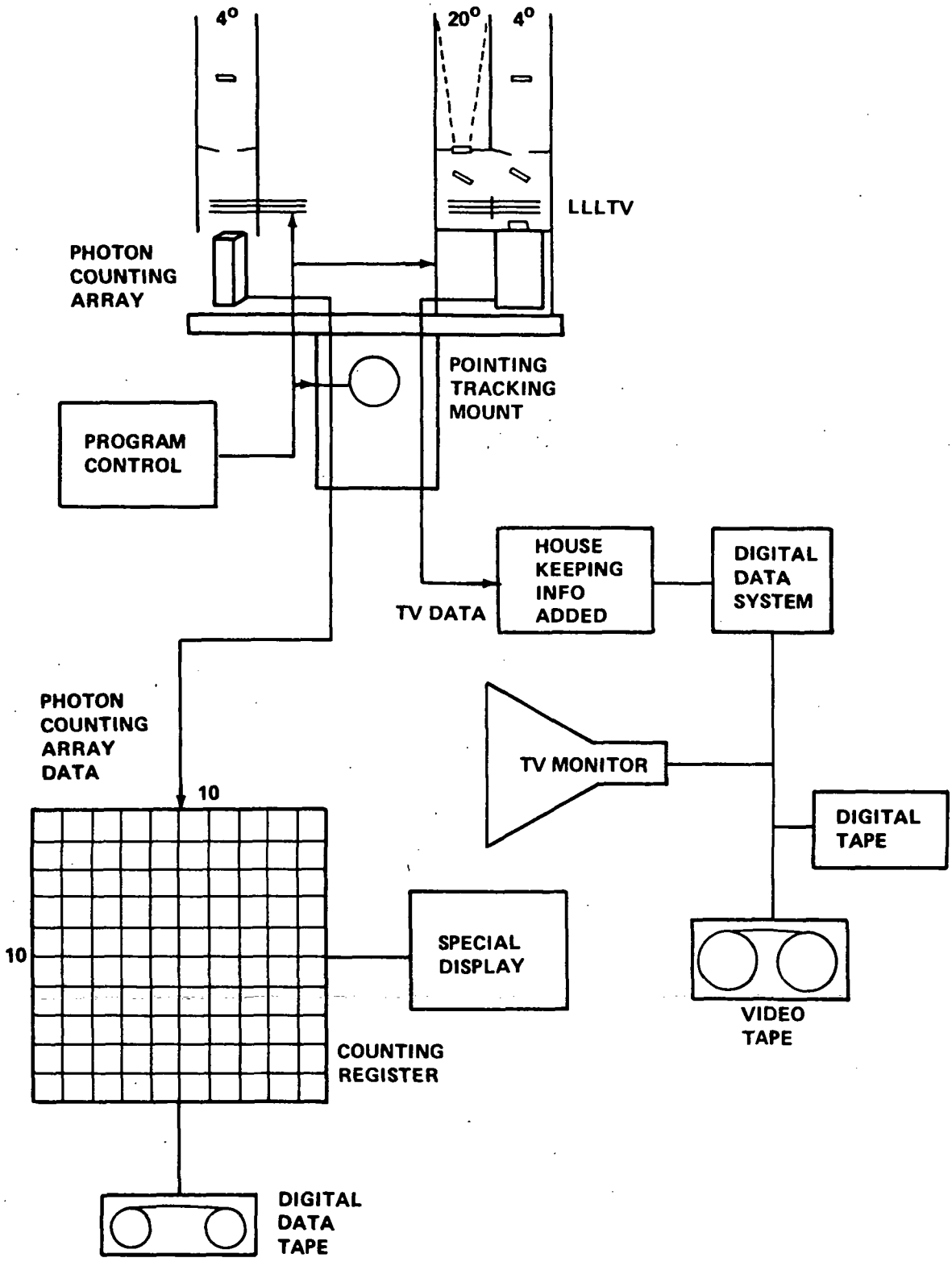

FIGURE 1. LOW LIGHT LEVEL IMAGING SYSTEM - SCHEMATIC

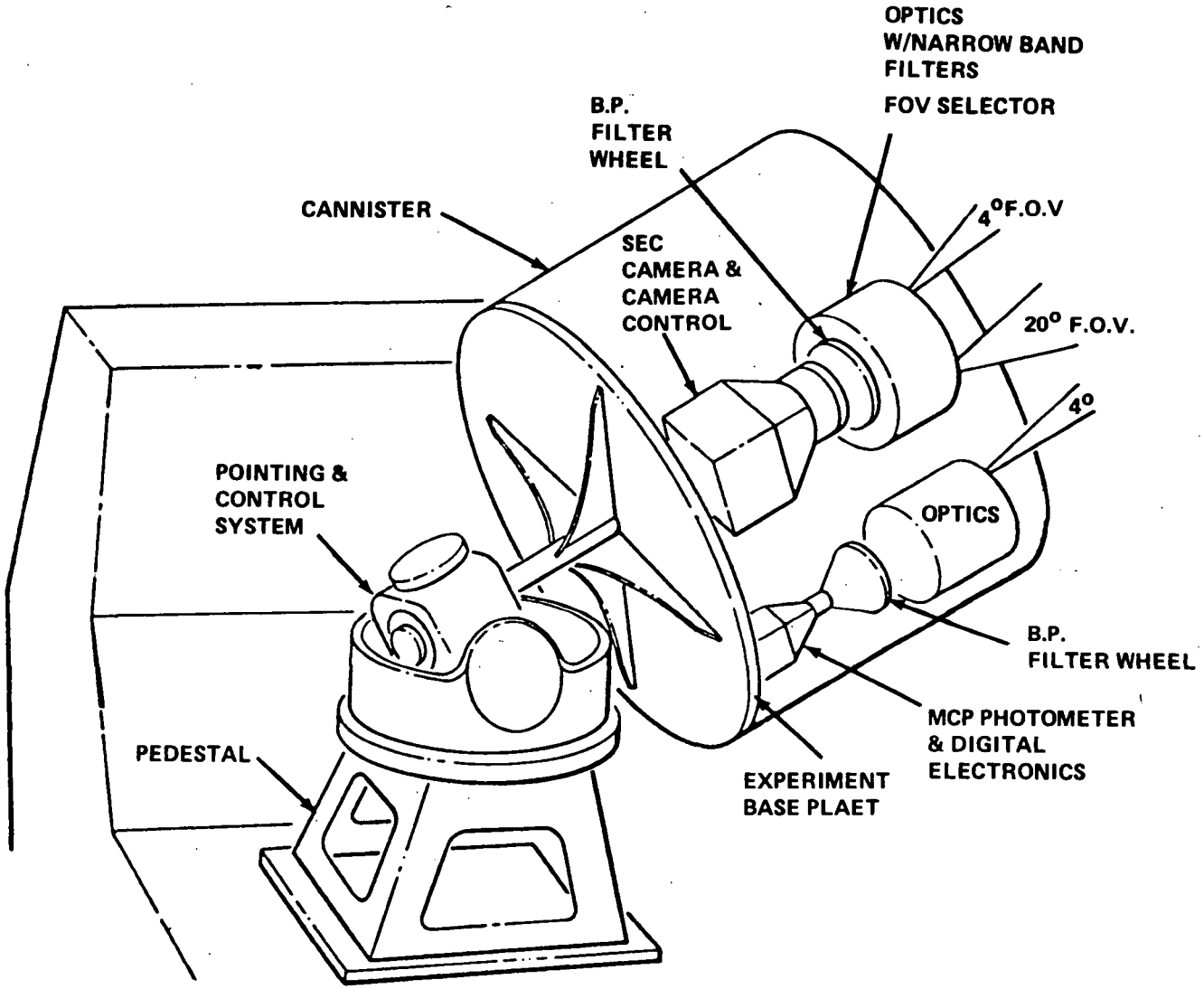

FIGURE 2. LOW LIGHT LEVEL IMAGING EXPERIMENT - CONCEPTUAL VIEW

SESSION II

SHUTTLE-BASED EXPERIMENTS

SIMULATION OF A COMETARY CONGLOMERATE OF FROZEN GASES AND DUST IN A ZERO-GRAVITY ENVIRONMENT

A Critical Evaluation of Possible Space Experiments

A. H. Delsemme
Dept. of Physics and Astronomy
The University of Toledo, Ohio

ABSTRACT

The cometary material is likely to be the last intact sample containing a volatile fraction accreted from the icy grains or condensed out of the gases of the primeval solar nebula, and it has never been in gravity fields larger than 10^{-4} g.

Since we do not have any experience of dust and snow accretion and sedimentation in these extremely weak gravity fields, the bulk properties of cometary material are totally unknown, and the clues given by observations of comets cannot be unambiguously interpreted.

It is therefore proposed to use the Shuttle (OFT experiments) or eventually Spacelab to study, in the absence of gravity:

1. the low-velocity accretion and the bulk properties of icy conglomerates simulating cometary material;

2. their sedimentation and bulk properties in very small acceleration fields (10^{-4} to 10^{-1} g);

3. their behavior when exposed to the direct solar flux.

INTRODUCTION

It is possible that the cometary snows either condensed, some five billion years ago, out of the gases of the primeval solar nebula, or that they accreted from those interstellar grains that were present in that nebula; in both cases, they could be the last intact samples of an important fraction of that nebula and they may be of a fundamental importance in unraveling the cosmogony of the solar system. In particular, since the volatile fraction of the cometary nucleus contains very large amounts of hydrogen, carbon, nitrogen, and oxygen, it is likely that their chemistry contains some of the information needed to understand the role and the fate of these important elements in the formation of the planets and in the appearance of life.

However, not only is the cometary chemistry rather uncertain, but the bulk properties of the icy conglomerate probably present in the cometary nucleus are totally unknown, mainly because it has never been exposed to any (large) gravity field. The gravity field at the surface of a cometary nucleus could typically be 10^{-4} or 10^{-5} g, and we do not have any experience of large systems of dust and ice that have been accreted in the absence of gravity, and have never been in gravity fields larger than these.

We suspect only that this "icy conglomerate" could be a very loose structure with almost no cohesive strength, in particular if it has been accreted at very slow velocities. The proposed research is not concerned with crystal properties or, by and large, solid state physics, because it is believed that microscopic properties are not very much perturbed by the presence or the absence of gravity. It is rather proposed to

concentrate on the more useful, although less glamorous bulk properties that could eventually lead toward the structural "geology" and evolution of the cometary nucleus. This type of information would be useful, not only to understand the clues given by the ground-based observations of comets, but also to clarify the meaning of the first imaging of a cometary nucleus, that could be obtained during a future flyby or rendez-vous mission, for instance to Comet Halley (1986).

NATURE OF THE COMETARY NUCLEUS

Coma and tail are transient phenomena originating from one single permanent feature: the cometary nucleus. No cometary nucleus has ever been seen but as a pinpoint of light, and data known with certainty are scarce. Although Lyttleton continues to argue that comets have no solid lump nucleus, he has never properly refuted the three major criticisms against his loose "sandbank" model, and a consensus has appeared among the other astronomers that has been described by Delsemme (1966) in his Report to I.A.U. Commission 15, and that can be summarized as follows:

Cometary nuclei have been stored for a large but unknown length of time on very large orbits, that may go half-way to the nearby stars but still are bound to the sun (the Oort's cloud of comets); hence they are permanent members of the solar system. Although their place of origin is still in dispute, they probably have never been heated above 100°K prior to their first passage through the inner solar system; in particular, wherever they were formed, their volatile fraction must have accreted or condensed at temperatures near 100°K. They have some cohesive strength which must be very small but not nil, although its order of magnitude is unknown. Their non-volatile material seems to be partially or totally

constituted by very fine dust, although some large chunks cannot be excluded at this stage.

The size distribution of the dust is poorly known, but it contains at least a large fraction of micron and submicron particles. This dust mainly contains silicate grains, although a small fraction of graphite grains cannot be ruled out. After their first passage in the vicinity of the sun, comets decay fast, losing much gas, icy grains and dust; at that time, a heating of the upper layers of the nucleus is not unlikely, that might change the dusty fraction into a crust; but a new comet coming straight from the Oort's cloud must have some kind of a cement to keep the dust together before its first passage near the sun. The cohesive strength could be provided by the snows of frozen gases or of solid hydrates of gases that are assumed to be its volatile fraction. The assumed "icy conglomerate" includes mainly water, probably rather large amounts of CO_2 (Delsemme and Combi 1976), HCN and CH_3CN, plus many compounds, including organic compounds, about which we have only incomplete spectroscopic clues. Even after one or several passages near the sun, the "crusty" surface of the nucleus must remain very friable and porous, because cometary fragments that sometimes reach the upper atmosphere of the earth are fragile and of a very low (although still not well-known) density.

We suspect that the shape of the cometary nucleus could be highly irregular, as suggested by other small bodies like asteroids, and Phobos and Deimos. However, if their cohesive strength were very low, but their density very high for snows, we could have more spherical bodies because even a moderately small gravity could crush the snows together.

Finally, we have circumstantial proofs that cometary nuclei rotate, but we do not know their rotation rate; we can only set upper estimates at which rate they would break into pieces by inertia. This is a possible origin for the observed splitting of many nuclei; this would imply that the asymmetrical vaporization, well established from non-gravitational forces, has a net impulse which does not always go through the center of mass of the nucleus; in some cases the spin could therefore be accelerated beyond the tensile strength of the nucleus. Disintegrations of cometary nuclei show very slow initial splitting velocities, probably too small to be measured, which implies values smaller than a few meters per second, as confirmed again by the recent splitting of Comet West. In particular, Sekanina (1976) has shown that the traditional approach yields velocities that are much too large, because it neglects the differential nongravitational accelerations. This suggests extremely low rotational velocities at breakup and therefore extremely low tensile strengths and low densities.

Numerically, we do not know much about any cometary nucleus. The average error bar for our assessments of the density, the thermal conductivity, and the tensile strength of any cometary nucleus could easily extend to three orders of magnitude; for the mass, two orders of magnitude; for the albedo, a factor of four and for the diameter, a factor of two. As mentioned before, our ignorance partially stems from the fact that cometary nuclei are too tiny to show an extended image in any telescope, and that we have no experience whatsoever with large, friable and porous systems in the absence of gravity, or more exactly in gravity fields of the order of 10^{-4} g.

Several fly-bys, or better, rendez-vous with different cometary nuclei, including at least some that have never been vaporized by the solar heat before, that is, coming straight from the Oort's cloud for the first time, would dramatically improve our understanding, but such an ambitious program contains almost insuperable difficulties and is not likely to be achieved during the 20th century anyhow.

However, the proper use of the Space Shuttle and Spacelab capabilities could dramatically improve our understanding of the bulk properties of an icy conglomerate of frozen gases and snows in the absence of gravity, and help our interpretation of the first imaging of a cometary nucleus (probe to Comet Halley 1986).

TARGETS OF THIS PROPOSAL

It is proposed to use the Space Shuttle and Spacelab capabilities to improve our understanding of the formation mechanisms and of the bulk properties of icy conglomerates of dust, water snow, frozen gases, and solid hydrates of gases, in vacuum and in the absence of gravity.

For this purpose, a few specific targets would be aimed at, namely:

Existence and Bulk Properties

To explore the range of existence and to measure the bulk properties of low-density icy conglomerate systems. The stress would be put on the lowest density range that can be achieved, by building up extremely fluffy, porous and friable clusters of "fairy castles" with long snow whiskers. At first, the exploration could be limited to pure water snow, pure carbon dioxide snow, solid hydrates of carbon dioxide, and mixtures of these snows with fine silicate dust in different proportions. More realistic icy conglomerate mixtures are probably difficult to define,

right now, and are unlikely to reveal large differences in bulk properties. However, if serious differences in bulk properties reflect the chemical differences in the nature of the snows, more realistic icy-conglomerate mixtures could be used later, incorporating a better understanding of cometary chemistry, that is likely to be gained from vacuum-ultraviolet studies of bright comets from 1977 to 1981.

Accretion Mechanisms

One of the techniques capable to achieve these porous structures is the very low-velocity accretion of snowy and fluffy grains in vacuum into large low-density clusters. By the same token, this technique could explore one of the most important mechanisms that has apparently played a basic role in the origin of the solar system: the accretion of the primeval nebula into cometary-size objects. Accretion is often used theoretically in models of the origin of the solar system, but theorists use arbitrary coefficients (for example a "sticking factor" of unity) because basic experiments have never been done, in particular for the very low-velocity range that can be realistically achieved only in the absence of any gravity.

Sedimentation in Acceleration Field

Starting from an icy conglomerate of the lowest possible bulk density, it is also proposed to study its sedimentation in an acceleration field covering the range from 10^{-4} to 10^{-2} g (conveniently obtained by centrifugation at small angular velocities) in particular in order to better understand the inside of the cometary nucleus. Here the sedimentation would be used not only to simulate gravity fields of the largest nuclei, but also to simulate the weight of the outer layers and gain an insight on snow compression in their cores.

Irradiation by Direct Sunlight in Space

Finally, icy conglomerates of different bulk densities would be exposed to direct sunlight in space, and their vaporization rate, their morphological changes (structure, density, albedo) the appearance of a crust, its destruction by further vaporization, the dragging away of dust and ice grains by vaporizing gases, the consequences of the photoelectric effect due to the ultraviolet light on the snows would be observed and recorded by different means including motion pictures. It is to be remarked that each of these specific targets, but particularly the last one requires the presence and the feedback of a experienced scientist actively engaged in cometary research, and are therefore particularly well suited to Spacelab capabilities.

DISCUSSION

What is a significant zero-g experiment?

We do not know much about zero-gravity conditions. However, we can try to establish a few guidelines. An experiment becomes significant in a zero-gravity environment, either if, in the presence of terrestrial gravity, the experiment is totally impossible; or if possible, it seems totally impossible to extrapolate it to zero-gravity conditions.

This implies that the forces of gravity are so overwhelming as compared with the forces involved in the experiment, that these latter forces are considerably perturbed or hidden. But the forces of gravity are the weakest. They are large only when all the other forces either have too short a range (as nuclear forces) or have been saturated to a high degree, like most electromagnetic forces for macroscopic amounts of matter. Typically, drop coalescence can be studied in zero-gravity

environment, with much larger drops than in the presence of gravity, because the amount of matter grows with the cube of the drop size, whereas surface tension grows only linearly.

Standing in contrast, crystal growing is unlikely to be much influenced microscopically by the absence of gravity, because the bond forces between atoms or ions are many orders of magnitude larger than gravity, However, when many crystals are mixed together, bond forces are not present outside individual crystals, second-order effects become overwhelming, and the bulk properties of materials are no more predictable from the properties of single crystals. In particular, bulk properties of snow have not been and cannot be predicted theoretically from the strength or the growth properties of individual ice crystals. These bulk properties (like snow density, thermal conductivity, albedo, etc.), typically are those that are going to play an important role in the morphology of a cometary nucleus.

Extrapolation from Terrestrial Snows

Bulk properties of water snows have been studied for a large range of static and dynamic conditions, in terrestrial snowfields and glaciers, and some of the extreme properties observed (like very low bulk densities) may already represent the best simulation of low gravity conditions, that could be obtained in earth-bound experiments. In particular, the very small terminal velocities of snow flakes may be interpreted as simulating a free fall in vacuum in a very low gravity field. However, their bulk properties are likely to have been considerably influenced by the presence of air. Even if we neglect the influence of air on the growth and bulk density of the snow flake

itself, as well as on the complex mechanism of snowflake accretion and growth from snow crystals, it is clear that the bulk densities observed in snow fields have never been accurately connected to known terminal velocities because in particular they also depend very much on the air turbulence.

Besides, the properties of snows of frozen gases and of their solid hydrates, mixed up or not with fine dust, have never been observed. Even if an exhaustive program of carefully controlled experiments were initiated now, by using air to slow down flakes of such an icy conglomerate in the presence of terrestrial gravity, the validity of their extrapolation to very weak gravity conditions and to the range of all gravities smaller than g, would remain forever dubious.

Size and Geometry of Zero-g Experiment

The larger the amount of the icy conglomerate, the more significant the experiments can be; however, apart from the previous general considerations, we have absolutely no guidelines on their best size. It seems however obvious that they must be at least an order of magnitude larger than a large ordinary snowflake, so that the geometry would not perturb its accretion. The other extreme is set by the capabilities of Spacelab. Within these capabilities, the law of diminishing returns suggests to keep them as small as possible. Since the previous considerations set the general size range between 30 cm and 3m, we tentatively adopt the smallest size for this preliminary estimate, for instance an average of 30 liters of icy conglomerate, that is 3 kg with a density of 0.1 kg/liter. This corresponds to a cube of 30 cm side for the snow chamber, and suggests an approximate volume of less than one cubic meter

for the whole apparatus. Thirty experiments, with the icy conglomerate being lost in space each time, imply a 100 kg supply of water and gases, and the total mass of the whole equipment can therefore be probably kept easily within a few hundred kilograms.

Vacuum and Temperature

It is submitted here that most of the experiments should be done in the vacuum of space, most of the time in the shadow of Spacelab itself (or of the Shuttle) with the exception of the vaporization studies that would take place directly in the solar-light flux. Not only the absence of gravity, but also the actual conditions of space itself are searched for here; the steady-state temperature of snow vaporization in vacuum and in solar light is in the vicinity of 200°K and will be reached in a time of the order of a few minutes after exposing the icy conglomerate in the flux of solar light.

For the other experiments, the distribution of the accretion temperatures in the primeval nebula is unknown, but since the condensation of gases probably took place around or below 100°K, we can assess that the important range lies around that temperature. This temperature should typically be reached automatically in the shadow of Spacelab, by steady-state vaporization of the snows and also by varying the heat flow coming from Spacelab, either by insulation or if impossible, by special cooling with liquid nitrogen.

CONCEPTUAL DESCRIPTION OF THE EXPERIMENTS

Snow Making

We'll call hereafter "snows" or "snowflakes," those snows of water or of frozen gases or of hydrates, mixed or not with dust. Different

procedures to produce snowflakes and to accelerate them to small velocities, should first be developed in a ground-based equipment. A sprayer spraying mist in vacuum could be used; the mist droplets would vaporize quickly while they would retain a preferential velocity towards a cold wall where the vapor could condense into snow; alternately, ice crystals and whiskers could be grown slowly in a low-pressure environment, like the saturated pressure of water vapor at low temperature, and they would be propelled later in vacuum. The production of particulate beams as described by Murphy and Sears (1963) could also be used as condensation cores. We call "snow gun" the equipment that will be finally developed, although its form may bear no resemblance with a gun. Much attention should be given to the development of an effective snow gun. Low bulk densities may require the growth of numerous snow whiskers without many crystal dislocation, which in turn may require difficult conditions for full success.

Snow Accretion

In the final experiments, the snow gun expels snowflakes in the absence of gravity and with a controlled slow velocity, into a metal cylinder (for instance thin black-anodized metal; size 30 cm x 30 cm) closed at one end. Since the experiments are taking place in space, protected either by screens or by the shadow of Spacelab from the direct radiation of the sun, the steady-state temperature of the cylinder and of the snows is kept in the vicinity of 100°K, mainly by radiative losses, partially also by a small vaporization of the snows. The temperature is not very critical, although some insulation, or some slight refrigeration using liquid nitrogen may be used to diminish or compensate the heat

losses coming from Spacelab. The accretion of snow is stopped when the metal cylinder is approximately filled up.

Mass, Volume and Thermal Measurements

A measurement of the mass of the snow filling the cylinder is needed. Since vapor losses are possible to space, a measure of the mass transferred is not accurate enough. It is proposed that the moment of inertia of the snow be measured, for instance by measuring the torque needed to accelerate the slow centrifuge described later for the sedimentation experiments, or by using the imbalance of the centrifuge in a feedback system also cescribed later. This implies that the cylinder be permanently incorporated within the centrifuge.

Other bulk properties of the icy conglomerate are also measured in situ, including total volume (by approximately filling up the cylinder, and integrating numerically the outer surface from photographs; alternately, a cutting blade could remove the snow excess protruding from the cylinder); thermal conductivity (by heat transfer thorugh a known temperature gradient), and tensile strength as described later.

Sedimentation and Cohesive Strength

The sedimentation of the icy conglomerate to higher densities under accelerations of 0.1 cm sec^{-2} to 100 cm sec^{-2}, is measured by centrifugation of the chamger. Different systems can be used to establish the moment of inertia and the mean radius of gyration of the snow during centrifugation. For instance, the out-of-balance introduced by the sedimentation of the icy conglomerate may be used in an electronic feedback system, to move a counterweight whose position will define the moment of inertia; the two moments will be solved for the girating radius and the mass of the snow.

The cohesive strength of the snows may also be measured after turning the cylinder 180° in the direction perpendicular to the centrifuge axis. The centrifugation rate is then slowly accelerated until the main body of snow splits into several chunks that will be ejected into space. For this purpose, the cylinder walls, but not the bottom--should be treated or covered with teflon.

Sublimation in Sunlight

The sublimation in sunlight is photographed by a movie camera, with the cylinder in the same position as before. Proper screens are removed or the rotation of Spacelab is used. The photoelectric effect of sunlight on the snows can be measured by the current collected by a wire grid located in front of the cylinder opening.

Thermal Conductivity

The technique used by West and Fountain (1975), to measure the thermal conductivity of lunar fines, could probably be used without much modification to measure the thermal conductivity of snows in the centrifuge.

DEVELOPMENT OF THE EQUIPMENT

It is clear that the previous description is conceptual only and that a long path must still be covered towards the development of a working equipment; during this development, it will become possible to make several experiments (although on higher density snows) in a cooled vacuum tank, and in the terrestrial gravity field. The equipment could be developed in any laboratory that possesses already the basic equipment needed, in particular a vacuum tank that is large enough; for instance, this could be done at Marshall Space Flight Center.

The Snowgun

Much attention must be devoted to the technological development of an effective snowgun: it is likely that several ideas should be tried and compared. However, in order not to stop the development of the centrifuge and its testing in a vacuum tank, a crude snowgun spraying water mist in vacuum would probably work. Even more simply, a nozzle introducing water vapor at a constant rate, controlled by a leak valve, would be satisfactory for early experiments in the terrestrial gravity field.

The Centrifuge

The development of the centrifuge does not seem to set any serious problem. A preliminary drawing is found in Figure 1. The water vapor A or the carbon dioxide A' (to be used in the first experiments) are introduced through the axis of the centrifuge D and injected towards the cylinder bottom F where it condenses as snow. After F is filled up with snow, the centrifuge (Motor D' coupled with belt and pulleys) is used to introduce an artificial gravity. Approximately 10 cm/sec^2 = 10^{-3} g is achieved with 5 rpm, and 0.1 g is reached for 60 rpm; therefore a range from 1 to 100 rpm would probably be quite satisfactory. Counterweight I is moved along screw J by motor G to remove the imbalance of the system, felt by piezoelectric sensors on ends of axis D and used in a feedback loop. Positions of counterweight I can be used to deduce the moment of inertia of the snow in sedimentation experiments. Motor H is used to turn cylinder with opening outside. Centrifugation is then used to measure tensile strength of snow, by observing its splitting into large chunks.

The different functions of the centrifuge can be tested in vacuum in terrestrial conditions, and tensile strength and sedimentation of higher density snows could already be studied, yielding data that could be significant per se, as well as compared later with those in zero gravity conditions.

Measurement Techniques for Other Physical Properties

The final choice of those other bulk properties of the snow that are going to be measured, will depend on the development and convenience of the different possible techniques. Mass and volume measurements have been already described tentatively, since they constitute the basic data to which all other measurements will be related.

The cohesive strength also seems one of the most fundamental data for which order-of-magnitude measurements would already bring important clarification on the splitting of the cometary nucleus. The proposed inertial splitting by centrifugation probably is sufficient for the type of data requested.

Heat transfer by thermal conductivity could probably be studied by measuring, at the steady-state, the temperature gradient established in the snow cylinder, by natural heating of one side by the sunlight, and natural radiative cooling of the (black) bottom of the cylinder towards space. From six to ten thermocouples, strategically placed within the cylinder, would be sufficient to study this thermal gradient at different points. A measurement of the albedo may not be as fundamental, because it is unlikely that very low densities would change the surface properties if the icy conglomerate. However, the geometric albedo, as seen from the camera, could be deduced before and at different times during the

vaporization, hopefully observing inhomogeneities and the appearance of a crust. A target with areas of known albedo should therefore be included in the camera field.

CONCLUSIONS

This report represents a first step towards a critical evaluation of those possible experiments in a zero-gravity environment, that could simulate the accretion, the sedimentation and the decay of cometary material in space. It assesses first the nature and the range of our ignorance on the bulk properties of cometary material. It gives the conceptual description of an experiment, and describes concrete suggestions on the possible development of the equipment, whose core would be a slow velocity centrifuge.

The next step would be to actually develop the Centrifuge, the Snowgun and the Measurement techniques, and test them in a vacuum chamber and at a liquid nitrogen temperature, but in presence of the terrestrial gravity. Measures of icy conglomerates in the density range 0.1 to 0.6 g cm^{-3}, in this equipment, could already yield rather significant results in an earth-bound laboratory, but the density range between 0.1 and 0.001 g cm^{-3} would probably be accessible in a zero gravity environment only. It is likely that even very crude results on the range of existence of low-density and low cohesive strength conglomerates of snow and dust, would have an important significance for our understanding of the physical nature of the cometary nucleus.

REFERENCES

Delsemme, A. H. (1976), Trans. I.A.U. XVI A part 1, 61, Reidel publ.

Delsemme, A. H., and Combi, M. R. (1976), Astrophys. J. 209, L149 and L153.

Murphy, W. K., and Sears, G. W. (1963), Preprint, Research Division, General Dynamics/Electronics, Rochester, N.Y.

Sekanina, Z. (1976), Preprint Series No. 616, Center for Astrophysics, Cambridge, Mass.

West, E. A., and Fountain, J. A. (1975), Rev. Sci. Instruments, 46, 543.

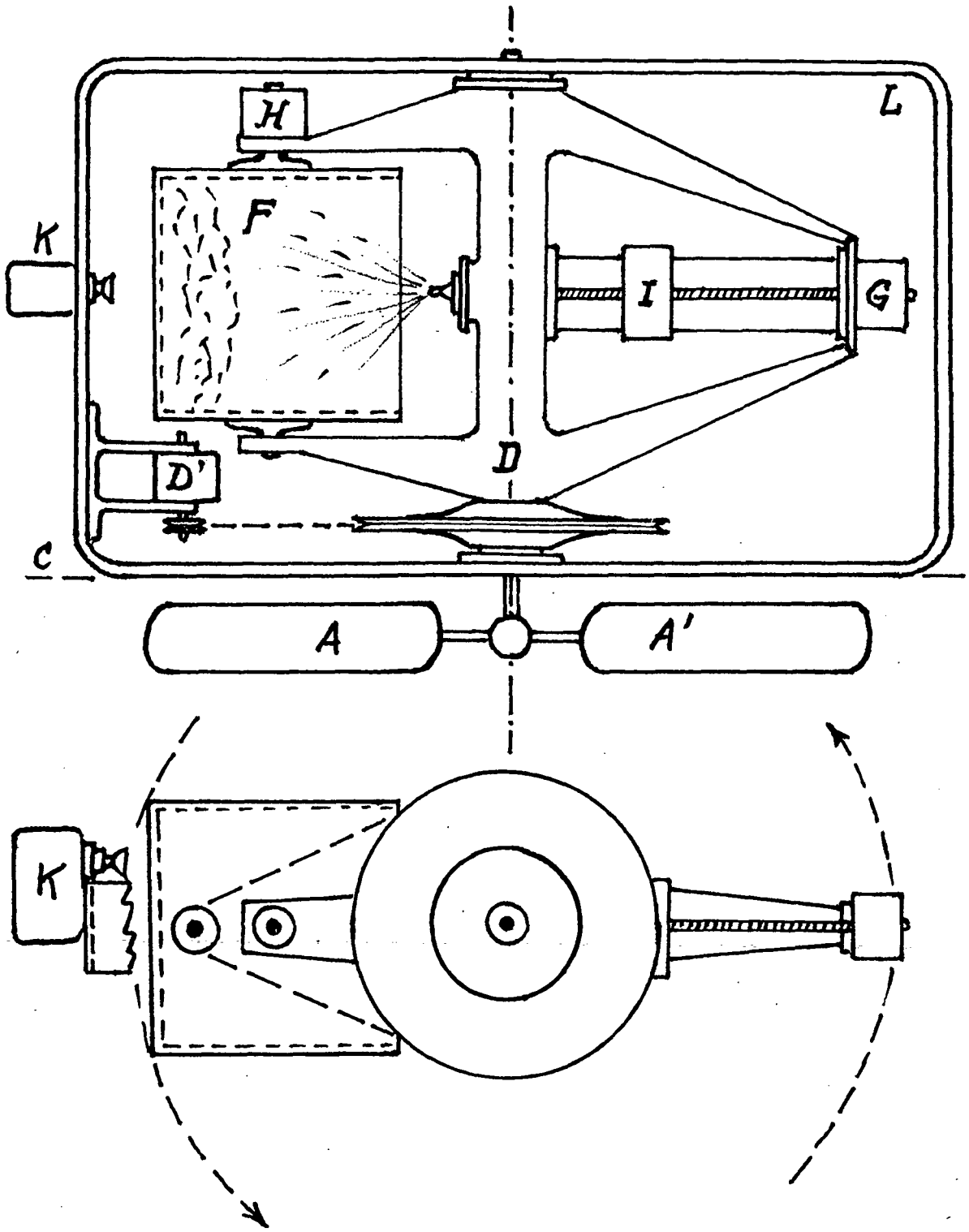

Figure 1.

SOLAR PHOTOCHEMISTRY USING THE SPACE SHUTTLE

William M. Jackson
and
Joshua Halpern
Department of Chemistry
Howard University
Washington, D.C. 20059

ABSTRACT

A continuing source of difficulty in cometary astrophysics is understanding the origin of C_2, C_3, NH and CO^+ species in comets. We propose an experiment to investigate these problems by continuously releasing suspected parent gases from the space shuttle and using a dye laser to selectively excite fragments produced as a result of solar photochemical decomposition of the molecules. The backscattered fluoresence will be gathered by a telescope, spectrally filtered and measured as a function of time after the laser pulse. We show that for reasonable estimates of the dissociation rate the expected signal is roughly described by $N_p(t) = N_o \exp[-t/\tau]$ for $t/\tau<10$, τ being the radiative lifetime of the daughter species, and typically of the order of 10^{-6} to 10^{-7} seconds. N_p is the number of photons reaching the detector per channel of width τ . N_o is calculated to be $\sim 10^6$. Thus the signals to be expected per pulse can be measured by analog techniques and the success of the experiment seems highly probable.

Introduction

A continuing source of difficulty in cometary astrophysics is understanding the origin of C_2, C_3, NH, and CO^+ species in comets. The C_2 and the NH radicals present difficulties because the most likely parents, ammonia and acetylene, do not form these radicals in a single photochemical process at the available solar wavelengths.[1] Further, since the observed emissions originate from triplet levels of the radicals it can be shown[1] that photodissociation through absorption of a single photon would violate selection rules and thus be unlikely to occur. The only currently reported single step photolysis source[2] of the C_3 radical is a minor product in the laboratory photodissociation of HC_2CH_3.

Substantial progress has been made in applying the results of laboratory studies to increase our understanding of photochemical processes that can occur in comets. Even with the reported progress and the prospects for future detailed studies there will always be difficulties associated with translating the laboratory results to the solar environment outside the earth's atmosphere. First, in the space environment there are no walls to complicate the interpretation of the results. Secondly, the time between collisions is orders of magnitude longer than it is in the laboratory, so that slow secondary processes can compete with the direct chemical reaction of these very liable species.

An ideal experiment would involve the release of suspected parent molecules one astronomical unit away from the sun in the interplanetary media. This ideal condition can not be met even in the proposed experiment, since the space shuttle does not reach interplanetary altitudes; it does of course operate at one astronomical unit.

In this proposal it will be shown that using the space shuttle one can obtain much of the needed information about photochemical processes that occur in comets by doing time resolved studies of the laser induced emission from the solar photodissociation fragments.

Proposed Space Shuttle Experiment

The proposed experiment consist of continuously releasing a gas from the space shuttle and using a pulsed tunable dye laser to selectively excite the fragments produced as the result of solar photochemical decomposition of the molecules. The collision time between molecules at the space shuttle's altitude is of the order of 13 seconds, thus a typical molecule will travel roughly 13 km before colliding with the ambient background gas. Any product formed by dissociation must be detected in times short compared to the collision time in order to insure that none of the observed products have been formed by collision with the ambient gas. Detection of the induced fluorescence as a function of both time and the laser wavelength will yield the rate of production of the species formed, the identity of the species, and the quantum mechanical state the species is formed in.

The spectra in Figure 1 is an example of the type of spectra that one can expect to obtain using laser induced fluorescence of the unstable species. This particular spectra is for CN radicals, but comparable spectrum may be expected for C_2, C_3, NH, and CO^+ species. It is important to be able to scan over a wide wavelength range, since a priori, we have no way of knowing exactly which rovibronic levels of the molecules are produced by the photodissociation process. In fact, determination of the rovibronic levels that the cometary radicals are produced in by solar radiation is valuable information and one of the aims of this ex-

periment. For example, this information can be used in explaining anomalies observed in the cometary spectra of the C_2 radical. The spectra of these radicals are well separated, so that there will be no problems of interpretation caused by overlapping lines and bands.

The 13 second exposure time of the parent molecule to solar radiation is short compared to the times that occur in comets. The calculated photochemical lifetimes for NH_3, C_2H_2, and HC_2CH_3 in cometary bodies at one astronomical unit have been reported as 2000, 5000, and 5000 sec respectively.[1] Thus one in 150 to 400 is a crude estimate of the fraction of the parent molecules decomposed during a 13 second exposure time. The success of the proposed method for studying the photochemistry of parent molecules relies on the extreme sensitivity of the laser technique. It has been reported[3] that in the laboratory one can detect densities as low as 10^5/cc or about 10^{-14} atm. We propose to use this high detection sensitivity to determine the mechanism for solar photodissociation of the proposed parent molecules.

Calculated Signal Strengths

In any fairly sophisticated experiment one should make a good estimate of its probable success and an evaluation of what will be learned if no signal is detected with all of the systems functioning. If no signal is detected, then one can conclude that acetylene, propyne, and ammonia are not the photochemical precursors for C_2, C_3, and NH in comets. This in turn would strongly suggest that collisions are the primary production mechanisms for these species or that some exotic molecule is the parent of these radicals. If forced to this last alternative then we must conclude the enviroment where comets are formed is stranger than is

currently believed.

The density of radicals formed from the photodissociation of a parent molecule has been computed by Haser.[4] The equation[5] he obtained for a freely expanding gas is,

$$(1) \qquad \rho = \rho_o(u_o/u_1)(r_o/r)^2\beta_o/(\beta_1-\beta_o)(\exp(-\beta_o x) - \exp(-\beta_1 x))$$

In this equation ρ is the density of the daughter molecule and ρ_o, the number density of the parent molecule. The β is the inverse of the mean distance traveled before dissociation which is the product of the flow velocity u, of the molecule times its lifetime τ, at one astronomical unit. ρ_o is the number density of the parent molecule, i.e., at the distance r_o. While it will not be possible to put a true artificial comet in space this equation can be adapted to our use if it is realized that r_o refers to a characteristic dimension of the emitter, such as the gross dimensions of a linear array of holes through which the gas is allowed to effuse. This equation then gives the lower limit of the radical density. If the parent molecules are released in such a way that one obtains a more directed flow, such as with nozzels[6] or multicappilary arrays,[7] the observed radical density could be much higher.

We can simplify the above equation since the argument of the exponential will be small for values of x less than 13 kilometers and $u_o\tau_o$ is much less than $u_1\tau_1$. There is both theoretical and observational evidence that the latter assumption is valid. O'Dell and Osterbrook[8] have determined the values of these products for the C_2 radical and found that they differed by an order of magnitude. The symmetry of Haser's equation does not, however, allow one to determine which of these values are larger. Jackson[1] in a recent review has calculated the photochemical lifetime of acetylene and has shown that it is of the order of 5000 seconds.

This is in reasonable agreement with the lowest determined lifetime of 10^4 sec of O'Dell and Osterbrook. The highest lifetime determined by these two authors is 100,000 seconds, forcing one to conclude that this is the lifetime of the C_2 daughter. The NH, C_2, and CN radicals probably all have lifetimes that are longer than their parents, since the suspected parent molecules will have a weaker bond than the daughters and therefore require longer wavelengths for photodissociation. The solar intensity[9] rises rapidly as the wavelength is increased from 100 nm to 300 nm, which will substantially reduce the photochemical lifetime of the parent relative to the daughter. Assuming that the daughter and parents have about the same flow velocities then β_o will be much greater than β_1.

The assumptions given in the above paragraph can be used to simplify to,

$$(2) \qquad \rho = \rho_o (r_o^2 / u_o \tau_o) \quad (x/r^2)$$

The laser pulse width is much smaller than the radiative lifetime of the excited radicals so that only a negligible fraction of these radicals will radiate while the laser is on. Under these circumstances the rate of laser excitation for an optically thin gas in which stimulated emission may be neglected can be calculated from equation 3.

$$(3) \qquad d\rho^* / dt = \sigma I \rho$$

In this equation ρ^* is the number density of the excited state, σ is the absorption coefficient of the radical, and I is the laser intensity in photons /cm^2 sec. Equation 3 may be multiplied by the cross sectional area, A_o, of the laser beam to yield an expression for N^* the number of excited molecules produced per unit path per sec.

(4) $dN^*/dt = \sigma I \rho A_o$

This differential equation only applies when the laser is on. Assuming the laser intensity is constant for a time t_o, then equation 4 may be integrated to yield.

(5) $N^* = I\sigma\rho A_o t_o = E\sigma\rho / h\nu$ where: E=energy of laser pulse
ν=laser frequency

When the laser pulse has passed a segment of length dr the excited molecules decay at the rate

(6) $$\frac{dN^*(r)}{dt'} = \frac{N^*}{\tau} = \frac{1}{\tau}\,\frac{E\sigma}{h\nu}\,\rho(r)\,\exp(-t'/\tau)$$

where τ is the radiative lifetime (in this experiment the effect of collisions upon the de-excitation of the molecules is negligible), and t', the local time at the segment centered about r, is less than $t-t_o$ and greater than $2r_o/c$, t being the time as measured at the detector. The number of photons received per centimeter per second by the detector from this segment is the rate of emission multiplied by the solid angle of the segment subtended by the detection system or

(7) $$\phi(r,t)\,dr\,dt = \frac{1}{\tau}\,\frac{E\sigma}{h\nu}\,\frac{A\rho(r)}{4\pi r^2}\exp\left[-(t - t_o - 2r/c)/\tau\right] dr\,dt$$

$\phi(r,t)$ is thus the contribution of a segment at r, where $c(t - t_o)/2 > r > r_o$, to the signal at time t. The rate at which the photons reach the detector from all excited molecules, $dN_p(t)/dt$ is, from eqs. (2), (5), and (7)

$$(8)\qquad \frac{dN_p(t)}{dt} = \Phi_o \left\{ \int_b^a dr\, \frac{(r - r_o)(t - 2r/c)}{r^4} + \int_{r_o}^{b} dr\, \frac{r - r_o}{r^4} \exp[-(t - t_o - 2r/c)/\tau] \right\}$$

where

$$\Phi_o = \frac{1}{\tau} \frac{E\sigma}{h\nu} \rho_o \frac{r_o}{v_o \tau_o} \frac{A}{4\pi} \; ; \; a = ct/2; \; b = c(t-t_o)/2$$

A is the area of the telescope.

The first integral is the contribution of the segment overlapped by the laser pulse and equals

$$(9)\qquad L = \frac{2t_o}{c^2 t^2} \left(1 - 2\frac{r_o}{ct}\right)$$

Now t_o is short compared to τ and all other significant times considered in this calculation and so as $t_o \rightarrow o$ L disappears. This must happen since in order to derive eq. (5) we had assumed that no excited molecules will fluoresce during the time it takes for the laser pulse to pass through the region dr about position r. The integral L is small compared to B and may be neglected.

The second integral

$$(10)\qquad B = \frac{8}{3}\frac{r_o}{c^3 t^3} - \frac{1}{3r_o^2} + \left(1 - \frac{2}{3}\frac{r_o}{ct}\right) e^{-t/\tau} \left[\frac{1}{2r_o^2} + \frac{1}{c\tau r_o}\right] + \frac{2}{c^2\tau^2}\left[Ei\left(\frac{t}{\tau}\right) - Ei\left(\frac{2r_o}{c\tau}\right)\right] - \frac{2}{c^2 t}\left[\frac{1}{t} + \frac{1}{\tau}\right]$$

where Ei (x) is the tabulated exponential integral. This can be simplified

by neglecting terms where appropriate ($2r_o/c\tau$ for example) and by defining $\alpha(x)$ as

$$\alpha(x) = \frac{Ei(x)}{\left[\frac{e^x}{x}\right]} \qquad x>2 \; ; \; \lim_{x\to\infty} \alpha(x) = 1$$

Then

$$(11) \qquad B \cong e^{-t/\tau}\left[\frac{1}{6r_o^2} + \frac{1}{c\tau r_o} + \frac{2}{c^2\tau^2}\ln\left(\frac{c\tau}{2r_o}\right)\right] + \frac{2}{c^2\tau t}\left[(\alpha(\tfrac{t}{\tau})-1) - \frac{t}{t}\right]$$

The gatewidth, of the detection system t_g, the radiative lifetime, τ, of the laser all limit the ultimate depth resolution ΔR of a LIDAR experiment. Kiddal and Beyer have defined ΔR by

$$(12) \qquad \Delta R \equiv (c/2)\ (t_o + \tau + \tau_g)$$

The radiative lifetimes of the radicals that will be studied in the present experiments is much greater than both t_o and τ_g so that ΔR is effectively $(c\tau)/2$.

The number of photons, N_p, reaching the detector per pulse in the interval from t to $t + t_g$ is from eqs (8) and (11)

$$(13) \qquad N_p(t) = \frac{t_g}{\tau}\ \frac{E\sigma}{h\nu}\ \frac{A}{4\pi}\ \frac{r_o \rho_o}{v_o \tau_o}\ B(t)$$

All of the quantities in this equation are known or can be calculated from known quantities. The only quantity that presents any particular difficulty

is σ, the absorption coefficient of the radical that one would like to detect.

The absorption coefficient for a single line is defined[10] by the following equation,

(14) $$I(\nu)I_o = \exp[-k\nu x] = \exp[-\sigma\rho_A x]$$

but $$\int k\nu d\nu = (h\nu_o/4\pi)\, B_{nm}\, \rho_A(1-\rho_{A*}/\rho_A)$$

where: B_{nm} = Einstein B coefficient for the transition

ρ_A = density of molecules in the J" rotational level

ρ_{A*} = density of excited molecules

For a line limited by Doppler broading one can integrate over the line profile and solve for B_{nm} in terms of the oscillator strength f. This then will give[10]

(15) $$\sigma' = k_o/c_A = [2/(\Delta\nu_D)][\ln 2/\pi]\ 1/2\ [\pi e^2/mc]f$$

This equation is valid for an atomic line, however for a molecular line f must be replaced[11] by $f_{nm}q_{v'v''}\, S_J/(2J'' + 1)$. The σ' can be converted to an absorption coefficient, σ, defined in terms of the total number density by multiplying by the fraction, $F_{J''}$, of the molecules in a given J" level and by the ratio of $\Delta\nu_D/\Delta\nu_l$ to account for the fact that the line width is determined by the laser line width.

(16) $$\sigma = (2/\Delta\nu_D)(\Delta\nu_D/\Delta\nu_l)\ [\ln 2/\pi]\ 1/2\ [\pi e^2/mc][f_{nm}q_{v'v''}\, S_J/(2J'' + 1)]F_{J''}$$

The oscillator strengths f_{nm}, Franck-Condon factors $q_{v'v''}$, and rotational line strengths S_J for the C_2 and NH radicals have all been measured so that they

present no particular difficulty in evaluating σ. The fraction of the molecules that are formed in a given J" level will be more difficult to determine since it is well known that free radicals are not necessarily rotationally equilibrated when produced by photodissociation. Recent experiments by the author[12] and his co-workers have shown that at least for some CN parent compounds the CN radicals initial rotational distribution may be characterized by a Maxwell-Boltzman distribution function with a high rotational temperature. This phenomena is illustrated in the plots in Figure 2. In light of these experiments it appears that $F_{J"}$ may be calculated from the Maxwell-Boltzman distribution function if a high rotational temperature is assumed. We will use this approach and assume a rotational temperature of 5000°K.

We are now in a position to estimate N_p for a given J" level of the C_2 or NH radicals using measured constants for these radicals along with assumptions about the experimental configuration. Figure 3 is a schematic drawing of how the laser transmitting and receiving telescope might look. We will assume that the receiving telescope is approximately 10" in diameter. We will further assume that the ρ_o at r_o is 10^{13} mole/cm^3 and that $r_o \sim$ 250 cm. Both of these latter quantities could be obtained with a long arrays of supersonic nozzels[6] or multicappillary arrays[7]. If either of these devices are used to release the gas then it will minimize the amount of gas that has to be carried on the space craft and released for the experiment.

The density at r_o was obtained by the following consideration: in a gas release system that is 3 cm high and 450 cm long the area from which gas is released is 1350 cm^2. Assuming we can carry 1.35×10^4 gms of gas and that the flash lamp will only last for 10^6 shots, this will limit the observation time to about 28 hours for the pulse rate of 10 cps. The flux of gas released

if the average molecular weight is 30 AMU is 2×10^{18} molec/cm^{2}sec corresponding to a density of 4×10^{13} molec/cm^3.

Figure 4 gives the results for the photons arriving at the telescope per laser shot for the maximum J" level of the NH and C_2 ground states. This figure shows that one can easily detect the resonance backscattered photons from the NH and C_2 radicals produced by the assumed solar photodissociation of either C_2H_2 or NH_3. Further there is a great deal of flexibility in the proposed system, since higher ρ_o may be obtained by releasing higher fluxes of the gas. Higher fluxes would permit us to look for even slower photodissociation processes and put firmer limits on the lifetimes of C_2H_2 and NH_3 in the solar radiation field.

The results in Figure 4 assume dye laser energies of the order of 10 millijoules per pulse of 0.1 A°. Recently, Davis and co-workers[13] have reported laser energies of this order of magnitude and bandwidths an order of magnitude smaller than 0.1 A° The laser they used to pump the dye laser was a frequency doubled Nd-Yag laser made by ILS Co. The advantage of this laser is that it can be supplied to military specifications so that it should be easy to certify for flight work. The dye laser that we need should be obtainable with a pump laser similiar to the one reported by Davis and co-workers. The actual design of the dye laser will have to be investigated since we want larger bandwidths and will want scan over larger wavelength ranges.

Conclusion

In the present paper we have shown that a gas release shuttle experiment can be used to determine if the C_2 and NH radicals are produced by the solar photodissociation of NH_3 and C_2H_2. The experimental detection of the

radicals can be accomplished with a Nd-Yag pumped dye laser. The Nd-Yag laser can already be supplied to military specifications and further development of dye laser appears to be technically feasible.

References

1. W.M. Jackson, J. of Photochem., 5, (1976), 107.

2. L. Stief, Nature, 237 (1974) 45.

3. W.M. Jackson, J. Chem. Phys., 59, (1973) 960.

4. L. Haser, Liege Inst. Astrophys. Rep., 394, (1957).

5. F.L. Whipple and W.F. Huebner, Ann. Rev. of Astron. and Astrophys., 14, (1976) 143.

6. J.B. Anderson, R.P. Andres, and J.B. Fenn, Adv. in Chem. Phys., 10, "Molecular Beams," Ed. J. Rozz, Interscience Publishers, New York (1966) 275.

7. J.G. Giordmaine and T.C. Wang, J. of App. Phys., 31 (1960), 463

8. C.R. O'Dell and D.E. Osterbrook, Ap. J, 136 (1962) 559.

9. W.M. Jackson, Molecular Photochem., 4, (1972), 142.

10. A.C.G. Mitchell and Mark W. Zemansky, "Resonance Radiation and Excited Atoms," Cambridge Univ. Press, (1971) 92.

11. G. Herzberg "Spectra of Diatomic Molecules," Van Nostrand Reinhold Co., (1950) 382.

12. M.J. Sabety-Dzvonik, R.J. Cody, and W.M. Jackson, Chem Physics Letters, 44, (1976) 131.

13. A. Moriarty, W. Heajss and D. Davis, Optics Comm., 16, (1976) 324.

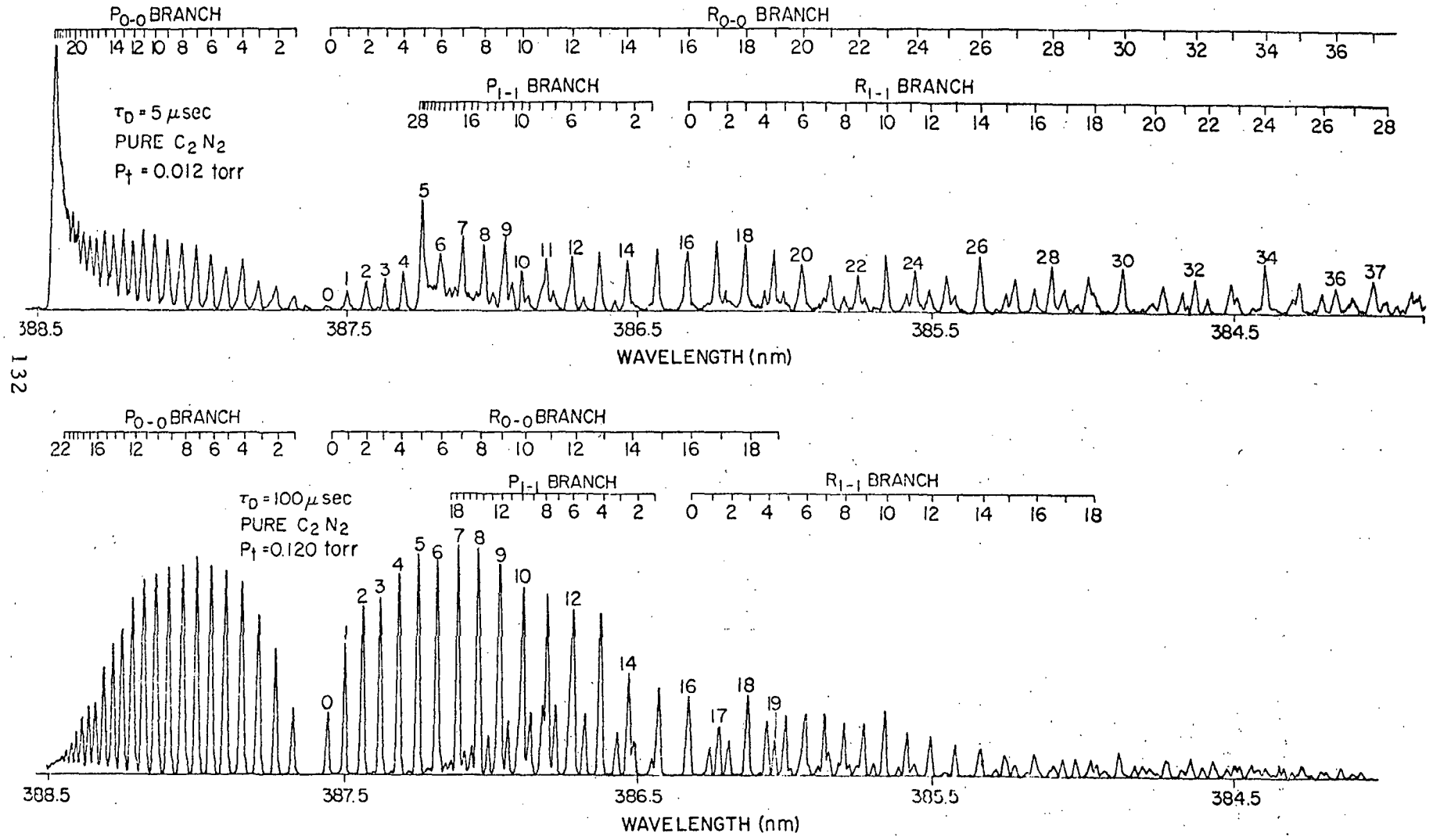

Figure 1. Laser excitation spectrum of the CN($B^2\Sigma \longleftarrow X^2\Sigma$) Violet System. The dye laser bandwidth was 0.01 nm.

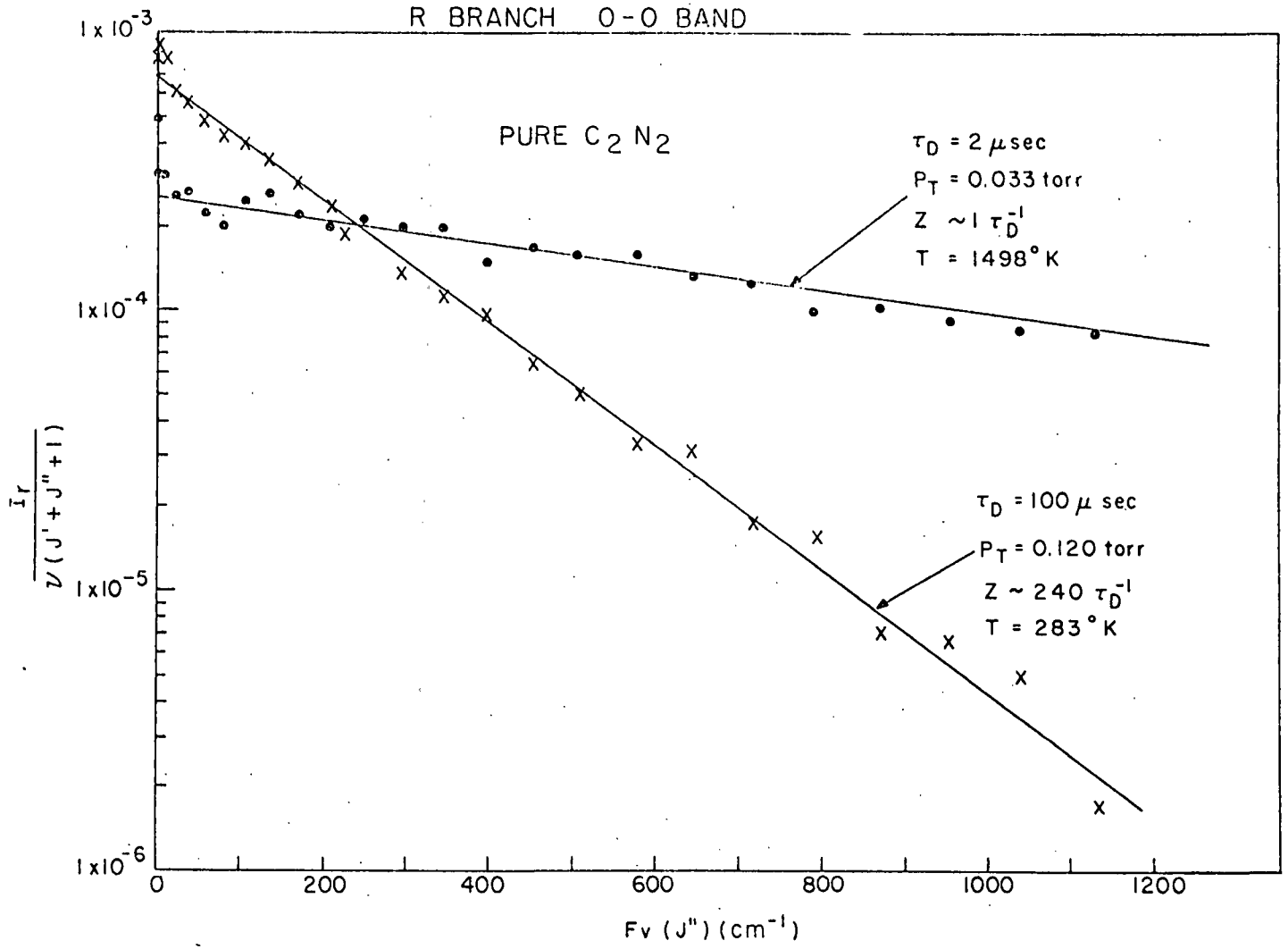

Figure 2. Normalized intensity probability versus rotational energy for the R branch 0-0 band in the CN ($B^2\Sigma \leftarrow X^2\Sigma$) violet system for two different delay times between the photolysis flash and the analyzing laser. For τ_{Delay} = 2 μsec the rotational temperature of the CN($X^2\Sigma$) molecules was 1498 K (●). For τ_{Delay} = 100 μsec the corresponding temperature was 283 K (-X).

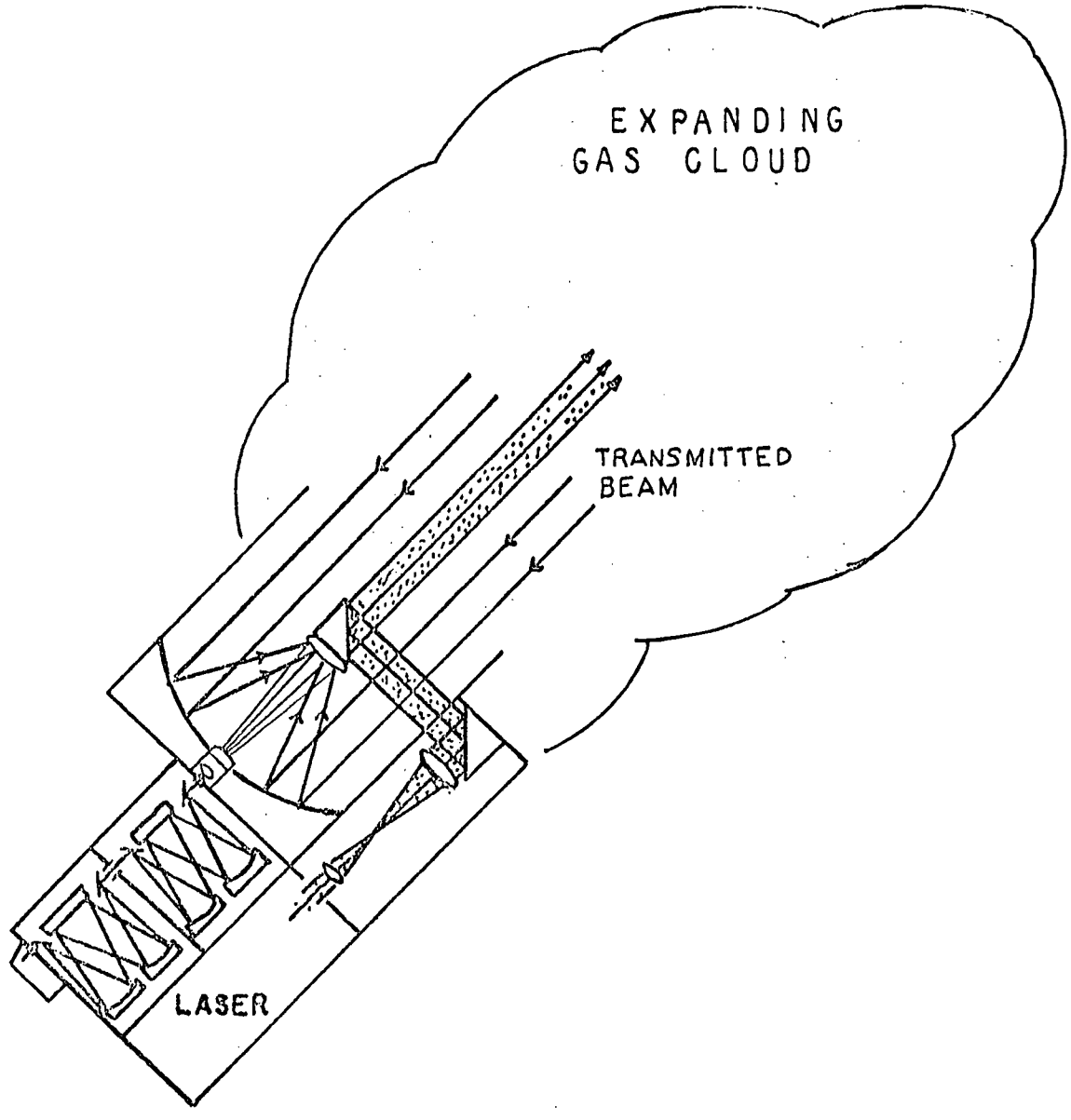

Figure 3. An example of the kind of LIDAR optical system proposed for this experiment.

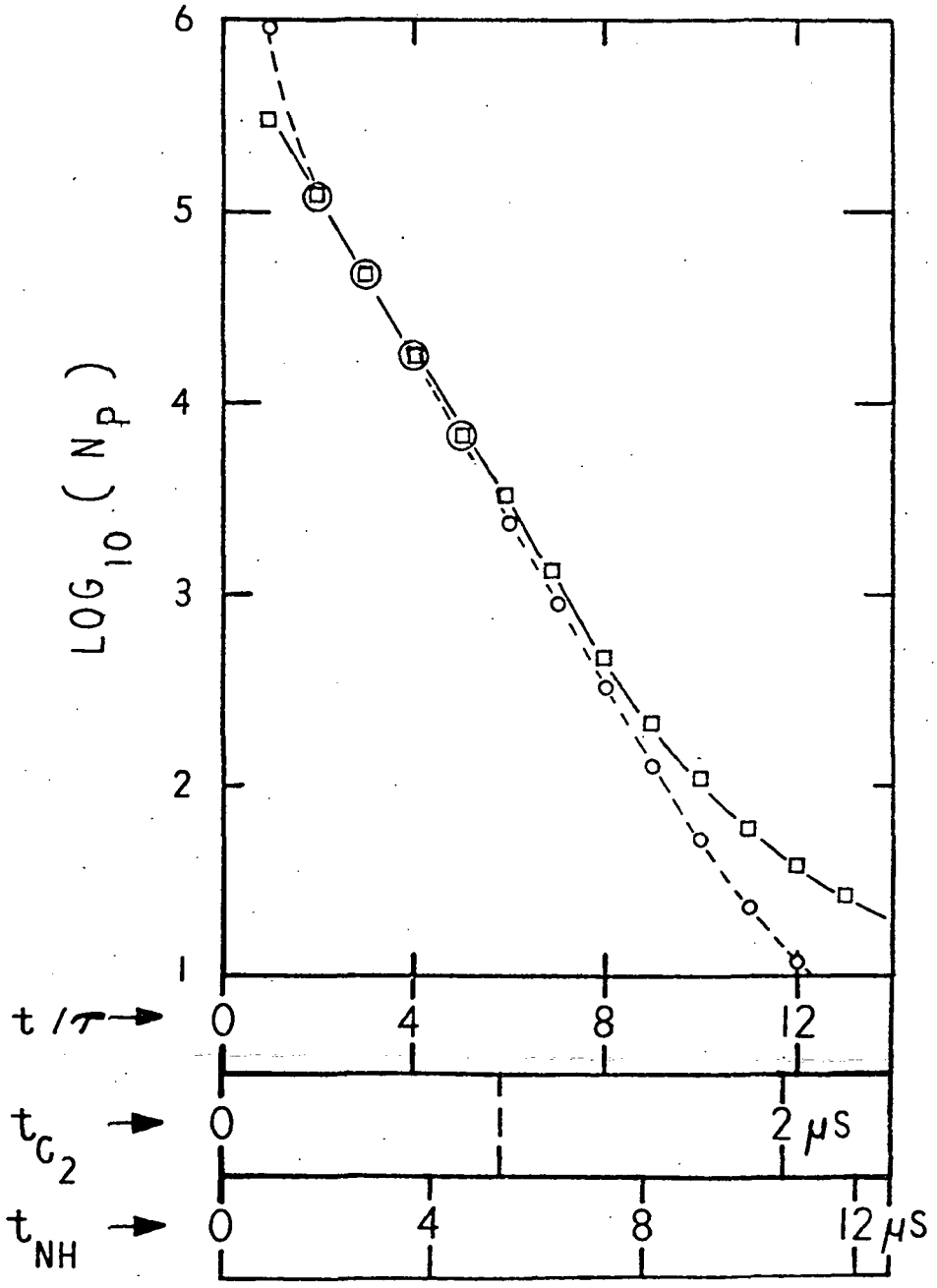

Figure 4. The calculated number of fluorescent photons striking the detector as a function of time after the laser pulse. The first time scale (t/τ) refers to the signals from both (□) C_2 and (o) NH. The two lower absolute time scales refer to the labeled radical. The signal, N_p, is per channel where the channel width equals τ.

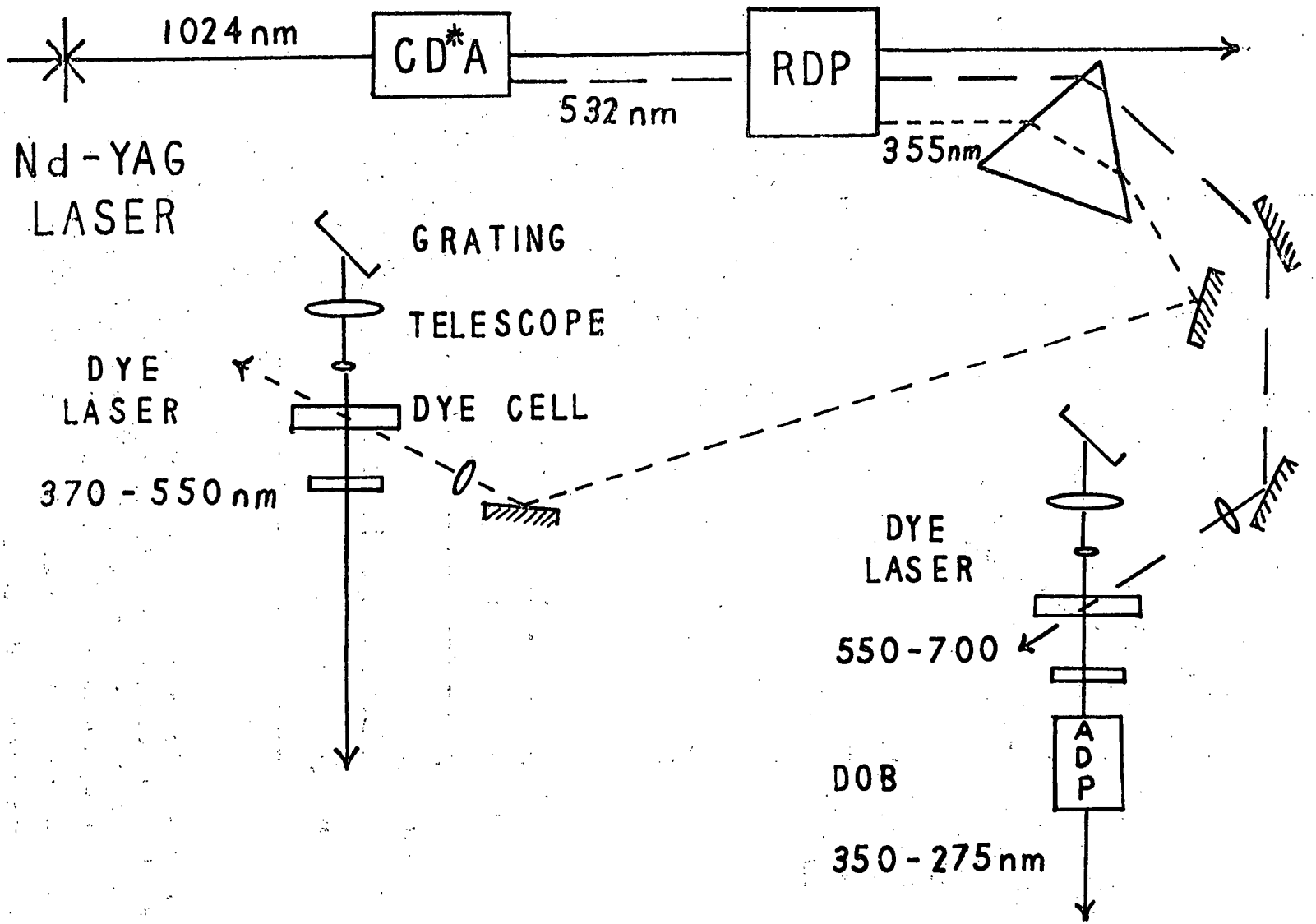

Figure 5. A possible configuration for the proposed Nd-Yad pumped doubled dye laser system.

D6

Cometary Nucleus Release Experiments and Ice Physics

W. F. Huebner
Theoretical Division
University of California, Los Alamos Scientific Laboratory
Los Alamos, New Mexico 87545

Some physical and chemical processes involved in the evaporation and sublimation of mixtures of frozen gases are discussed. Effects of zero gravity, vacuum and solar radiation are emphasized. Relevant experiments that can be carried out with the aid of the Space Shuttle are proposed.

The mass of a comet nucleus is of the order of 10^{10} to 10^{12} tons. An ice release experiment from the Space Shuttle will involve several 10 kg up to possibly about 10 tons. Since the rate of sublimation (i.e., vaporization) per unit surface area is the same for an artificial comet nucleus as for a real nucleus the density of the vapors escaping in three dimensions is $n(r) \approx n_0 \cdot (R/r)^2$. Here r is the distance from the center of the nucleus of a test volume of gas and n_0 is the gas density just above the unclear surface, it is independent of the nuclear radius R. The half life against dissociation and ionization of the molecules, τ, depends primarily on the solar radiation. Thus the range of the molecules $r_0 = v\tau \sim 10^4$ km is about the same for a real and for an artificial comet since the escape velocity is about the same. In an artificial comet ion and radical chemistry will have only a very minor effect because the density of the active constituents is too small. Similar arguments have been presented by Öpik (1965) on the brightness of an artificial comet, and by Jackson and Donn (1968). A new factor would be: coordinated radio observation from the ground of the developing coma of an artificial comet. To fill the half-power beam width of a, say 36 ft, radio telescope with a column density of $\sim 10^{13}$ molecules per cm^2 at a line transition wavelength $\lambda \sim 1$ cm requires about 10 tons of ice in a spherical shell of several meters in diameter

and a few cm thickness. The parameters depend also on the altitude of the release, the dipole moment of the molecule and the length of desired observing time.

The main area of my discussion will be concerned with the ice surface and the space just above the surface, i.e., the physics and chemistry of ice sublimation. A surface area of $1m^2$ or less is sufficient in almost all of the proposed experiments. Four categories should be cosidered:

1. Ground-based laboratory experiments. These are done in a vacuum, with artificial light and in the presence of gravity.
2. Onboard experiments on the Shuttle. Here experimental environment are vacuum, possibly direct solar radiation but with truncated ultraviolet radiation and "zero gravity".
3. Release experiments from the Shuttle. The residual earth's atmosphere may not provide a vacuum as ideal as in the above two categories, but the solar radiation spectrum is complete and gravity is "zero". Ground-based observations, e.g., with radio telescopes, should be coordinated.
4. Theoretical support, i.e., interpretation of the observations and modeling, should be closely coordinated with the above three categories.

Solar wind interaction cannot be incorporated unless a release is made above the magnetosphere.

Care should be taken that no clear ice, i.e., without air (gas) bubbles is used. Such ice is "black", it does not scatter light. Cometary ice probably has a flaky or grainy structure.

Desirable measurements include:

1. The rate of gas production, i.e., rate of sublimation.
2. The albedo as a function of wavelength, angle of incidence and angle of reflection. Related to the albedo is the infrared emissivity as a function

of wavelength and surface irregularity (plane emissivity, hemispherical emissivity, etc.).

3. The surface characteristics as a function of time. Sublimation can cause very irregular surfaces.
4. The temperature of the surface.
5. The ice-grain size and velocity distribution as a function of distance from the surface.
6. The dust-grain size and velocity distribution.
7. The composition of the gas, i.e., the particle density of the radicals, ions, and electrons.
8. The velocity and total density of the gas.
9. The state of excitation and the radiation emitted by the gas molecules.
10. The heat conduction into the ice.

The above measurements will vary with the composition of the icy conglomerate. Desirable compositions of the ice component would include:

1. Various pure components such as H_2O, CO_2 and highly volatile compounds with large dipole moments. Water has been studied most extensively, its properties can therefore be used for calibrations.
2. Pure compounds with dust of known particle size distribution.
3. Mixtures of compounds without dust.
   a. Homogeneous mixtures. These may turn into layered mixtures if the volatile component is sublimated preferentially.
   b. Layered in various orders of volatility.
   c. Heterogeneous mixtures, such as pockets of volatiles enclosed in H_2O ice. This may result in actions similar to the ones found in a frying pan. If, e.g., a small amount of water is covered with a larger amount

of light oil, then the oil will completely cover the water. When heated the oil, being less volatile, can reach a higher temperature then the boiling temperature of the water. The water will form vapor bubbles that pop out of the oil with high speed. If such a bubble has to travel some distance through the oil, the water may even become super heated and be released explosively. In either case small amounts of oil are dragged along with the escaping water. Similar results can be expected from volatile frozen gases enclosed in less volatile ice, and may explain outbursts in comets. Rate of heat conduction into the interior would be an important criterion.

4. Mixture of icy compounds with dust of known particle size distribution. Subheadings a, b, c the same as in 3 above.

Desirable compositions of the refractory dust grains might include:

1. Silicates, because they have been identified in the infrared spectra of comets.
2. Metals:
   a. Iron should be considered because it is a good catalyst. It may cause observable changes in the chemical composition of the coma gases.
   b. Sodium should be considered. It has been observed in comet spectra and it is also a good donor of electrons which also may affect the chemical composition of the coma.

The proposed measurements on the outlined compositions will yield valueable information on the physics and chemistry of sublimation from comet ices. E.g., they will indicate the effective latent heat of sublimation of the icy conglomerate and they will indicate the change of the latent heat with depletion of the volatile components. The composition of the dust may alter the heat conduction into the interior and lead to a better understanding of cometary activity.

Many of the experiments should be carried out first in ground-based laboratories. Many of the surface characteristics will depend on the degree to which icy grains or flakes are compacted and should be carried out in a "zero gravity" environment. Experiments involving measurements of radicals, ions and electrons, the effects of metallic grains on these, and the interaction of the gas with radiation should be performed outside of the Space Shuttle.

REFERENCES

Jackson, W. M. and Donn, B., 1968, Icarus 8, 270.

Öpik, E. J., 1965, Irish Astron. J. 7, 32.

DUST CONTENT AND PARTICLE RELEASE EXPERIMENTS

Zdenek Sekanina
Center for Astrophysics
Harvard College Observatory and
Smithsonian Astrophysical Observatory
Cambridge, Massachusetts 02138

I. Introduction

Since dust particles are carried away from a comet nucleus by sublimating ices, the effects from the ambient earth's atmosphere on Shuttle-based simulation experiments at lower altitudes are of the same concern to the studies of the dust behavior as they are to the investigation of the volatile component. Also, since the experimental modeling could realistically be performed on a linear scale that is at least three orders of magnitude smaller than required by the true conditions in comets, severe problems of extrapolation may arise in the interpretation of some of the simulation results. Subject to these limitations, future dust-release experiments made on "artificial comets" could prove fruitful, as they would test the correctness of our understanding of the fundamental properties of the dust-emission mechanism in comets, and at the same time insight into the behavior of dust particles after expulsion would be gained.

II. The Dust Release Mechanism

The general solution to the problem of dust emission from comets was submitted by Probstein (1968), who applied a fluid-dynamics approach. He treated the innermost coma of a comet as a spherically

symmetric continuum source flow of a two-phase dusty gas, and found that significant dust-gas interaction is confined to the immediate vicinity of the nucleus. The terminal particle velocity was calculated as a function of two parameters: one of them is the ratio of the mass-emission rate of the dust to the production rate of the gas, the other measures the degree of accommodation of the particle to the ambient gas-velocity field.

A meaningful experimental test of this mathematical model of the release mechanism can only be performed, if, apart from other requirements, the manufactured dust grains realistically approximate the actual cometary particles in composition, structure and other characteristics. This would unquestionably be a very difficult task to accomplish in the near future, since the present level of knowledge of the physical nature of cometary dust is in many a respect less than satisfactory. Table I presents the basic information that is available; it can perhaps serve as a basis for a future guide to particle manufacturing, but in its present form it leaves too many important questions unanswered. The information is compiled from various sources, such as Whipple (1950, 1951), Jacchia et al. (1967), O'Dell (1971), Ney (1974), Brownlee et al. (1976), Millman (1976), Ney and Merrill (1976), Sekanina (1976a, b) and Weinberg and Beeson (1976), to list several of them; and relies upon a number of assumptions, such as the relation between cometary dust and Browlee's extraterrestrial particles.

The straightforward application of Probstein's (1968) approach

TABLE I

THE NATURE OF COMETARY DUST

Aspect	Source of Information	Basic Information
Chemical composition	Meteor spectra	H, O, C, N, Fe, Si, Mg, Ca, Ni, others
	Infrared data	Silicates
	Particle collections	Chondritic, FSN, olivine/pyroxene, others
Physical structure	Meteor studies	Average density 0.3 and 0.8 g/cm^3, respectively, for photographic and radio meteoroids (millimeter to centimeter size range); strength $\sim 10^{5\pm}$ dynes/cm^2; irregular shape?
	Particle collections	Some irregular, very porous aggregates of 0.1 μm sized grains; others compact ablation products
Optical properties	Spectrophotometry in visible and infrared	Albedo ∿0.2; effect of reddening (on an average, +0.2 in B-V); effect of phase angle
	Polarimetric data	Generally high polarization, occasionally negative
Size distribution	Dust-tail studies	Sizes from <1 μm to >>1 mm; number varies inversely as 4th to 5th power of size; probably a relatively sharp cutoff at lower limit but tailing off toward upper limit
	Infrared data	Micron sized particles; also larger than 10 μm
	Polarimetric data	Submicron sized particles; possibly steep slope
Dust inside nucleus	Comet models	Distribution very uncertain; various patterns likely
Amount of dust	Dust-tail studies	In dust-rich comets near sun: dust ≐ gas in mass

to a small artificial comet launched from the Space Shuttle gives the "initial" velocities, i.e., velocities acquired through the interaction with outgoing gas, that range from about 1 m/sec for millimeter-sized particles to several tens of m/sec for micron-sized ones. These are comparable in magnitude with velocities to which the particles would be accelerated by solar radiation pressure over an orbital arc of about 100 km (Table II). The effect of the pressure exerted by the solar light reflected and scattered by the earth — a small fraction of the direct solar radiation pressure — is here neglected.

III. Particle Behavior After Ejection

The studies of dust tails of comets indicate that the radiation pressure and attraction of the sun are the two dominant forces controlling the motions of ejected dust particles after their interaction with the escaping volatile substances has been terminated. That does not exclude the possibility that the particles are subjected to additional forces, such as the electrostatic charge, the effects of the solar wind and of the solar magnetic field, etc. However, many of these effects could only be studied on an artificial comet placed in a trajectory outside of the earth's magnetosphere.

Potentially interesting results might emerge from the comparison of the observed particle-size distribution with the manufactured one. During the ejection process particles are exposed to forces that could

TABLE II

MOTIONS OF DUST PARTICLES RELEASED FROM AN ARTIFICIAL COMET

Object's diameter: 5 meters
Particle bulk density: 1.2 gram/cm^3
Production rate at 1 AU from sun: 8 gram/sec (H_2O), 40 gram/sec (CO_2)
Scattering efficiency for radiation pressure: 1

Particle diameter	Particle velocity (m/sec) acquired					
	From outgassing (reached within 50 meters of the comet)		From solar radiation pressure			Radiation pressure / Solar attraction
			Distance from comet (km)			
(μm)	H_2O comet	CO_2 comet	1	10	100	
1000	0.76	1.2	0.11	0.34	1.1	0.001
100	2.4	3.7	0.34	1.1	3.4	0.01
10	7.6	12	1.1	3.4	11	0.1
1	24	37	3.4	11	34	1

perhaps crumble very fragile grains into smaller fragments, in which case the particle-impact rates registered by dust detectors at various distances from the artificial comet would exceed the predicted rates (Table III).

There are indications that effects of particle fragmentation and evaporation are observed in outer sections of cometary dust tails (Sekanina 1976b). Particle evaporation cannot be properly simulated on an artificial comet orbiting as far from the sun as 1 AU; the cause of fragmentation is so far unclear and chances for its simulation cannot be assessed at the present time.

Photometry of individual dust particles released from an artificial comet would be possible only at close range. Table IV shows that a centimeter-sized grain observed from a distance of 100 meters should be about as bright as Jupiter from the earth. Photometry could serve to check some of the results based on impact rates.

IV. Conclusions

To summarize, we believe that limited experimentation with the dust released from an artificial comet is possible, but that the quality of simulation of the physical conditions of dust in comets should first be improved. Results from missions to real comets, the continuing ground-based observations, and the theoretical and laboratory work will hopefully provide the necessary information in the relatively near future.

TABLE III

IMPACT RATES OF DUST PARTICLES RELEASED FROM AN ARTIFICIAL COMET

Object's diameter: 5 meters
Production rate at 1 AU from sun: 8 gram/sec
Dust-to-gas mass-flux ratio: 1
Differential particle-mass distribution law: $m^{-2}dm$
(m from m_{min} to 10^3 grams)

	Impact rate ($cm^{-2}sec^{-1}$)		
m_{min}	Distance (km) of detector* from comet		
(g)	1	10	100
10^{-14}	160	1.6	0.016
10^{-13}	17	0.17	0.0017
10^{-12}	1.8	0.018	0.00018

* At rest with respect to comet.

TABLE IV

BRIGHTNESS OF DUST PARTICLES RELEASED FROM AN ARTIFICIAL COMET

Geometric albedo: 0.2
Phase angle: 0°

	Apparent B magnitude		
Particle diameter	Distance (km) of photometer from particle		
(mm)	0.1	1	10
10	-2.8	2.2	7.2
1	2.2	7.2	12.2
0.1	7.2	12.2	17.2
0.01	12.2	17.2	22.2

Acknowledgment

This work has been supported by Grant NGR 09-015-159 from the National Aeronautics and Space Administration.

References

Brownlee, D. E., Tomandl, D., Blanchard, M. B., Ferry, G. V., and Kyte, F. (1976). NASA TM X-73, 152.

Jacchia, L. G., Verniani, F., and Briggs, R. E. (1967). Smithson. Contr. Astrophys. 10, 1.

Millman, P. M. (1976). In "Interplanetary Dust and Zodiacal Light", Springer, Berlin-Heidelberg, p. 359.

Ney, E. P. (1974). Icarus 23, 551.

Ney, E. P., and Merrill, K. M. (1976). Science 194, 1051.

O'Dell, C. R. (1971). Astrophys. J. 166, 675.

Probstein, R. F. (1968). In "Problems of Hydrodynamics and Continuum Mechanics", Soc. Industr. Appl. Math., Philadelphia, Pa., p. 568.

Sekanina, Z. (1976a). In "The Study of Comets", NASA SP-393, Washington, D.C., p. 537.

Sekanina, Z. (1976b). In "The Study of Comets", NASA SP-393, Washington, D.C., p. 893.

Weinberg, J. L., and Beeson, D. E. (1976). In "The Study of Comets", NASA SP-393, Washington, D.C., p. 92.

Whipple, F. L. (1950). Astrophys. J. 111, 375

Whipple, F. L. (1951). Astrophys. J. 113, 464.

Spectroscopy of Small Cometary Particles

by

Peter M. Millman
Herzberg Institute of Astrophysics
Ottawa, Ontario

INTRODUCTION

In this review I will summarize briefly our knowledge of chemical composition derived from the spectroscopy of small cometary meteoroids, when they enter the earth's atmosphere at high velocity and become visible as meteors. For statistically reliable results it is necessary to have a large number of observations, and this requires the photography of relatively faint meteors, which are considerably more numerous than the bright fireballs. During the last thirty years, in the post-war period, the improvement in observational techniques and cameras has made it possible to extend the range of spectrographic data from cometary particles of mass between a kilogram and a gram down to those of only 10^{-2} or 10^{-3} grams in mass. The corresponding increase in the number-value of the statisitcs has been from less than 100 data points to several 1000.

Increased observational efficiency has been achieved by the development of very fast lens systems of radical designs, a great improvement in the speed of photographic emulsions and, more recently, by the employment of image-orthicon and vidicon systems which incorporate electronic image-intensification and record on the standard video tape used for television. Another important aid in meteor spectroscopy has been the availability of efficient transmission gratings large enough to cover optical objectives up to 15 or more cm in diameter.

THE NATURE OF METEOR SPECTRA

A typical meteor spectrum consists of the low excitation atomic lines of the elements common in chondritic meteorites, Fe, Mg, Si, Na, Ca, Ni, Mn, Cr, Co, Al, Ti, for example (see Figs. 1&2), plus a faint background of the band systems of molecules such as N_2, FeO, and probably CN, CH, and others. Meteor spectra are primarily a result of collision excitation in vapour consisting of a mixture of meteoroid and atmospheric atoms and molecules. Unfortunately, the theoretical and laboratory work necessary for converting the spectral line and band intensities to numbers of atoms in the meteoroid has not been done in most cases.

Values for relative abundances of Fe, Mg, Ca, Ni, and Na have been given by Millman (1972a, 1972b) and Harvery (1973), and reviewed by Millman (1976b, 1977). These relative abundances agree well with those of carbonaceous chondrites, type I, and with the values for upper-air metallic ions and the electron microprobe analyses of a few meteoroids collected in the upper atmosphere of the earth.

LIGHT, VOLATILE ELEMENTS

On the basis of the commonly observed out-gassing from comet nuclei when they are near the sun, one would expect to find in comet fragments considerable quantities of the light volatiles such as H, C, and O. Hydrogen appears quite regularly in the spectra of bright, fast meteors such as the Leonids and Perseids (see Fig. 1), while the presence of carbon may be assumed from the identification of such molecules as CN and CH. Oxygen is certainly a common component in the radiating vapour of a meteor, but it is impossible to estimate the fraction of the O atoms which originate in the atmosphere. We can say that there is good

qualitative evidence for the presence of light, volatile elements in cometary meteoroids but we can give no quantitative values for abundances of these elements.

From first principles it is likely that a smaller percentage of the light volatiles will contribute to the composition of the meteoroids of smaller mass detected at the earth's mean distance from the sun, since here solar energy will tend to vaporize the light-element ices - especially for the small meteoroids with a relatively large surface-to-mass ratio. The above supposition is supported by the observational evidence that cometary meteoroids of smaller mass have higher mean bulk densities (Verniani 1967, 1973).

In the future further information concerning H, C, N, and O in the luminosity of meteors may come from both the spectra of very brilliant fireballs, photographed with high-resolution spectrographs (Ceplecha, 1971), and the spectra of relatively faint meteors, recorded in large numbers at low resolution on video tape with several types of electronic, image-intensifying equipments. In the first case various systems of molecular bands appear with some detail as a faint background to sharp atomic emission lines, while in the second case a faint band structure can be seen in the early part of the meteor trail before the atomic lines are fully developed (Millman et al., 1971; Cook et al., 1973; Millman and Clifton, 1975).

CURRENT PROGRAMS

With the help of SIT Vidicon systems, studies are now being made of the spectra of various major meteor showers to see if there is

evidence for a significant difference in the chemical composition of the meteoroids associated with different comets or cometary orbits. Aircraft operated by NASA have been employed on this project to overcome problems of both bad weather and inaccessible observing locations (Millman 1973, 1976a).

One obvious possibility in this field is to extend observations of meteor spectra into the ultraviolet by using Shuttle-operated spectrographs. A recent study (Meisel 1976) has noted the atomic lines of interest that should be strong in meteor spectra in the wavelength range from 1000 Å to 3000 Å. These include lines of H, P, S, Mg, Ca, Mn, and Fe. A full utilization of such observations to give quantitative chemical information on cometary meteoroids can only be made if we have a great deal more data on the emission cross sections and the luminous efficiencies of the relevant atoms and molecules when radiating under conditions which simulate those in the upper atmosphere.

REFERENCES

Ceplecha, Z. 1971

"Spectral data on terminal flare and wake of double-station meteor No. 38421 (Ondřejov, April 21, 1963)", Bull. Astron. Inst. Czech., vol. 22, pp. 219 - 304.

Cook, A.F., Hemenway, C.L., Millman, P.M. and Swider, A. 1973

"An unusual meteor spectrum", in Evolutionary and Physical Properties of Meteoroids, NASA SP-319, Washington, D.C., pp. 153 - 159.

Harvey, G.A. 1973

"Elemental abundance determinations for meteors by spectroscopy", J. Geophys. Res., vol. 78, pp. 3913 - 3926.

Meisel, D.D. 1976

"A study of meteor spectroscopy and physics from earth-orbit; A preliminary survey into ultraviolet meteor spectra", NASA CR-2664, Washington, D.C., pp. 1 - 78.

Millman, P.M. 1972a

"Cometary meteoroids", in Nobel Symposium 21, From Plasma to Planet, edited by A. Elvius, Almqvist & Wiksell, Stockholm, pp. 157 - 168.

Millman, P.M. 1972b

"Giacobinid meteor spectra", J. Roy. Astron. Soc. Canada, vol. 66, pp. 201 - 211.

Millman, P.M. 1973

"Airborne observations of the 1972 Giacobinids", J. Roy. Astron. Soc. Canada, vol. 67, pp. 35 - 38.

Millman, P.M. 1976a

"Quadrantid meteors from 41,000 feet", Sky and Telescope, vol. 51, pp. 225 - 228.

Millman, P.M. 1976b

"Meteors and interplanetary dust", in Interplanetary Dust and Zodiacal Light, edited by H. Elsässer and H. Fechtig, Springer-Verlag, Berlin-Heidelberg-New York, pp. 359 - 372.

Millman, P.M. 1977

"The chemical composition of cometary meteoroids", Proceedings of IAU Colloquium No. 39, Lyon,Aug. 17-20, 1976, in press, University of Toledo, Ohio, U.S.A.

Millman, P.M. and Clifton, K.S. 1975

"SEC Vidicon spectra of Geminid meteors, 1972", Canadian J. Phys., vol. 53, pp. 1939 - 1947.

Millman, P.M., Cook A.F. and Hemenway, C.L. 1971

"Spectroscopy of Perseid meteors with an Image Orthicon", Canadian J. Phys., vol. 49, pp. 1365 - 1373.

Verniani, F. 1967

"Meteor masses and luminosity", Smithsonian Contrib. Astrophys., vol. 10, pp. 181 - 195.

Verniani, F. 1973

"An analysis of the physical parameters of 5759 faint radio meteors", J. Geophys. Res., vol. 78, pp. 8429 - 8462.

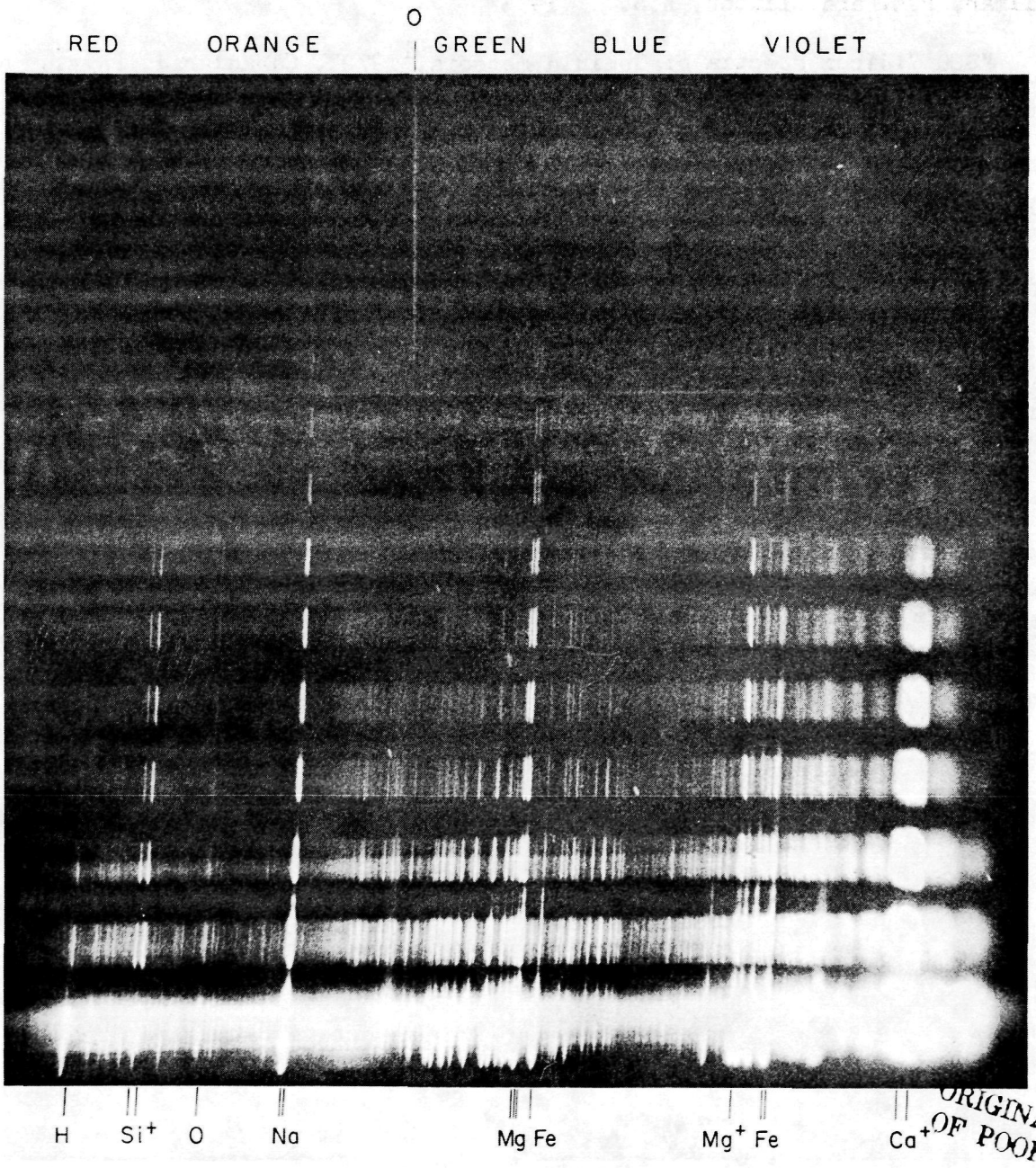

Figure 1. The photographic spectrum of a bright Perseid meteor, secured at the Springhill Meteor Observatory of the Herzberg Institute of Astrophysics near Ottawa, Ontario, on 12 August 1968 at $08^h\ 00^m\ 22^s$ UT.

This meteor was visually estimated to have a luminosity equivalent to -6 stellar magnitude. The visual train remained visible for 12 seconds and the radar echo endured for 305 seconds. The photograph was taken with a Leitz lens, focal length 75 mm, aperture ratio f/2.0, and a Bausch & Lomb transmission grating, 600 lines/mm blazed for 5500 Å. An occulting shutter, open to closed ratio 1:1, covered the lens 20 times per second, producing the horizontal gaps in the spectrum. Emulsion was Agfa Isopan Record developed in hyfinol.

The meteor moved vertically downward as the spectrum is here reproduced. Prominent lines of the metallic elements Fe, Mg, Na, Ca, and Si have been identified as well as lines of the light volatiles H and O. The forbidden oxygen green line at 5577 Å appears early at the top and shows no shutter breaks since it has an effective duration of a second or more. Other lines, with very brief duration characteristics, appear in the shutter breaks near the bottom. Exposure duration was only 60 seconds as it was just 4 days past full moon and the sky was bright. The meteor spectrum is in the first order of the grating, while the short star trails in the zero order appear as small slanted bright spots. The lens was focused for the green-red region, so the violet end of the spectrum is badly out of focus.

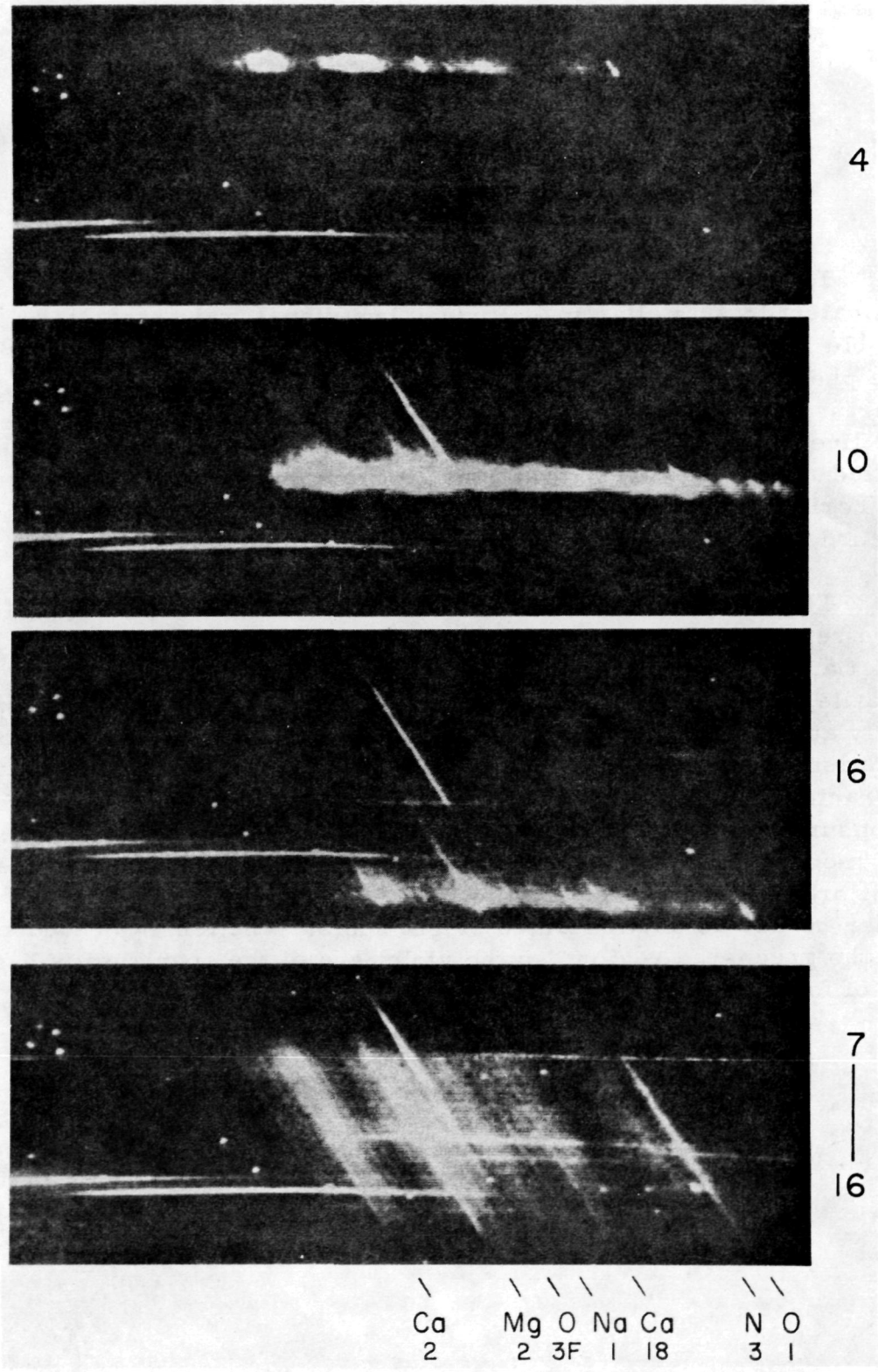

Figure 2. A Geminid meteor spectrum recorded on video tape by K. S. Clifton at the Mt. Hopkins Observatory, Arizona, on 14 December 1974 at $10^h\ 21^m\ 16^s$ UT.

The recording instrument was an SEC vidicon used with an Oulde Delft Rayxar lens, focal length 105 mm, aperture ratio f/0.75 and a Diffraction Products transmission grating, 300 lines/mm, blazed for 5000 Å. Spectrum was recorded on video tape by an Ampex 660C tape recorder, bandwidth 4.2 MHz.

This equipment produces 30 complete frames per second. Identifying field numbers appear at the right for the first three records. The fourth record represents an integration of ten frames, a technique which assists in the correct identification of lines in the spectrum and which produces a better star field for use in height calculations. Some of the more prominent atomic lines have been identified at the bottom of the figure.

N81-24137

REVIEW COMMENTS OF SHUTTLE-BASED COMETARY EXPERIMENTS

C. R. O'Dell
Marshall Space Flight Center

The experiments considered by the various authors in this session can be classified according to their morphological nature. In order to plan for comet relevant Shuttle experiments and payloads, I've grouped the experiments along the line of the earlier speakers with slight variations.

PROPOSED SHUTTLE COMETARY EXPERIMENTS

On-Board	Determination of Bulk Properties and Processes (Within Solids) Observations of Exposure Panels (Near Surface Phenomena)
Overboard	Gas/Dust Shells Observation from Shuttle Observation by Sub-satellites

One set of experiments is genuinely an on-board type, e.g., Delsemme's experiment for the determination of bulk properties. He talked about taking materials much like what one would think the nucleus should be and determining

the characteristics like density, conductivity, tensile strength, etc. The advantage of Shuttle is that one can work in low gravity, which cannot be done on earth. An enormous variety of characteristics can be covered that hopefully allows one to model, from outside to inside, a favorite comet model of the nucleus. These are on-board experiments that can be done in one of the Spacelabs.

A related (or extended) version of this is Huebner's on-board experiments of observations at or near exposed panels. Instead of just using orbit for low gravity, one is using the low gravity plus vacuum (not the best vacuum but a high vacuum) and the direct access to solar radiation for exposing panels to space. One can observe properties both at and near the surface itself, and look at variations in the nature of the surface with the time exposed to these conditions. One can look at the material coming off these surfaces for such things as the velocity of escape and the physical form of the ejected material. A wide variety of samples can be covered. Huebner talked about mixtures which vary in gas to dust ratio, the physical state (homogeneous - highly inhomogeneous), and various types of particles and ices. With these experiments we are looking at and near the surface or, in some cases, looking at the plume being created from the panel.

The next type of experiment I'll call the overboard experiment. This is what Sekanina and Jackson discussed. In these cases we are talking about hollow shells with the sample material of ice or ice plus dust on the outside giving a large surface area. This mass is thrown overboard. One knows exactly what it is when observations are begun. This experiment can be done on the same mission as the on-board experiment. Since the Shuttle transportation costs are about $20 million per flight, a majority of a payload for one discipline, especially a small discipline, isn't going to get too many flights per year.

There is a dispersion of opinion about what kind of ice is relevant to be put on the surface, e.g., what kind and how much water. Clearly, one can cover a variety of molecular types and various dust types. The theory of the interaction of radiation with idealized particles is well confirmed and applied to the interpretation of dust tails; but, there are some things we know that must be true, although we are unable to model them today. I would identify two of these as (1) the question of charges on particles (how they build up and vary), and (2) the effect of the irregular shapes of particles. The particles of the Brownlee photographs, even when one looks at the small subcomponents of the whole, look like irregular particles. The determination of the basic effects of irregular parti-

cles is needed for modeling and interpretation of actual observations. It is difficult to get enough dust overboard to observe, although it may be observed by direct scattered light for a very large size, while cooled infrared instruments would allow observations of small particles at lower densities and might be the preferred way to make direct observations of the dynamics of these dust particles.

It is also difficult to get enough gas to directly observe. It is certainly very difficult to create an artificial comet that can be studied well from the ground. Even observations from the Shuttle are difficult. Jackson suggests the best way to do observations is with a mass spectrometer since one is working with low densities. The ideal way of doing this is to put a series--he illustrated three--of satellites (very much like the ones put on interplanetary missions) in the plume of the artificial nucleus. One can also envision conditions where something is thrown overboard and the Shuttle is flown along that plume. The ability to maneuver the spacecraft in three dimensions is now rather sophisticated and we should consider it.

Finally, on both of the overboard experiments there are serious questions about whether or not anything meaningful can be done. Jackson was initially pessimistic but then reconsidered. The effects of the residual atmosphere moving past the experiment (e.g., artificial nucleus) at

8 km/sec and interacting in both a reactive and momentum manner can be very serious. It is so serious that one would have to understand this interaction with great precision before it would allow the determination of information about the nucleus. It is a small comet signal superimposed on a large atmospheric signal. There is a zero order experiment, mentioned by Jackson, that can be done. Although the sun (light source) is not present in the earth's shadow, it doesn't mean that all the atomic species will decay. Neither will all the electrons recombine. The light simply goes off when the experiment is in the earth's shadow. You should be able to see the difference in a plasma with the light source on and with the light source off. The atmosphere is always there. One can observe with the atmosphere plus a light source and with the atmosphere and no light source.

Jackson: I don't think the hydro-dynamics problem is as much of a problem as what happens in the chemistry interaction.

Keller: I don't think the chemistry will occur because the density is much too low in that case - the chemistry you expect to occur in a comet.

Jackson: What you're saying is that the experiment won't work and one can do some calculations to determine whether it will work by calculating what the relative lifetimes are for the chemistry.

Keller: Are you talking about the chemistry between the oxygen atmosphere and the gas released?

Jackson: Yes, what the relative lifetimes are of the chemistry of the oxygen and the electrons, and the ions with the cometary gases that you release. The chemistry caused by the photon interaction with the gas that you release. Those lifetimes are of the order of 10^3 - 10^4 seconds. I know what the rate constants are for the interactions. You can then make a calculation of what percentage of the fragments you get for a certain kind. The photon interaction can be compared to the gas interaction.

Now it is highly probably that the gas interaction is going to give you a different product than the photon interaction. The whole question is if you are getting enough.

O'Dell: Millman has said that there is a certain possibility to make meteor observations looking down into the atmosphere in a new wavelength range which always holds surprises. In addition, it makes possible the opportunity to do some calibrations using artificial, well known objects of a known mass range. It will check the methods that people have been employing over the years. It is very nice to confirm something like this in an experimental way.

SPECIAL SESSION

D,10

THE STATUS OF COMETARY SCIENCE

Fred L. Whipple
Center for Astrophysics
Harvard College Observatory
and
Smithsonian Astrophysical Observatory

Abstract

The nature of the cometary nucleus and the observable phenomena induced by the Sun are now sufficiently well understood to justify sophisticated scientific planning and extensive effort directed toward the solution of specific problems. The broad basic problem is to determine the chemical composition and physical structure of the nucleus. The rapidly accumulating information about the nucleus can eventually lead to an understanding of the processes and location of cometary origin. The role of comets in the evolution of solar system will then become evident, including possibly a major contribution to the volatiles of planets and even the elements necessary for the development of life on Earth.

New dimensions to our understanding of comets are now being contributed from the ground by radio, infrared, remarkably improved sensing equipment and phenomenal computers. From space, vehicles and platforms rise above our obscuring atmosphere to expose the entire electromagnetic spectrum for scrutiny. The development of new theory for the complex chemistry and physics in cometary atmospheres can now be justified by the increasing wealth of observations. Conversely, new observations can be tuned for testing theories. Fine

examples of constructive interplay between theory and observation lie in the field of plasma physics applied to the ion tails of comets and in the field of gas-phase chemistry applied to the problem of parent molecules in the cometary nucleus.

Space experiments and space probes now promise a quantum jump in our understanding of comets, their origin and their relation to us as living beings.

INTRODUCTION

As I see the ultimate goal in cometary science, it is to determine the chemical composition and the physical structure of the nuclei of comets. When we know enough about the nucleus we can tell where, how and when comets were formed. With this solid information as to their origin we can evaluate their function in the evolution of the solar system. On the way to this goal we can learn to understand the physics of a number of cometary phenomena. When we get space missions to comets we can make more rapid progress in answering questions about the nucleus. Once having understood the role that comets played in the evolution of the solar system, we can find out what role they may have played in providing volatiles on the Earth from which the life giving elements may have come. Whether their role was a major or a minor one is a critical and fundamental question.

Now, as we all know, knowledge of comets has been expanded enormously through the observation of comet Kohoutek, 1973XII, which was extensively supported by NASA. We have now beautiful infrared techniques, radar results, remarkable new instrumentation, ground-based equipment and computers which are far better than anything we could dream of 30 or 40 years ago when I used to do a lot of computing. With these we have made phenomenal progress in understanding comets. Space vehicles have enabled us to study cometary emissions into the far ultraviolet. We now can study the entire electromagnetic spectrum of comets. The huge amount of new information justifies the expenditure of great effort in developing new theories and in ground-based laboratory studies. The latter I would like to see greatly expanded so that we can understand the physics and chemistry of the cometary atmosphere. Then of course, having new theories, we will have to be more explicit and fine tune our observations to check and disprove these theories. This constructive interplay between theory and observation is beautifully illustrated in the dynamics of ion tails and in gas-phase chemistry, which are just getting underway to solve the problem of parent molecules and other cometary problems. My favorite pictures of comets are C/Kohoutek in ordinary light and in the 1416 Å line, Lyman alpha of hydrogen. I'm fond of the first because

it was taken by the first observatory devoted entirely to comets and asteroids, and of the second, at the same scale and time, because it was taken from Skylab (Fig. 1). The pictures show us how little we knew about comets before we could observe Lyman alpha. The circle gives the scale, the Sun's diameter at the comet. Dr. Lillie helped make the first observations of Lα, of Comet Bennett.

COMET SPLITTING

Now Comet West 1975n is perhaps the greatest comet of the century. It came in without too much fuss and feathers, and was observed almost as thoroughly as C/Kohoutek. At an early meeting about C/Kohoutek, I mentioned that I hoped it would split. Unfortunately, it did not, but C/West did. This is a very dusty comet so that photographs in the red showing the dust tail and blue showing the ion tail look entirely different.

Near perihelion a great brightening occurred because the comet split into at least four components. Figure 2 from the New Mexico State University Observatory at Las Cruces shows the development of these components from March 8 to March 24. Marsden and Sekanina believe component A to be the main body because it seems to follow a Newtonian orbit. Component C is well separated by the middle of March and in late March it is moving out at a very high rate of speed. Component D is moving very slowly and B somewhat more rapidly with respect to A.

A photograph of the nucleus by Giclas on April 1 shows that C is nearly gone, hardly visible; all these components showed tails at some time.

We once thought that components of split comets left the main component at an appreciable velocity, if only some 10 to 30 meters per second. But this assumption never gave satisfactory Newtonian orbits. Sekanina conceived the idea that the components separate almost at zero velocity. The non-gravitational forces arising by jet action from the sublimated gases cause separation. He finds that the subsequent orbits, with different non-gravitational forces, join back together at the time of splitting and fit the observations excellently.

Comet West illustrates what must happen to all comets with multiple nuclei. The components must separate because of differential jet forces! A very interesting second phenomenon concerns component C. It was the last one to separate, some 10 days after perihelion, and lasted about 3 or 4 weeks. Sekanina finds it was moving out with an acceleration of more than 10 times B and about 20 or so times the acceleration of D. When you calculate from the acceleration the amount of mass in component C the dimension is perhaps some 30 meters. Its short life and high acceleration show that it was much smaller than others. But the smallest component was, at times, brighter than the larger components. Now, how can this be?

An icy conglomerate comet, after some solar heating should develop layered structure with the dust and less volatile ices on the outside. Inside is matter of much greater volatility. Now it is a truism that for any solid whatsoever, when broken into two pieces, the new areas exposed on the two pieces are identical. If the inside of the comet contains very active material, the two broken pieces expose equal amounts. When oriented towards the Sun properly the small component can be just as bright as the large one. In addition fragmentation may increase the effective area of the small piece. Indeed when observations are available the right times, almost all split comets show this phenomenon: the little piece may disappear but at times it will be brighter than the big piece which persists.

ICES AND RADIAL NON-GRAVITATIONAL FORCES

For many comets the accelerations radially from the Sun have been determined by deviations from gravitational orbits. The radial force per unit area can be calculated on the basis of: a) sublimation equal to absorbed solar radiation divided by the latent heat of vaporization, and b) force radially to the Sun proportional to the momentum of the escaping gas corrected for the geometry of an assumed spherical nucleus.

The calculated radial force is thus proportional to $\pi R^2(1-A)$ where R is the radius and A is the albedo. The

acceleration is the force divided by the mass, $4\pi\rho R^3/3$, where ρ is the density, taken as 1.3 gm/cm^3. Equating this theoretical acceleration to the observed non-gravitational acceleration provides a numerical value of (1-A)/R.

At extreme solar distances where old short-period comets are usually inactive, photometry provides the well-known quantity area-times-albedo or, as the square root, $RA^{1/2}$. From these numerical values, a solution is then possible for R and A for the nucleus of a comet. The derived quantity from the product is $(1-A)A^{1/2}$, a quantity that maximizes at 0.3849 when A=1/3. It provides a limiting check on the basic assumptions and, therefore, on the basic physical properties of the nuclei. The check is made, with the latent heat of vaporization for water ice, as an upper limit to the product $R_1A_1 \leq 0.20$ where A_1 is the radial non-gravitational term as used by Marsden, Sekanina and Yeomans (1973) and $R_1=RA^{1/2}$ km, directly observed.

I have applied the method to ten short-period comets of perihelion distance, q, less than 1.5 AU for which the values of A_1 are applicable. The results are shown in Table I where r_o (AU) is the maximum solar distance at which the comets were observed.

The results are consistent with water ice as the subliming material except for P/Tuttle, in which case the

determined value of A_1 is undoubtedly too large. About half the comets appear to be "spotty," that is, they sublime more slowly than if uniformly covered with water ice. If constituted of a more volatile material they would be even more spotty or R_1A_1 would become even smaller.

The radii in Table I have been determined with small values ($\leq 1/3$) for the albedo. I do not trust this method really to give reliable radii, but probably the order of magnitude is correct, $R \approx 0.4$ to 1.7 km for these old comets. Higher values of A may be quite correct for newer comets, however.

I cannot yet apply the method to periodic comets of larger q because of the assumptions regarding sublimation made in the calculations by Marsden, et al. Nevertheless we have strong evidence supporting water ice as the primary sublimating agent for old comets.

Delsemme and Rud (1973) have shown for three comets the combination of observed H_2O loss and photometry at great solar distances leads to determinations of the radii that appear reasonable. Thus water ice could be the major action agent for somewhat younger comets. For comets that are very bright with much larger perihelion distances than 1.5 AU, some of them periodic and some single apparition comets, ice is not adequate because, at 3 to 4 AU from the Sun, water ice would be completely inactive with negligible vapor

pressure. Nothing should happen at all. Some comets are active beyond 4 and 5 AU, up to 11 or 12 AU. So, we know that there must be more volatile materials.

For some comets of a single apparition, H_2O ice is not volatile enough to produce the observed radial accelerations. For at least one comet, Bennett 1970II, however, the gas production rates, as studied by Delsemme and Rud cannot be reconciled with the observed non-gravitational radial acceleration and the theory of this paper. I suspect that this acceleration is actually spurious, being produced by apparent displacements of the observed nucleus from the true nucleus radially away from the Sun. Such displacements have been observed by Malaise (1976). For C/Bennett I find that the displacements need not exceed some 3300 km.

The physical characteristics of comets vary with their orbits and with their age. New comets on their first near solar passage from the Oort cloud are extremely active. The activity appears to fall statistically with increasing age as measured by reduced orbital period. This sequence must represent a corresponding layering of structure from the surface of a new comet inwards.

Marsden and Sekanina point out that comet discoveries with very large perihelion distances of 4 to 5 AU have mostly been new comets. Why are there so few returning comets of large q? Probably because new comets return as fainter

objects. Here we have evidence that new comets may rather rapidly lose a thin outer layer of extreme volatility.

I find that I didn't listen to Bertram Donn as I should. He suggested (1976) that while comets are in the Oort cloud they are exposed to cosmic rays for presumably the age of the solar system. The amount of energy injected near the surface is tremendous. Figure 6 shows data based upon observations at very high altitude from balloons, giving the ionization energy from cosmic rays deposited as a function of depth in water ice. For integration over 4.6×10^9 yr the measurement unit of 10,000 cal gm^{-1} is rather staggering. For water ice, which is the most difficult to sublimate, the latent heat vaporization is only 640 cal gm^{-1}. The induced radiation gives up to about 50,000 calories per gram or nearly 60 times the amount of energy required to vaporize water ice in the outer meters of a new comet. Of course, vaporization does not occur as the surface temperature in deep space needs be only some 10 K or less to radiate away the energy, including also any likely radioactive energy from within.

What would actually happen to an icy conglomerate mix after this much bombardment by cosmic rays? I know of no data that are directly applicable, although graphite in piles can store some 50 cal gm^{-1}! From certain laboratory data Donn feels that polymerization might be the major effect,

producing more complex molecules but probably reducing rather than increasing the volatility of the end product. Figure 7 shows a schematic representation of crystal damage by a primary near the end of its path or by a secondary. Momentarily a great deal of heat is generated in the interstitial lattice, which partially heals at room temperature. In a very cold environment at only a few degrees absolute the crystalline structure must suffer enormous damage, being transformed into an amorphous structure. Hence significant exothermic energy in the form of defects, vacancies and radicals must be added to produce the extraordinary activity observed in some new comets. I consider laboratory experiments as urgently demanded to simulate the cometary environment in deep space.

I am fascinated with Brownlee's pictures of high-altitude particles that appear very likely to be cometary stuff (Fig. 8). On a scale of only a few tenths of a micron the internal structure looks like fish eggs, incidentally, about the size of interstellar dust. But they form single pieces strong enough to withstand entrance into the atmosphere. Since they are like nothing else we know and have the expected composition, they are probably cometary. I think this is one of the most exciting aspects of comet research today. Do we really have pieces of comets in the laboratory?

A word about the nucleii of comets. Outside is a very thin layer, I call frosting, producing the activity in very new comets. On the other hand, the very old comets of short period contain mostly water ice and fairly compact meteoritic material. Perhaps this is a core just outside of which may be an inner mantle. Water ice may still be the major material that sublimates to produce the activity of the "not-quite-so-old" comets, i.e., the periodic comets of longer period and those of larger perihelion distances. Between the inner mantle and the "frosting," however, is a (thick?) region containing a considerable fraction of ices that must be much more volatile than water ice. This outer mantle provides the material for the activity of the split pieces of C/West, for example.

As these outer regions sublime away to space, an old and originally very large comet such as P/Encke wastes away to some sort of a core. Several thousands revolutions about the Sun for P/Encke with q only 0.3 AU leave a rather inactive body. Does this inner core turn into an earth crossing asteroid? We don't know whether any of these asteroids are comets. Many people believe they are. I have always stood on the fence on that subject because there is yet no proof, not until we can get missions to comets and asteroids to see what that material is like. In any case, there is a huge

reduction in activity from new to old comets. Part of this effect undoubtedly comes from increasing coherence of the material with depth. Recall that the activity of comets arises only by sublimation of ices at the surface; the gas must carry along the meteoroidal material. We know that the latter constitutes a good fraction of the total mass and is somewhat consolidated. At least it sticks together to some extent. A crust of such material could only be broken by "explosive" pockets as Huebner has discussed. I wonder to what extent the activity is controlled by increased cohesiveness with depth rather than by chemical changes in composition.

As to the origin of these layered comets there are several possibilities. Perhaps the first accumulation was a meteoritic core on which ice was deposited, a theory which Öpik rather likes. On the other hand, the cloud of dust and gas may have been very cold and homogeneous to begin with, containing enough radioactivity to produce a certain amount of vaporization. The heat conductivity is extremely poor in such a body so that heat would be transferred by the sublimation of material which would then move outward to cooler regions and recondense. In that way perhaps the inner part will consolidate without the need for much gravity, which is very small in comets.

All in all, however, the fact that comets exist and are so active shows that the meteoritic material cannot be the major matrix material. Activity would halt very quickly as the gas from the subliming ice would have to seep out through the porous poorly conducting solid. Clearly the solids must be introduced as finely divided unconnected tiny particles. I rather suspect most of these particles (interstellar grains?) are surrounded with ice when they collect and are insulated by ice so that they do not stick together. We know that the cometary meteoroids are very fragile. A small increase in the strength of the meteoritic material would very much reduce the activity and perhaps form an impervious crust.

It may not be clear until we go to comets whether the major variable with depth in comets is the coherence of the meteoritic material or chemical variation. So far we see little difference in the ratio of water (from lyman alpha and OH) to the solids for the few comets in which they have been measured. Also there appears to be no great compositional change systematically from new comets to old comets as measured by that ratio. The problem remains.

So far I have discussed the nature of the nucleus. I have not treated much of the very beautiful work that has been done on other aspects, the C/Kohoutek results, new

results on the molecules by radio and the progress that has been made in understanding the gas-phase chemistry, nor the great progress that's being made in ion tails. There has barely been time enough to talk about the subjects closest to me.

Cometary science is now at a point where we can justify highly sophisticated and expensive techniques in studying comets. We have a sound enough basis that we know how to get results of importance by good detailed planning and execution, and we have enough basis to justify laboratory experimentation on the important physical processes involved. We can justify expensive calculations and theory, based perhaps upon not quite the right premises but theory that will enable us to make new relevant observations or to use the old observations more effectively. All of this, of course, again, leads to the study of the nucleus, which I mentioned at the first. It then leads to an understanding of the role of comets in the evolution of the solar system. I think that we can say with confidence that shuttle-based cometary science and, in particular, missions to comets, can lead to a true quantum jump in our understanding. Eventually we will discover the degree to which comets provided the atoms that make up our own bodies.

Table I

Data for Periodic Comets with q≤1.5 AU

Comet	q AU	r_o AU	R_1 km	A_1	R_1A_1 km	A^3 (calc)	R (km)
Honda-Mrkos-Pajdusakova	0.56	1.2	0.48	0.1	0.05	0.008	1.2[4]
Giacobini-Zinner	0.99	2.5	0.70	0.3[1]	0.21	--	1.2[5]
Tuttle	1.02	2.0	2.01	0.32[1]	0.64	--	3.5[5]
Finlay	1.08	2.0	0.26	0.5[1]	0.13	0.07	0.7[4]
Tuttle-Giacobini-Kresak	1.15	1.7	0.14	0.66[2]	0.09	0.033	0.4[4]
D'Arrest	1.17	2.8	0.28	0.8[2]	0.22	--	0.5[5]
Schaumasse	1.20	2.8	0.88	0.4[2]	0.35	--	1.5[5]
Tempel 2	1.37	3.6	0.53	0.1[1]	0.05	0.010	1.4[4]
Jackson-Neujmin	1.43	1.9	0.20	0.8	0.16	0.12	0.5[4]
Borreley	1.45	3.0	0.66	0.09	0.06	0.013	1.7[4]

1 Maximum value if variable
2 Most recent value
3 Lower value of A adopted, ρ=1.3
4 A adopted as 0.15
5 A adopted as 1/3

REFERENCES

Bowen, I.S., Millikan, R.A. and Neher, H.V., 1938, Phys. Rev. 58, 855-861.

Chadderton, L.T. and Torrens, I.M., 1969, Fission Damage in Crystals, Methuen & Co. Ltd., London.

Delsemme, A.H. and Rud, D.A., 1973, Astr. Astrophys., 28, 1.

Donn, B., 1976, "The Study of Comets," NASA SP-393, 611-619.

Malaise, D., 1976, "The Study of Comets," NASA SP-393, 740-749.

Marsden, B.G., Sekanina, Z. and Yeomans, D.K., 1973, Astr. J., 78, p. 211.

For further reference material see:

"The Study of Comets," NASA SP-393, 1976.

Reports of the International Astronomical Union, Commission 15.

"Physical Processes in Comets," by F. L. Whipple and W. F. Huebner, Ann. Rev. Astr. Astrophys., 14, 1976.

The material of the present paper is taken largely from "The Constitution of Cometary Nuclei," by F. L. Whipple, Preprint No. 637 of the Center for Astrophysics, 1976, to be published in the Proceedings of the IAU Colloquium No. 39, Lyons, France. The work was largely supported by NASA Grant No. 7082.

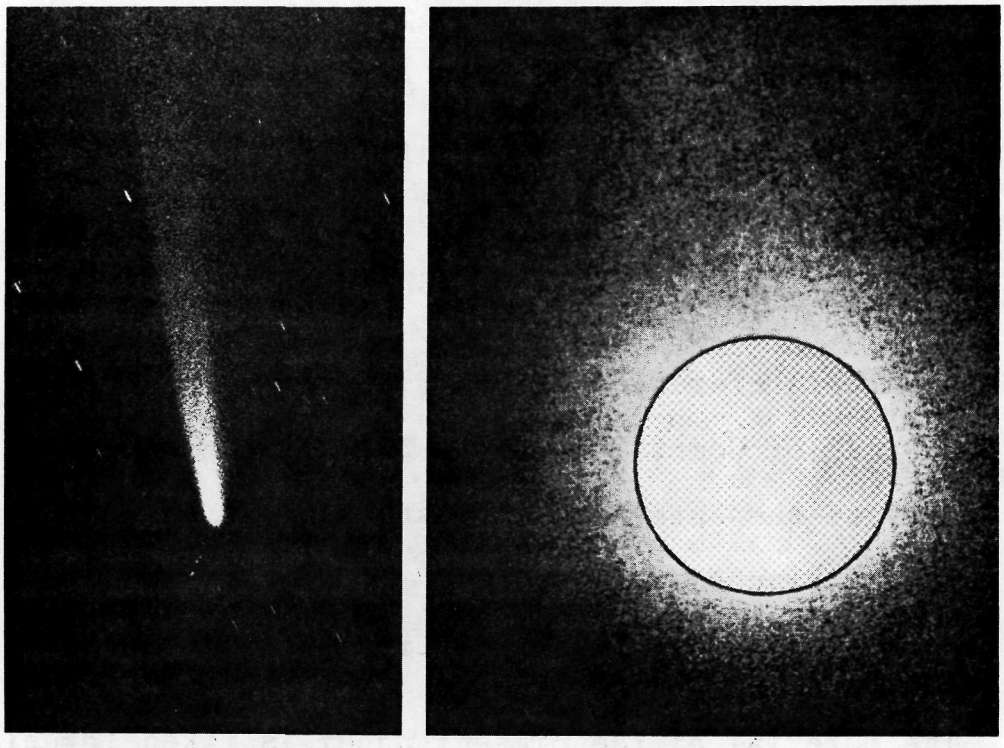

(a) (b)

Figure 1. Comet Kohoutek, 1973XII, Dec. 25.9, 1973. (a) Photograph, Comet and Asteroid Observatory, South Baldy, New Mexico. (b) NASA Skylab photograph in far-ultraviolet hydrogen Lα radiation. Both photographs are on the same scale as is the Sun's disk (circle) at same projected distance.

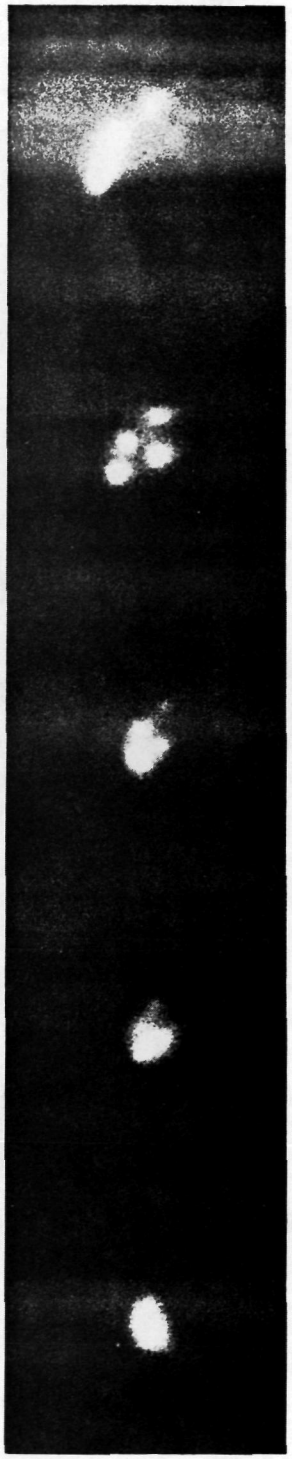

Mar. 24.5

Mar. 18.5

Mar. 14.5

Mar. 12.5

Mar. 8.5

1976

Figure 2. Nucleus of Comet West, 1975n, on 5 dates. Component A, lower left; B, upper right; C, lower right; D, middle left. Scale on March 24.5: A to B = 16.3". Distance from Earth: 0.88 to 1.09 AU, March 5.5 to 24.5. From A. S. Murrell and C. F. Knuckles, New Mexico State University Observatory.

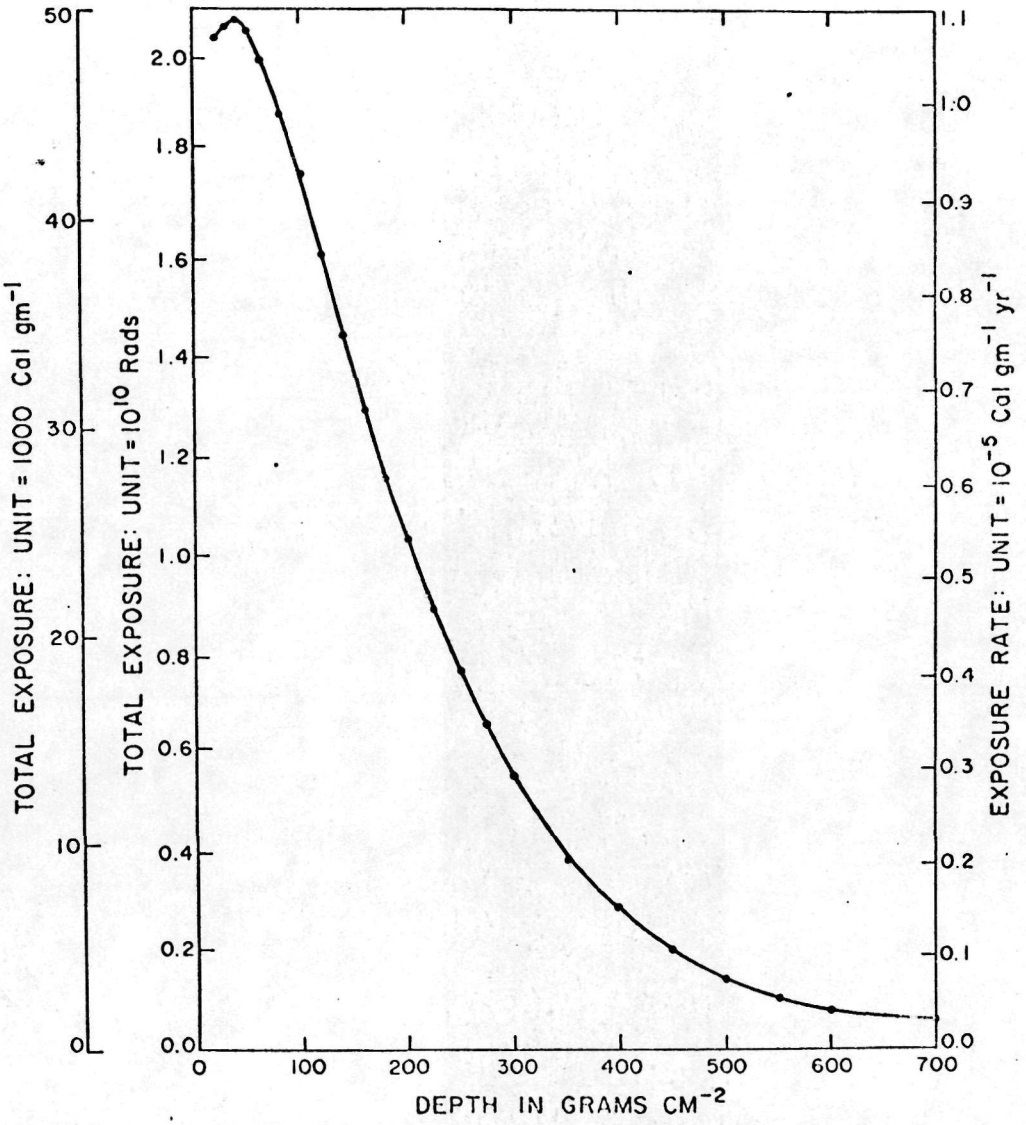

Figure 3. Ionizing exposure by cosmic rays in comets as function of mass depth: total exposure over 4.6×10^9 yr (left) and exposure rate (right), based on Bowen, Millikan and Neher, 1938.

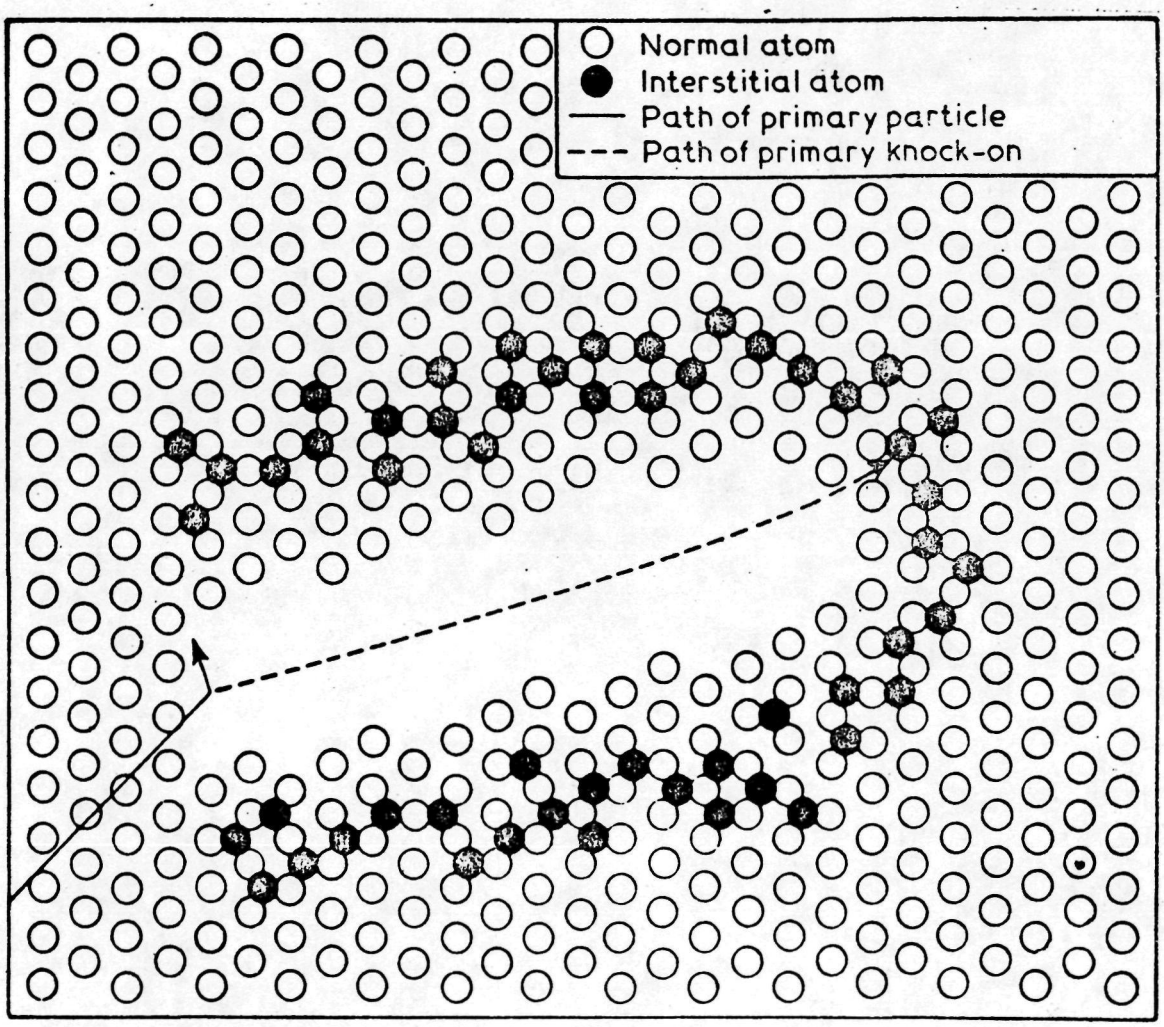

Figure 4. Brinkman displacement spike of high-energy fragment in crystal. (From Chadderton and Torrens, 1969).

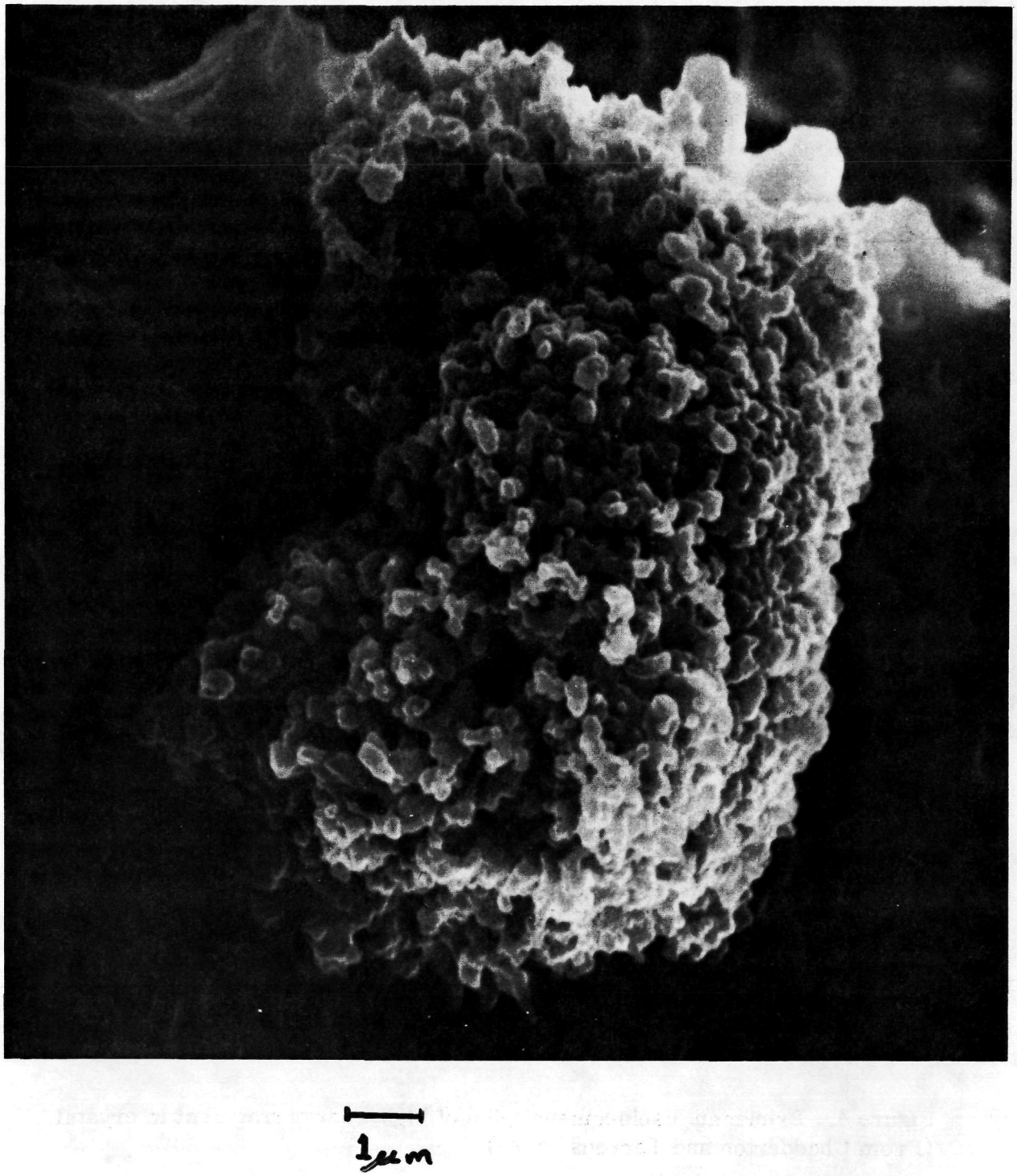

Figure 5. Particle collected at an altitude of 20 km by Donald E. Brownlee and his collaborators.

SESSION III

SHUTTLE-BASED OBSERVATIONS

SHUTTLE-BASED OBSERVATIONS

M. Dubin
Science Manager of Spacelab Research
Goddard Space Flight Center

I would like to say a few introductory words which, I guess, is the prerogative of the chairman. I will not mention the specific history of cometary research by NASA, which I have spent upwards of a dozen years managing at NASA Headquarters. I think it is not worthwhile talking here about the astronomical activities of the IR programs that have developed and have been used for comet observations. I think you are fairly familiar with the programs using manned systems from Gemini to Skylab. Of course, the Skylab cometary work is well documented and I hope you have the report on Comet Kohoutek. What I want to do is to outline some of the progress in science in relation to the Space Shuttle and to bring the working group up to date about what has been happening.

Beginning about 1970-71 John Naugle began an activity of the use of the Space Shuttle and Spacelab. Prior to this, there were a number of studies on the use of space stations. In 1971, a symposium was held at Langley Research Center on science in the sortie mode using the Space Shuttle, and there followed a workshop for NASA scientists at Goddard in 1972, which was published in a series of documents. There then was organized ten discipline working groups and meetings and another series of doc uments on the uses of the Space Shuttle was published in May 1973. In 1973 there was a National Academy of Science summer study on the scientific use of the Shuttle which was published in 1974. Some of you have copies of this material and it is relevant in some respects to the theme of this working group. In addition to the above, there have

been a number of follow-on activities and studies that are clearly relevant and I'm not sure that you are familiar with, i.e., the Astronomy Spacelab Payloads Studies at the Goddard Space Flight Center that continued for several years (about three years) and the AMPS activity, (AMPS stands for the area of Atmosphere, Magnetosphere and Physics-in-Space). Each of these programs involved a number of people, some workshops, and an expenditure of study funds of several million dollars in these areas. I am not sure that you are familiar with the AMPS program which was begun at Marshall and later transferred to Goddard.

At Goddard there was organized in January 1976, a Shuttle Spacelab Payloads Project Office covering the fields of (1) solar physics, (2) astronomy with optical instruments (3) high energy astrophysics, (4) atmospheric research and magnetospheric physics and (5) Earth observational studies. The reason for reviewing all these activities is that within the context of the cometary physics field there are a number of devices and instruments that are already in the planned program; for example, the astronomy studies at Goddard, which are published in a six volume report Astronomy Spacelab Payloads Study, incorporated various types of instruments as, i.e., telescopes, spectrometers, which are expected to be available in the Spacelab program. A variety of pointing devices with arc second stability were studies: The European large pointer called the Instrument Pointing System for telescopes, a smaller pointer which is the size of one of the Spacelab pallets and which can simultaneously point two independent instrumented canisters. Within the context of the workshops and studies, rocket instruments like the UV Schwarzschild camera were included, similar to the instrument used to

observe comet West in early March from an Aerobee rocket; the results will be reported in this next session.

In the AMPS study also, comet investigations have been included. In the astronomy studies, comets were considered to be of secondary scientific importance; if bright cometary apparition appeared, it would be observed in a manner of OAO observations of Comet TSK. In the case of AMPS, there were some experiments identified relating to comets. One set of observations involved meteor observations and artificial meteors. Another experimental area, which is fairly extensive, is the study of chemical releases notably explosive releases, the releases of ionized plasmas, as barium, shape-charged barium and other chemicals like sodium, lithium or other resonant fluorescent species. In addition, within that same study, there is for example the laser resonance experiment and its evolution as a means of probing chemical releases.

By way of introduction, I want to mention to the working group that cometary physics has been treated more as a secondary area in all the previous work up to the present time. I would hope that this working group, possibly, would take the lead in evolving an advocacy group, a planning group, that would actually "sell" the program, or get it through the competition for available resources, to advance the program in physics of comets. As an example, the AMPS phase B study which was carried out by TRW and by the Martin Company included devices for releasing subsatellites or controlling subsatellites for releasing chemicals at different locations from the Shuttle, i.e., at geo-stationery altitudes and outside the magnetosphere with observations of these releases from the Shuttle. These experiments have a great similarity to what was already discussed.

With regard to these reports, the Academy Study was available in print in 1974. It is called The Scientific Uses of Space Shuttles, Space Science Board National Research Council National Academy of Sciences, Washington, D. C., 1974, a GPO publication. The Goddard report is a series of reports which may be available through the Goddard Space Flight Center.

I think most of you know that proposals are required by NASA and they are submitted in response to announcements. However, what is needed in the organization of comet research proposals is a program plan for physics of comets as a guide for peer groups reviewing proposals. For example, there is not, at the present time, a peer group for review of comet physics proposals, that will look at proposals in a manner commensurate with the type of physics we are talking about. To this end, an advocacy group and a program plan of cometary physics covering several years into the future could turn out to be valuable.

In regard to the present status of the Spacelab program, the Spacelab I and II missions and Orbital Flight Test missions experiment proposal due date has already passed. These Shuttle missions cover the period 1979 and 1980. It turns out that the flight schedule is expected to accelerate after that time reaching 4 or 8 missions in 1981 and from 6 to 10 missions in 1982.

Perhaps I should outline also how the comet program used to work in the past. It used to be poor, in the sense that for astronomical observations there was no program, except observations of orbits of comets by a few dedicated observers like E. Roemer, except in the case of a very bright comet. Only a few bright comets appeared - Ikeya-Seki in 1965 in which a rocket experiment turned out negative UV results; Tago-Sato-kosaka in

1970; and Bennett in 1970, an excellent, very bright comet. We are going to cover some of the ultraviolet results in this session, including the Lyman alpha detection and hydroxyl detection from these comets. There were no further bright comets until Kohoutek in 1973. Then, right after that, there was Comet Bradfield in 1974 and West in 1976. I think that the future will be similar if the comet is not bright we probably won't look at it. However, we can now observe with the new devices and the instruments in orbit with the longer viewing time and it will be possible to look at much dimmer comets which are between 5th and 10th magnitude. This will tremendously improve the astronomical set of observations. For example, in Bennett, we found only two lines, hydroxyl and Lyman alpha, we found the additional lines of OI (λ1304) and the CI (λ1541) in Kohoutek but that's all. That was enough for Paul Feldman to argue that there was enough carbon generated in that comet to be about equilivant to the water molecule evolution within a factor of ten, which is very significant. For comet West, there is a fabulous set of results by comparison. You will see these in this session. The spectroscopy of comets in the ultraviolet is superb. The spectroscopy of comets in the infrared is poor at the present time, and it is a new field in terms of molecular species.

OMIT TO P.265

ULTRAVIOLET AND INFRARED OBSERVATIONS OF COMETS: RECENT RESULTS AND PROSPECTS FOR THE SHUTTLE ERA

C. B. Opal and G. R. Carruthers *
Naval Research Laboratory
Washington, D. C.

Abstract

Recent observations in the ultraviolet and infrared, particularly during the apparition of Comet Kohoutek, have considerably increased our knowledge of comets. New atomic and ionic species (H, C, O, and C^+) have been identified with ultraviolet instruments on spacecraft. Improved observations of the OH radical in the near ultraviolet have been made from space and from high-flying airplanes. Recent ground-based infrared measurements indicate that cometary dust is very similar to that in the interstellar medium. Large regions of the infrared will be opened up when infrared instruments are operated in space, making it possible to detect the more abundant parent molecular species such as H_2O and CO_2. Other expected atoms and molecules such as N, CO, and H_2 will be detectable in the ultraviolet. Instrumentation applicable to these observations includes sounding-rocket class instruments, Spacelab facility instruments such as SUOT and SIRTF, and the free-flying LST. From these spacecraft data, a better picture of the composition of cometary nuclei will emerge, revealing much about the composition and conditions of the solar nebula during the formation of the solar system.

I. Introduction

Interest in comets has increased in recent years because the space program has spurred greater interest in the solar system as a whole. And Comet Kohoutek stimulated many observations, including a number from spacecraft. We will describe some of the recent observations, particularly those in parts of the optical spectrum not studied before. We will also discuss how observational capabilities will be expanded by future space systems--particularly the space shuttle--and how these expanded capabilities will help us to learn more about the nature of comets and their origin. This, in turn, will aid our understanding of the origin and history of the solar system.

A comet, as seen when it is close enough to the sun to be observable to the unaided eye, consists of a diffuse spherical halo called the coma, which is the brightest part of the comet that is ordinarily observable, and a tail (actually consisting of two independent parts, both of which generally point away from the sun). According to the currently favored "dirty snowball" model, the source of the phenomena associated with a comet is a nucleus, consisting largely of ice, which sublimes and sheds particles as the comet warms on approaching the sun. This nucleus has yet to be resolved with a telescope, but is probably a few km in diameter. As it evaporates the ice releases embedded dust and exotic molecules, forming the coma. Radiation pressure acting on the dust grains blows them away from the nucleus, producing the dust tail. The outflowing molecules are dissociated by sunlight, forming a succession of free radicals and finally atoms. Some of the molecules and atoms are ionized, forming a plasma which is dragged backward by the solar wind to produce the ion tail.

Figure 1. Comet Kohoutek photographed in the visible from South Baldy Mountain, New Mexico on January 11, 1974. (JOCR photo, courtesy NASA) Note that the smooth dust tail and kinked ion tail point in slightly different directions.

The solar system is believed to have formed from the contraction and condensation of a cloud of interstellar gas consisting mostly of hydrogen and helium, with about 1% by mass of heavier elements. The sun, other stars, and the interstellar medium have nearly identical compositions. Comets are now thought to originate in the very outermost portions of the solar system--the orbit of Uranus and beyond. In the outer solar system, the low temperatures that prevailed during condensation and agglomeration of primordial solar nebula

* Member AIAA

allowed condensation of the volatile H_2O, NH_3, and CH_4, forming "cometesimals". In contrast, only the less abundant refractory dust particles (silicates, iron, etc.) were incorporated into planetesimals in the inner solar system, where temperatures were 300 K or more. The cometesimals then aggregated to form comets, the cores of the outer planets and their satellites, in the same manner as the planetesimals formed the inner planets and asteriods. The satellites of the outer planets and comets are probably still very similar to the original solar nebula condensate in their composition; whereas the outer planets themselves gravitationally accumulated large amounts of the still more abundant (but non-condensible) hydrogen and helium, and became more like the sun in composition.

Comets are the most accessible samples of the original solar nebula condensate; hence the study of comets is very important to our understanding of the early phases of formation of the solar system.

II. The Neutral Coma

Our best chance of learning about the volatile component of the cometary nucleus is from studying the neutral coma.

In the visible, the strongest emissions from neutral species are due to bands of free radicals such as CN and C_2. Although it is possible that some of these radicals were trapped in the ices, it is much more likely that they are photodisintegration products of larger, stable molecules. None of the potential parent molecules has been detected in the optical spectrum--in fact, the only stable molecules yet detected (HCN, CH_3CN) have been seen through their emission of microwaves. Unfortunately, it is very difficult to derive abundances from microwave measurements, because the excitation conditions are poorly known.

Probably the most abundant constituent of most comets is water. Its photodissociation products, OH and H, can be observed from the ground, but only with difficulty because of complications from ozone absorption and geocoronal hydrogen emissions. In fact it was not generally realized how really strong the OH emissions at 3090 A really were until they were observed in Comets Tago-Sato-Kosaka and Bennett by OAO-2. The OAO also discovered a strong signal at 1216 A from sunlight scattered from atomic hydrogen. (See Fig. 2.) The hydrogen region was very extensive and could be mapped out to millions of kilometers. The reason for the great extent is that momentum is shared equally between the two fragments of a dissociation process, hence light atoms like hydrogen fly away from the comet more rapidly than other species. Also, atomic hydrogen is fairly long-lived in the solar radiation field as compared to heavy molecules.

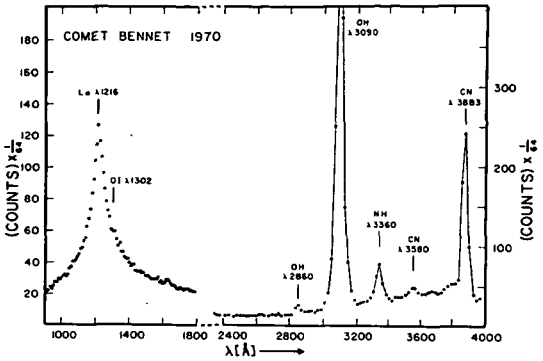

Figure 2. Objective spectrum of Comet Bennett obtained by OAO-A2. The 1216 A Lyman alpha line of H dominates the spectrum; it appears broad because of the large extent of the hydrogen cloud. Note the strong OH features near 3000 A.

The first real images showing the great extent of the hydrogen cloud were obtained with an NRL ultraviolet camera which was carried on an Aerobee rocket in early 1974 to observe Comet Kohoutek. A similar camera was also carried on the Skylab 4 mission. The observed cloud extended some 10^7 km from the nucleus, making it the largest object in the solar system after the heliosphere. Figure 3 shows equal brightness contours of the rocket image. The effect of solar Lyman-α radiation pressure is to deflect the atoms in the down-sun direction, which causes the more distant contours to become elliptical. Contour mappings like these make it possible to determine quite accurately the outflow velocity of the atomic hydrogen and the rate at which it is being produced by the comet.

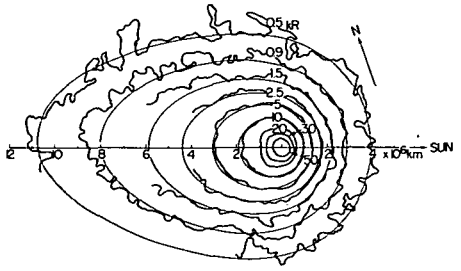

Figure 3. Equal brightness contours of the hydrogen cloud surrounding Comet Kohoutek observed from a sounding rocket on Jan. 8, 1974. The elliptical shape is caused by pressure of sunlight acting on the atoms. Solid lines are a theoretical fit to the data.

Similar observations were made with

the Skylab instrument, both before and after perihelion. Figure 4 shows the rate of production of atomic H as a function of distance from the sun. Note that the production rate was nearly constant and about the same both inbound and outbound, except for a brief outburst near perihelion. This is not what one would expect; ideally the rate of production of H should depend on the inverse square of the distance from the comet to the sun. It is also interesting that this comet was much brighter in the visible before perihelion than after. Clearly the production of dust (as seen in the visible) and the production of gas (as seen in the ultraviolet) were not following the same patterns.

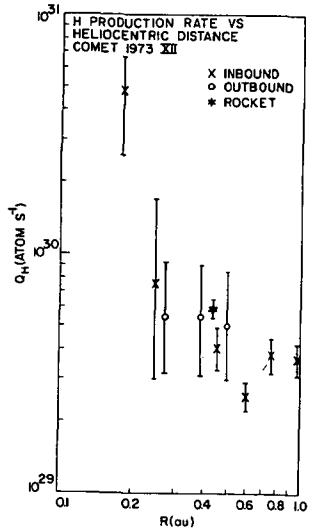

Figure 4. Hydrogen production rate of Comet Kohoutek as a function of distance from the sun, based on ultraviolet observations from Skylab 4 and the Jan. 8 rocket flight. Note the tremendous increase in output near perihelion, but relatively constant output otherwise, both inbound and outbound.

An important reason for studying atomic hydrogen is that even if water is not the dominant constituent, hydrogen is still likely to be one of the most abundant atoms in the head of the comet. Thus, even if we can't see the original parent molecules, we can infer a good deal about them from a comparison of the relative abundances of other atoms as compared to hydrogen.

The abundant neutral atoms, O, C, and N (like H), can best or only be observed in the far ultraviolet wavelength range (below 3000 A) which is inaccessible to ground-based observations. The abundances of atoms other than H were first measured from a pair of sounding rockets in January 1974. Scanning spectrometers covering the range 1200-3200 A were flown by Johns Hopkins University. An objective spectrograph covering the 1250-2000 A range was flown by NRL (on the same payload which contained the Lyman-α camera). Figure 5 shows part of the JHU spectrum. All of the features between 2000 and 3200 A are due to airglow except for the very strong cometary OH emissions in the 3090 and 2840 A bands. The feature at 1657 A (and a weaker one at 1561 A) are from atomic carbon in the comet. The features at 1304 and 1356 A are mainly atomic oxygen airglow, with a contribution from the comet at 1304 A. Monochromatic images of the comet at 1304 A and 1657 were obtained with the NRL spectrograph; Figure 6 shows isodensity tracings of the 1304 A image. Although these data were noisy, it was possible to determine the brightness and size of the oxygen coma and hence the rate of production of oxygen. Similar results were obtained for carbon.

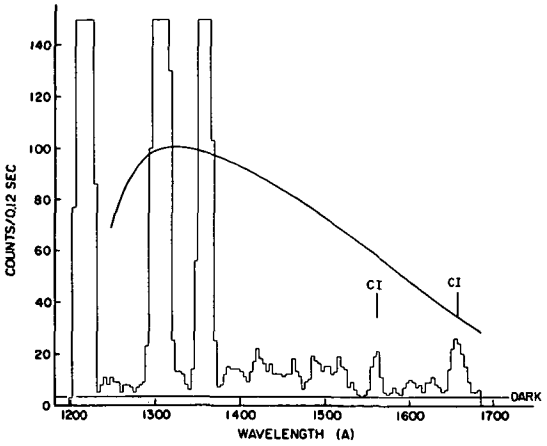

Figure 5. Ultraviolet spectrum of Comet Kohoutek obtained with a scanning spectrometer carried on a sounding rocket on Jan. 5, 1974. Carbon features are present at 1561 and 1657 A. Other features are due primarily to airglow, but part of the 1304 A atomic oxygen and of the 1216 A atomic hydrogen emissions are cometary.

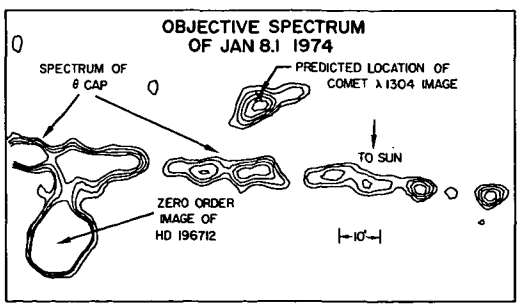

Figure 6. Equal brightness contours of the atomic oxygen cloud (obtained on the Jan. 8 rocket flight). The oxygen cloud is much smaller than the hydrogen cloud because the oxygen atoms move outward

more slowly and are more rapidly lost through ionization.

The results of the rocket experiments are ambiguous. The amount of O and OH observed was not as large as would be expected if most of the H came from dissociation of water. There seemed to be about as much carbon as oxygen. The fourth expected major atom, N, was not observed. These results imply either that organic substances and other complex molecules are a major component of the nucleus, or that O and OH become ionized or otherwise disappear from view more rapidly than we think. Observations of O^+ and OH^+ simultaneous with observations of O and OH are needed to clarify the situation.

The exploration of cometary spectra at wavelengths not accessible from the ground has only begun. With more sensitive ultraviolet instruments, we should be able to detect emissions from atomic nitrogen, carbon monoxide, and perhaps other molecules such as NO, N_2, and H_2. Extensions further into the ultraviolet (below Lyman-α) are needed to observe N, N^+, and Ar.

It is difficult to interpret the far-ultraviolet spectra of comets because the solar ultraviolet spectrum, which excites cometary emissions, consists of discrete emission lines rather than a continuum (as in the near ultraviolet, visible, and infrared). Therefore, the efficiency of a solar line in exciting a cometary emission varies drastically with the Doppler shift (due to the radial velocity of the comet relative to the sun). Thus, the solar line can be Doppler-shifted partially or completely off the corresponding cometary absorption line, and the observed emission is determined not only by the abundance of the particular specie in the comet, but also by the radial velocity, the width of the solar emission line, and the width of the cometary absorption line. Therefore, observations must be made over a range of radial velocities, including in particular the very short time interval near perihelion when the radial velocity passes through zero (and where the solar radiation is most intense). The velocity shift is more favorable for observing atomic oxygen before perihelion than after perihelion, because the solar Lyman-β line can excite the oxygen 1304 A emission (though not as efficiently as the solar 1304 A lines, most effective near zero radial velocity). Conversely, molecular hydrogen emission (also excited by the solar Lyman-β line) is best observed after perihelion.

The infrared has hardly been touched. Although (unlike the ultraviolet) there are numerous "windows" in the infrared where interference from the earth's atmosphere is relatively low, difficulties are produced by the fact that atmospheric emissions and absorptions due to OH, H_2O, CO_2, etc. make it hard to observe these same species in extraterrestrial objects. Also, in the far infrared, the atmosphere emits a thermal (black body) continuum, which also interferes with the observation of faint sources.

So far, only upper limits for known or expected cometary constituents such as H_2O, NH_3, CO_2, and CH_4 have been obtained by ground-based infrared observations. Undoubtedly, the higher sensitivity obtainable with cryogenically-cooled space telescopes will result in the detection of these and other parent molecules. There is observational evidence that comets shed flakes of ice when they are far from the sun; at present, the infrared signature of ice particles near 2 μ has not been detected because when comets are close to the sun, the ice evaporates too close to the nucleus to be observable with ground-based resolutions, and when comets are far from the sun, too few ice particles are released to be detectable with available ground-based sensitivities.

In addition to limited spectral coverage, ground-based cometary observations suffer through most of the accessible wavelength range from foreground glow due to atmospheric emissions and scattering of sunlight. The latter is particularly important when comets are close to the sun, and hence must be observed near sunset or sunrise. Also, however, ground-based observations (even with the largest telescopes) are limited in resolution to about 1 arc second by atmospheric turbulence and motions. Observations with a large, diffraction-limited space telescope will give 0.1 arc sec resolution capability and freedom from atmospheric foreground. This will allow resolution of the cometary nucleus and the "transition zone" in which volatized parent molecules are dissociated to form the coma. Thus, new spectral identifications may be made even in the visible wavelength range, as well as in the extended spectral range accessible from space.

III. The Dust Tail

The smallest dust particles released by the sublimation of "dirty ice" are blown away by the radiation pressure of visible sunlight and disperse outward through the solar system. The larger, heavier ones spread out gradually in the comet's orbit, forming a meteor stream. These shower meteors, however, generally are still too small and friable to survive entry to the earth's atmosphere, and do not reach the ground. Some information about their composition (particularly the relative abundances of the heavier metallic elements) can be inferred from the visible spectra of these meteors, but the most abundant non-volatile constituents such as mineral compounds of silicon, oxygen, and carbon, cannot be observed in the visible spectrum. Samples of the dust

by high flying airplanes and, most recently, samples gathered in foils on Skylab, have provided additional information. But the samples have been modified by the impact and have been altered by being near the sun for some time, so they may not be representative of the major dust component of the comet.

Data on fresh dust must come from studying the dust tail directly. In the visible, the dust simply reflects sunlight and, except for some polarization, the scattered light does not reveal much about the size distribution, structure, or composition of the dust. In the ultraviolet there is so little sunlight to reflect that the tail has not yet been detected. Most of our information on the dust comes from infrared measurements.

Figure 7 shows broadband and visible measurements of the brightness of the dust tail of Comet Kohoutek which were made at several sun-comet distances by E. P. Ney at U. of Minn. The broad peak in the visible spectrum is simply reflected sunlight; it gets fainter as the comet recedes from the sun. The broad peak in the infrared is thermal radiation from the dust. The wavelength of the peak is determined by the temperature of the dust. Note that, as expected, the peak moves to longer wavelengths as the comet recedes from the sun and the grains cool down. The temperature of the grains is higher than the predicted temperature of a black body at the same distance from the sun. This indicates that the grains have difficulty radiating their heat, which would be the case if the grains were smaller than the typical infrared wavelength they are trying to emit; this sets the upper limit on the size of a typical cometary dust particle at a few microns. The fact that the reflectivity of the grains doesn't change much in the visible means that they are larger than visible-light wavelengths, in other words, bigger than a few tenths of a micron. Thus the infrared spectrum gives a good idea of the size of the particles. Also, there is usually a peak near 10 microns which can be attributed to metallic silicate material. The infrared signature of the dust is identical to that of interstellar dust, which indicates that comets may hold some of this cosmic dust in cold storage in essentially unaltered form.

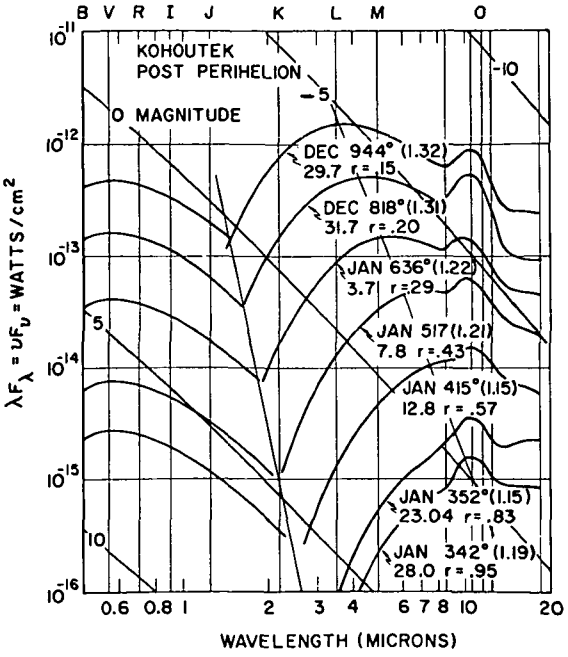

Figure 7. Broadband visible and infrared measurements of the dust tail of Comet Kohoutek over a range of sun-comet distances. The peak in the visible is reflected sunlight, that at longer wavelengths is thermal emission from the dust.

It is important to make ultraviolet measurements of the dust to see whether it has characteristics identical to interstellar dust in that portion of the spectrum as well. In particular, the dust should have an absorption band near 2200 A and should scatter more strongly to shorter wavelengths. These measurements can only be made in space by a sensitive ultraviolet spectrometer.

IV. The Ion Tail

Ion tails are formed through a complex and poorly understood interaction of the gases in the coma with the solar wind. The ions apparent in the visible spectrum are clearly not produced by photoionization, since they do not originate from a diffuse region but rather from confined regions near the nucleus. Among the ions present are CO^+, N_2^+, OH^+, CH^+, and H_2O^+. The latter was identified recently in spectra of Comet Kohoutek, and in old comet spectra through some recent laboratory and theoretical work on the spectrum of ionized water. Probably most of the ions present simply don't show up in the ground-accessible spectrum. Expected ions which are observable only in the vacuum ultraviolet include O^+, C^+, N^+, Si^+, and many others.

Because of the difficulties in

interpretation, ion tails do not yet tell us very much about the composition of the nucleus. Rather, they are of interest for what they tell us about the solar wind. In fact, the existence of the solar wind was first postulated by Biermann on the basis of the existence of ion tails. The direction of the tail allows one to determine the speed of the solar wind. Since comets can go closer to the sun and farther out of the ecliptic than existing spacecraft, they provide a unique means of studying the solar wind in these regions.

Ground-based observations of ion tails when the comet is near the sun are hampered by twilight, which washes out the tail, and by the fact that the lifetimes of the ions which can be observed in the visible are short close to the sun, making the tail short. The closest to the sun an ion tail has ever been observed is .18 a.u.; this observation was made in the far ultraviolet. Figure 8 shows an image in the 1250-1600 A band of Comet Kohoutek at that sun-comet distance, obtained during the Christmas Day EVA on Skylab 4 with the NRL S-201 ultraviolet camera. Although the emitting species has not been identified spectroscopically, it is probably the long-lived carbon ion. Incidentially, there was no twilight problem with this measurement; in fact, it was made in broad daylight! Unfortunately the earth was almost in the plane of the comet's orbit, which means that the viewing geometry was very poor for determining the speed of the solar wind. This type of measurement will have to await a comet with a more favorable orbit.

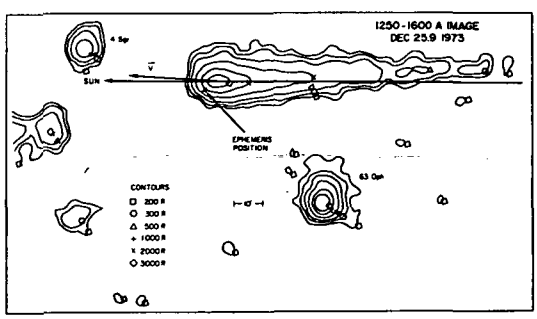

Figure 8. Brightness contours of Comet Kohoutek in the 1250-1600 A band on Christmas Day, 1973 from Skylab (same camera as used for the H observations). This is probably an ion tail of C^+. Note that the tail does not point exactly away from the sun, owing to comet motion and non-radial flow of the solar wind. This is the closest to the sun that an ion tail has been observed.

Desirable observations for the future are measurements of ion tails at high ecliptic latitudes and near the sun. Spectroscopic observations of ion tails in the ultraviolet, to identify and measure the emissions, are necessary. Also, high-resolution spectra in the visible and other spectral regions would tell us more about the velocity distribution of the ions near the head and in the tail, from which one could hope to better understand the interaction of the coma gases with the solar wind and the subsequent acceleration process. It is important to obtain a self-consistent, well-calibrated set of observations over the largest possible portion of the comet's trajectory, as it approaches and recedes from the sun. (Incidentally, not only twilight problems, but also the vagaries of weather, make this very difficult to do from the ground.) Also, higher-resolution imagery (from a space probe or a telescope in earth orbit) is needed to resolve the details of the ion tail origin close to the nucleus.

V. Future Prospects

It is clear that there are huge gaps in our understanding of comets. We will now turn our attention to some of the ways of filling these gaps which will be available in the future. We will concentrate on those made possible by future spacecraft.

An obvious thing to do is send a spacecraft to a comet to take high resolution pictures of the nucleus, to sample its atmosphere with a mass spectrometer, to measure the size distribution of the dust, and perhaps to somehow sample the nucleus itself. The most desirable type of comet to study is one that has never been near the sun before--a so-called "new" comet. Unfortunately, a slow fly-by of, or rendezvous with, such a comet is extremely difficult. For one thing, most comets are discovered only a few months before perihelion, which makes preparing a spacecraft for the mission virtually impossible. For another the energy requirements for rendezvous are enormous. The minimum delta v required for a parabolic comet orbit is more than 20 km/sec; 50 km/sec is more typical. This is clearly out of the question for conventional chemical rockets, although it could be achieved with solar electric propulsion. There are also difficulties associated with dust near the nucleus, which could obscure it from view and which would present serious hazards to a spacecraft undergoing a high-speed fly-by. The best prospect for a direct cometary mission in the near future seems to be a slow fly-by of one of the less spectacular periodic comets. These require smaller delta v's and have dust production low enough for the nucleus to be observable and for the spacecraft to survive undamaged. It would also be possible to target a spacecraft with a non-cometary mission near a comet at a safe distance; in fact this is being studied as a possibility for the third Helios mission. Even granted that a fly-by is undertaken in the near future

there will still be an important role for near-earth observations.

We anticipate that there will be further sounding rocket experiments, since they offer the advantages of quick response time and good economics for a single-purpose objective such as a comet study. Unfortunately it is not practical to use sounding rockets for synoptic studies of the comet's passage through perihelion, where the most interesting changes take place.

An orbiting observatory would provide the necessary time coverage, but because of the high cost and the unpredictability of comet observing opportunities, building a satellite solely for a comet-study mission would be difficult to justify. Thus, future orbital observations of comets will be made primarily from spacecraft designed for other purposes.

The most promising prospect for near-earth observations in the near future is provided by the space shuttle. The flexibility, large recoverable payload capacity, short preparation time, and relatively low cost of Spacelab missions will be ideal for comet studies. One of the major orbital facilities planned for launch on the shuttle is the Large Space Telescope (LST). This will be a diffraction-limited, 2.4 meter aperture telescope with angular resolution of 0.1 arc sec (10 times the best ground-based resolution) and capable of observations over the entire spectral range from about 1000 A in the far ultraviolet to 1000 microns in the far infrared. It will be capable of low-resolution spectrometry in the 1000-8000 A wavelength range, high resolution spectrometry in the 1150-3100 A wavelength range, and high-resolution direct imagery. It will, therefore, be a powerful tool for the study of comets. The space shuttle will also serve as a first stage for deep-space missions, utilizing solar-electric as well as chemical upper stages, which could be used for in-situ probing of comets.

In addition to its use as a launch vehicle for automated spacecraft such as LST, and as a booster stage for deep-space missions, the shuttle can be used as a platform from which to make short-term astronomical observations (7 to 30 days in the Spacelab mode of operation), followed by return of the shuttle and its instrument complement to the earth.

Proposed Spacelab missions include major facility instruments, such as the Spacelab Ultraviolet/Optical Telescope and the cryogenically-cooled Spacelab Infrared Telescope Facility, both of which will be quite useful for cometary studies. The Spacelab mode of operation, however, can also incorporate a large number of smaller, independent instruments directed toward a common objective. It will be possible to assemble a diverse payload designed specifically to study comets and to fly it on short notice. One can envision a group of small "sounding-rocket class" instruments, covering the optical spectrum from the near infrared to the extreme ultraviolet. Because the instruments would be recoverable, film recording could be used in many cases, resulting in greatly simplified instrument design. For the middle and far infrared, cryogenically cooled instruments could be carried. Data retrieval in this case could be in the form of on-board recording analogous or even practically identical to that used in a terrestrial observatory. Various specialized instruments could be carried as well.

VI. Conclusions

In summary we emphasize again that we have yet to find out (for certain) what comets are made of. When we do, we will have some important clues about what the solar nebula was made of and how it condensed to form the solar system. To find out what comets are made of, we must make sensitive instruments covering the whole spectrum and carry them above the atmosphere. Of the methods available for doing this, the shuttle holds the most promise: it provides the advantages of flexibility, low cost, quick response time, and retrievability, all of which combine to make it an ideal platform for comet watching.

VII. Bibliography

Many of the recent papers on comets have appeared in the December 1974 issue of Icarus (V. 23) and in the Proceedings of IAU Colloquium No. 25. Several reviews are scheduled for publication in the near future.

VIII. Acknowledgments

We thank A. Code, J. C. Brandt, E. P. Ney, and P. D. Feldman for providing illustrations.

D12

ULTRAVIOLET SPECTROSCOPY OF COMETS

Charles F. Lillie
The University of Colorado at Boulder

Introduction:

Since the first ultraviolet observations of comets were obtained in 1970 (Code et al., 1972), considerable progress has been made in both observational techniques and the interpretation of their spectra. The recent rocket observations of Comet West by groups at the University of Colorado, Johns Hopkins University, and Goddard Space Flight Center produced the most detailed ultraviolet spectra currently available. Ultraviolet spectra offer a special insight into the physics of comets because most of the abundant atomic and molecular species present in the coma, H, C, O, CO, CO_2, OH, CN, NH, have resonance transitions in the 1000 to 4000 A region of the spectrum.

Impact of the Space Shuttle

As an observing platform for advanced instrumentation, the Space Shuttle has the potential for great advances in the study of comets. Ground-based observatories are severely hampered in their studies by the earth's atmosphere.

In many respects, comets are most interesting during perhelion passage when the production rate of dust and gas is at a maximum. Unfortunately, this event takes place in only a few days, during which the comet can only be observed for a brief period just before sunrise or after sunset and is seen through a long path length in the earth's atmosphere

which produces image blurring, absorption of light, and enhanced sky brightness due to scattered light and airglow. More often than not, it seems, the weather is bad just when key observations are to be made. And, of course, ground-based measurements are only possible in the visible and near infrared where the features are mainly due to trace constituents of the comet: CN, C_2, C_3, CH, NH.

By contrast, the Space Shuttle orbits the earth 15 times each day, far above the atmosphere. With its rapid turnaround time and frequent launch schedule, it should be possible to fly an integrated payload to observe newly discovered comets at perihelion passage at wavelengths from the extreme ultraviolet to the far infrared or sub-millimeter range.

In addition to high spectral resolution measurements, it will be possible to obtain nearly diffraction-limited images through narrow bandwidth filters which isolate specific atomic and molecular species such as H, O, CO, CO_2^+. And we will be able to observe the comet every 95 minutes, 15 times each day, to follow temporal changes in the production rate of atoms and molecules due to solar activity, which occur with time scales shorter than a day.

Cometary Spectra

We have perhaps the most complete spectral coverage for comet West (1976). Figure 1 shows its spectrum in the 3000 to 5800 A region, where the dominant features are due to C_2, C_3, and CN. These data were obtained from Boulder when the

comet was low in the sky, and the OH feature at 3090 A was absorbed by ozone in the earth's atmosphere. Satellite observations show OH λ3090 is approximately twice as strong as CN λ3883. Figure 2 shows Andy Smith's spectrum of comet West in the 1600-4000 A region with a rocket-borne Schwartzschild camera. It illustrates the increasing richness of cometary spectra as one goes further into the ultraviolet. As a rule, the information content per unit wavelength interval seems to be inversely proportional to the wavelength. Here we see not only a strong, over exposed OH λ3090 feature, but many previously unobserved features due to CO^+, CO_2^+, CS, and Si. The underlying continuum is due to sunlight scattered by dust; its density decreases toward long wavelengths due to vignetting in the camera. The CI λ1657 and CN λ3883 features show weakly at the extreme edges of the spectrum. This is but one of 30 or 40 density profiles from Smith's observations which have not yet been analyzed.

Figure 3 is a reproduction of the rocket observations of comet West by Feldman and Brune (1976). In the 2000 to 3200 A region we again note the CO^+ first negative band and the first positive band of CO_2^+. Shortward of 1700 A, the spectrum is dominated by features due to atomic carbon and oxygen. The Lyman alpha feature of atomic hydrogen, at λ1216, not shown here, is the strongest single emission feature of comets. Figure 4 shows the ultraviolet observations of Comet West obtained by Barth, Lawrence, and Rottman.

In addition to the features due to C and O we note the Fourth Positive Band of CO, including what may be the (5-0) transition at 1393 A.

Interpretation of the Spectra

The obvious information to be derived from a study of these spectra includes the density, temperature and composition of the coma and tail of the comet as a function of distance from the nucleus and, by repeated observations over a period of time (several weeks if possible) how these properties vary with heliocentric distance. In order to determine these parameters, it is necessary to understand the excitation mechanism for the observed features. We should also like to determine the production rate of dust and gas in the comet as a function of heliocentric distance. Given this information, it will then be possible to construct models for the coma of the comet and to study the gas phase reactions which occur in the collisional region of the coma. At the boundary of the coma, and in the tail of the comet, we should also like to understand the interaction of the cometary plasma with the solar wind and the interplanetary magnetic field.

In addition to providing a better understanding of comets, these studies are relevant to research on the CO_2-rich atmospheres of Venus and Mars whose spectra resemble in many ways the ultraviolet spectra of comets.

Comet Bennett

Many of the features in the spectra of comet West had been detected earlier in the OAO-2 observations of comet Bennett (1970 II). Because the OAO-2 spectrometer was an objective grating instrument (Code et al., 1970) a strong signal due to Lyman alpha was measured at all grating positions. Figure 5 shows the spectrum of comet Bennett in the 1250 to 1800 A region with the contribution of Lyman alpha removed. It shows, for the first time, (Lillie, 1975) the CO Fourth Positive Bands, as well as OI λ1304, CII λ1335, CI λ1657, and possibly [OI] λ1356.

Comparing the spectrum of comet Bennett with that of comet West, we note a great decrease in the strength of the CI lines relative to OI, and an enhancement of the emission rate in the 1350 to 1450 A. Although these difference may be due to differences in composition, it seems more likely to be a result of the different heliocentric distances at which they were observed: 0.39 a.u. for West, and 0.82 a.u. for Bennett.

We have fit synthetic spectra to these data, assuming a Boltzmann distribution of line strengths for the Fourth Positive System and find a good correlation in the 1450 to 1800 A region. In order to fit the 1850 to 1450 A region, however, it is necessary to assume the higher vibrational bands are far more populated than one would expect. We have examined the possibility that the emission features in this wavelength interval are due to the CO ($d^3\Delta_i$-$X^1\Sigma^+$) system,

but no conclusion could be reached with the limited information on this band system which was available to use.

We may also use the OAO data to calculate the lifetimes of these atomic and molecular species against charge-exchange and photoionization. Since the ultraviolet spectrometer is an objective grating instrument, it provides information on the spatial distribution of the emitting species (Keller and Lillie, 1974). Additional information can be obtained by comparing the emission strength measured in the 1x8 arcmin spectrometer slit with that in the 10' diameter field-of-view of the ultraviolet photometers. When we compare these observations with the intensity variations predicted by Haser's (1957) parent-daughter model for the radial expansion and dissociation/ionization of cometary gasses, we find the lifetimes for O and CO listed in Table 1. These values are a factor of $\sim$12 smaller than those in the literature, suggesting that an additional process is contributing to their destruction.

Given the lifetimes of these species we may also calculate the rate at which they are produced in the coma, if we know the excitation mechanism. Normally the emission lines are due to the resonant-fluorescence of solar radiation, although the strong [OI] λ1356 line must originate by another process. If we use the lifetimes from the literature, the hydrogen production rate, 6×10^{29} atom-s^{-1}, is consistent with previous measurements (Keller and Lillie, 1974; Keller and Thomas, 1975), and the value for oxygen,

2×10^{29}, is nearly right for it to be produced by the photodissociation of water; but CO is far more abundant than expected, a factor of 4-6 greater than hydrogen. We get the same result if we integrate over the entire CO Fourth Positive System from 1400 to 1800 A.

If we use the observed lifetimes of the species, (see Table 1) the oxygen production goes up to $\sim 2 \times 10^{30}$ atom-s^{-1}, which is consistent with Delsemme and Combi's (1975) production rate for oxygen in comet Bennett at the heliocentric distance (0.82 a.u.), based on observations of the [OI] λ6300 line. However, the production rate of CO is increased to $\sim 2 \times 10^{31}$ molecule-s^{-1}, which seems far too high.

TABLE 1 -- Column Densities and Production Rates

Species	$\lambda_{(A)}$	$B(s)_{(R)}$	$g(\frac{photon}{mol\text{-}sec})$	$\tau(s^{-1})$	f	$Q_{(mol\text{-}s^{-1})}$
HI	1216	70,000	2.5×10^{-3}	2.2×10^{6}	0.0033	6.1×10^{29}
OI	1304	3,420	3.1×10^{-6}	1.5×10^{5}	0.53	2.2×10^{30}
CI	1657	220	3.5×10^{-5}	2.5×10^{5}	0.46	8.5×10^{27}
CII	1335	1,260	4.9×10^{-6}	2.5×10^{5}?	0.46	3.5×10^{29}
CO	1510	440	2.2×10^{-7}	1.9×10^{4}	0.92	1.8×10^{31}
H_2	1608	≤ 30	1.4×10^{-7}	$\sim 10^{8}$	0.001	$\leq 3.3 \times 10^{29}$

We have examined other excitation mechanisms: dissociative recombination of CO_2^+,

$$CO_2^+ + e^- \rightarrow CO^* + O,$$

would require a similarly high production rate, and collisional excitation by electrons would require unreasonably

high electron densities. Perhaps chemiluminescence due to gas phase reactions in the collisional region of the coma, within $3x10^4$ km from the nucleus, is the answer.

Cometary and Planetary Spectra

Since a comet is influenced by many of the same factors which affect the atmospheres of the planets: solar radiation, solar wind, and the interplanetary magnetic field, and they can be studied at a large range of heliocentric distances: $0.10<r\leq 5$ a.u., we can gain new insight in the physics of planetary atmospheres by their study. In particular, we may compare them with the C, O, CO, and CO_2 atmospheres of Mars and Venus.

Figure 6 shows the spectrum of Mars' atmosphere (Barth et al., 1972) in the 2000-4000 A region. The CO_2^+ λ2890 feature is present, but instead of the CO^+ First Negative Bands found in Comet West, we have the Cameron Bands of CO which are the result of electron excitation. On the other hand, in both the comet and Mars we see the CO Fourth Positive Bands, CI, OI, and, of course, atomic hydrogen.

In the spectrum of Venus (Rottman and Moos, 1973; Figure 7) the CO Fourth Positive and the λ1400 emission line is abnormally strong, as in the case of Comet Bennett. Other features in the 1350 to 1450 A region are blended into the [OI] λ1356 and λ1400 features at the low resolution of this spectrum.

The spectra of Mars and Venus resemble those of comets in many respects, but also differ in subtle ways. Compara-

tive studies of the ultraviolet spectra of these planets and comets at different heliocentric distances ($0.1<r<2.0$ a.u.) should provide much insight into physical processes in planetary atmospheres and cometary comae.

Summary

This discussion indicates the current state of our understanding of the ultraviolet observations of comets, and it suggests the Shuttle could make an enormous contribution in this area. Of course, what is required to resolve the discrepancy between our observations of comet West and comet Bennett is a long-duration ($\sim$30 to 45 days) study of several comets, both dusty and gaseous, "new comets," and those which have previously approached the sun. The rocket observations represents "snapshots" taken when the comets were bright and close to the sun (0.34 to 0.39 a.u.), with relatively low spectral resolution (10 to 20 A).

Extended observations from the Shuttle would permit us to follow variations in the production rate of gas and dust and changes in the structure of the tail and coma as comets approach and recede from the sun. We should be thinking at this time of payloads which are tailored to cometary observations from the Shuttle; one which covers the accessible wavelength range at moderate and high spectral resolution, and permits monochromatic imaging at high spatial resolution; and which can be flown with minimal preparation, within two to three months after the discovery of a comet. We must try to get out of our present situation in which one

uses the instruments that are available (but designed for other purposes) when a bright comet comes along. The questions which are being posed by the ultraviolet observations demand specialized instrumentation.

References

Code, A. D., Houck, T. E., Lillie, C. F., 1972, "Scientific Results from the Orbiting Astronomical Observatory (OAO-2)," ed. A. D. Code, NASA Sp-310, 109.

Feldman, P. D., Brune, W. H., 1976, Astrophys. J. Letters 209, L45.

Lillie, C. F., 1975, Bull. Amer. Astron. Soc. 7, 507.

Code, A. D., Houck, T. E., McNall, J. F., Bless, R. C., Lillie, C. F., 1970, Astrophys. J. 161, 377.

Haser, L., 1957, Bull. Acad. Roy. Sci. Belgique 43, 740.

Keller, H. U., Lillie, C. F., 1974, Astron. and Astrophys. 34, 187.

Keller, H. U., Thomas, G. E., 1975, Astron. and Astrophys 39, 7.

Barth, C. A., Stewart, A. I., Hord, C. W., Lane, A. L., 1972, Icarus 17, 457.

Rottman, G. J., Moos, H. W., 1973, J. Geophys. Res 78, 8033.

Delseme, A. H., Combi, M. R., 1975, Bull. Amer. Astron. Soc. 7, 507.

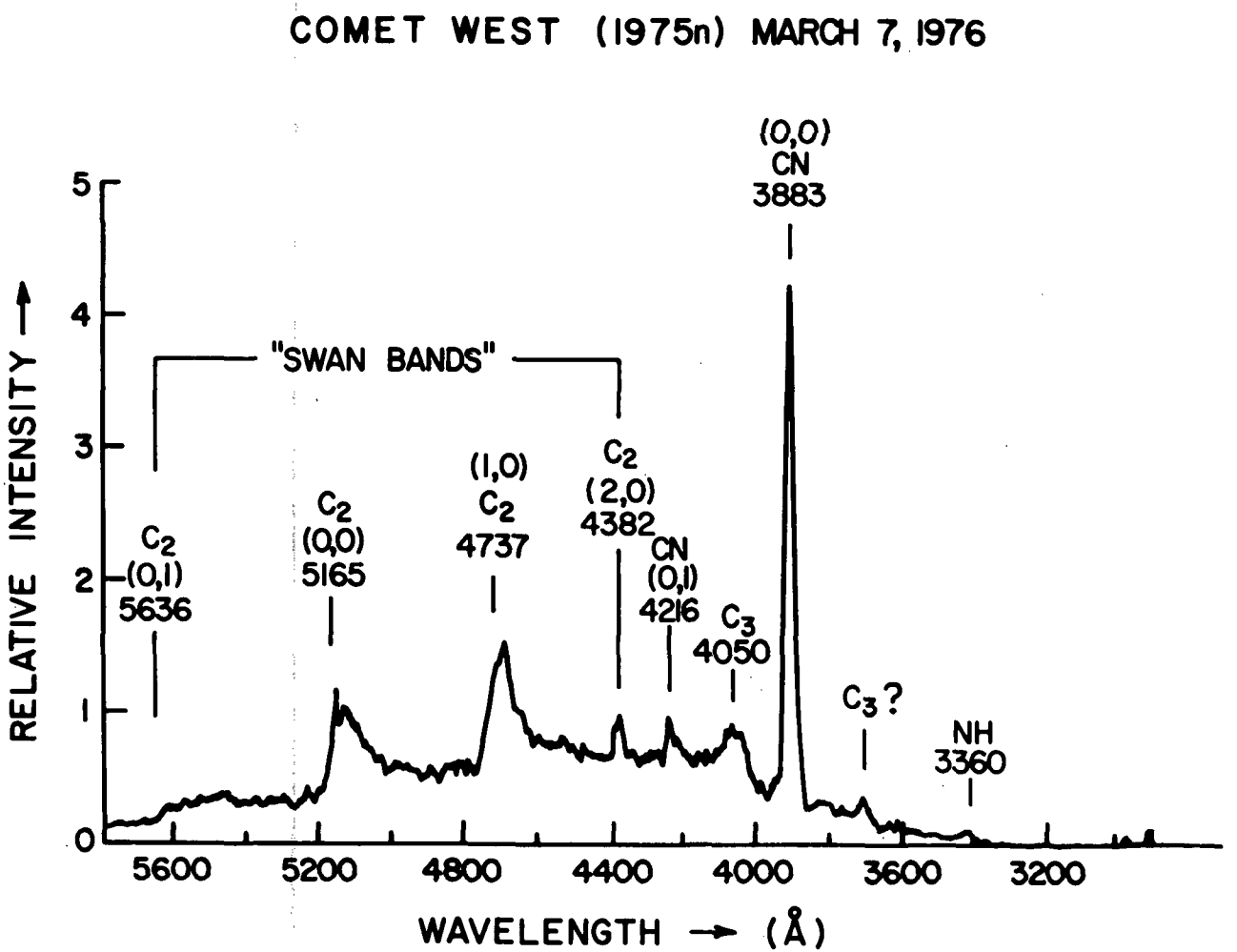

Figure 1. The spectrum of comet West in the 3000-5800 A region, observed from Boulder, Colorado, on March 7, 1976, with an 1/8-meter spectrometer and 15 A resolution. No correction has been made for atmospheric extinction.

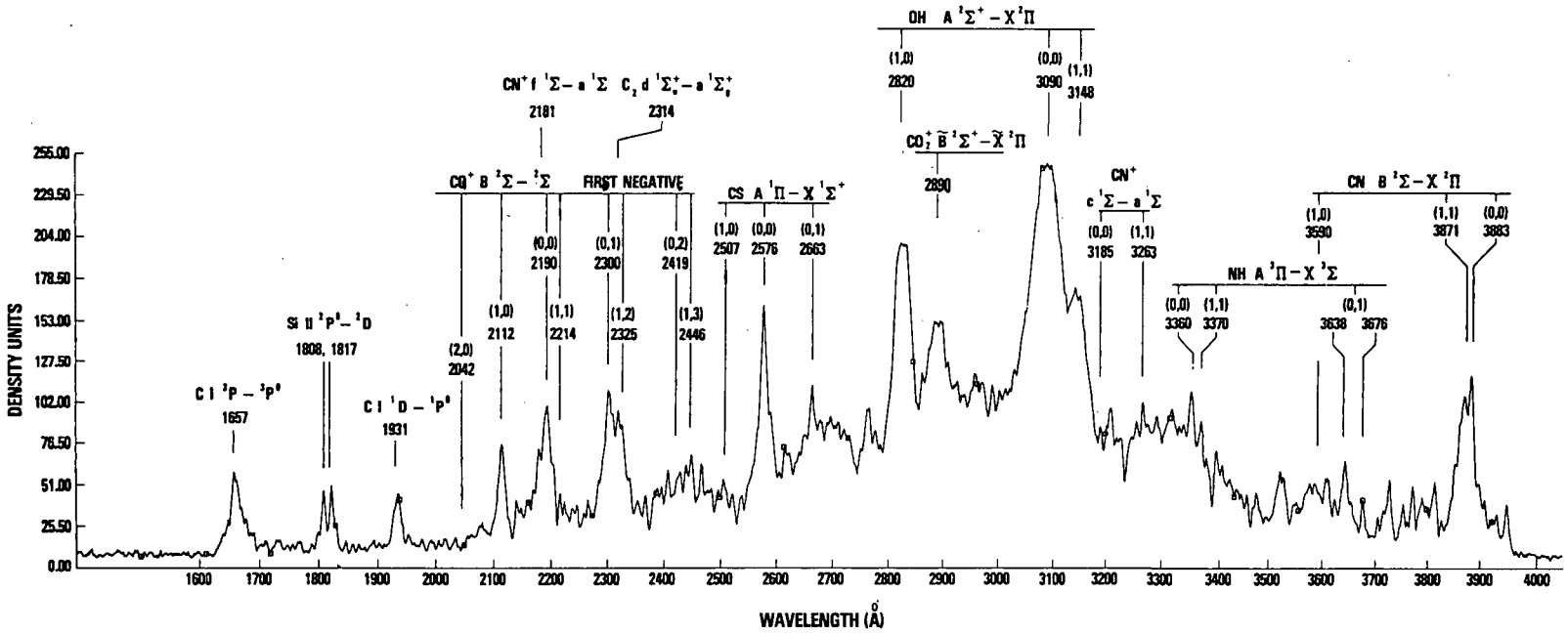

Figure 2. The spectrum of comet West in the 1600 to 4000 A region, obtained by A. Smith with a Schwartzschild camera on a sounding rocket launched from White Sands Missile Range (WSMR).

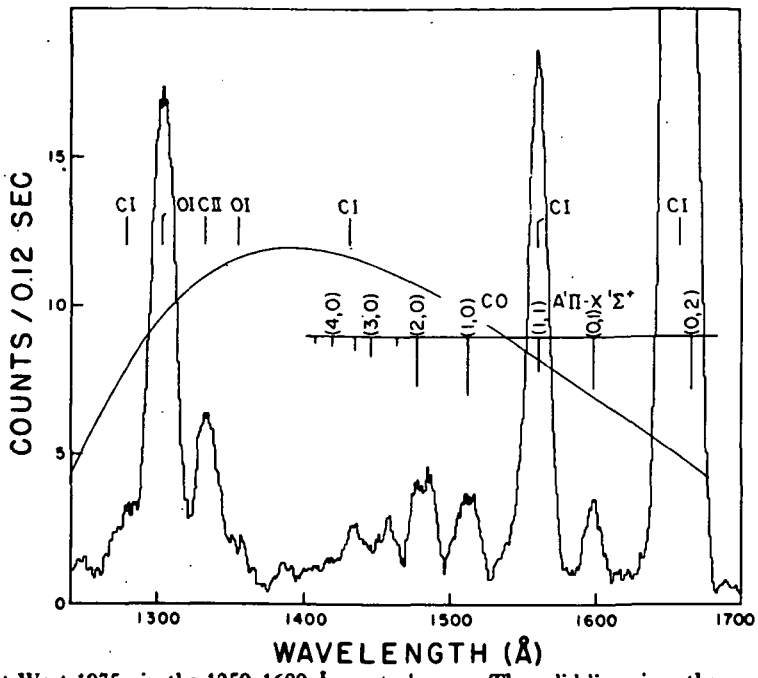

Spectrum of comet West 1975n in the 1250–1680 Å spectral range. The solid line gives the response of the spectrometer to a source of uniform spectral brightness. The peak of the C I λ1657 line is off-scale at 79 counts per 0.12 s.

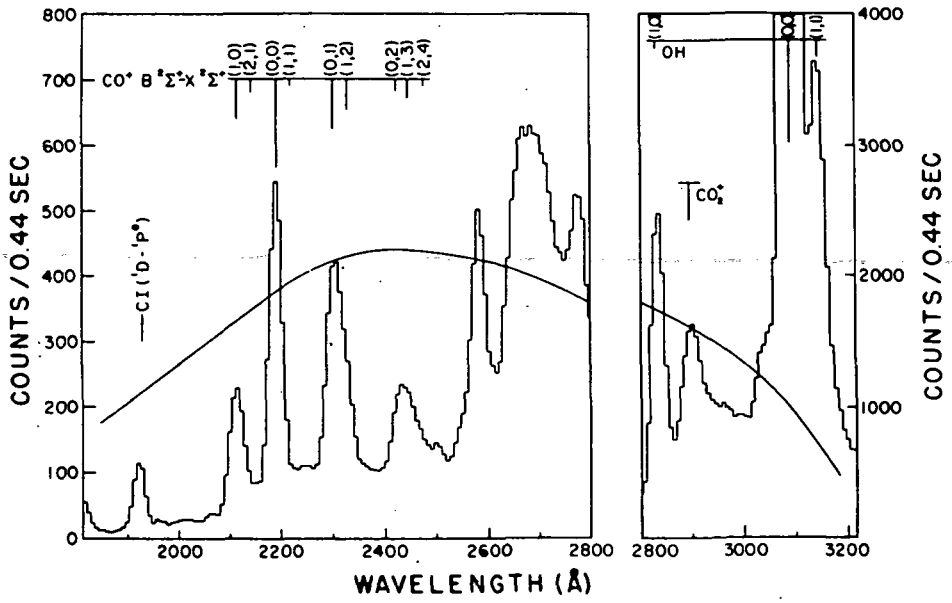

Same as Fig. 1 for the 1800–3200 Å spectral range. The off-scale value of the (0, 0) OH band is 55,000 counts per 0.44 s.

Figure 3. The ultraviolet spectrum of comet West obtained by P. Feldman with ultraviolet spectrometers on a sounding rocket launched from WSMR on March 5, 1976.

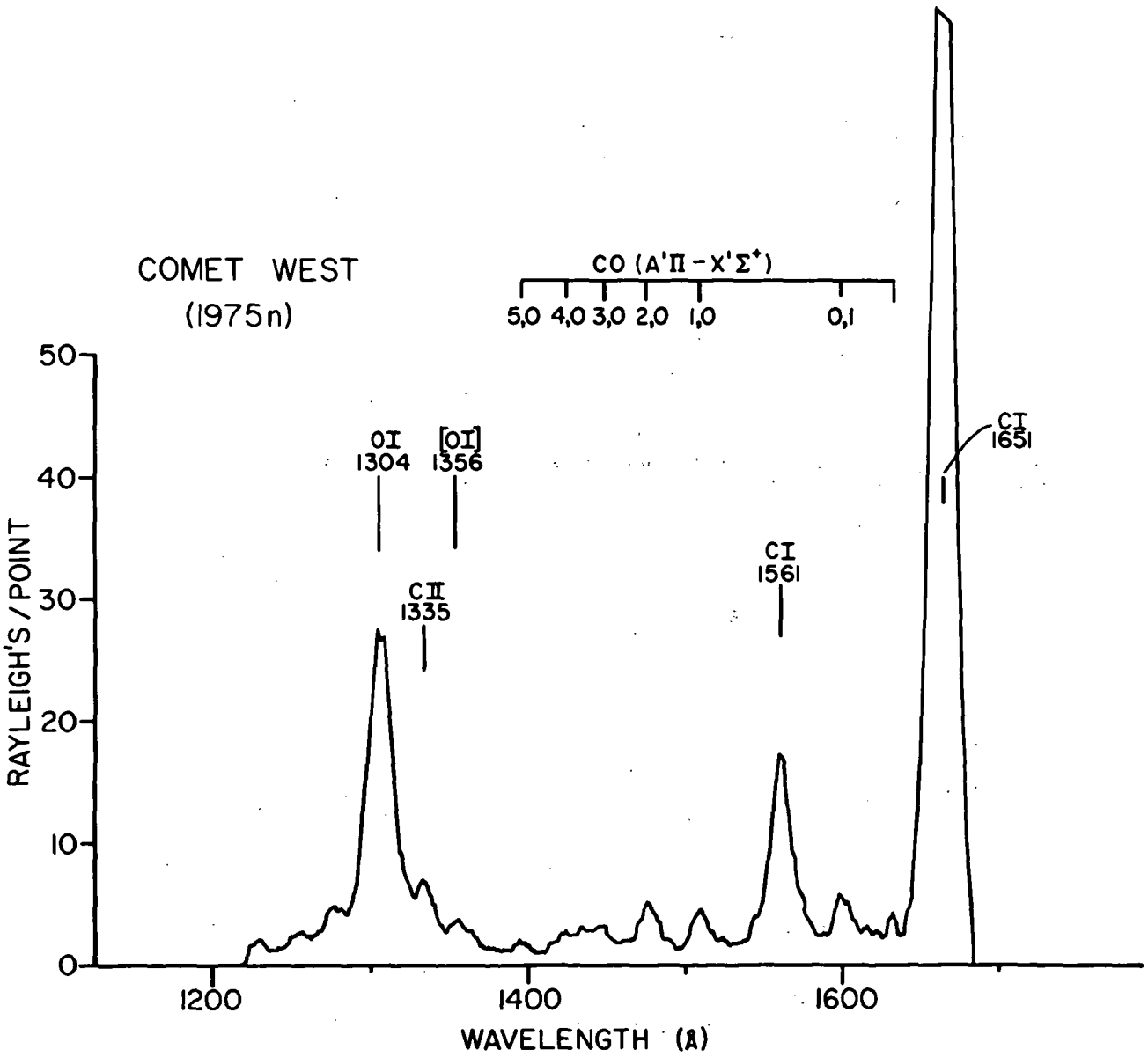

Figure 4. The spectrum of comet West in the 1250 to 1800 Å region obtained by Barth et al. with a sounding rocket launched from WSMR on March 5, 1976.

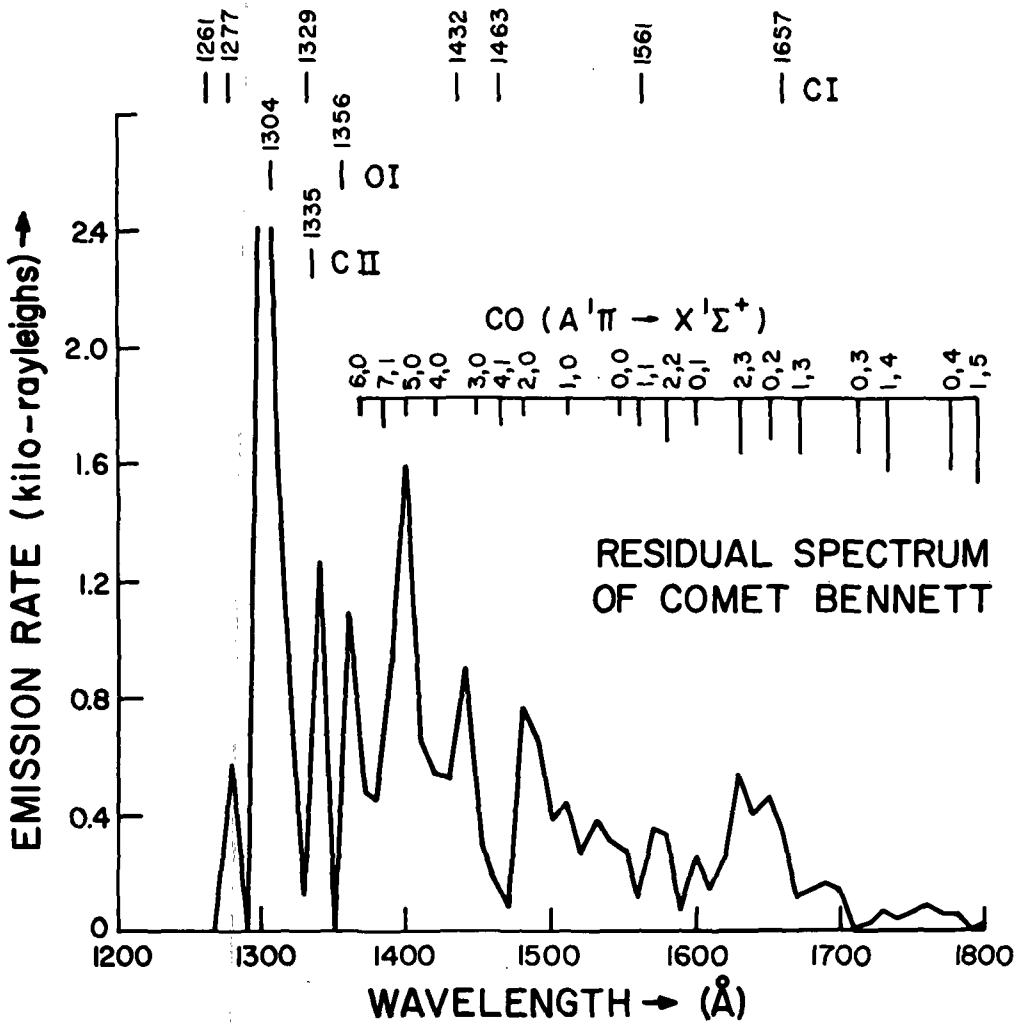

Figure 5. The spectrum of comet Bennett (1970 II) in the 1250 to 1800 A region obtained from OAO-2 in April 1970. It is the sum of six individual scans, at a resolution of approximately 15 A.

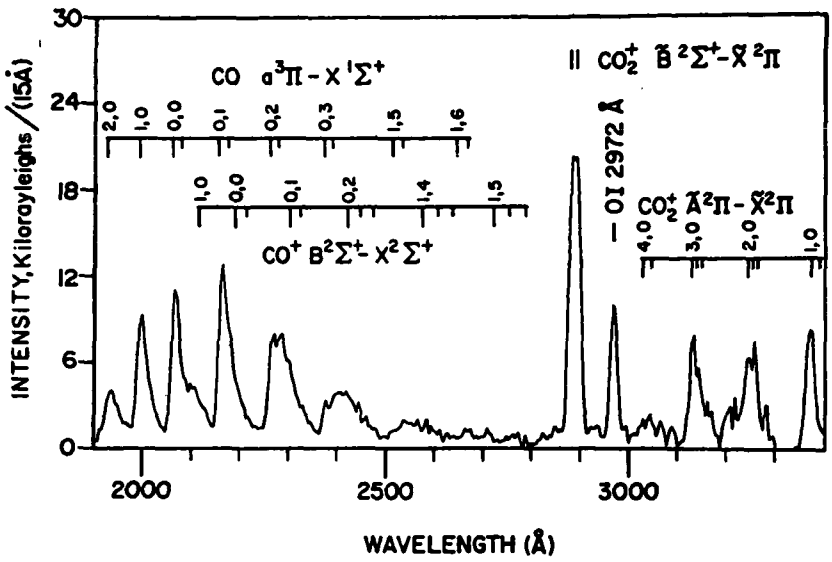

Mars airglow spectrum 1900–3400 Å. This spectrum is the result of averaging 120 individual limb observations with 15-Å resolution.

MARINER 9: MARS AIRGLOW SPECTROSCOPY

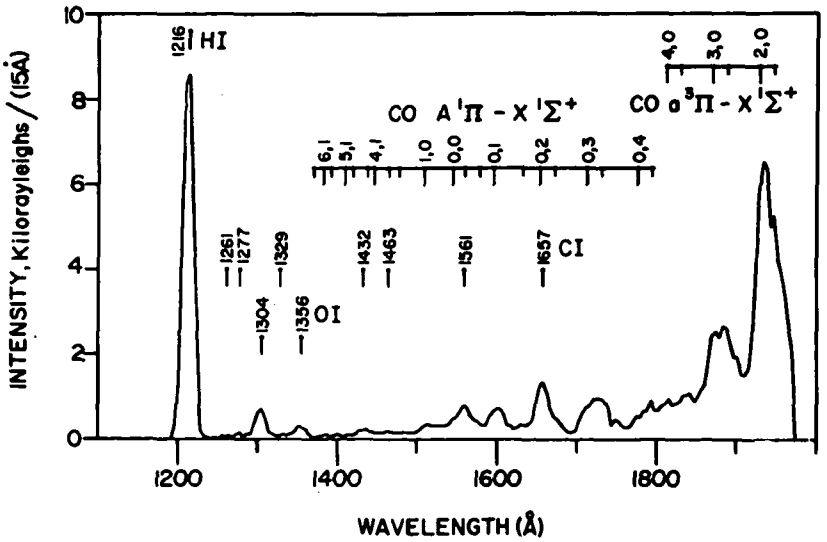

Mars airglow spectrum 1100–1900 Å. This spectrum also is the result of averaging 120 individual limb observations with 15-Å resolution.

Figure 6. The airglow spectrum of Mars' atmosphere observed from the Mariner 9 spacecraft at a resolution of 15 A.

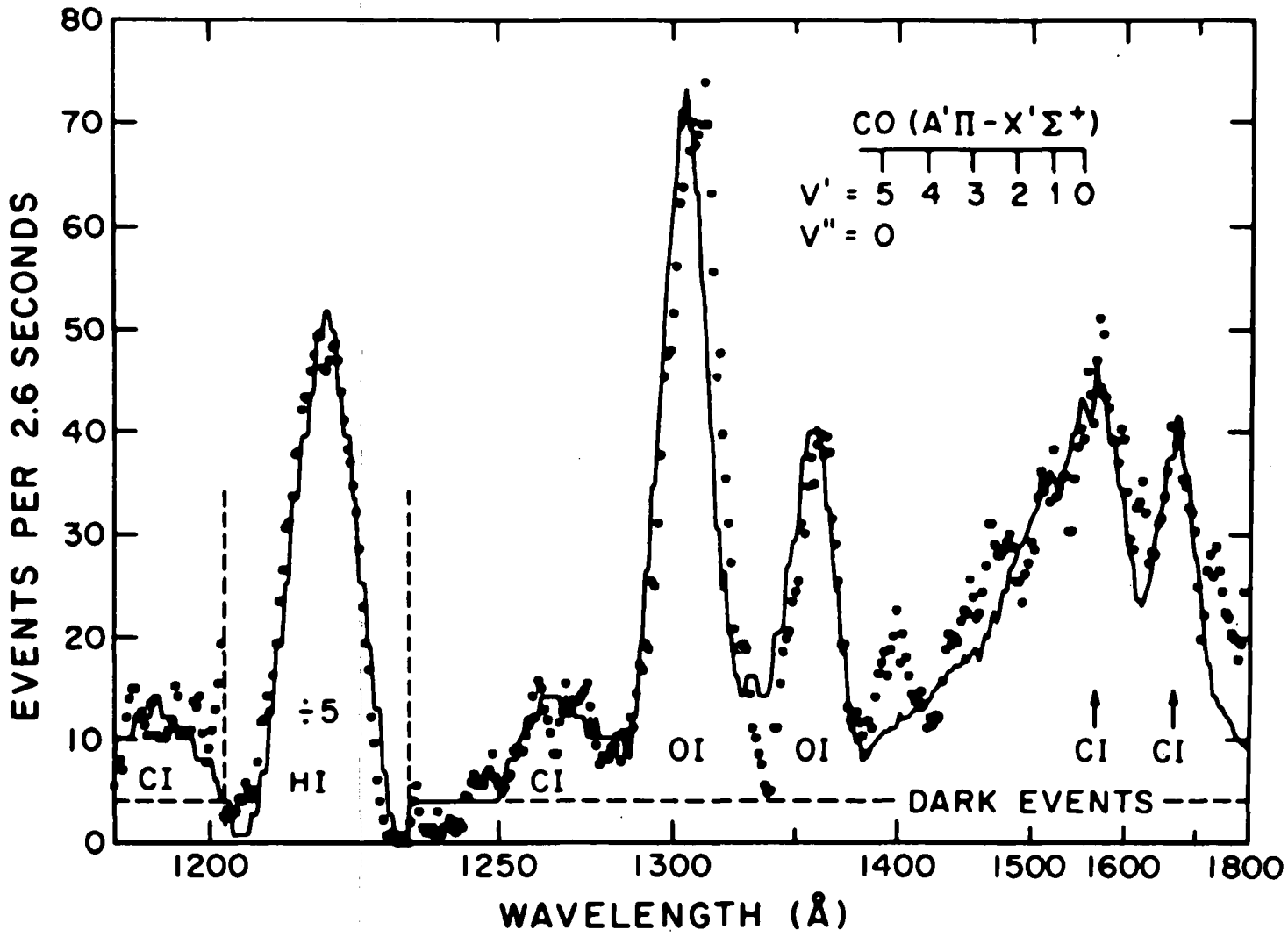

Figure 7. The spectrum of Venus in the 1150 to 1800 A region of the spectrum. The resolution varies from ~15 A at 1200 A to ~100 A at 1800 A.

OH OBSERVATIONS

Michel FESTOU
Service d'Aéronomie du CNRS
Verrières le Buisson
FRANCE

The OH emission has been observed from the ground since 1941 (Comet Cunningham 1940 c)(Swings et al., 1941) in the UV range.(0-0) and (1-1) bands of the $A^2\Sigma^+-X^2\Pi_i$ transition were identified. Then IR was detected and more recently radio-observations were conducted successfully on Comets Kohoutek (1973 XII) and West (1975 N) at 18 cm. The OH emission is one of the strongest arguments which have led to the icy model for the nucleus developped by Whipple (1950). With OAO2 observations in 1970 (Code et al.) of both emissions of H and OH of comet Tago-Sato-Kosaka (1969 g) begins a new epoch for the OH radical : as a matter of fact since that time we have quantitative measurements. H and OH observations can be used to check the validity of the icy model.

As far as we describe the H cloud as a very large object, we can assume the H-source to be ponctual. But in order to explain observations of the central part of the cloud, the source must be assumed as extended, and consequently we have to know the OH lifetime. It is why we attempted to obtain photographs of the OH emission from the Convair 990 airplane (Blamont et al., 1974).

The photographic technic from the ground has some inconvenients : in a single photograph we cannot reach the isophotes beyond two scalelengths of the OH radical from the nucleus owing to the rather small available time exposure (the comet is always following or preceding the Sun). Another difficulty bound to the long observationnal duration is the necessity to correct the proper motion of the comet with respect to the stellar field (whence a limited spatial resolution). As demonstrated by the easy detection of the OH emission in comet Bennett (1970 II) (Keller and Lillie, 1974), the future is to developp experiments from Earth-orbiting plateforms. However some problems will be raised as the necessity to account for stray-light coming directly from the Sun or diffused by the Earth. The principal improvements will be a better sensitivity (no atmospheric absorption + new technics)and an increase of the available time for measurements.

The analysis of OH isophotes provides two informations : the production rate of H_2O (the most probable parent of OH) and the dissociative-lifetime of the radical. This last parameter is model dependent : until now all observations in the cometary coma have been studied with the Haser's model which principal features are a radial and uniform expansion velocity of the molecules. This assumption is certainly uncorrect since the dissociation of the parent almost leads to an excess of energy (Keller, 1971) essentially converted into the kinetic energy of the products. We have computed a new model where the H_2O and the OH velocities are vectorially added and we have compared it with our OH observations of comet Kobayashi-Berger-Milon (1975 H) obtained from La Foux-d'Allos (France) in August, 1975. Thus we have

determined a lifetime of about 3×10^5 seconds (at 1 A.U.) instead of 2×10^5 s by an Haser's analysis. The uncertainty is $\pm 10^5$ s. Consequently all determinations of the OH production rates are model-dependant since they necessitate the exact value of the OH lifetime. Considering that H_2O is the parent of OH, there are two sources of H : if we are looking directly on the nuclear region, we observe the first component of hydrogen (produced by dissociation of H_2O, the H velocity is $\sim$ 20 km s^{-1} if there is no thermalisation by collisions) and looking farther we observed the H-atoms coming from the dissociation of OH. The knowledge of the OH lifetime is helpfull to construct such a model. The H and OH production rates must be compatible with the common origin hypothesis : that is the case when we compare the H/OH ratio in comets Bennett, Kohoutek and K.B.M., at least within a factor of 2. Another consequence of the H_2O presence in comets is that it is not possible to describe the Lyman-alpha emission as the result of the superposition of two emissions due to two populations of atoms having maxwellian velocity distributions centered at 8 and 20 km s^{-1} respectively : the first one indicates that collisions occur precisely where the second is created and thus there is necessarely a single population, what is inconsistent. In the same way, to utilize a 4 km s^{-1} component is purely artificial since a 8 km s^{-1} maxwellian distribution contains a lot of 4 km s^{-1} atoms.

Coming back to the advantages that can be reached in space, what are the objectives which can be looked at ? OH is the best indicator of the H_2O presence and a systematic survey of its emission is desirable. The measured production rates, reduced to 1 A.U., in the three

comets mentionned above are between 2 and 5 x 10^{29} molecules s^{-1}. This can reflect a common size for these objects. The comet Encke, for which we have H-observations, has a much lower production rate. It will be interesting to know if it is characteristic of the short period comets. The high value of the g factor for OH (and OD) and the low signal due to the dust at 3100 Å allow us to attempt a measurement of the OD/OH ratio in very bright comets. In our laboratory we have obtained spectra of a mixture of OD and OH. It was rather easy to detect a 10^{-3} - 10^{-4} ratio, but we were limited by small satellite lines of OH. The lines of the (1-0) bands of OD and OH are separated by many angströms and the continuum is very low, but this band is 20 times less intense than the (0-0) (Feldman, 1976). Note that the interpretation of the observation of the OD/OH ratio, if it is positive, may be certainly more difficult that the direct measurement of the D/H ratio at Lyman-alpha (to be done outside the geocorona). The Lyman-alpha and the OH emissions can be used to detect comets since they are very intense and well isolated. Neglecting the problem of the geocoronal Lyman-alpha absorption, the choice of the observing wavelength is dependant of the Sun-comet distance R. If R > 2 A.U., the Lyman-alpha emission is limited by the interplanetary background, while the OH emission is only limited by the zodiacal light (is there a threshold in the OH emission versus R ?). If R < 0.5 A.U., for a 2° field of view and a low production rate (no saturation effect), it is best to use the Lyman-alpha wavelength (a comet 10 times fainter than Encke could be easily detected at 0.5 A.U.). If 0.5 < R < 2 AU the two wavelengths are almost equivalent but the objects in the

OH light are much more stellar at Lyman-alpha and the determination of their position can be easier. Do not forget here that a one week mission risk to be insufficient to obtain meaningfull results, especially in a detection experiment.

References

I - Swings P., Elvey C.T., Babcock H.- 1941

Ap. J. 94, 320

II - Whipple F.L.-1950

Ap. J., 111, 375-394

III - Code A.D., Houck T.E., Lillie C.F. - 1972

NASA SP. 310, 109.

IV - Blamont J.E., Festou M. - 1974

Icarus, 23, n° 4, 538-544

V - Keller H.U., Lillie C.F. - 1974

Astr. and Astrophys. 38, 413.

VI - Keller H.U., - 1971

Mitt. Astron. Ges. 30, 143-148

VII - Feldman P.D. - 1976

Personnal communication.

D14

N81-24142

HYDROGEN LYMAN ALPHA OBSERVATIONS

H.U. Keller

Max-Planck-Institut für Aeronomie, Katlenburg-Lindau, FRG

The intention of this contribution is to give a brief status report on theoretical models dealing with the interpretation of the cometary Lyman alpha (L_α) observations. L_α is the resonant line of hydrogen at λ 121.6 nm. It is the most prominent emission feature in the cometary vacuum ultraviolet. The existence and general extensions of a hydrogen halo around comets had been conceived in the late sixties (Biermann 1968). One of the main clues for high gas production rates were the observations of a cometary component of the forbidden OI[630.0 nm] in the early sixties.

The first satellite observations revealed strong L_α signals of the two medium bright comets Tago-Sato-Kosaka (1969 IX) and Bennett (1970 II). These new data triggered some effort to create more elaborate models for the interpretation of the hydrogen halo. I will not dwell on the early models and their refinements but rather briefly describe the most recent results.

The UV observation of comet Bennett by the University of Colorado photometer (Keller and Thomas 1973) showed that the dimension of the hydrogen halo was more than 1/5 a.u. Figure 1 displays the model isophotes for the observational scans across the hydrogen cloud (Keller and Thomas 1975). They show the influence of the relatively strong solar L_α pressure force pushing the hydrogen atoms in an antisolar direction. This repellant force can even overcome the gravitational attraction. The iso-

photes are not at all circular as for the small optical coma. The hydrogen halo shows also a strong curvature due to the orbital motion of the

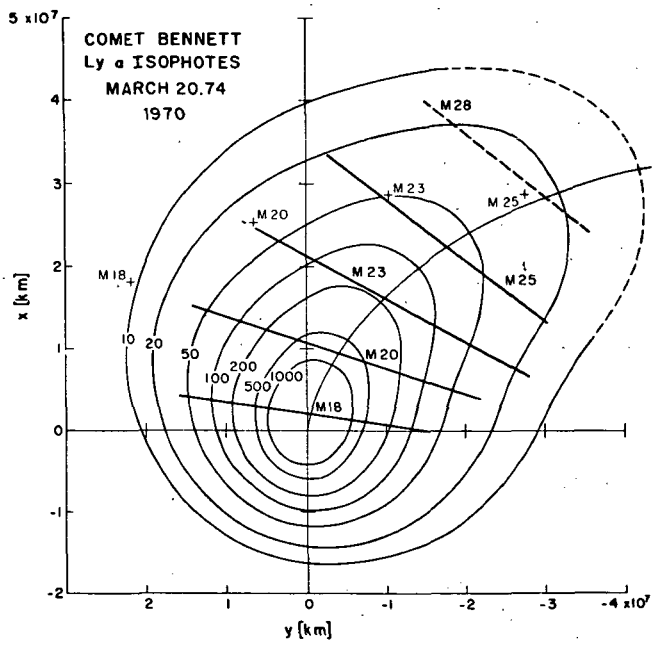

Fig. 1. Lα isophote map of a model calculation for 20.74 March. The x coordinate points in antisolar and the y coordinate in the direction of the cometary motion. x and y lie in the orbital plane of the comet. The cometary nucleus is located at the origin. Two velocity components $v_H = 7$ and 21 km s^{-1}, $F_\odot = 5 \times 10^{11}$ ph s^{-1} cm^{-2} Å^{-1} and $t_H = 1.3 \times 10^6$ s are used. The isophotes are labeled with relative apparent emission rates. 10 corresponds to 8.86 R for $Q = 5.9 \times 10^{29}$ H atom s^{-1} at 1 a.u. ($n = 2$). Heavy lines are scans of the OGO–5 University of Colorado photometer at their particular geometrical position depending on the observational date (M 28 dashed). The crosses (+) are defined by the x and y coordinates of the earth at the times when the maximum intensities were observed. The curved line is the syndyname

Keller and Thomas (1975)

comet (very much in analogy to the visible dust tail). The line-of-observation was almost perpendicular to the cometary orbital plane revealing the curvature most effectively. The stronger the solar L_α flux the less curvature can be seen. This curvature can therefore be used to determine the solar L_α intensity independent of any absolute calibration of the instrument. The relative intensity distribution across the hydrogen halo determines the strength of the curvature and hence the solar L_α

intensity scattered by the comet.

This type of model assumes an optically thin emission (certainly not correct for the surroundings of the nucleus out to less than 10^6km) and takes the effects of the orbital motion of the comet and the gradients of the forces of gravitation and radiation pressure into account. The following cometary parameters can be determined:

1) The production rate of hydrogen, Q_H, and its variation with heliocentric distance, r.
2) The mean outflow velocity, v_H.
3) The hydrogen lifetime, t_H.

We shall now discuss these parameters using L_α observations of comet Kohoutek (1973 XII) taken by the electrographic camera of the Naval Research Laboratory (Opal et al. 1973; Meier et al. 1976). A camera was installed on Skylab and observed the comet for a period of about two months centered around perihelion time. A second camera was flown on a sounding rocket on June 8, 1974, (r = 0.43) producing the best observation (Fig. 2). For this observation the line-of-sight lay almost in the orbital plane perpendicular to the sun-comet direction. Therefore, the effect of the curvature <u>in</u> the orbital plane appears only as a rather slight asymmetry. We (Keller and Meier 1976) had to give up the convenience of the earlier model and refine the calculations by introducing an arbitrary geometry but neglecting the variations of forces over the size of the observed hydrogen cloud (which is considerably smaller than that observed by the OGO-5 photometer, see Fig. 1). The intensity of the solar L_α line had to be assumed because the curvature could not be seen due to the projection. With a solar flux of $F = 3.7 \times 10^{11}$ph $cm^{-2}s^{-1}Å^{-1}$

at 1 a.u. we obtained $Q_H = 6 \times 10^{29} s^{-1}$, and $t_H = 2 \times 10^6 s$ reduced to 1 a.u. A potential law $Q_H \propto r^{-n}$ was assumed for the time variation of the

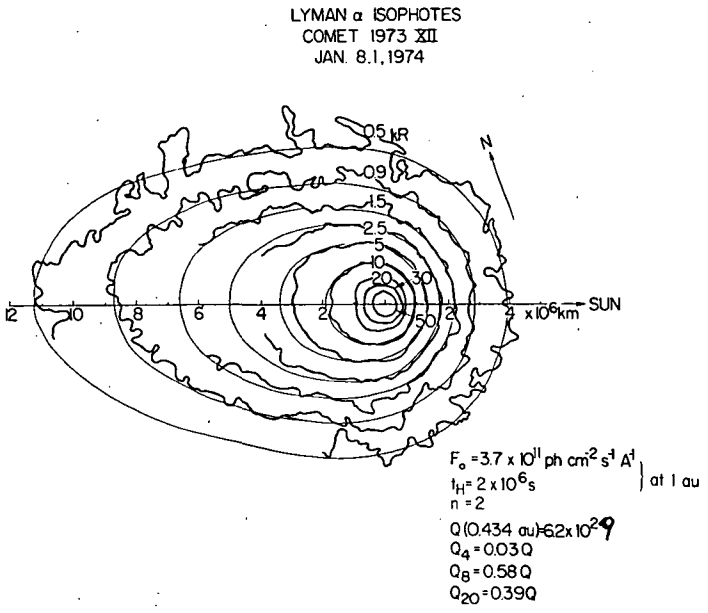

Fig. 2 Observed and computed isophotes from the rocket Lα imagery. Airglow and film backgrounds have been removed. No data are shown in portions of the antisolar direction, owing to an instrumental ion spot at the center of the field; the outermost isophote is not completed in the lower left of the figure because of a scratch on the film. The smallscale variations in the data are due to grain variations in the film, and densitometer noise

Meier et al. (1976)

production yielding an exponent n = 2. As for the above mentioned OGO-5 observations of comet Bennett it was not possible to fit the isophotes with a one parametric Maxwellian velocity distribution of the outstreaming hydrogen atoms. A combination of 60% atoms with $v_H = 8$ km s^{-1} and 40% with $v_H = 20$ km s^{-1} resulted in a good fit to the observations. While the outflow velocity of 8 km s^{-1} had been found in early investigations (Keller 1971; Bertaux et al. 1973), a second, higher velocity component had to be introduced for fitting with the more sophisticated models. It

should be pointed out that the mean velocities 8 and 20 km s^{-1} were not the result of the fit but had been chosen a priori and only the ratio of the productions of atoms of the two distributions was varied. 20 km s^{-1} was chosen because the hydrogen atoms may be produced from dissociation of water (see below). The interpretation of this result is that the actual velocity distribution of the outflowing hydrogen atoms (which is certainly not Maxwellian) has to have a high velocity component.

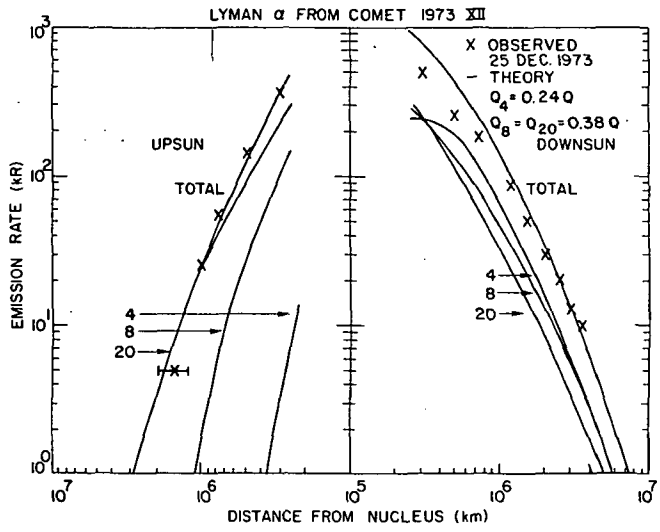

Fig. 3. Upsun and downsun emission rate profiles for the EVA observation. The horizontal error bar in the last upsun data reflects the spread in distance of the outermost isophote

Notice the change in curvature of the 4 km s^{-1} profile in the downsun direction near 5 10^5 km due to atmospheric absorption

Meier et al. (1976)

Figure 3 displays upsun and downsun intensity profiles of the Skylab observation of comet Kohoutek on Dec. 25, 1973 (r = 0.18 a.u.) Here we had to introduce a third, low, velocity component with 4 km s^{-1} to achieve a good fit to the isophotes.

The number of parameters makes it advisable to investigate their influence on the fit rather carefully to uphold their physical meaning. An

easy method to do so is demonstrated in Figure 4. Three models with v_H = 4, 8, and 20 km s^{-1} were calculated resulting in the isophotes shown on the first row of Fig. 4. The second row shows isochrones connecting points where the mean lifetime of the hydrogen atoms in the line-of-sight column is equal.

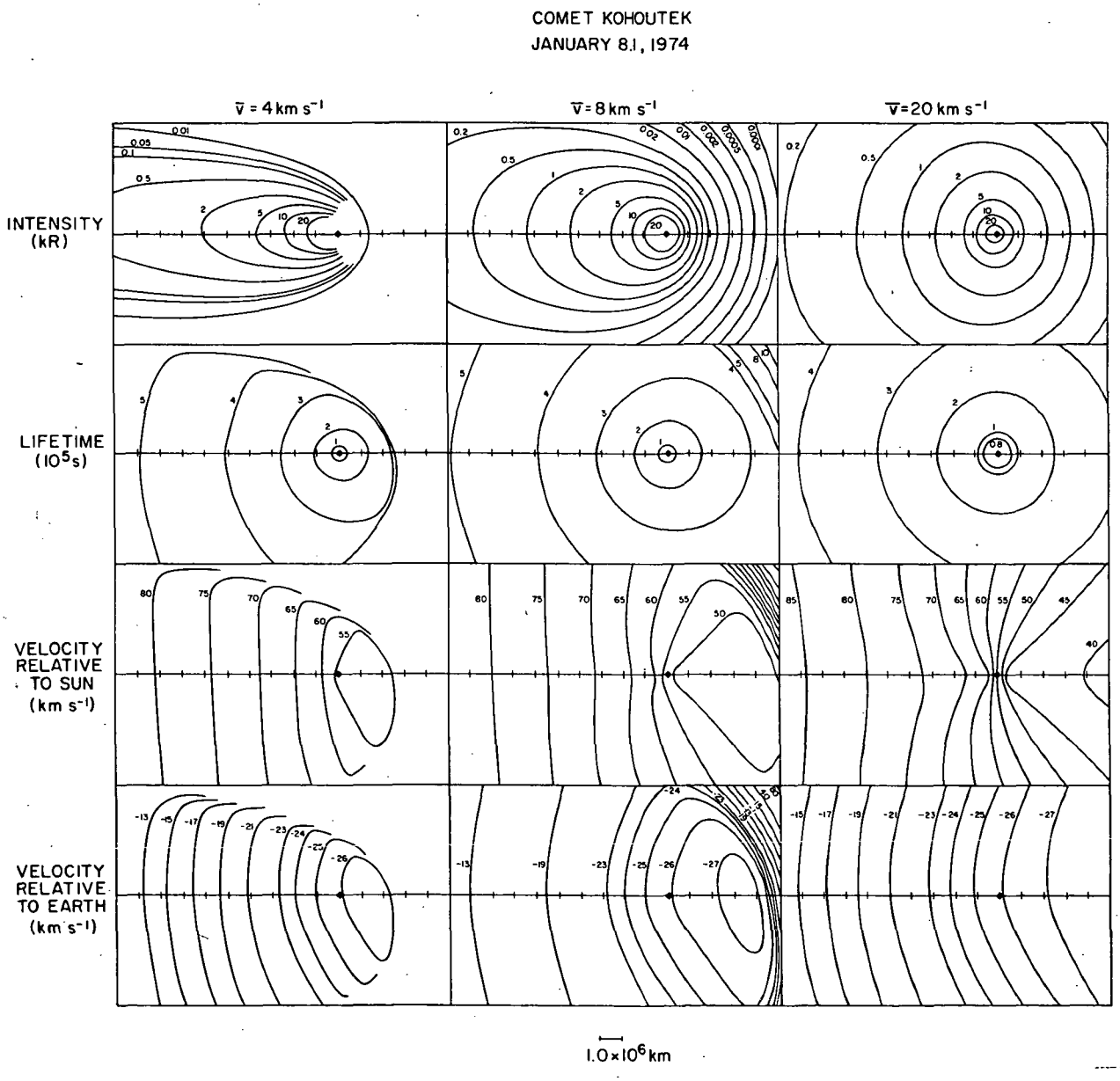

Fig. 4. Isophotes, isochrones and isotachs of the radial velocities for models with mean velocities of 4, 8 and 20 cm s^{-1} For illustration purposes, the following values of the parameters were adopted at 1 a. u. for each model: $F_\odot = 3.7\ 10^{11}$ ph $cm^{-2}\ s^{-1}\ A^{-1}$, $t_H = 2\ 10^6$ s, $n = 3$, $Q_H = 10^{29}\ s^{-1}$. The position of the nucleus is indicated by a dot, the sun is to the right.

The solar L_α line is self-reversed. The excitation of the hydrogen atoms depend on their radial velocity component with respect to the sun. The influence of this Doppler shift can be judged using the plots in the third row displaying isotachs.

Even more important than the variation of the solar excitation may be the geocoronal absorption of the cometary L_α signal. Since the geocorona extends to more than 10^5km from the earth most satellites fly inside. The optical depth of the terrestrial hydrogen in the center of the absorption line depends on the observational geometry; a typical value is 10. The isotachs of the fourth row of Fig. 4 permit determination of the influence of this absorption, which often is only important in a small region of the cometary halo. The geocoronal line is narrow compared to the cometary emission line and to the dispersion of the radial velocity component. A first order approximation of this absorption is included in our models. E.g., it was important for the Skylab observations on Dec. 25. In general, all the diagrams show an asymmetry with respect to the sun comet line. The faint isophotes show a slight intensity enhancement even on the sunward portion of the plots. This is due to a contribution of old hydrogen atoms of the far tail which is turned around and seen in this particular observational projection as faint background mainly on the upper parts of the plots. The situation can be compared to the appearance of an anomalous dust tail.

We have strong indications that H_2O is an important, or even the dominant, parent molecule of the observed hydrogen. H and OH are produced in a ratio of about two to one. This ratio was constant for $0.8 < r < 1.2$ a.u. for two comets (Keller and Lillie 1974, 1977). The water mole-

cules are dissociated into H and OH by solar photons (Table I). Most of the excess energy of this process is converted into kinetic energy of the hydrogen atoms yielding velocities bigger than 16 km s^{-1}. The second dissociation of OH into O and H is badly known, no laboratory measurements exist. The question is whether the observed 8 km s^{-1} component can be connected with this dissociation process. For more details see Keller (1976a).

Table

H_2O Photodissociation			
$H_2O+h\frac{c}{\lambda}$			
λ: 1365–1860 Å	70% →	$H(^2S)+OH(X^2\pi)+E_{kin}$ (>1.5 eV, $v_H>16$ km s^{-1})	60%
		H_2+O [a]	10%
$\lambda<1365$ Å	30% →	$H(^2S)+OH(X^2\pi)+E_{kin}$ (~ 5 eV?, $v_H\sim 30$ km s^{-1}?)	28%
		$H(^2S)+OH(A^2\Sigma^+)+E_{kin}$ (<0.4 eV, $v_H<9$ km s^{-1})	<1%
		H_2+O [a] $2H+O$ [a]	2%
OH Photodissociation			
$OH+h\frac{c}{\lambda}$			
λ: 2610 Å	→	$H(^2S)+O(^3P)+E_{kin}(\sim 0.4$ eV) [b]	
$\lambda\sim 1500$ Å	→	$H(^2S)+O(^3P)+E_{kin}(\sim 4$ eV) [c]	
$\lambda\sim 1000$ Å	→	$H(^2S)+O(^1S)+E_{kin}(\sim 4$ eV) [d]	

[a] ^3P, ^1D, ^1S depending on λ.
[b] Predissociation via $A^2\Sigma^+v'=2$.
[c] Dissociation via $^2\Sigma^-$ or $^4\pi$.
[d] Dissociation via $B^2\Sigma^+$.
E_{kin} estimated using the Franck-Condon principle

Keller (1976a)

The appearance of the low velocity component with about 4 km s^{-1} in the pre-perihelion observation on Dec. 25, 1973 can be explained by thermalization of hydrogen atoms which are created in the inner coma. At this small heliocentric distance the cometary gas production is high, extending the collisional zone around the nucleus. The parent molecules dissociate shortly after evaporation from the nucleus because of the in-

creased solar flux. This interpretation yields an additional argument that the 8 km s^{-1} component is not due to thermalization but is intrinsic to the creation processes of the hydrogen atoms (Keller 1976b).

The explanation of the origin of the predominant 8 km s^{-1} velocity component seems to be one of the central questions which ought to be investigated and solved. Possibly experiments could be performed using the Space Shuttle to study the photodissociation of OH and the resulting excess energies liberated in this process.

Because hydrogen is the dominant atomic species produced by comets the L_α observations are representative for the overall gas output and its variation with heliocentric distance. They provide the best means to monitor the evolution of an incoming comet and are an important feature for the characterization of a comet.

Space Shuttle will make it possible to observe comets with a variety of instruments simultaneously. This will enable us to combine L_α observations with information gained at other wavelengths and so help to solve the question of the nature of the original parent molecules and their dissociation processes.

Observations over an extended heliocentric distance interval of comets, perhaps with more than one shuttle mission, will provide essential information of the scalelengths of the species. These scalelengths vary with r^2 if the destroying process depends on the strength of the solar flux. This, combined with the variation of the intensities of the emissions with r, will provide clues on the creation and excitation mechanisms. E.g., a long living species can be observed out to several scalelengths if the comet is close to the sun and vice versa the scale-

length of a short lived parent molecule may be resolved at larger distances. The knowledge of the scalelength of a species is essential for the determination of its production rate. Theoretical dissociation rates are very uncertain.

Monitoring the strong L_α signal and hence the variation of the total gas production out to 2 to 3 a.u. is possible. Thus the predicted rather rapid decline of the gas production at around 2 a.u. will be observable. There the insolation cannot any longer overcome the high evaporation heat of water ice. Observations of a large number of well known periodic comets (such as comet Encke) will be possible. The determination of their gas productions could tell us whether there are systematic differences between periodic and "new" comets.

References

Bertaux, J.L., Blamont, J., Festou, M. 1973, Astron. Astrophys. 25, 415

Biermann, L. 1968, JILA Report 93

Keller, H.U. 1971, Mitt. Astron. Ges. 30, 143

Keller, H.U. 1976a, Space Sci. Rev. 18, 641

Keller, H.U. 1976b, Mitt. Astron. Ges. 38, 150

Keller, H.U., Thomas, G.E. 1973, Astrophys. J. 186, L87

Keller, H.U., Lillie, C.F. 1974, Astron. Astrophys. 34, 187

Keller, H.U., Thomas, G.E. 1975, Astron. Astrophys. 34, 187

Keller, H.U., Meier, R.R. 1976, Astron. Astrophys. 52, 273

Keller, H.U., Lillie, C.F. 1977, Astron. Astrophys. to be published

Meier, R.R., Opal, C.B., Keller, H.U., Page, T.L., Carruthers, G.R. 1976, Astron. Astrophys. 52, 283

Opal, C.B., Carruthers, G.R., Prinz, D.K., Meier, R.R. 1974, Science 185, 702

The Study of Cometary Plasmas Using Artificial Comets Launched from the Space Shuttle

D. A. Mendis*

Department of Applied Physics and Information Science

University of California, San Diego

La Jolla, California 92093

The extension of the range of observation from the visual to the ultraviolet on the one hand, and to the infrared and radio on the other hand, within the last decade, has produced a significant advance in our knowledge of comets. It is doubtful if there has been a corresponding increase in our understanding of comets. Perhaps the real progress here has been the growing realization that comets are more complex beasts than had hitherto been thought.

The infrequent and unexpected apparition of comets as well as their transient nature contribute to the difficulty of the systematic and sustained study of comets. It is therefore desirable to supplement the study of these natural phenomena with simulations in both the terrestrial and the space (earth orbiting) laboratory, as well as in the "free space" environment.

Of course, these simulations will be based on our current views of comets, and will therefore be largely useful in establishing the plausibility of some and the invalidity of others. Hopefully the happy circumstance of serendipity may provide us insights that we are not actively seeking. Furthermore, the controls we exercise on our experiments will enable us to cut through the bewildering welter of cometary phenomena and study them piecemeal.

With regard to shuttle based experiments, earlier speakers have emphasized the importance of on-board experiments, using particularly the "zero-gravity" environment in the study of cometary snows.

Others have discussed release experiments from the shuttle, particularly with the view of studying the neutral coma. Clearly the absence or near absence of "wall effects" is an advantage in this case, and so is the negligible attenuation of the solar spectrum at high exospheric altitudes. The existence of "zero-gravity" here is not crucial.

The observational difficulty of such a coma and its lack of 'photometric similarity' to a real comet, mainly by virtue of our situation within it, has already been discussed by Öpik (1965). This needs to be kept in mind, even though Öpik overestimated the expansion velocity and consequently the size of the artificial coma substantially, by assuming a free-expansion rather than a diffusion of the artificial comet gases into the ambient environment.

This leads us to the second and more important difficulty, which is the lack of 'dynamical similarity' between the artificial and the real comet.

At typical shuttle altitudes (h) there is still a substantial residual atmosphere, mainly of neutral atomic oxygen, with a typical temperature of about 1500°K. When $h \approx 300$ km typically $n(o) \approx 10^9$ cm^{-3}, and $n(e^-) \approx 2 \times 10^6$ cm^{-3}, whereas when $h \approx 700$ km (which corresponds to the maximum altitude of the shuttle) $n(o) \approx 10^7$ cm^{-3} and $n(e^-) \approx 5 \times 10^5$ cm^{-3}. The shuttle will also be moving with a speed of 7-8 km sec^{-1} with respect to the ambient atmosphere.

Suppose the artificial comet released from the shuttle space laboratory consists of a frosting of snow (predominantly H_2O with traces of CO_2, etc.) 1 cm thick deposited on a light hollow spherical shell of radius 1 m. Then it would have a mass of perhaps 100 kg or less and will continue to be active for several weeks.

This "comet" will be subject to a neutral wind with $n \approx 10^9$ cm^{-3} and $v \approx 7.8$ km sec^{-1}, if it is at an altitude of 300 km above the earth. While this will not have an appreciable effect on decelerating the 'comet'; it will be basic to the size and shape of the artificial coma. Due to the small size of the artificial comet, a 'free particle' approach is appropriate even for regions close to the nucleus, unlike in the case of a real comet. However, the cometary molecules will be strongly decelerated by collisions with the oxygen atoms of the ambient neutral wind. The trajectories of the cometary molecules will be enveloped within a paraboloid whose apex is at a distance $D \approx \lambda(u_o/w)$ from the nucleus, where u_o and w are respectively the initial speed of the cometary molecules and the wind speed, and λ is the effective mean free path of the cometary molecules ($\approx 1/n_a \alpha$). On substitution we find that D is only about 2 km, and the latus rectum of the paraboloid $L \leq 10$ km.

Also the oxygen atoms of the neutral wind have energies ≥ 5 eV which are sufficient to dissociate the 'cometary' molecules with a time scale of only 10-20 sec. Furthermore, the cometary species will be ionized by charge exchange with the ions of the corresponding 'ion wind'

with a time scale of 500-1000 sec.

The dynamic interaction of this terrestrial 'ion-wind' ($n_i \approx 2 \times 10^6$ cm^{-3} and $w \approx 7.8$ km sec^{-1}) with the artificial cometary ionosphere is also completely different from that of the solar wind with the natural cometary ionosphere. The equitorial magnetic field at $h \approx 300$ km is about 0.3 Γ and therefore the terrestrial 'ion-wind' is highly sub-Alfenic, unlike the solar wind. Consequently there will be negligible distortion of the field lines and the cometary ions will merely diffuse along these undistorted field lines as they are swept back into the wake.

If the artificial comet released from the shuttle is merely a mixture of neutral gases (e.g. H_2O, CO_2, N_2, etc.), so as to reduce the payload, this cloud will be brought to rest with respect to the ambient medium in a line scale $\tau \approx \langle n_i \rangle R / n_a w$, which may be on the order of only a minute, for typical values of $\langle n_i \rangle R$. The neutral gas cloud, which would be somewhat squashed in the forward direction, will then begin to diffuse into the ambient medium. The dynamical development of any single neutral species, neglecting sources and sinks, is then governed by the diffusion equation (with spherical symmetry):

$$\frac{\partial n}{\partial t} = D\left(\frac{\partial^2 n}{\partial r^2} + \frac{2}{r}\frac{\partial n}{\partial r}\right) \qquad (1)$$

where D is the diffusion coefficient $= kT/m\nu$ (ν being the collision frequency). If initially there was a uniform spherical cloud of radius r_o

and density n_o, then the solution of (1) is (Shklovskii and Kurt, 1961) given by,

$$n(r,t) = \frac{n_o}{2}\left[\mathrm{erf}(x) + \mathrm{erf}(y) + \frac{1}{r}\sqrt{\frac{Dt}{\pi}}\{\exp(-x^2) - \exp(-y^2)\}\right] \qquad (2)$$

where

$$x = \frac{r_o - r}{2\sqrt{Dt}} \quad ; \quad y = \frac{r_o + r}{2\sqrt{Dt}}$$

and

$$\mathrm{erf}(x) = \frac{2}{\sqrt{\pi}}\int_o^x \exp(-\xi^2)\, d\xi .$$

The diffusion speed

$$v_D = -\frac{D}{n}\frac{dn}{dr} \qquad (3)$$

and the radius of the cloud $R(t)$ (when it is much larger than r_o) is given approximately by

$$R(t) \approx \sqrt{Dt} \qquad (4)$$

The expansion speed of the cloud is then given by

$$V(t) = \dot{R}(t) \approx \frac{D}{2R(t)} \qquad (5)$$

and $V(t) \ll v_{th}$, when $R(t) \gg 5$ km.

What all this shows is therefore, that on account of the existence of a substantial residual ambient atmosphere at typical shuttle altitudes,

artificial comets released from the shuttle will not simulate the natural ones either physically or dynamically.

In order to obtain a proper simulation, it is not sufficient to merely reach higher altitudes, where the effects of the residual ambient atmosphere would be smaller. It is necessary to reach outside the terrestrial magnetosphere where the artificial comet can have a direct interaction with the solar wind.

This may conceivably be achieved with the help of a small booster rocket, attached to the cometary payload, which uses the shuttle as a launching pad. Best viewing conditions may be obtained with a high inclination orbit which reaches apogee at a distance $r_A \approx 50\ R_\oplus$, on the tail side of the magnetosphere, but well above the magnetotail.

It appears that artificial 'comets' were launched by the Russians outside the magnetosphere early in their space program, when 1 kg of Na vapor was released at an earth distance of about 19 $R_\oplus$ (Shklovskii, 1961). But the purpose of this 'comet' was merely to serve as a method for optical tracking of space vehicles.

We are, of course, interested in studying the nature of the comet solar-wind interaction.

The two primary agents responsible for the observed (transient) cometary phenomena are solar radiation and the solar wind. It is generally believed that solar radiation is responsible for the evaporation of cometary snows and also largely responsible for the dissociation and

and ionization of the resulting gas molecules. More recently, it has been suggested (Ip and Mendis, 1975, 1976) that the solar wind, which is responsible for the shaping and maintaining of the plasma tail, would play an indirect but dominant role on the dissociation and ionization of the cometary gases too.

The idea here is that the 'folding umbrella' morphology of cometary tail streamers is associated with the 'folding' of interplanetary field lines into the cometary tail and the build up of an associated cross tail current (see Fig. 1). It is argued that a large current ($\sim 10^8 - 10^9$ A) of keV electrons can be generated this way, and that at least a part of this current may be eventually discharged, along the field lines, into the cometary ionosphere, due to a partial or total disruption of the cross-tail current (see Fig. 2). Dissociation and ionization of cometary species can then take place sporadically on a time scale of only $10^3 - 10^4$ sec under favorable conditions, which is in agreement with the early observations of Wurm (e.g. see Wurm, 1961). These times are orders of magnitude smaller than the typical photodissociation and photoionization time scales of $10^5 - 10^6$ sec at 1 AU.

Since the identification of the dominant dissociation and ionization process is vital to the future development of cometary physics, it seems that a space experiment directed specifically towards this end is highly desirable.

Conceivably, with the simultaneous release of about 50 kg of a mixture of Ba and H_2O (and perhaps also CO) vapor at $r \approx 50\ R_\oplus$ we

can produce an observable "comet" (with a total brightness comparable to that of an "average" H_2O dominated comet of 1 km radius at a heliocentric and geocentric distance of 1 AU) in order to simulate the comet-solar wind interaction described in Figs. 1 and 2. The purpose of the Ba (which is photoionized within an extremely short time $\leq$ 100 sec, Haser, 1967) is to capture the interplanetary magnetic field lines and fold them back into the tail. As discussed earlier a strong electric discharge through the coma would result, causing dissociation and ionization of the H_2O and CO with a predicted time scale of about 10^3 - 10^4 sec. The actual time scales for these processes may be estimated from the appearance and distribution of the H_2O^+, CO^+ and OH emissions in the visual region, and compared with prediction, in order to test the validity of this proposed mechanism.

If an experiment of this nature is at all feasible, then we could extend it also to study other details of the comet-solar wind interaction. The stability of the comet-solar wind interface and the fine structure of the plasma tail are amongst these.

Acknowledgments

This research was supported in part by the following grants: NASA-NSG-7102 of the NASA Planetology Program, NASA NGR-05-009-110 of the NASA Physics and Astronomy Program, NSF-MPS74-23501 and NSF-MPS74-21195 of the Solar System Astronomy Program of the National Science Foundation.

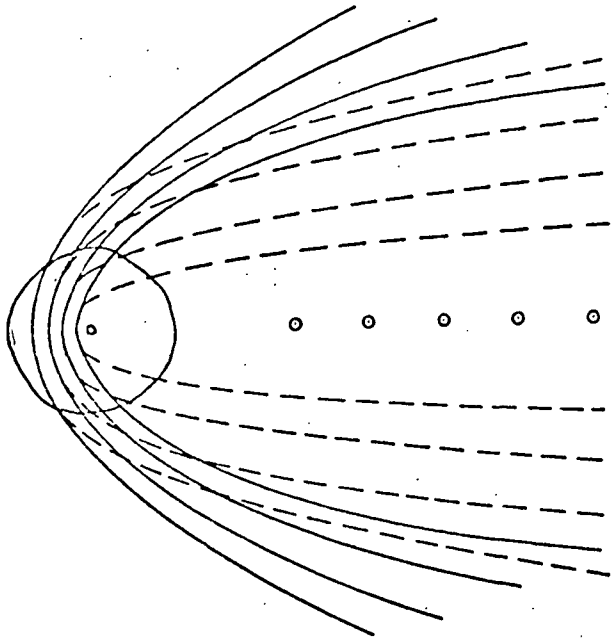

Fig. 1

The 'folding umbrella' morphology of cometary tail streamers and the generation phase of the neutral sheet cross tail current.

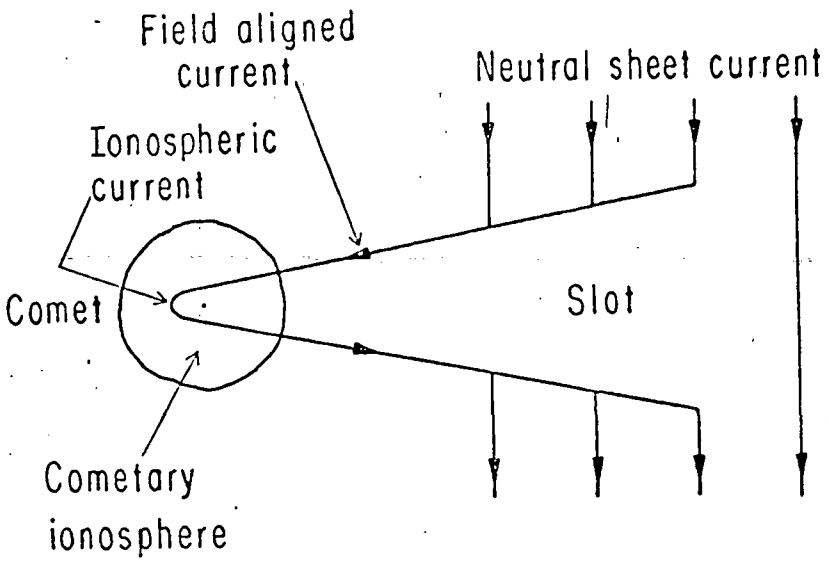

Fig. 2

Disruption phase of the cross-tail current, causing field aligned flow and a strong ionization in the inner coma.

References

Ip, W.-H. and Mendis, D. A., 1975, Icarus, 26, 601

Ip, W.-H. and Mendis, D. A., 1976, Icarus, 29, 147.

Öpik, E. J., 1965, Irish. Astron. J., 7, 32.

Shklovskii, I. S., 1961. Artificial Earth Satellites (Ed. L. V. Kurnosova), Vol. 4, p. 445.

Shklovskii, I. S. and Kurt, V. G., 1961, Artificial Earth Satellites (Ed. L. V. Kurnosova), Vol. V, p. 92.

Wurm, K., 1961, Astron. J., 66, 362.

APPENDIX A

Editors' Comment: Various missions to comets have been and are being planned. The experimentation and observations from the Shuttle base should provide significant insight into the selection of missions to comets. This brief description of a possible rendezvous mission with Comet Halley is presented to indicate the possible role that cometary research may take in the future.

THE HALLEY RENDEZVOUS VIA SOLAR SAILING MISSION DESCRIPTION

L. D. Friedman

The Solar Sail trajectory to Halley's Comet provides a path through unexplored regions of our solar system to yield a rendezvous with this famous celestial visitor. Comets are believed to hold clues about the origin of our solar system and its subsequent history, for they, unlike planets, have not undergone internal processes altering their primitive composition. A typical comet comes from the far outer reaches of the solar system once in recorded history--these comets are usually active and undoubtedly would provide many indicators for scientific studies if their coming could only be predicted. The short period comets, in contradistinction, can be predicted, but because they come near the Sun so often they are nearly "burnt out" and are far less active. Halley's Comet is the compromise--long period enough to be active and bright, yet having sufficient visits to be a predictable target for exploration.

But although Halley's Comet is a tantalizingly close target (in its last visit its tail actually touched the Earth), it is an elusive one. Halley comes through the solar system backwards (retrograde) and, like ships passing in the night, normal flybys provide too brief a visit to learn much. To achieve a rendezvous (matching position and velocity) or slow flybys of speeds associated with planetary missions, we must, in effect, stop our vehicle and turn it completely around. Mathematically, this means we must wipe out orbital angular momentum and then reverse it. This has the effect of turning the orbital plane over. Of course, simultaneously we must reduce the orbital energy from that of Earth's (which has a period of 1 year) to that of Halley's (which has a period

of 76 years). The finding of a trajectory to accomplish this is due to J. Wright, formerly of Battelle Columbus Laboratories.

The Solar Sail trajectory can be modified easiest when it is near the Sun, hence the angular momentum change is done in a near solar orbit. Similarly, acceleration can only be provided while the vehicle flys outward from the Sun, thus the energy change to match Halley's orbit is done primarily with an outward loop after the inclination change.* The energy change is a much easier job than is the flipping of the orbital plane.

The trajectory is depicted in Fig. 1. Following launch, a 9-month cruise phase takes the vehicle to a 0.3 AU circular orbit about the Sun. This orbit is called the "cranking" orbit since, while here, the orbit is "cranked" from a low inclination, over the pole to an angle of 163°. Approximately once per two months the vehicle orbits the Sun while the solar radiation force modifies the inclination about 10° per orbit. After about 1-1/2 to 2 years the orbital plane has been flipped to nearly that of Halley's.

This period should provide some very exciting opportunities for solar observations and exploration of new regions of our solar system, for this would be the first spacecraft ever to fly significantly out of the ecliptic plane, and it would repeatedly do so near the Sun affording many observation opportunities. Solar polar observations are possible in addition to monitoring activity at all ecliptic latitudes and longitudes.

*Solar Electric Propulsion trajectories differ in that they cannot utilize full solar power near the Sun because of temperature limitations, but they can accelerate while flying in toward the Sun by pointing of the thruster. Thus, the SEP trajectory is very different.

After the near 160° orbit is achieved, the orbit is "pumped" out to an aphelion near 2 AU (almost to the asteroid belt, but above it and not quite deep enough into it to be dangerous) where it leisurely turns around to fly in front of Halley going just slow enough to be gradually overtaken by the comet. (The sail can fly outward or inward simply by orienting the sail angle to add or reduce orbital speed). The rendezvous takes place after Halley's perihelion since the sail cannot gain much energy while flying in toward the Sun. This turns out to be no scientific limitation since a near perihelion rendezvous could not occur with the vehicle near the comet. The latter is too active at that point and would probably destroy the instruments observing it. The rendezvous is planned for a distance about 1 AU from the Sun, while outbound. After this, the spacecraft would stay with the comet flying in and around it exploring and observing the nucleus, the coma and the tail. The sail would be jettisoned after the rendezvous, before the spacecraft flys close to the nucleus. The total velocity change achieved by the sail on the mission is approximately 125 km/s (or 225,000 mph)--if the sail were kept connected to the spacecraft for three more days after rendezvous it would escape the solar system.

The rendezvous approach is shown in Fig. 2. It is designed to provide a cautious exploration plan, one in which the vehicle gradually approaches the active regions from a direction outside the main flow of particles. The spacecraft will have 500 m/s (enough to move it almost 200,000 miles per week, 10 different times) velocity impulse from chemical propellant to move it after rendezvous. This will enable detailed cometary exploration.

The nominal mission plan calls for a launch in January 1982, with rendezvous near 1 AU in March 1986. The sail would be visible to the naked eye on Earth for months after launch. If the sail is heavier than anticipated or if its development takes longer so that launch is not possible until as late as July 1982, then the rendezvous point is moved further out to 2 to 2.5 AU. After July 1982, it may be better to not move the rendezvous point further away, but to let the intercept be a slow flyby. Even with a January 1983 launch, a 5 km/s flyby is possible. An October 1983 launch yields a 15 km/s flyby.

The mission schedule presently calls for a full-scale Shuttle test in early 1981 or late 1980. If this can be dispensed with and if the development program has proceeded without adverse surprises, then a 1981 launch could be used to permit either an earlier rendezvous or else a somewhat farther out cranking orbit. This latter could ease temperature requirements on the sail material.

Solar sailing to Halley's Comet affords an exciting opportunity for space exploration--to a large, active, famous, unique target and to a new environment near and over the Sun. The mission plan is challenging, but the options for variations from it offer sufficient contingency to permit justifying acceptance of the challenge. The two-year sail development program is now underway, aimed at project readiness in October 1978, and at launch readiness for a test on the Shuttle in late 1980.

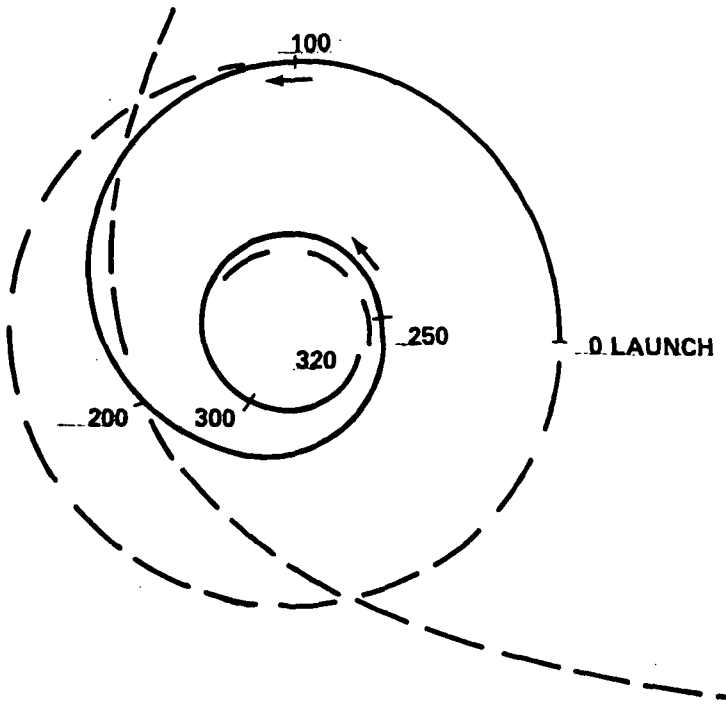

FIG. 1a HALLEY RENDEZVOUS TRAJECTORY; EARTH TO CRANKING ORBIT

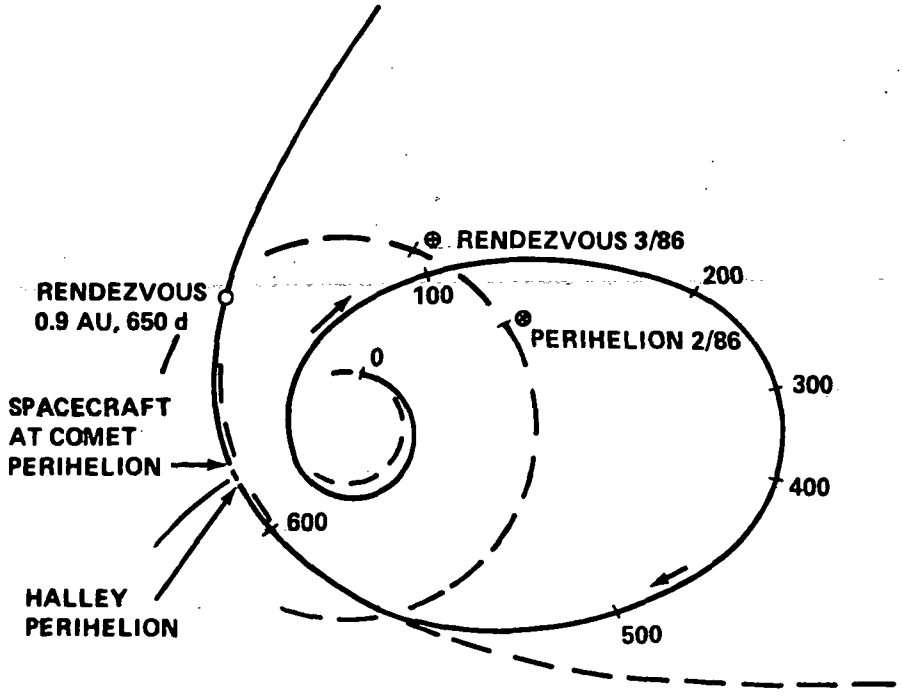

FIG. 1b HALLEY RENDEZVOUS TRAJECTORY: CRANKING ORBIT TO RENDEZVOUS

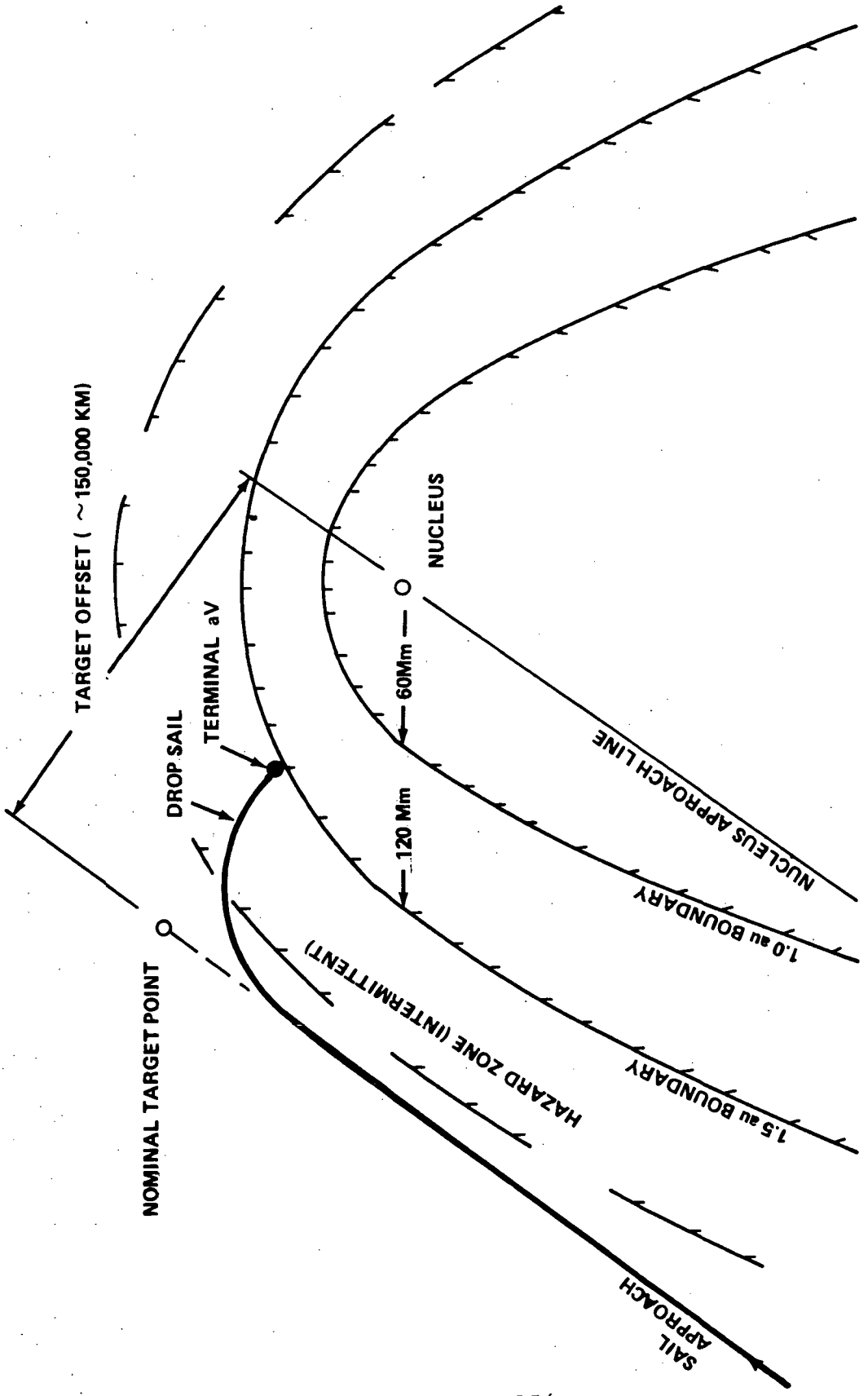
TARGET OFFSET (~150,000 KM)
TERMINAL aV
DROP SAIL
NUCLEUS
60Mm
120 Mm
NUCLEUS APPROACH LINE
1.0 au BOUNDARY
1.5 au BOUNDARY
HAZARD ZONE (INTERMITTENT)
NOMINAL TARGET POINT
SAIL APPROACH

FIG. 2

OMIT TO END

APPENDIX B

SHUTTLE-BASED COMETARY SCIENCE WORKSHOP PARTICIPANTS

Kenneth S. Clifton (Stu)
Code ES64
NASA/MSFC
Huntsville, Alabama 35812

Dr. Nicholas C. Costes
Code ES81
NASA/MSFC
Huntsville, Alabama 35812

Dr. Armand H. Delsemme
Department of Physics and Astronomy
University of Toledo
Toledo, Ohio 43606

Dr. Bertram Donn
Code SG, Cometary Physics
NASA Headquarters
Washington, D. C. 20546

Dr. Maurice Dubin
Code 680
NASA/GSFC
Greenbelt, Maryland 20771

Dr. M. Festou
Service D'Aeronomie du CNRS
B. P. No. 3
91-Verrieres-le-Buisson
France

Dr. G. Allen Gary
Code ES62
NASA/MSFC
Huntsville, Alabama 35812

Dr. Walter F. Huebner
Los Alamos Scientific Laboratory
Box 1663
Alamos, New Mexico 87544

Dr. William M. Jackson
Department of Chemistry
Howard University
Washington, D. C. 20059

Dr. H. U. Keller
Max Planck Institut für Aeronomie
Postfach 20
D-3411 Katlenburg-Lindau 3
Germany

R. Lavender
Code JA61
NASA/MSFC
Huntsville, Alabama 35812

Dr. C. F. Lillie
Laboratory of Atmospheric and
Space Physics
University of Colorado
Boulder, Colorado 80302

Dr. Charles A. Lundquist
Director, Space Sciences
Laboratory, ES01
NASA/MSFC
Huntsville, Alabama 35812

Dr. Asoka Mendis
Department of Applied Physics
University of California
San Diego, California 92110

Dr. Peter M. Millman
National Research Council of Canada
Ottawa, Ontario
Canada K1A 0R6

Dr. Robert J. Naumann
Code ES71
NASA/MSFC
Huntsville, Alabama 35812

Dr. C. R. O'Dell
Associate Director for Science
NASA/MSFC
Huntsville, Alabama 35812

Dr. Chet Opal
Code 7124
Naval Research Laboratory
Washington, D. C. 20375

Jerry K. Owens
Code ES64
NASA/MSFC
Huntsville, Alabama 35812

Dr. Zdenek Sekanina
Smithsonian Astrophysical Observatory
60 Garden Street
Cambridge, Massachusetts 02138

Dr. Ernst Stuhlinger
Adjunct Professor
The University of Alabama in Huntsville
P. O. Box 1247
Huntsville, Alabama 35807

Dr. Fred L. Whipple
Smithsonian Astrophysical Observatory
60 Garden Street
Cambridge, Massachusetts 02138

☆U.S. GOVERNMENT PRINTING OFFICE 1977 – 740-049/277 REGION NO. 4